An Investigation of Zwitterionic Magnesium Complexes as Ziegler-Natta Polymerisation Catalysts

by

Daniel José Loroño González

Doctor of Philosophy

University of Edinburgh

2004

To Juan, José, Maylim and my Mum

For their love and support in everything I have done

Declaration

I declare that this thesis has been entirely composed by myself and that the work described herein is my own work except where clearly mentioned either in acknowledgement, reference or text. No part of the work referred to in this thesis has been submitted in support of an application for another degree or qualification from this or any other University of institute or learning. Certain of the results have been published previously.

Daniel José Loroño González

Contents

Abstract

This thesis is concerned with the synthesis and chemistry of series of zwitterionic magnesium complexes, with the aim of providing the first evidence of zwitterionic potential magnesium polymerisation catalysts. The positive charge on the magnesium centre can be stabilised by preparing zwitterionic species incorporating existing and specially developed chelating nitrogen donor ligands.

Chapter One serves as general introduction about ethylene polymerisation throughout the periodic table, and the polymerisation activity of magnesium complexes supported by bidentate nitrogen donor ligands.

Chapter Two describes the synthesis of a series of magnesium complexes using $[K\{H_2B(pz)\}_2]$ ligand. Predominately $[\{H_2B(py)\}_2Mg(THF)n]$ (n: 1 or 2) bis-chelate complexes are obtained in order to satisfy the electronic requirement of magnesium. The charge transfer from the ligand has the effect of neutralising the formal Mg^{2+} charges, and this does not produce zwitterionic complexes. Schlenk equilibrium suggests a solvation and association, by which $MgCl_2$ is formed, and associations by μ–bridging halide predominate.

Chapter Three describes the synthesis of three different borate-centred ligands suggested for zwitterionic magnesium complexes, and this chapter is divided into three main sections. The first section deals with the synthesis of $[R_2B(CH_2NEt_2)_2]^-$ (R: Me or Ph) ligands and describes the chemistry of these systems. The $[\{Ph_2B(CH_2NEt_2)_2]\}Li]$ complex can be obtained but no reactivity is observed with Grignard reagents. The second section is concerned with the reactivity of isonitrile ligands to produce borate-centre ligands. The third section deals with the synthesis and chemistry of pyridyl borate ligands, whilst a series of $[\{R_2B(2\text{-}py)\}Mg(R')THF]$ (R: Me or Ph) complexes can be obtained as shown by ^1H, ^{13}C and ^{11}B analyses.

Chapter Four explores the chemistry of boron supported by the β-diketiminate ligand. Complexation of β-diketiminate ligand with boron results in the formation of several reaction products, *via* radical processes and provides the first

evidence of borane carbene analogue, $[HC(MeCNAr')_2B]$ (Ar': 2,6-diisopropylphenyl). The redox behaviour of these systems is discussed.

Chapter Five describes the synthesis of a series magnesium complexes using $[R_2AFA(H)]$ (R: Cy, AFA; 6-aminofulvene-2-aldimine) ligands. Co-ordination of the cyclopentadienyl (η^5-Cp) portion of the ligand results in complexes of zwitterionic character in which a positive charge resides on the magnesium. Schlenk equilibrium suggests a solvation and association, by which $MgCl_2$ is formed to provide complexes $[(R_2AFA)Mg(Cl)Et_2O]$ and $[[(R_2AFA)_2Mg]$. Ethylene polymerisation studies of $[(R_2AFA)MgMe]$ were implemented and revealed that the compound is inactive under both mild and forcing conditions.

Chapter Six explores the technique of high-resolution X-ray diffraction in the complex of $[Mg\{(pz)_3BH\}_2]$. The topological properties of $\rho(r)$ and $\nabla^2\rho(r)$ have been investigated, and the nature of the B-N and Mg-N bonding investigated.

Acknowledgements

There are a number of people whom I would like to thank without whose help this thesis would have been impossible.

Firstly, I would like to thank Dr Philip Bailey and Dr Simon Parsons who gave me the opportunity to do a PhD, for their ideas, encouragement, support, friendship and patience throughout my time in Edinburgh.

A special thanks must go to Dr Lesley Yellowless and Colin Pulham, for advice and discussions at various stages of my PhD, especially because they always have time for everyone.

I will be forever grateful to Dr Hamish McNab for his friendship and the enjoyable discussions about Organic Chemistry.

I owe a great debt of gratitude to Dr Steve Liddle, Dr Andrew Parkin, Dr Bob Coxall and Dr Garry Smith for training me in the arts of air sensitive techniques and the X-ray crystallography skills.

It is a pleasure to acknowledge the skill and help of the technical staff of the Chemistry Department. In particular, John Millar, Wesley Kerr and Alan Taylor.

I also extend my grateful thanks to the Bailey and Parsons groups who contribute to carry out this research, for their day to day support and company (Lab's 85 and N2.15).

Finally, I would not even have contemplated working had it not been for the continuous underpinning of love and encouragement from my beloved family, Juan, José and Maylim. To my Mum for their support and also for putting up with me all these years.

Abbreviations

%	percent
δ	chemical shift
β	beta
γ	gamma
λ	wavelength
ν	wavenumber
ε	ellipticity
°	degree
θ	circle diffraction angle
ρ(r)	electron density
$\nabla^2\rho(r)$	Laplacian
°C	degree centigrade
Å	angstrom
AFA	6-aminofulvene-2-aldimine
AIM	atoms in molecules
Ar	aromatic
Ary	aryl
Atl	aminotroponiminste
atm	atmosphere
BCP	bond critical point.
Bp	hydrobis(pyrazolyl)borate
BP	bond path
Br	broad
Bu	butyl
BuLi	butyl lithium
^{t}Bu	tertiary butyl
CCD	Charge-Coupled-Devices
$CDCl_3$	deuterated chloroform

CH_2Ph	benzyl
CHN	elemental analysis
Cp	cyopentadienyl
CP	critical point
Cp*	pentamethylcyclopentadienyl
CSD	Cambridge Structural Database
CV	cyclic voltammogram
Cy	cyclohexyl
d (NMR)	doublet
D_2O	deuterated water
DCM	dichloromethane
DEPT	Distortionless Enhancement by Polarization Transfer
DFT	Differential Fourier Transform
DMF	Dimethyl formamide
DMSO-d_6	deuterated dimethyl sulfoxide
E	exponential (to the power of 10)
EIMS	electron impact mass spectroscopy
EPR	electron paramagnetic resonance
ES	electrospray
Et	ethyl
et al	*et alli* (and others)
Et_2O	diethyl ether
EtOH	ethanol
FABMS	fast atom bombardment mass spectroscopy
FT-IR	Fourier Transform-Infra-Red spectroscopy
g	gram
g (EPR)	*g* value (for a free electron, $g_e = 2.0023$)
h	hour
HF	Hartree-Fock
HOMO	Highest Occupancy Molecular Orbital
IAM	independent atom model
^iPr	isopropyl

IR	infra-red
K	kelvin
KRMM	κ'- restricted multipole model
L	ligand
LS	least squares
LUMO	Lowest Occupancy Molecular Orbital
M	molar
m	*meta*
M	Mol dm^{-3}
m (IR)	medium
m (NMR)	multiplet
m.p.	melting point
m/z	mass per unit charge
MAO	methylaluminoxane
Me	methyl
MeCN	acetonitrile
MeLi	methyllithium
MeOH	methanol
MHz	mega hertz
min	minute
mL	millilitre
mm	millimetre
MMAO	modified methylaluminoxane
mmHg	millimetres of mercury
mmol	millimoles
mol	moles
MS	Mass Spectroscopy
NMR	Nuclear Magnetic Resonance
Np	Neopentyl
o	*ortho*
p	*para*
p.s.i	pound per square inch

Ph	phenyl
ppm	parts per million
py	pyridyl
pz	pyrazolyl
q (NMR)	quartet
R	alkyl
R_{int}	Independent reflections
s (NMR)	singlet
SOMO	Single Occupancy Molecular Orbital
T	temperature
t (NMR)	triplet
$TBABF_4$	tetrabutylammonium tetrafluoroborate
$TBAPF_6$	tetrabutylammonium hexafluorophosphate
THF	tetrahydrofuran
TMEDA	tretamethylethylenediamine
TMBuNC	1,1,3,3-tetramethylbutylisonitrile
TMS(NMR)	tetramethyl silane
Toluene-d_8	deuterated toluene
Tp	hydrotri(pyrazolyl)borate
UV/vis	ultra violet/visible
VSCC	valence shell charge concentration
VSEPR	valence shell electron pair repulsion
w (IR)	weak
Z	number of asymmetric units per unit cell
cm^{-1}	wavenumber

Compound Numbers

No.	Compound
1	$[K\{H_2B(pz)_2\}]$
2	$[\{H_2B(pz)_2\}Mg(CH_3)THF]$
3	$[\{H_2B(pz)_2\}Mg(THF)(\mu\text{-}Cl)_2Mg(THF)_2\{(pz)_2BH_2\}]$
4	$[\{H_2B(pz)_2\}_2Mg(THF)]$
5	$[\{H_2B(pz)_2\}_2Mg(THF)_2]$
6	$[\{H_2B(pz)_2\}Mg(CH_2Ph)THF]$
7	$[\{H_2B(pz)_2\}Mg(THF)_3][B(CH_2Ph)_4]$
8	$[K\{B(CH_2Ph)_4\}]$
9	$PhSCH_2NEt_2$
10	$Et_2NCH_2Si(Ph)Me_2$
11	Ph_2BCl
12	$[\{Ph_2B(CH_2NEt_2)_2\}Li(THF)]$
13	[ArNC(Me)Li] (Ar: 2,6-dimethylphenyl)
14	$[ArNC(Me)SiMe_3]$ (Ar: 2,6-dimethylphenyl)
15	$[ArNC(Me)C\{Si(Me)_3\}NAr]$ (Ar: 2,6-dimethylphenyl)
16	$[ArNC(Me)Si(Ph)Me_2]$ (Ar: 2,6-dimethylphenyl)
17	$[\{ArNC(Me)CNAr\}_2]$ (Ar: 2,6-dimethylphenyl)
18	[TMBuNC(Bu)Li]
19	$[TMBuNC(Bu)SiMe_3]$
20	Me_2BBr
21	$[\{Me_2B(2\text{-}py)_2\}Li]$
22	$[Me_2B(2\text{-}py)_2(H)]$
23	Dimethylboronium bis(2-pyridyl)borate
24	dimeric dimethyl(2-pyridyl)borane
25	$[\{Me_2B(2\text{-}py)_2\}Mg(Me)THF]$
26	$[\{Me_2B(2\text{-}py)_2\}_2Mg]$
27	Ph_2BBr
28	$[\{Ph_2B(2\text{-}py)_2\}Li(THF)]$

29 $[Ph_2B(2\text{-}py)_2(H)]$

30 $[\{Ph_2B(2\text{-}py)_2\}Mg(Me)THF]$

31 $[Ar'N{=}C(CH_3)C(H){=}C(CH_3)N(H)Ar']$; (Ar': 2,6-diisopropylphenyl)

32 $[HC(MeCNAr')_2Li(Et_2O)]$(Ar'=2,6-diisopropylphenyl)

33 $[HC(MeCNAr')_2BCl_2]$ (Ar'=2,6-diisopropylphenyl)

34 $[HC(MeCNAr')_2B(Cl)Me]$ (Ar'=2,6-diisopropylphenyl)

35 $[HC(MeCNAr')_2BCl]^{\bullet}$ (Ar'=2,6-diisopropylphenyl)

36 $[\{HC(MeCNAr')_2BOK\}_2]$ (Ar'=2,6-diisopropylphenyl)

37 $[HC(MeCNAr')_2BO]$ (Ar'=2,6-diisopropylphenyl)

38 $[Li\{BMe_4\}]$

39 $[C_5H_4{=}C(H)Nme_2]$

40 $[\{H(Cl)CNMe_2\}Cl]$

41 $[\{C_5H_3\text{-}(HCNMe_2)_2\}Cl]$

42 $[Cy_2AFA(H)]$

43 $[Ph_2AFA(H)]$

44 $[(4\text{-methyl})Ph_2AFA(H)]$

45 $[(2,6\text{-dimethyl})Ph_2AFA(H)]$

46 $[(2,4,6\text{-trimethyl})Ph_2AFA(H)]$

47 $[(Ph_2AFA)_2Mg]$

48 $MgMe_2$

49 $[(Cy_2AFA)_2Mg]$

50 $[(Cy_2AFA)Mg(Cl)Et_2O]$

51 $[\{(Cy_2AFA)MgBr\}_2]$

52 $[(Cy_2AFA)Mg(Me)THF]$

53 $[(Cy_2AFA)Mg(Me)]$

54 $[K\{HB(pz)_3\}]$

55 $[Mg\{(pz)_3BH\}_2].2[CHCl_3]$

Chapter 1:

Introduction

1.1 Background

The area of catalysed alkene polymerisation has been intensively studied and explored since the discovery of the low pressure polymerisation of ethylene and propylene by Ziegler and Natta.[3] Karl Ziegler discovered ethylene polymerisation in the reaction products of aluminium alkyl compounds and transition metal compounds like the halides of titanium, vanadium, and zirconium.[4] As Natta discovered, heterogeneous polymerisation catalysts polymerise propene with a very high degree of stereoselectivity in the formation of isotactic polyolefins,[2,5] where adequate models were proposed to explain the induction of stereoregular polymer growth by the chiral environment of the catalysts centres (Figure 1.1).[6]

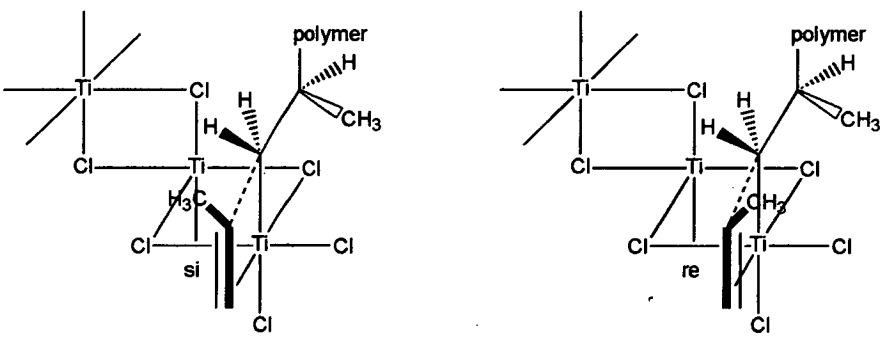

Figure 1.1 Model for the stereospecific polymerisation of propene at a chiral Ti centre on the edge of a $TiCl_3$ crystal. The olefin adopts that enantiofacial orientation which places the olefin substituent *trans-* to the polymer chain at the incipient C-C bond (left); a *cis-* orientation of olefin substituent and polymer chain is disfavoured (right).

The use of co-catalyst, such as triethylaluminium (Et_3Al), in these systems is essential, its role being to alkylate Ti atoms on the catalyst surface (Figure 1.2).[7] The application of co-catalysts has been accompanied by growth in the understanding of the chemistry involved, and the mechanistic studies have usually followed commercial application, but the information from these studies has been valuable in the optimisation of reaction conditions and in development of new catalysts.[8]

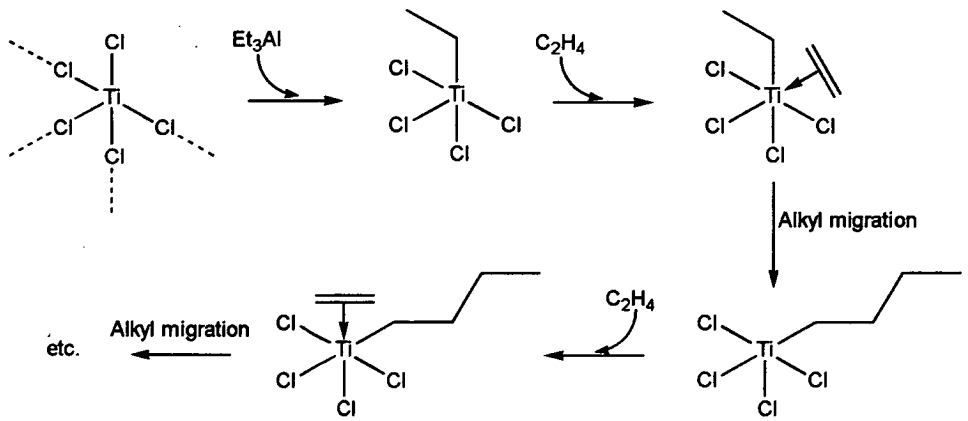

Figure 1.2 Schematic model of alkene polymerisation on the surface of a Ziegler-Natta catalyst.

1.1.1 Catalytic Activation Using Methylaluminoxane

After the development of the first Group 4 so-called "metallocenes" by Wilkinson *et al.*,[9] the use of these complexes as polymerisation catalyst have facilitated greater control of polymer structure and properties.[10] The homogeneous reaction mixture of dicyclopentadienyltitanium dichloride (Cp_2TiCl_2) and the co-catalyst diethylaluminium chloride (Et_2AlCl) or dimethylaluminium chloride (Me_2AlCl) catalyse the formation of polyethene with moderate activity at pressures as low as 1 bar,[9-11] but there was no industrial application due to the reduction to inactive titanium(III) species. The system of $Cp_2Ti(R)Cl/RAlCl_2$ (R: Me or Et), however, showed a polarisation of $Cp_2Ti(R)$-Cl bond by the Lewis-acidic aluminium atoms of the type $[Cp_2(R)Ti^{\delta+}\cdots Cl\cdots Al^{\delta-}RCl_2]$ where an electron deficient species could be suggested.[6-11] Moreover, experiments of Reichert and Meyer demonstrated that addition of water increased the rate of polymerisation in titanocene catalysts, whilst the formation of aluminoxanes was suggested.[12] Sinn and Kaminsky studied the system of $Cp_2ZrMe_2/AlMe_3$ where a hydrated form of trimethylaluminum, methylaluminoxane (MAO),[13] afforded extremely active catalysts when combined with zirconium metallocenes. The methylaluminoxane is poorly characterised, where the molecular weight can be situated between 900-1200 with a $[\{MeAlO\}_n]$ core, while the modified MAO (MMAO), however, prepared by the controlled hydrolysis of a mixture of trimethylaluminum (TMA) and triisobutylaluminum, has emerged as

an alternative activator.[14] Advantages of MMAO include its improved solubility in aliphatic solvents and enhanced solution storage stability.[14]

1.2 Catalytic Activation by Methyl or Alkyl Abstraction

Cationic metallocene complexes of the type $[Cp_2MR]^+$ (R: alkyl) have been identified as the catalytically active species in the polymerisation of α-olefins by the homogeneous Ziegler-Natta catalysts.[15] They are highly electron deficient and extremely reactive, whilst their efficiency as catalysts has been shown to be influenced and limited by the nature of the counteranion.[15,16] The stability of cationic metal alkyl complexes $[Cp_2MR]^+$ is increased by the basicity and the weakly co-ordinating anions such as $[BPh_4]^-$, $[B(C_6H_4F)_4]^-$, $[MeMAO]^-$ or $[B(C_6F_5)_4]^-$, where the most active catalysts are obtained.[17] More recently the activation of Cp_2TiMe_2 has been possible by methyl abstraction with $[B(C_6F_5)_3]$ or $[Ph_3C][B(C_6F_5)_4]$ (Figure 1.3), but the formation of dinuclear methyl complexes of the type $[\{Cp_2MMe\}_2(\mu\text{-}Me)]^+$ (M: Zr or Hf) or $[\{Cp_2M(\mu\text{-}Me)_2\}AlMe_2]^+$, however, have been reported by addition of $[Cp_2MMe_2]$, $[Ph_3C][B(C_6F_5)_4]$ or $AlMe_3$ to *in situ* generated $[Cp_2MMe]^+$ species, respectively (Figure 1.4).[18] The methyl abstraction of $[Cp_2ZrMe_2]$ by using $[B(C_6F_5)_3]$ has been reported,[19] and the resulting ion pair adopts a methyl-bridged structure (Figure 1.5).

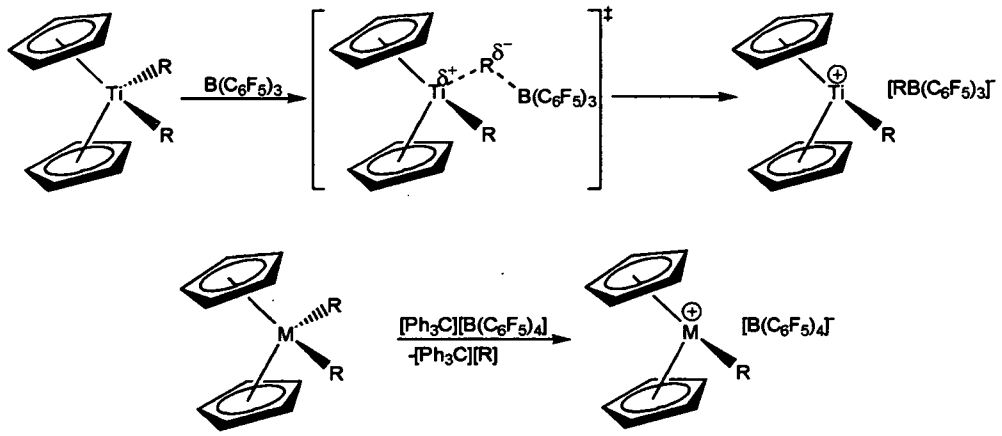

Figure 1.3 Methyl or alkyl abstraction from $[Cp_2MR_2]$ by a Lewis acid reagent like $B(C_6F_5)_3$ or $[Ph_3C][B(C_6F_5)_4]$.

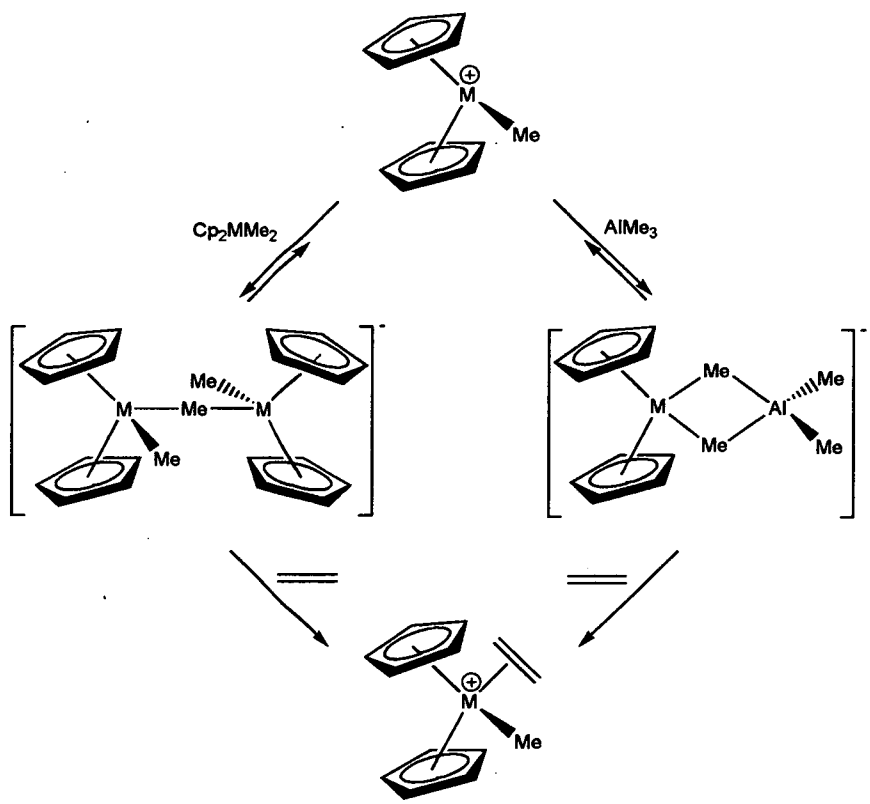

Figure 1.4 Methyl bridged active complexes generated by addition of $[Cp_2MMe_2]$ or $AlMe_3$ to *in situ* $[CpMMe]^+$ species.

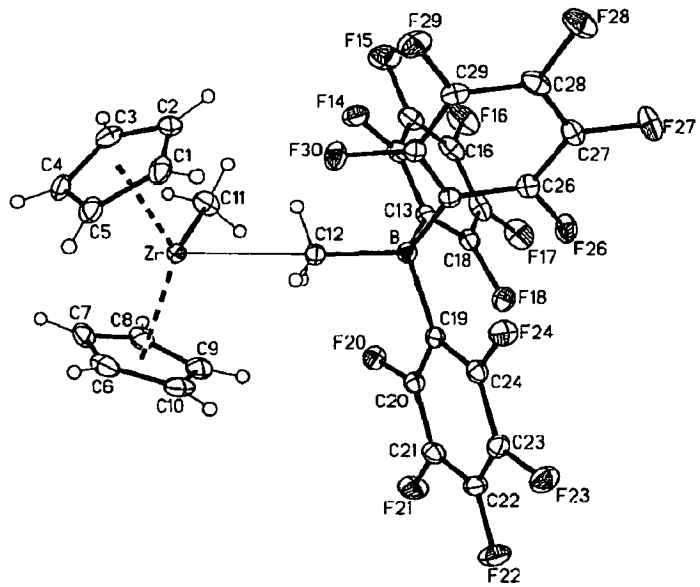

Figure 1.5 Methyl bridged structure of $[Cp_2ZrMe][MeB(C_6F_5)_3]$

Alkyl abstraction from azazirconacycles represents a competitive reaction for $B(C_6F_5)_3$ where the nitrogen would be preferentially abstracted to produce a zwitterionic catalyst complex (Figure 1.6).[20] The different characteristics which zwitterionic metallocenes present as donor-acceptor complexes, higher solubilities, preactivated single-component and base-free, could play an important role in the activity and overall selectivity of catalytic reactions. The ability of counterions derived from $B(C_6F_5)_3$ to co-ordinate to metal centres has been investigated and it can be reduced by complexation with CN^- or cyanometals to produce compounds like $[CN\{B(C_6F_5)_3\}_2]^-$ or $[M\{CNB(C_6F_5)_3\}_4]^{2-}$, where the negative charge should be delocalized over the boron atoms. Although alkene polymerisation catalysts reported have provided higher activation of metallocene dialkyls with $[Ph_3C][CN\{B(C_6F_5)_3\}_2]$, solutions of the metallocene salts of $[L_2ZrMe][CN\{B(C_6F_5)_3\}_2]$ tend to decompose slowly, due to anion dissociation into BPh_3 and $[Ph_3BCN]^-$.[20,21] In contrast, the higher Lewis acidity of $B(C_6F_5)_3$ make its dissociation less feasible and it results more commercial available.[21] The principle on which the normal Ziegler and Natta polymerisation is based is mainly upon co-ordinative unsaturation and insertion reactions and attacks on co-ordinated ligands by electrophiles or nucleophiles (Figure 1.7).

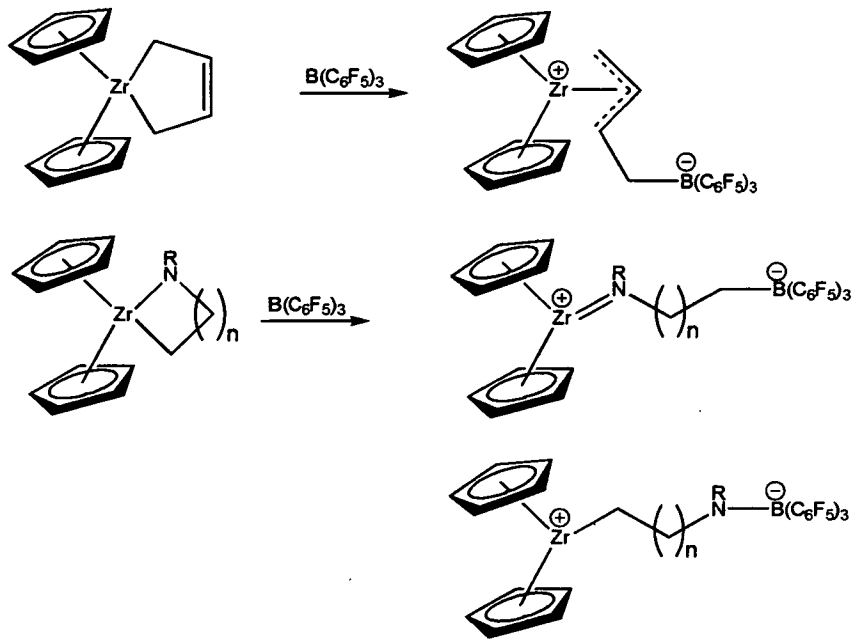

Figure 1.6 Zwitterionic complexes produced by the methyl abstraction from azazirconacycles complexes with $B(C_6F_5)_3$.

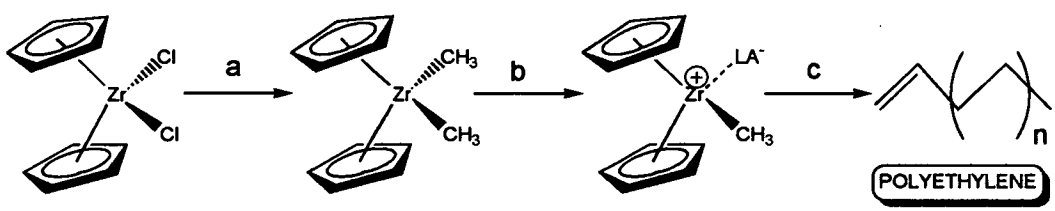

Figure 1.7 Ziegler-Natta polymerisation reaction; a) alkylating reagent, eg. MeLi or MAO; b) strong Lewis acid, eg. MAO, $B(C_6F_5)_3$, or $[Ph_3C][B(C_6F_5)_4]$; c) excess of C_2H_4.

1.3 Zwitterionic Metallocene Complexes

Jutzi and Seufert reported the first boron substituted cyclopentadienyl complexes (a, Figure 1.8),[22] However, Bochmann *et al.*[23] described the synthesis of [{(pentafluorophenyl)boryl}cyclopentadienyl] half-sandwich complexes of titanium and zirconium in which the strong Lewis acidic substituent on the cyclopentadienyl ring make it an interesting active complex for polymerisation. Moreover, an equilibrium for R transference is also possible, where further treatment with LiCp produces the respective metallocene complexes (b, Figure 1.8).[24] On the other hand, the synthesis of complexes with boron-substituted cyclopentadienyl ligands where

the anion is incorporated into the bridge, or the ligand transference provide an extra stability for self activating complexes (c and d, Figure 1.8).[25]

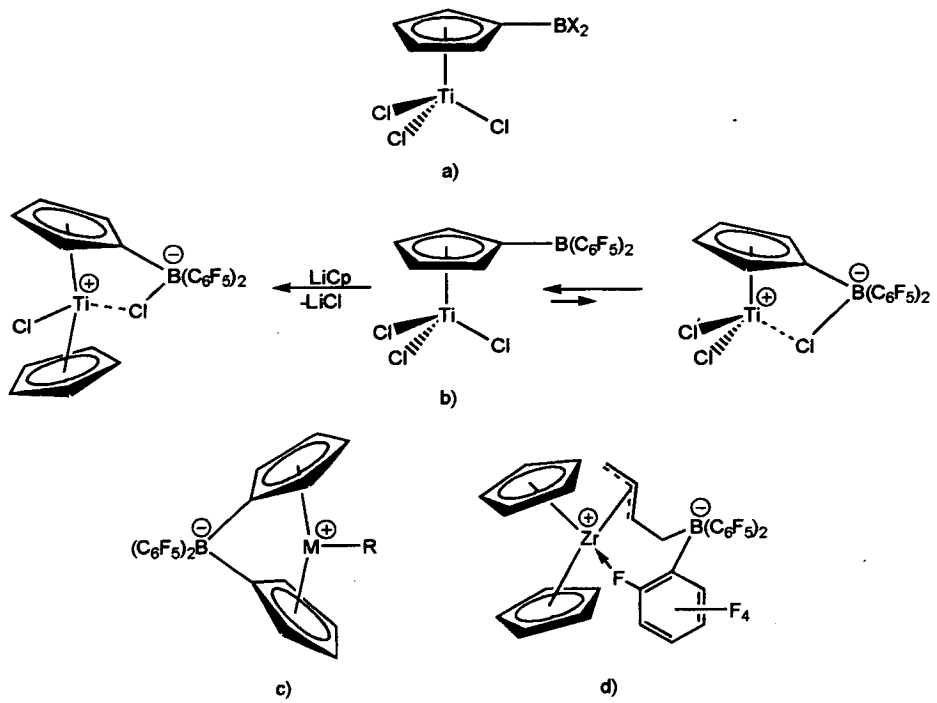

Figure 1.8 a-b) half-sandwich and metallocene complexes containing a Lewis acidic substituents on the cyclopentadienyl ring; c-d) stability of zwitterionic complexes by electron and ligand transfer.

1.3.1 Ethylene Polymerisation of Zwitterionic Metallocene Complexes

The zwitterionic feature of organotransition metal complexes has only recently become an influential factor in the design of a formal positive charge at an electropositive transition metal atom. The ability of zwitterionic species to produce high polymerisation activity levels can be exemplified using zwitterionic zirconium metallocene species, where the addition of an excess of ethylene to Erker's zwitterion (Figure 1.9) produces multiple additions in the main chain, and the process terminates by a β-hydrogen transference. Once the β-hydrogen transferral has happened, the reaction continues operating a normal polymerisation according to the Scheme shown in Figure 1.9.[24-25]

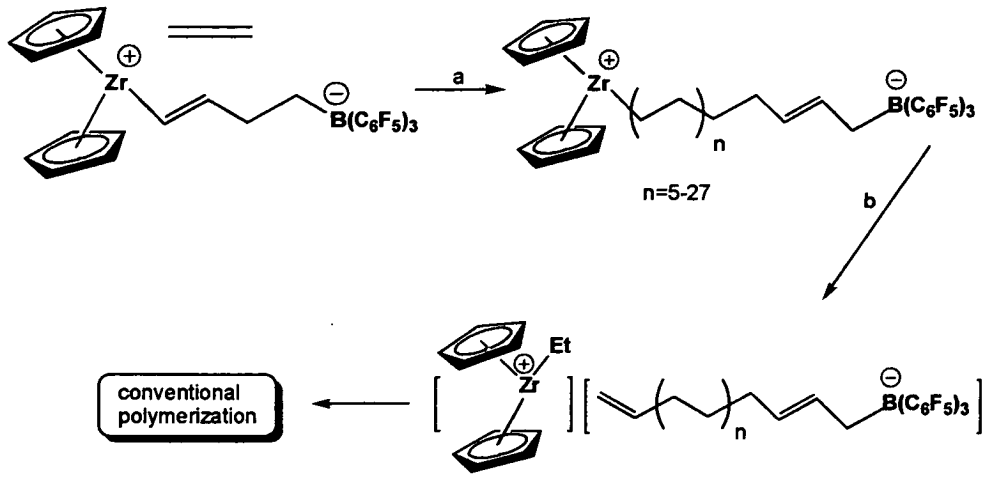

Figure 1.9 Erker's [Cp_2Zr(butadiene)/$B(C_6F_5)_3$]-derived girdle zwitterion. The fate of girdle zwitterions. a) C_2H_4, excess; b) β-hydrogen transfer.

The electron counting formalism employed for the unsaturated active catalysts is very important, where most of the species known are electron deficient containing 14 electrons $[Cp_2ZrR]^+$ or lower electron count of 10 for $[(R_2N)_2ZrR]^+$ or 6 for $[ZrR_3]^+$ which result in more electrophilic and therefore potentially more active catalyst complexes.[24-25] The ligand also plays an important role over the polymerisation-active metal complex where the steric protection is very important to prevent changes in the geometry and the co-ordination number. Moreover, control over the polymerisation is often compromised by intramolecular co-ordination processes.

1.4 Effect of the Ligand Over the Catalytic Activity

The selection of metal-ligand combinations suitable for polymerisation-active centres has been at the heart of the discovery process, and one of the most noteworthy advances in this regard has been the increased prominence of late transition metal systems.[26-28] Perhaps one of the most significant advances in the general understanding of the factors responsible for stabilising active catalysts during the period of 1994-1997 was the recognition that bulky substituents can play a crucial role, not only in stabilising the active site, but also in controlling chain-

transfer processes. However during the last 25 years, highly active systems based on ligands bearing relatively small substituents have also been discovered, and serve to emphasise that there is no single rule for ligand selection that is applicable to all metals.[26-28]

Calculations have shown that the co-ordination number and geometry characteristic of a particular metal have to be given due consideration. The ground-state geometry of $[Cp_2ZrMe]^+$ is pyramidal, whilst complexes of trivalent metals such as scandium and lanthanides are trigonal planar but the pyramidal geometry is better adapted for olefin co-ordination (a, Figure 1.10).[26] In addition, the catalytic activity of cyclopentadienyl-amide transition metal complexes have proved very successful (b, Figures 1.10).[27]

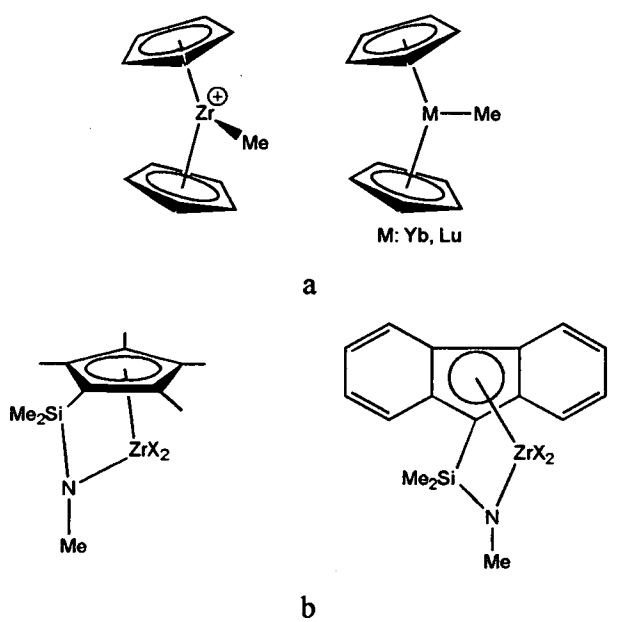

Figure 1.10 Effect of the ligand: a) geometry effect of the metal; b) Cyclopentadienyl-amide metal complexes.

The design of most of the ligands incorporate diimine or bipyridine ligands, whilst porphyrins have also been used as ancillary ligands to support zirconium and hafnium alkyl complexes. However, these complexes proved unreactive towards ethylene. Terminal oxygen donors such as phenoxide ligands have been used successfully in olefin polymerisation catalysis.[28] Jordan *et al.*[29] have shown the application of [N,O] chelating ligands in Group 4. Trithiacyclonane derivatives have

been synthesised for which low activity was reported with MAO as cocatalyst.[30] There is a rich co-ordination chemistry of phosphine ligands with late transition metals, but the strong σ-donor capacity of these ligands had been presumed to be more suited to catalytic reaction requiring nucleophilic metal centres.[31] This appears to be supported by the low ethylene polymerisation activity observed for the diphosphinide complex (Figure 1.11), which is sterically similar to α-diimine complexes, and suggests that the polymerisation activities in the Group 10 metal system are strongly dependent upon the nature of the donor.[32] Pringle, Wass, and co-workers have observed, however, high ethylene polymerisation activities for nickel precursors containing disphosphine ligands.[33] In addition, monoanionic [P,O] ligands on Group 10 metals have also been studied for the Shell Higher Olefin Process (SHOP) for ethylene oligomerisation.[34] Finally, Guan *et al.*[35] have shown low ethylene polymerisation activity for nickel complexes bearing neutral imino-phosphine ligands.

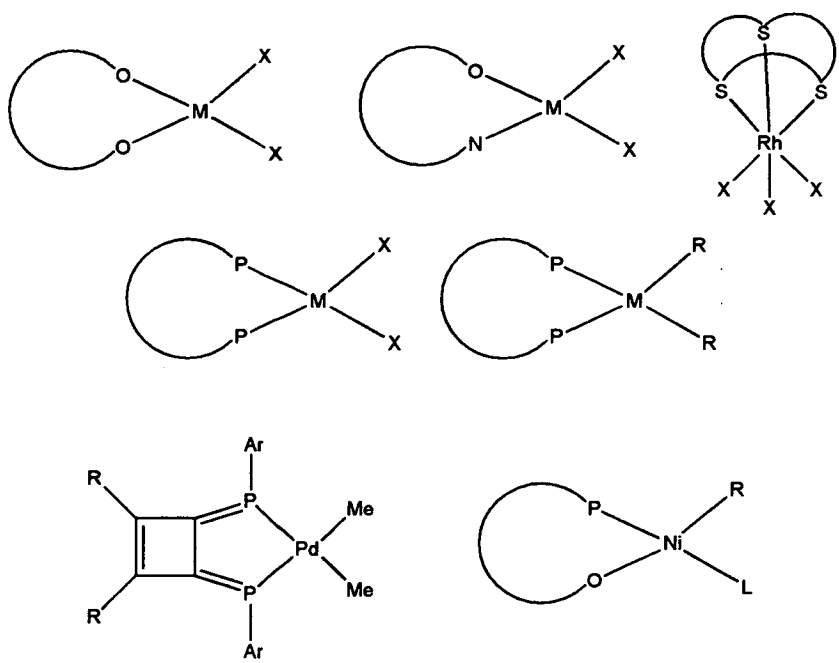

Figure 1.11 Nature of the donor base ligand: application of [O,O], [O,N], [S,S,S], [P,P] and [P,O] chelating ligands used with transition metals.

1.5 Activity of Transition and Lanthanide Metal Complexes

Although soluble metal salts were used commercially as catalysts for acetylene reactions as early as 1910, broad use of soluble catalysts did not begin until the 1940s.[1-15] More broadly, the introduction of many new, polyamide, and vinyl polymers between 1940 and 1960 called for worldwide development of new processes for production of the monomers.[3-5] The introduction of well defined, single-site organotransition metal olefin polymerisation catalysts in the early 1980s highlighted the possibilities for controlling and dramatically improving the properties of commodity polymer products such as polyethylene and polypropylene.[3-5]

Some of the most significant recent developments have occurred with late transition metal systems, whilst through the 1990s the Group 4 metallocenes and half-sandwich titanium-amide complexes have been at the forefront of these developments, and these catalysts are increasingly finding their way into commercial operations.[31-34] Chiral group 4 ansa-metallocenes play an important role in stereoselective catalysis, and the development of efficient synthetic methods for these compounds has been an important challenge.[36] Reports on nickel catalyst systems through the period 1998-2001 have exceeded those for titanium during the previous 4 years period, while catalysts based on iron have strongly signposted the way for further technologically significant advances, and systems based on copper have started to emerge, while a role for zinc has been identified in catalysed chain growth.[33-36] Olefin polymerisation using manganese complexes has yet to be reported, but there is no reason to suspect that this situation will not be rectified before too long. For other catalytic processes, generally several orders of magnitude lower activities are observed for Mn(II) or Mn(III) complexes bearing ligands which give highly active catalysts with other late or early transition metals. The reductive processes in the presence of alkylating agents might be responsible for the poor catalyst performance.[35-47] Some examples of transition and lanthanide metal complexes can be seen in Figure 1.12

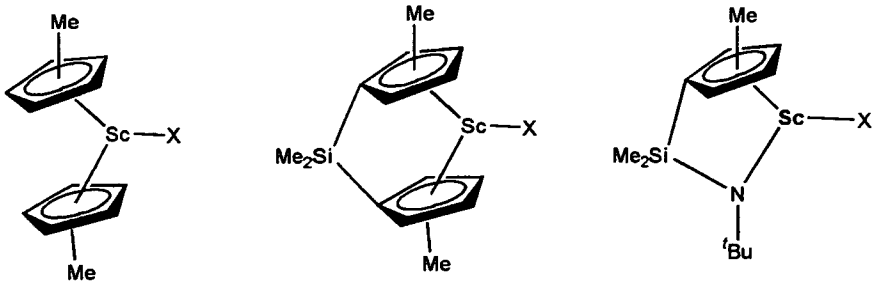

Group 3

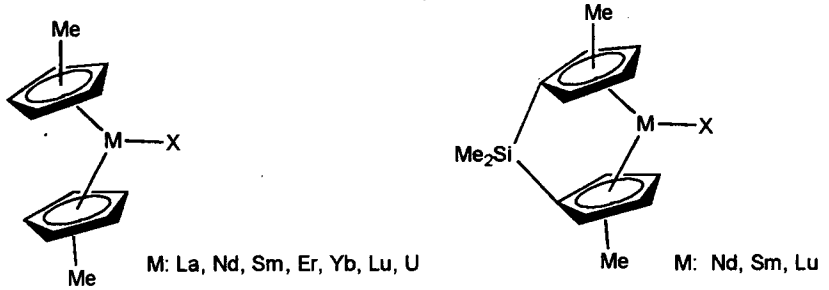

Group 3

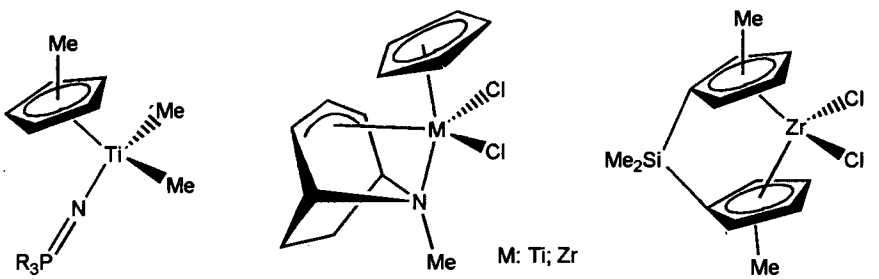

Group 4-

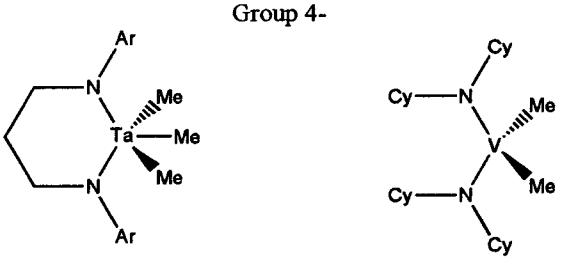

Group 5

Figure 1.12 Some examples of transition and lanthanide metal complexes used as olefin polymerisation catalysts.[38-41]

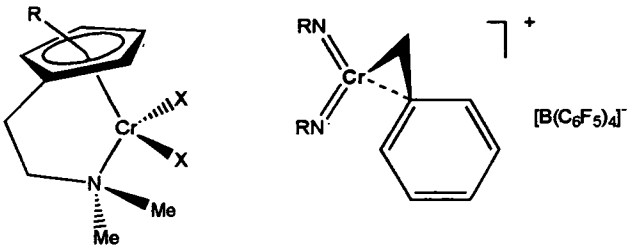

Group 6

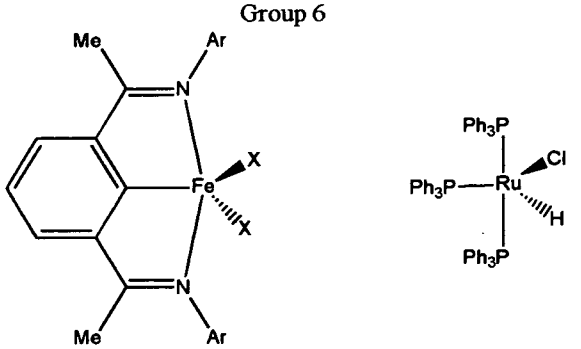

Group 8

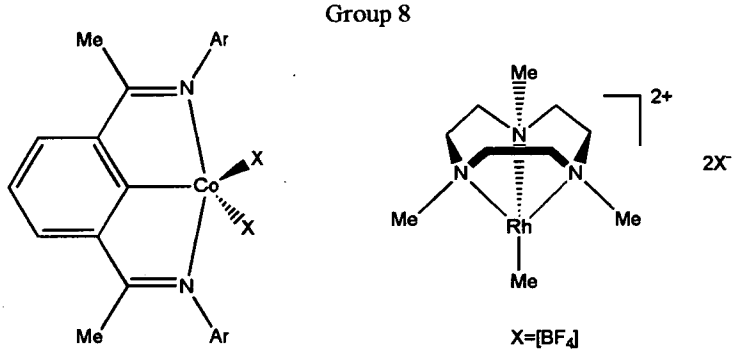

Group 9

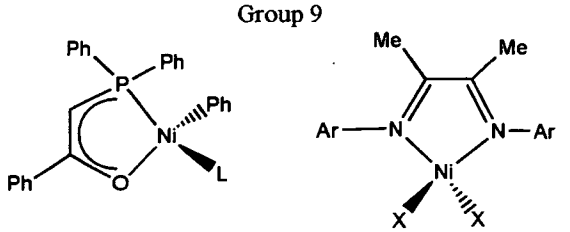

Group 10

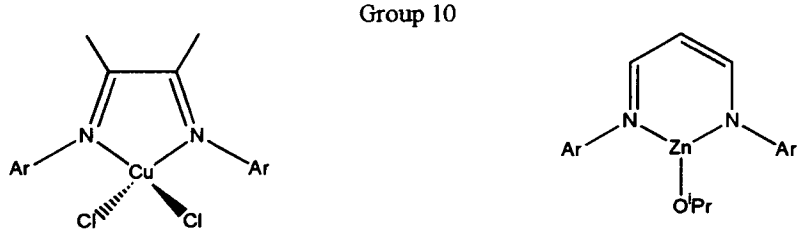

Group 11 Group 12

Figure 1.12 (Continued) Some examples of transition and lanthanide metal complexes used as olefin polymerisation catalysts.[42-47]

1.6 Main Group Metal Catalysts

Coles and Jordan[37] and Gibson[48] have showed the potential for cationic aluminium alkyls as ethylene polymerisation catalysts. The aluminium procatalysts reported thus far contain monoanionic bi- and tri-dentate chelate ligands (L-X) of the general form [(L-X)$AlMe_2$], which are synthesised by the reaction of the relevant ligand system with $AlMe_3$. To obtain an active catalyst system cationic species are generated on further reaction with $B(C_6F_5)_3$ or $[Ph_3C][B(C_6F_5)_4]$ in some hydrocarbon or chlorocarbon solvents (but no reactivity has been reported using toluene or dichloromethane). The cationic aluminium alkyls so derived display low activities as ethylene polymerisation catalysts and they produce polymer of high[37](*Mw* 176000-272000) or moderate[48] (*Mw* 13000-23000) molecular weight. Sen *et al.*[49] reported polymer of high molecular weight, linear homo- and copolymers of ethene and propene, *via* a catalyst system consisting of alkyl aluminium compounds activated by suitable Lewis acids. However, although the ethylene polymerisation under mild conditions has been reported, this area still remains controversial. Several classes of aluminium, gallium and thallium dialkyl compounds [(L-X)MR_2] that incorporate bidentate, monoanionic, nitrogen-based L-X- ligands, including amidinates, guanidinates, aminotroponiminates, β-diketiminate, bulky thioamidate, and thioureido have been studied intensively (Figure 1.13).[37,50-55] Representative examples include the monoamidinate compounds [{$MeC(N^iPr)_2$}MMe_2] (M: Al, Ga, In, Tl),[41] [{$MeC(NSiMe_3)_2$}MMe_2] (M: Al, Ga, In, Tl).[53,54] Group 13 amidinate compounds are of interest as precursors to nitride materials and as selective reagents and catalysts.[55] Amidinate ligands have been used extensively in other main group, transition metal, and *f*-block co-ordination chemistry.[56]

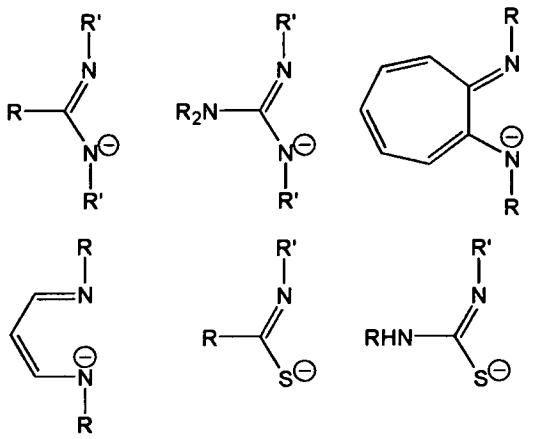

Figure 1.13 Some monoanionic ligands used with main group metals.

1.7 Activity of Magnesium Complexes

Grignard reagents have been known from the beginning of the 1900s, and synthetic applications have been well-established as tools in organic chemistry. Grignard was the first to separate the overall reaction into two steps, the first being the reaction of alkyl halide and magnesium in ether to form the reagent that now bears his name and the second being the reaction with a carbonyl compound to give the corresponding alcohol after hydrolysis.[57] After 1930, other reagents, especially organolithium reagents, were developed as alternatives. A general disadvantage of organolithium compounds, however, is their lower stability and higher cost. Therefore, organomagnesium chemistry remains important and is still standard in many synthetic procedures.[57]

The crystallographic study of organomagnesium compounds started around 1964 with the investigation of the simple Grignard phenylmagnesium bromide and ethylmagnesium bromide, which were found to be tetrahedral containing co-ordinated ether molecules.[57] Dimeric structures can result if organomagnesium compounds are crystallised from a weakly co-ordinating solvent like ether. For steric reasons the co-ordinative power of the solvents is too low to break organomagnesium complexes down into monomers. Solvent-free dimethylmagnesium was reported to have been prepared in 1929.[58] A crystal structure study in 1964,[59] however, showed that the compound forms high polymer chains with methyl bridges. An X-ray powder

diffraction study of diethylmagnesium also showed a polymeric chain structure with bridging ethyl groups and tetrahedral co-ordination of the magnesium (Figure 1.14).[60]

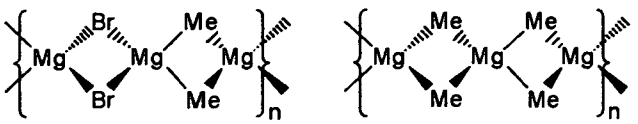

Figure 1.14 Polymeric structure of MeMgBr and Me_2Mg.

Dialkyl magnesium compounds can be prepared from an ether solution of the Grignard reagent by shifting the Schlenk equilibrium[61] by precipitating magnesium chloride with dioxan, filtration or centrifugation, crystallisation and drying the etherate in *vacuum* at 100 °C to obtain a microcrystalline powder. Intramolecular co-ordination strongly influences the structure of organomagnesium compounds. Co-ordinating solvent molecules are successively substituted by intramolecular ligands, and eventually the complex becomes completely saturated by "intermolecular solvatation" (Figure 1.15). In addition, co-ordination numbers can be induced which are unusually high in organomagnesium chemistry. Although conventional Grignard reagents are usually prepared in diethyl ether or other donor solvents, organomagnesium compounds have for many years also been obtained in hydrocarbon media in the absence of a donor, or without use of any solvent.[59-64] The use of hydrocarbons is economical since they are cheap and present relatively low fire hazards. Furthermore, the unsolvated organomagnesium compounds are only sparingly soluble in hydrocarbons.

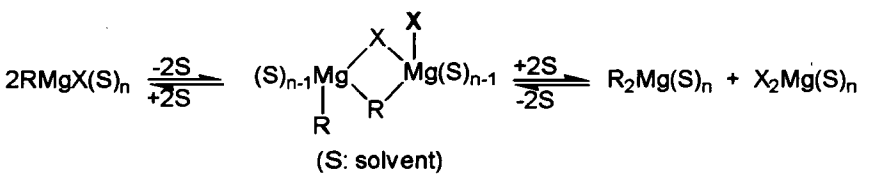

Figure 1.15 Effect of the donor solvent by Schlenk equilibrium.

Whereas the Grignard reagents in donor solvents are solvated by at least two solvent molecules per magnesium, those obtained in the presence of catalytic amount

of donor substances are only partially solvated.[57,59] As the solvating agent is firmly bound to the Grignard reagent, such solutions possess almost all the advantages of unsolvated organomagnesium halides in non-solvating media. However, the partially solvated Grignard reagents exhibit several properties different from those of both conventional Grignard reagents and unsolvated organomagnesium compounds.[62] The reaction of mono-solvated alkylmagnesium bromide with ketones in benzene or toluene give higher yields of addition products in comparison with those in ether.[65] Partially solvated Grignard reagents have also been used in large scale industrial processes,[62,65] but little information on their chemical and physical properties or on the details of their production are available in the open literature.

With the electronic structure of the magnesium atom having a [Ne]$3s^2$ electronic configuration and a strongly electropositive character, magnesium has a tendency to become Mg^{2+}. This tendency is not fully realised in organomagnesium compounds, but does result in strongly polarised bonds with other elements, including those to carbon. In comparison to lithium, the electronegativity of magnesium is higher (Li 0.98, Mg 1.31); accordingly, the Mg-C bond is more covalent. In the presence of polarizable electron-rich organic compounds, especially Lewis bases such as ethers or tertiary amines, organomagnesium compounds form complexes: the polymeric structures which are present in the solvent-free species are broken down to form lower aggregates or monomers.[57-62] In solvents like benzene, or toluene, most organomagnesium reagents retain their polymeric nature and have therefore a low solubility. For this reason, organomagnesium chemistry is almost always performed in ethereal solvents. Despite the synthetic importance and widespread use of Grignard reagents, the chemistry of well characterised simple mono-alkyl magnesium systems is surprisingly undeveloped.[57]

The complexation of the organomagnesium species with polydentate nitrogen donor ligands is also now attracting interest with a number of advances in understanding of the structure, bonding and reactivity of the Mg-C bond.[63] The oligomeric structure of commercial dibutylmagnesium [^{s}Bu(^{n}Bu)Mg] can be treated with *N,N,N',N'*-tetramethylethylenediamine (TMEDA) and undergoes preferential crystallisation of a distorted tetrahedral mononuclear arrangement [(^{s}Bu$_2$Mg)(TMEDA)] (a, Figure 1.16).[62] The same tetrahedral magnesium

arrangement has been observed for $[(Me_2Mg)(TMEDA)]$[64] and $[(Ph_2Mg)(TMEDA)]$ (b, Figure 1.16).[66] In contrast, monomeric structures of octahedral magnesium arrangements can be given when bidentate anions such as $[Ph(2\text{-}Py)N]^-$ and the solvent are involved (Figure 1.17).[67]

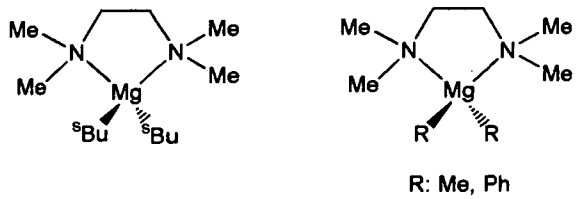

a b

Figure 1.16 Tetrahedral mononuclear magnesium arrangement for: a) $[(^sBu_2Mg)(TMEDA)]$; b) $[(R_2Mg)(TMEDA)]$.

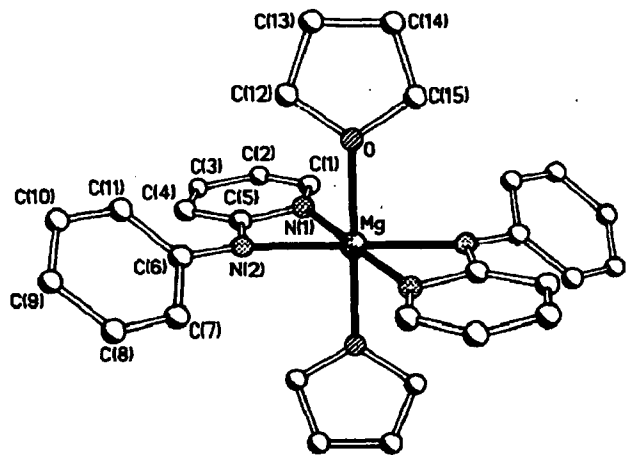

Figure 1.17 Octahedral mononuclear magnesium arrangement of $[(L_2Mg)(THF)_2]$; (L: $[Ph(2\text{-}Py)N]^-$).

Hydrides of metals from Groups I, III and IV have been used to react with ethylene and other olefins.[68] Jordan has reported the ability of certain cationic methyl aluminium amidinate complexes to catalyse ethene polymerisation,[69] the first such main group metal system to do so, and Brookhart and Gibson extended activity to the later transition metals.[45,46] The only groups of metals in the periodic table yet to be shown to exhibit alkene polymerisation activity are those of the *s*-block, and an investigation of their potential is overdue.

Evidence of reaction of dialkyl magnesium or diethylmagnesium with olefins has been provided by Podall and Foster,[70] where the reaction conditions and products are summarised in Table 1.1. The results of the solvent study indicated that polar solvents favour the alkylation reaction.

Table 1.1 Reactions of Et_2Mg with some alkenes.[70]

Mg catalyst	Solvent	Alkene	Conditions	Products
Et_2Mg	Ether	Ethylene	100°C, 740 p.s.i.g., 3h	45% Et_2Mg, 2.8% n-hexymagnesium, 2.5% vinylmagnesium, 2.5% MgH_2, 13% ethynylmagnesium complexes
Et_2Mg	n-hexane or n-heptane	Ethylene	100°C, 600-900 p.s.i.g	Liquid hydrocarbon ranging from C10 and small amount of solid polymer
Et_2Mg	Benzene	Ethene	140°C, 800 p.s.i., /hydrolysis	25%nC_5H_{12}, 26%nC_7H_{16}, 24%C_9H_{20}, 7%$nC_{13}H_{28}$, 3%$nC_{15}H_{32}$, 1%$nC_{17}H_{36}$, 0.2%$nC_{19}H_{40}$.

Sen and Kim[71] have published the invention of active ethene and/or α-olefin oligomerisation or polymerisation catalysts systems comprising of both an alkyl magnesium component and a Lewis acid component. At high pressures of between 700 – 900 psi of ethene, using either $B(C_6F_5)_3$ or $AlCl_3$ activators, they report the activity of R_2Mg (R: butyl or neopentyl) in producing polymers (Table 1.2).

Table 1.2 Activity of some alkyl magnesium components with ethene.[71]

R_2Mg	Activator	Solvent	Conditions	Productivity (kg/mol.h)	Polymer
Bu_2Mg	$B(C_6F_5)_3$	C_6H_5Cl	700 psi/60 °C	112.0	Solid
Bu_2Mg	$B(C_6F_5)_3$	Toluene	700 psi/60 °C	11.1	Solid
$(Neopentyl)_2Mg$	$B(C_6F_5)_3$	Toluene	700 psi/60 °C	7.2	Solid
Bu_2Mg	$B(C_6F_5)_3$	C_6H_5Cl	700 psi/60 °C	14.4	Solid
Bu_2Mg	$AlCl_3$	C_6H_5Cl	700 psi/60 °C	56.6	Liquid
$(Neopentyl)_2Mg$	$AlCl_3$	C_6H_5Cl	700 psi/60 °C	23.8	Liquid

1.7.1 Mono-Alkyl Magnesium Complexes Supported by β-diketiminate Bidentate Nitrogen Donor Ligands

The development of three-coordinate mono-alkyl magnesium systems that have a vacant co-ordination site, or effectively a protected vacant site, have been designed as potential catalytic agents,[72] where the preferred type of bonding would be sp^2. The electronic and steric properties of the ligand system may protect the metal centre and prevent unwanted reactions such as complex dimerization in order

to allow the development of new modes of reactivity. The chemistry of bulky nitrogen-ligated organomagnesium species has attracted increasing attention in both transition metal and main group co-ordination chemistry,[73] whilst the bulky β-diketiminate ligand systems have been recently investigated by Bailey *et al.*[74] where polymerisation activity has been found to be absent. The ligand [Ar'N=C(R)CH=C(R)N(H)Ar']; (Ar'=2,6-Diisopropylphenyl, R=Me or ^{t}Bu) can be treated with one equivalent of ^{n}BuLi in THF at low temperature with stirring to provide a lithiated complex (a-b, Figure 1.18). The lithiated complex can be further treated with an equivalent amount of Grignard reagent to provide a tetrahedral magnesium sphere (c-d, Figure 1.18).[72-74]

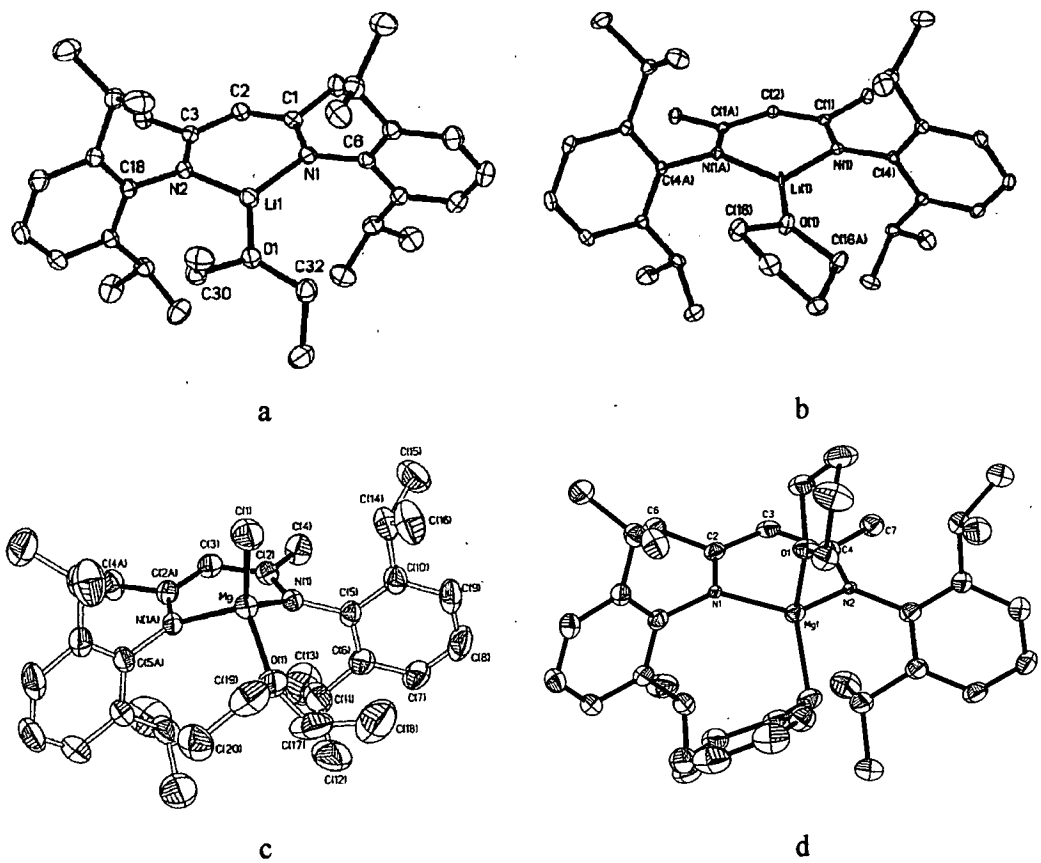

Figure 1.18 a-b) Molecular structure of [η²-HC{C(CH₃)NAr'}₂Li(Et₂O)] and [η²-HC{C(CH₃)NAr'}₂Li(THF)]; c-d) Molecular structure of [η²-HC{C(CH₃)NAr'}₂Mg(CH₃)(Et₂O)] and [η²-HC{C(CH₃)NAr'}₂Mg(CH₂Ph)THF].

Solvent free magnesium complexes may be prepared by heating the corresponding Et_2O/THF solvated complex obtained under *vacuum* (Figure 1.19).

Both the steric bulk of the ligand and the R group, contribute to the production of either an alkyl bridged dimeric species or a three co-ordinate monomeric species. Clearly the bulk of the ^{t}Bu groups in the 1,3 position on the ligand backbone is sufficient to produce the desired 3-coordinate monomeric species (Figure 1.20).[72]

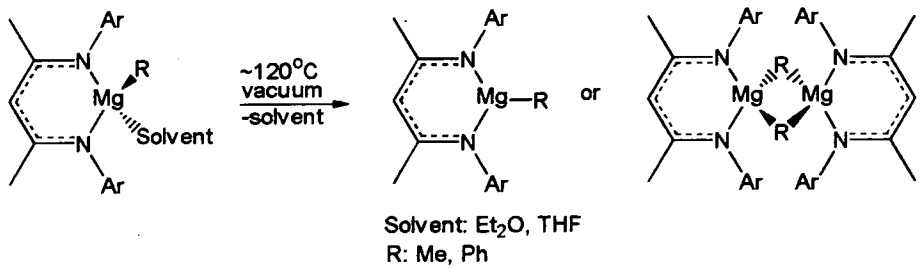

Figure 1.19 Synthesis of solvent free three co-ordinate magnesium atom supported by β-diketiminate bidentate nitrogen donor ligand.

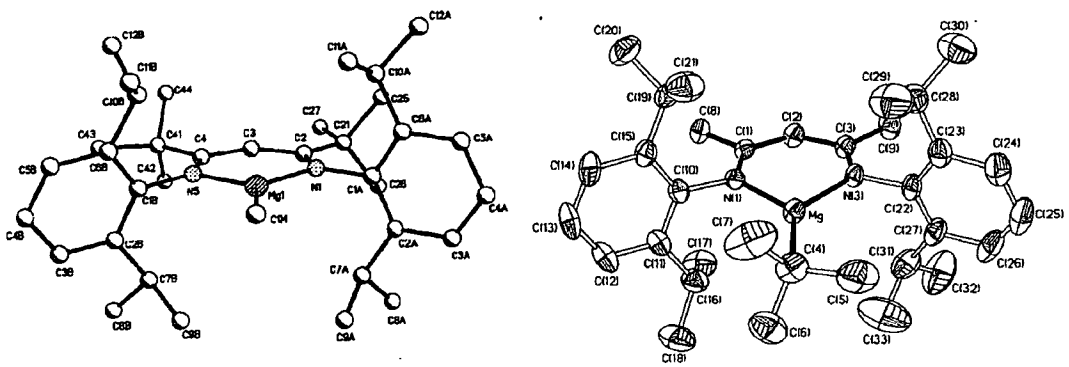

a b

Figure 1.20 Molecular structure of: a) [η^2-HC{C(CH$_3$)NAr'}$_2$MgCH$_3$]; b) [η^2-HC{C(CH$_3$)NAr'}$_2$MgC(CH$_3$)$_3$].

1.7.2 The Oxygenation of Organomagnesium Complexes

Magnesium alkoxides and aryloxides are used in a wide range of applications including as reagents in organic synthesis, and play and important role in oxidation reactions as additives in polyolefin catalysis.[75-78] The mono-alkyl magnesium complex can be treated with oxygen, where a mechanism has been proposed to proceed *via* a two-step process oxidation, followed by metathesis (Equations 1 and 2).[77-79]

$$RMgX + O_2 \longrightarrow ROOMgX \quad \text{(oxidation)} \quad \text{(Equation 1)}$$

$$ROOMgX + RMgX \longrightarrow 2\ ROMgX \quad \text{(metathesis)} \quad \text{(Equation 2)}$$

A radical chain mechanism according to Equations 3-5 has been suggested for the insertion process, and this may be followed by O-O cleavage *via* σ-bond metathesis in the presence of an excess of the alkyl complex (Equation 6).[75-79] Evidence of the formation of methyl peroxide species has been suggested by Bailey *et al.*[74] before decomposition to the methoxy-bridged dimer (Figure 1.21).

$$LnM\text{-}R + O_2 \longrightarrow LnM\text{-}OO^{\bullet} + R^{\bullet} \quad \text{(initiation)} \quad \text{(Equation 3)}$$

$$R^{\bullet} + O_2 \longrightarrow ROO^{\bullet} \quad \text{(Equation 4)}$$

$$LnM\text{-}R + ROO^{\bullet} \longrightarrow LnM\text{-}OOR + R^{\bullet} \quad \text{(propagation)} \quad \text{(Equation 5)}$$

$$LnM\text{-}OOR + LnM\text{-}R \longrightarrow LnM\text{-}OR \quad \text{(Equation 6)}$$

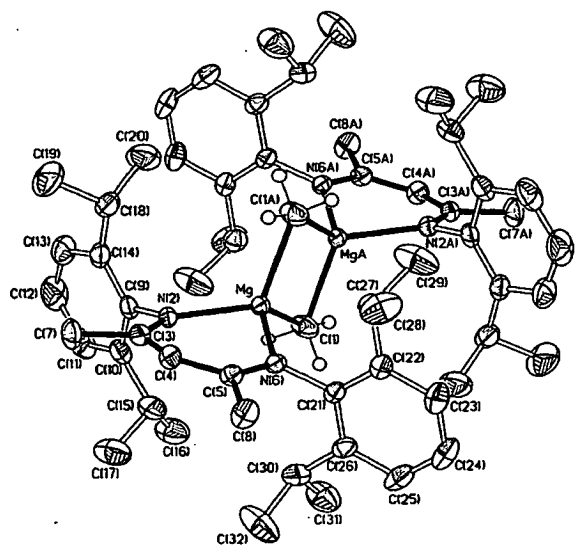

Figure 1.20 Methoxy bridged magnesium dimer supported by β-diketiminate bidentate nitrogen donor ligands.

1.8 Project Aim

The project has been designed to generate a range of zwitterionic mono-alkyl magnesium complexes containing a range of ligands. The possible complexes obtained of type [L^2MgR] (L^2: monoanionic ligand; R: Methyl or Benzyl) will provide the first examples of zwitterionic potential magnesium polymerisation catalysts (eg. Figure 1.21) which will be of significant interest due to their electronic structure which could promote increased activity.

In summary, a positive charge on the magnesium centre could be stablised by preparing zwitterionic species incorporating both existing and specially developed chelating nitrogen donor ligands. The intention in designing such species is twofold. First to provide an electrostatic barrier to dimerisation of the unsaturated species *via* alkyl bridging, and second, to provide a more highly electrophilic metal centre in an overall neutral catalystic complex. The nature of the B-N and Mg-N bonding could be investigated using high-resolution X-ray diffraction (Chapter 6). In this manner a discernible pattern of polymerisation activity should emerge which can be correlated with metal site and overall catalyst charge, and this will provide valuable guidance in the development of the next generation of alkene polymerisation catalysts.

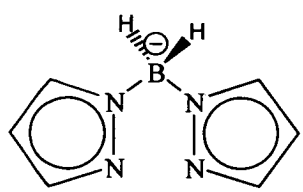

Chapter 2: Boron-Pyrazole Chemistry

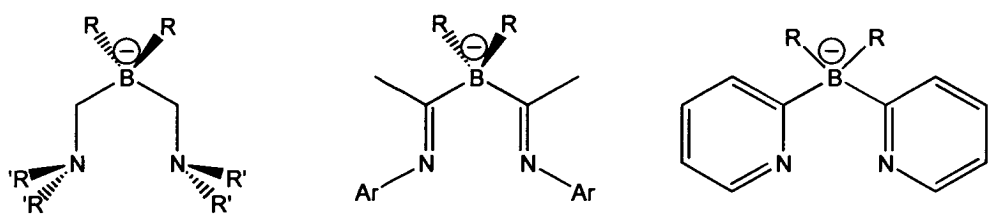

Chapter 3: New borate centred ligands for zwitterionic metal complexes

Figure 1.21 Some ligands synthesised and tested for reactivity with Grignard reagents.

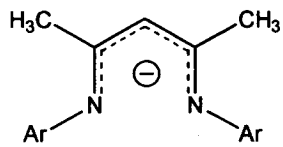

Chapter 4: β-Diketiminate systems

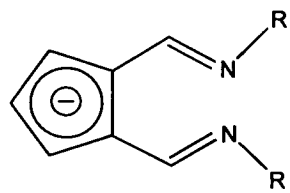

Chapter 5: 6-Aminofulvene-2-aldimine derivatives

Figure 1.21 (continued) Some ligands synthesised and tested for reactivity with Grignard reagents.

1.9 References

1 B. L. Shaw, and N. I. Tucker, *Organo-Transition Metal Compounds and Related Aspects of Homogeneous Catalysis*, Pergamon Press, **1975**, 781.

2 G. W. Parshall, *Homogenoeus Catalysis-The Applications and Chemistry of Catalysis by Soluble Transition Metal Complexes*, John Wile & Sons, Inc., **1980**.

3 K. Ziegler, E. Holzkamp, H. Breil and H. Martin, *Angew. Chem.*, **1955**, *67*, 541; K. Ziegler, *Angew. Chem.*, **1964**, *76*, 545; G. Natta, *Angew. Chem.*, **1956**, *68*, 393; G. Natta, *Angew. Chem.*, **1964**, *76*, 553.

4 K. Ziegler, E. Holzkamp, H. Breil and H. Martin, *Angew. Chem.*, **1955**, *67*, 541.

5 M. Bochmann, *J. Chem. Soc., Dalton Trans.*, **1996**, 255.

6 P. Cossee, *Tetrahedrom Lett.*, **1960**, *12*, 17; P. Cossee, *J. Catal.*, **1964**, *3*, 80; A. Zambelli, G. Gatti, C. Sacchi, W. O. Crain and J. D. Roberts, *Macromolecules*, **1971**, *4*, 475.

7 C. Elschenbroich and A. Salzer, *Organometallics - A Concise Introduction*, John Wile & Sons, Inc., **1989**, 423.

8 E. Chen and T. J. Marks, *Chem. Rev.*, **2000**, *100*, 1391.

9 G. Wilkinson, P. L. Pauson, J. M. Birmingham and F. A. Cotton, *J. Am. Chem. Soc.*, **1953**, *75*, 1011.

10 H. H. Brintzinger, D. Fischer, R. Mülhaupt, B. Rieger and R. M. Waymounth, *Angew. Chem. Int. Ed. Engl.*, **1995**, *34*, 1143.

11 D. S. Breslow and N. R. Newburg, *J. Am. Chem. Soc.*, **1959**, *81*, 81; J. C. W. Chien, *J. Am. Chem. Soc.*, **1959**, *81*, 86

12 K. H. Reichert and K. R. Meyer, *Makromol. Chem.*, **1973**, *169*, 163.

13 H. Sinn and W. Kaminsky, *Adv. Organomet. Chem.*, **1980**, *18*, 99; A. Andresen, H. G. Cordes, J. Herwig, K. Kaminsky, A. Merck, R. Mottweiler, J. Pein, H. Sinn and H. J. Vollmer, *Angew. Chem.*, **1976**, *88*, 689; A. Andresen, H. G. Cordes, J. Herwig, K. Kaminsky, A. Merck, R. Mottweiler, J. Pein, H. Sinn and H. J. Vollmer, *Angew. Chem. Int. Ed. Engl.*, **1976**, *15*, 630; W. Kaminsky and R. Steiger, *Polyhedron*, **1988**, *7*, 2375.

14 A. H. Trullo, *Chem. Eng. News*, **2001**, *43*, 38.

15 W. Kaminsky, J. Kopf, H. Sinn and H. J. Vollmer, *Angew. Chem.*, **1976**, *88*, 688; R. F. Jordan, C. S. Bajgur, R. Willet and B. Scott, *Am. Chem. Soc.*, **1986**, *108*, 7410; R. F. Jordan, R. E. LaPointe, P. K. Bradley, N. C. Baenziger, *Organometallics*, **1989**, *8*, 2892; R. F. Jordan, P. K. Bradley, N. C. Baenziger and R. E. LaPointe, *J. Am. Chem. Soc.*, **1990**, *112*, 1289; Y. W. Alelyunas, R. F. Jordan, S. F. Echols, S. L. Borkowsky and P. K. Bradley, *Organometallics*, **1991**, *10*, 1406; M. Bochmann and L. M. Wilson, *J. Chem. Soc., Chem. Commun.*, **1986**, 1610; M. Bochmann, L. M. Wilson, M. B. Hursthouse and M. Motevalli,

Organometallics, **1988**, *7*, 1148; M. Bochmann, L. M. Wilson, M. B. Hursthouse and M. Motevalli, *Polyhedron*, **1989**, *8*, 1838.

16 J. J. W. Eshuis, Y. Y. Tan, A. Meetama, J. H. Teuben, J. Renkema and G. G. Evans, *Organometallics*, **1992**, *11*, 362.

17 W. E. Piers, *Chem. Eur. J.*, **1998**, *4*, 1; M. Bochmann, A. J. Jaggar, and J. C. Nicholls, *Angew. Chem.*, **1990**, *102*, 830; M. Bochmann, A. J. Jaggar and J. C. Nicholls, *Angew. Chem., Int. Ed. Engl.*, **1990**, *29*, 780; M. Bochmann, A. J. Jaggar and J. C. Nicholls, *J. Organomet. Chem.*, **1992**, *424*, C5; X. Yang, C. L. Stern and T. J. Marks, *Organometallics*, **1991**, *10*, 840; A. D. Horton and J. H. G. Frijns, *Angew. Chem.*, **1991**, *103*, 1181; A. D. Horton and A. G. Orpen, *Organometallics*, **1991**, *10*, 3910; A. D. Horton, *J. Chem. Soc., Chem. Commun.*, **1992**, 185.

18 M. Bochmann, T. Cuenca and D. T. Hardy, *J. Organomet. Chem.*, **1994**, *484*, C10; A. R. Siedle, R. A. Newmark, J. N. Schropfer and P. A. Lyon, *Organometallics*, **1991**, *10*, 400; M. Bochmann and S. J. Lancaster, *J. Organomet. Chem.*, **1995**, *497*, 55; H. Sinn and W. Kaminsky, *Adv. Organomet. Chem.*, **1980**, *18*, 99.

19 I. A. Guzei, R. A. Stockland and R. F. Jordan, *Acta Cryst.*, **2000**, *C56*, 635.

20 B. Temme and G. Erker, *J. Organomet. Chem.*, **1995**, *488*, 177.

21 S. J. Lancaster, D. A. Walker, M. Thornton-Pett and M. Bochmann, *Chem. Commun.*, **1999**, 1533; D. A. Walker, M. Thornton-Pett and M. Bochmann, *J. Am. Chem. Soc.*, **2001**, *123*, 223.

22 P. Jutzi and A. Seufert, *J. Organomet. Chem.*, **1979**, *169*, 373.

23 R. Duchateau, S. J. Lacaster, M. Thornton-Pett and M. Bochmann, *Organometallics*, **1997**, *16*, 4995.

24 S. J. Lancaster, S. Al-Benna, M. Thornton-Pett and M. Bochmann, *Organometallics*, **2000**, *19*, 1599.

25 C. T. Burns, D. S. Stelck, P. J. Shapiro, V. Ashwani, K. Kunz, C. Kehr, T. Concolino and A. L. Rheingold, *Organometallics*, **1999**, *18*, 5432.

26 T. K. Woo, L. Fan and T. Ziegler, *Organometallics*, **1994**, *13*, 432; P. L. Watson and G. W. Parshall, *Acc. Chem. Res.*, **1985**, *18*, 51.

27 D. D. Devore, F. J. Timmers, D. L. Hasha, R. K. Rosen, T. J. Marks, P. A. Deck and C. L. Stern, *Organometallics*, **1995**, *14*, 3132.

28 S. Fokken, T. P. Spaniol, J. Okuda, F. G. Sernetz and R. Mülhaupt, *Organometallics*, **1977**, *16*, 4240.

29 E. B. Tjaden, D. C. Swenson, R. F. Jordan and J. L. Petersen, *Organometallics*, **1995**, *14*, 371.

30 G. J. P. Britovsek, V. C. Gibson and D. F. Wass, *Angew. Chem., Int. Ed.*, **1999**, *38*, 429, and references therein.

31 P. Van Leeuwen, P. C. J. Kamer, J. N. H. Reek and P. Dierkers, *Chem. Rev.*, **2000**, *100*, 2741.

[32] S. Ikeda, F. Ohhata, M. Miyoshi, R. Tanaka, T. Minami, F. Ozawa and M. Yoshifuji, *Angew. Chem., Int., Ed.*, **2000**, *39*, 4512.

[33] N. A. Cooley, S. M. Gree, D. F. Wass, K. Heslop, A. G. Orpen and P. G. Pringle, *Organometallics*, **2001**, *20*, 4769.

[34] J. Heinicke, M. Koesling, R. Brull, W. Kein and H. Pritzknow, *Eur. J. Inorg. Chem.*, **2000**, 299.

[35] Z. Guan and W. J. Marshall, *Organometallics*, **2002**, *21*, 3580.

[36] B. Thiyagarajan, R. F. Jordan and V. G. Young, *Organometallics*, **1998**, *17*, 281; B. Thiyagarajan, R. F. Jordan and V. G. Young, *Organometallics*, **1999**, *18*, 5347.

[37] M. P. Coles and R. F. Jodan, *J. Am. Chem. Soc.*, **1997**, *119*, 8125.

[38] M. D. Fryzuk, G. Giesbrecht and S. J. Retting, *Organometallics*, **1996**, *15*, 3329; S. Hajela, W. P. Schaefer and J. E. Bercaw, *J. Organomet. Chem.*, **1997**, *532*, 45.

[39] D. G. H. Ballard, A. Coutis, J. Holton, J. McMeeking and R. Pearce, *J. Chem. Soc. Chem. Commun.*, **1978**, 994; G. Jeske, H. Lauke, H. Mauermann, P. N. Swepston, H. Schumann and T. J. Marks, *J. Am. Chem. Soc.*, **1985**, *107*, 8091.

[40] S. J. Skoog, C. Mateo, G. G. Lavole, F. J. Hollander and R. G. Bergman, *Organometallics*, **2000**, *19*, 1406; A. J. Ashe, S. Al-Ahmad, X. G. Fang and J. W. Kampf, *Organometallics*, **1998**, *17*, 3883; D. Stephan, J. C. Stewart, F. Guerin, R. Spence, W. Xu and D. G. Harrison, *Organometallics*, **1999**, *18*, 1116.

[41] S. Feng, G. R. Roof and E. Y. X. Chen, *Organometallics*, **2002**, *21*, 832; S. Al-Benna, M. J. Sarsfield, M. Thornton-Pett, D. L. Ormsby, P. J. Maddox, P. Bres and M. Bochmann, *J. Chem. Soc., Dalton Trans.*, **2000**, 4247.

[42] R. Emrich, O. Heinemann, P. W. Jolly, C. Krüger and G. P. J. Verhovnik, *Organometallics*, **1997**, *16*, 1511.

[43] M. P. Coles, C. I. Dalby, V. E. Gibson, W. Clegg and M. R. J. Elsegood, *J. Chem. Soc., Chem. Commun.*, **1995**, 1709.

[44] V. C. Gibson, M. J. Humphries, K. P. Tellman, D. F. Wass, A. J. P. White, and D. J. Willians, *Chem.Commun.*, **2001**, 2252.

[45] M. S. W. Chan, L. Q. Deng and T. Ziegler, *Organometallics*, **2000**, *19*, 2741; A. C. Gottfried and M. Brookhart, *Macromolecules*, **2001**, *34*, 1140.

[46] V. C. Gibson, A. Tomov, D. F. Wass, A. J. P. White and D. J. Willians, *J. Chem. Soc., Dalton Trans.*, **2002**, 2261.

[47] L. R. Rieth, D. R. Moore, E. B. Lobkovsky and G. W. Coates, *J. Am. Chem. Soc.*, **2002**, *124*, 15239.

[48] M. Bruces, V. C. Gibson, C. Redshaw, G. A. Solan, A. J. P. White and D. J. Williams, *Chem. Commun.*, *1998*, 2523.

[49] J. S. Kim, L. M. Wojcinski II, S. Lin and J. C. Sworen, A. Se, *J. Am. Chem. Soc.*, **2000**, *122*, 5668.

[50] E. Ihara, V. G. Young and R. F. Jordan, *J. Am. Chem. Soc.*, **1998**, *120*, 8277.

[51] I. A. Guzei and R. F. Jordan, *J. Am. Chem. Soc.*, **1999**, *121*, 8673.

[52] A. V. Korolev, E. Ihara, I. A. Guzei, V. G. Young and R. F. Jordan, *J. Am. Chem. Soc.*, **2001**, *123*, 8291.

[53] D. Kottmair-Maeieron, R. Lechler and J. Weidlein, *Anorg. Allg. Chem.*, **1991**, *593*, 111.

[54] R. Lechler, H. D. Hausen and J. Weidlein, *J. Organomet. Chem.*, **1989**, *359*, 1.

[55] J. Barker, N. C. Blacker, P. R. Phillips, N. W. Alcock, W. Errington and M. G. H. Wallbridge, *J. Chem. Soc., Dalton Trans.*, **1996**, 431; R. Duchateau, A. Meetsma and J. H. Teuben, *J. Chem. Soc., Chem. Commun.*, **1996**, 223.

[56] F. T. Edelmann, *Coord., Chem., Rev.*, **1994**, *137*, 403; J. Barker and M. Kilner, *Coord., Chem. Rev.*, **1994**, *133*, 219.

[57] A. G. Pinkus, *Coord. Chem. Rev.*, **1978**, *28*, 173; Cotton and Wilkinson, *Advanced Inorganic Chemistry*, 4th Ed., Wile and Sons, Inc., **1980**, 286.

[58] H. Gilan and R. E. Brown, *J. Am. Chem. Soc.*, **1930**, *52*, 4480.

[59] E. Weiss, *J. Organometal. Chem.*, **1964**, *2*, 314.

[60] E. Weiss, *Organometal. Chem.*, **1965**, *4*, 101.

[61] W. Schlenk and W. Schlenk Jr., *Chem. Ber.*, **1929**, *62*, 920.

[62] N. D. R. Barnett, W. Clegg, R. E. Mulvey, P. A. O'Neil and D. Reed, *J. Organomet. Chem.*, **1996**, *510*, 297.

[63] R. Han and G. Parkin, *J. Am. Chem. Soc.*, **1990**, *112*, 3662; R. Han, M. Bachrach and G. Parkin, *Polyhedron*, **1990**, 1775; G. E. Coates and J. A. Heslop, *J. Chem. Soc. A.*, **1968**, 514.

[64] D. Thoennes and E. Weiss, *Chem. Ber.*, **1978**, *111*, 3381.

[65] G. P. Canone, F. H. Caron and G. Lemay, *Tetrahedron*, **1982**, *38*, 3563.

[66] T. Greiser, J. Kopf, D. Thoennes and E. Weiss, *J. Organomet. Chem.*, **1980**, *191*, 1.

[67] K. W. Henderson and R. E. Mulvey, *J. Organomet. Chem.*, **1992**, *439*, 237.

[68] D. T. Hurd, *J. Am. Chem. Soc.*, **1948**, *70*, 2053; A. T. Whatley and R. N. Pease, *J. Am. Chem. Soc.*, **1954**, *76*, 835; H. C. Brown and B. C. Subbarao, *J. Org. Chem.*, **1957**, *22*, 1136.

[69] M. P. Coles and R. F. Jordan, *J. Am. Chem. Soc.*, **1997**, *119*, 8125; US Pat., 5, 777, 120, July 7 1998; C. E. Radzewich, I. A. Guzei and R. F. Jordan, *J. Am. Chem. Soc.*, **1999**, *121*, 8673.

[70] H. E. Podall and W. E. Foster, *J. Org. Chem.*, **1958**, *23*, 1848.

[71] A. Sen and J. S Kim, *ExxonMobil Reseach and Engineering Company, USA.* WO 2000073359, **2000**, 20001207.

[72] V. C. Gibson, J. A. Segal, A. J. P. White, D. J. Williams, *J. Am. Chem. Soc.*, **2000**, *122*, 7120; M. Westerhausen, N. Makropoulos, B. Wieneke, K. Karaghiosoh, H. Nöth, H. Schwenk-Kircher, J. Knizer and T. Scifert, *Eur. J. Inorg. Chem.*, **1998**, 965; H. Vielbrock, U. Behrens and E. Weiss, *Angew. Chem. Int. Ed. Engl.*, **1994**, *33*, 1257.

[73] M. Cheng, A. B. Attygalle, E. B. Lobkovsky and G. W. Coates, *J. Am. Chem. Soc.*, **1999**, *121*, 11583; V. C. Gibson, P. J. Maddox, C. Newton, C. Redshow, G. A. Solan, A. J. P. White and Williams, *Chem. Commun.*, **1998**, 1651; P. H. M. Budzelar, A. B. Van Oort and A. Orpen, *Eur. J. Inorg. Chem.*, **1998**, 1485; J. Feldman, S. J. McLain, A. Parthasarathly, W.

J. Marshal, C. J. Calabrese and S. A. Arthur, *Organometallics*, **1997**, *16*, 1514; M. Rahim, N. J. Taylor and S. Xin, *Organometallics*, **1998**, *17*, 1315; F. S. Mair, D. Scully, A. J. Edwards, P. R. Railthby and R. Snaith, *Polyhedron*, **1995**, *14*, 2397; C. F. Caro, P. B. Hitchcock and M. F. Lappert, *Chemm. Commun.*, **1999**, 1433; F. Cosledan, P. B. Hitchcock and M. F. Lappert, *Chem. Commun.*, **1999**, 705.

74 P. J. Bailey, C. M. E. Dick, S. Fabre and S. Parsons, *J. Chem. Soc., Dalton Trans.*, **2000**, 1655; P. J. Bailey, R. A. Coxal, C. M. E. Dick, S. Fabre and S. Parsons, *Organometallics*, **2001**, *20*, 798; S. Liddle, End of grant report, C.O. P. J. Bailey, *School of Chemistry*, University of Edinburgh, Sept., **2001**.

75 G. Stork and L. Bauer, *J. Am. Chem., Soc.*, **1953**, *75*, 4372; J. H. Song, S. T. Rhie and E. K. Ryu, *Synth. Commun.*, **1995**, *25*, 1801; S. Kanemasa, M. Nishiuichi and E. Wada, *Tetrahedron Lett.*, **1992**, *33*, 1357.

76 P. Sobota, J. Utko, J. Ejfler and L. B. Jerzykiewicz, *Organometallics*, **2000**, *24*, 4929; L. R. Rieth, D. R. Moore, E. B. Lobkovsky and G. W. Coates, *J. Am. Chem. Soc.*, **2002**, *124*, 15239.

77 C. W. Poster and C. Steel, *J. Am. Chem. Soc.*, **1920**, *42*, 2650.

78 A. P. Dove, V. C. Gibson, E. L. Marshall, A. J. P. White, and D. J. Williams, *Chem. Commun.*, **2002**, 1208.

79 G. Stork and L. Bauer, *J. Am. Chem. Soc.*, **1953**, *75*, 4372; J. H. Song, S. T. Rhie and E. K. Ryu, *Synth.Commun.*, **1995**, *25*, 1801; S. Kanemasa, M. Mishiuichi and E. Wada, *Tetrahedron Lett.*, **1992**, *33*, 1357.

Chapter 2:

Potassium Dihydrobis(1-pyrazolyl)borate and Grignard Reagents

2.1 Introduction

2.1.1 Background

The present Chapter involves attempts to explore the chemistry of bis-chelating dihydrobis(pyrazoly)borates (Bp) with Grignard reagents, in order to synthesise mono-alkyl magnesium complexes (Figure 2.1). The effect of the B-N and Mg-N bonds will be explored to prevent the complexes from dimerization. Finally, alkene polymerisation will be tested for any mono-alkyl magnesium complex obtained.

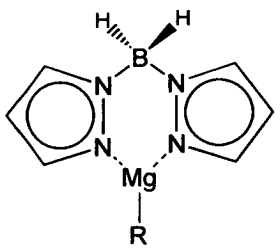

R= Me, CH_2Ph

Figure 2.1 Zwitterionic magnesium complexes proposed from the reactivity of Bis-chelating dihydrobis(pyrazolyl)borate with Grignard reagents.

Boron-pyrazole chemistry has yielded novel classes of boron heterocycles, chelating ligands, and transition metal compounds.[1] The 1-boryl-pyrazole fragment has remarkable electronic and geometric characteristics which produce stabilisation of complexes by using a pyrazolide ion through its co-ordination or through dimerization.[2] The activation of pyrazole by a borohydride ion suggests the existence of a five-centre transition state (Figure 2.2).[3] The co-ordination of pyrazole and borohydride ion occurs through the release of an H_2 molecule, where the hydrogen atom at the second position in the pyrazole system and any hydrogen atom from the borohydride ion have to be sufficiently close to allow hydrogen-hydrogen atom contact.[4]

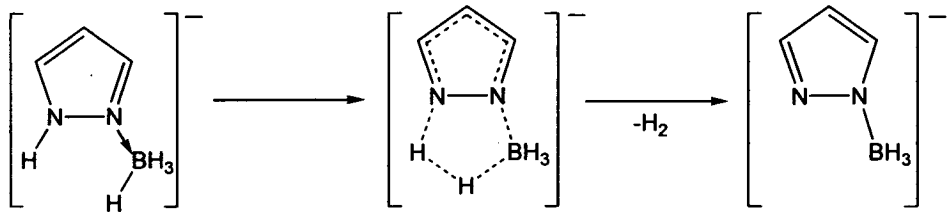

Figure 2.2 Borane-pyrazole and its five-membered ring transition state.

The reactivity of the borohydride ion with pyrazole is thought to proceed in a way that combines some important characteristics of first- and second-order (S_N1 and S_N2) nucleophilic displacement reactions.[4,5] Poly(1-pyrazolyl)borates can be prepared by heating an alkali metal borohydride with pyrazole, where the di-, tri-, and tetra(1-pyrazolyl)borates complexes are obtained by maintaining temperatures of approximately 110, 180, and > 210 °C, respectively.[2] The oxidative and hydrolytic stability of poly(1-pyrazolyl)borates increases with a decreasing number of hydrogens attached to boron.[2,5] A second approaching pyrazabole could undergo a S_N1 reaction, resulting in a well stabilised alkali metal complex (Figure 2.3). The synthesis of a tripodal ligand may present steric effects in the transition state, and the non-coordinating nitrogen atom is orientated towards the metal ion rather than towards the hydrogen to be eliminated. The introduction of a fourth pyrazolyl group involves an obstructed boron atom which suggests a slow nucleophilic displacement of first-order (S_N1).[2]

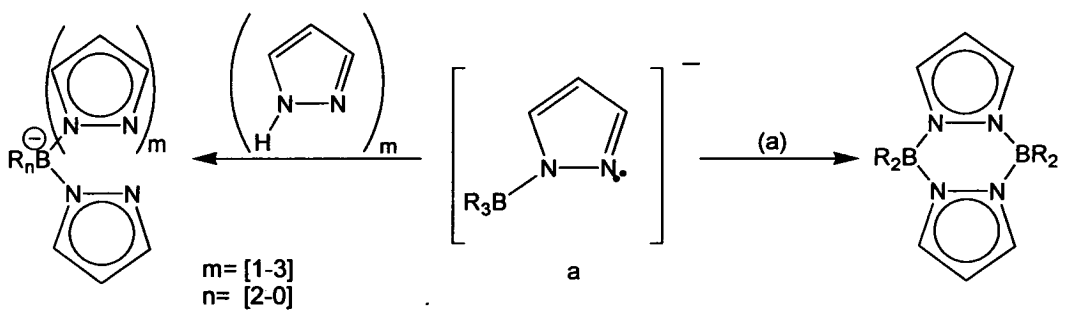

Figure 2.3 Mechanism of pyrazabole formation and dimerization or through co-ordination with a pyrazolide ion.

Carbon substituted pyrazaboles can be obtained from substituted pyrazoles, and the reactions proceed in a similar manner to the unsubstituted pyrazole reactions.[4] Moreover, a strong electron-withdrawing substituent in the pyrazoles

produces a slow reaction rate as a result of the reduced nucleophilicity of the 2-nitrogen atom.[1,4] In addition, the reaction of BR_3 and pyrazole will also depend on the R group on the boron atom, whose reactivity has an order of halogen > hydrogen > alkyl > aryl.[1] Although several methods have been tested in order to give pure substituted poly(1-pyrazolyl)borates complexes, their properties are not sufficiently different to produce separations from the mixture of products, resulting in poor yields.[6]

2.1.2 Bis(pyrazoly)borate Chemistry

The co-ordinating ability of the bis(1-pyrazolyl)borate ions, $[R_2B(pz)_2]^-$, has favourable electronic and geometric properties compared to the β-diketonate ion (Figure 2.4a). The non-coordinating electrons on each nitrogen atom make possible the formation of complexes with a range of transition metal ions (Figure 2.4b).[1,7]

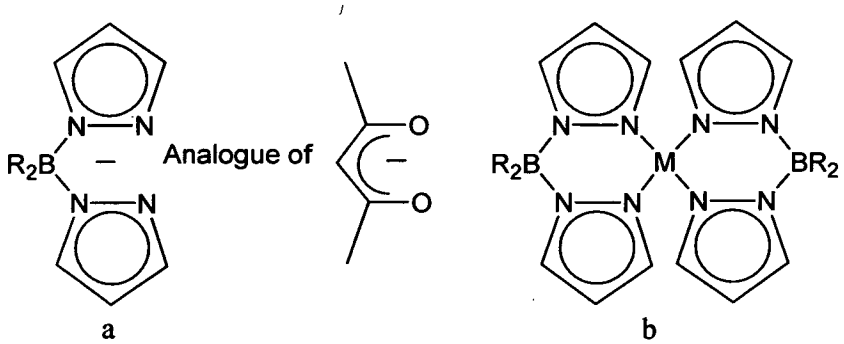

Figure 2.4 a) Bis(pyrazolyl)borate ion and relationship with β-diketonate ion. b) Chelate with a divalent transition metal.

The geometrical disposition of the boron, nitrogen and the metal atoms in the chelate (Figure 2.5) induce a puckered pseudoboat conformation (or scorpionate conformation), where the pseudoaxial R group has been described as a protector screen and may also produce bonding to the metal.[1,7,8] The structure illustrated in Figure 2.5 may show changes in bond angles and distances, which produce variation in depth of the constituent boat conformation.

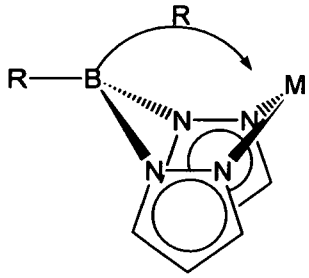

Figure 2.5 The "Scorpionate" or boat structure and the versatility of co-ordination for poly(pyrazolyl)borates.

Monomeric complexes $[\{H_2B(pz)_2\}_2M]$ with most divalent first-row transition metal have shown high stability and solubility, except for the Fe(II) and Mn(II) derivatives.[1] The isomorphous stuctures for Ni and Cu complexes are square planar, whilst complexes of Mn, Fe, Co, and Zn are tetrahedral.[9] The presence of alkyl substituents in the 3- and 5- positions enhance the stabilising effect on the synthesis of stable organometallic compounds with non-inert gas configurations (e.g. $[R_2B\{3,5\text{-}R'_2pz\}_2Mo(CO)_2\text{-}\pi\text{-allyl}]$) (Figure 2.6a).[10] The powerful effect of a CN substituent in position 4 has been investigated,[11] and co-ordinating ability is not compromised by the presence of sterically interfering 3 and 5 substituents in pyrazoles (Figure 2.6b).[11-14]

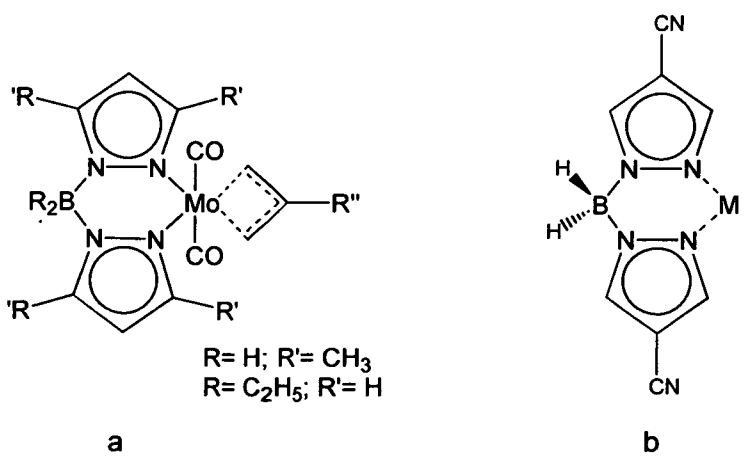

Figure 2.6 a) Bidentate mono chelate possessing a 16-electron configuration. b) Bidentate mono chelate containing organic functional groups.

Metal adducts of the halogenated ligands often show very different physical and chemical properties relative to their non-halogenated analogues.[15] Polyfluoro-

and polybrominated ligands (Figure 2.7) commonly improve the volatility, oxidation resistance and halo-carbon solubility of metal complexes.[15,16] Polysubstituted bis(1-pyrazolyl)borate ligands have also been known to increase the activity of certain metal catalysed reactions.[17,18] The design of new polyfunctional ligands that provide non-coordinating sulphur atoms capable of supporting a monomeric tetrahedral zinc centre,[19,20] has prompted the suggestion that this is critical for the effective functioning of natural product.

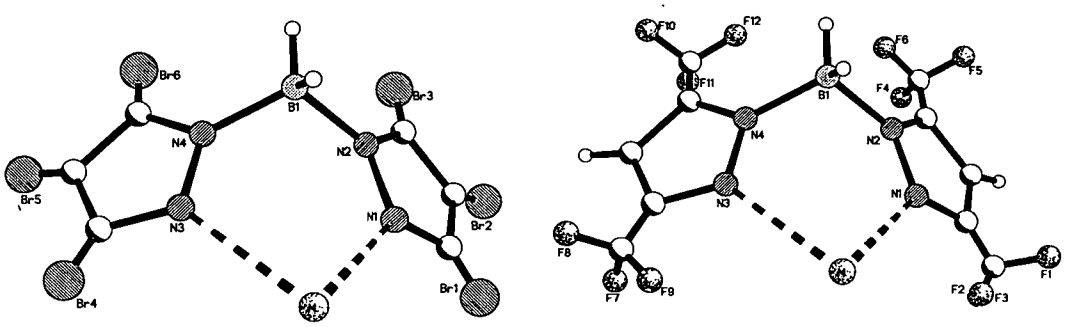

a b

Figure 2.7 a) Metal complex of dihydrobis(3,4,5-tribromopyrazolyl)borate, b) Metal complex of dihydrobis[3,5-bis(trifluoromethyl)pyrazolyl]borate.

2.1.3 Tris(pyrazoly)borate Chemistry

The co-ordinating ability of the tris(1-pyrazolyl)borate ion, $[RB(pz)_3]^-$, may be attributed to a more highly favourable delocalizable charge using its three rings than the bis(1-pyrazolyl)borate ion, and it could be compared to a cyclopentadienide ion (Figure 2.8a).[1,7] "Octahedral" complexes (C_{3v} tripodal symmetry) may be obtained when divalent transition metals are used with the tris(1-pyrazolyl)borate ion (Figure 2.8b), whilst trivalent transition metals form similar, but charged complexes. Trofimenko has also reported the preparation of metal complexes using a tris(1-pyrazolyl)borate ions where steric effects induce the formation of tridentate complexes.[1]

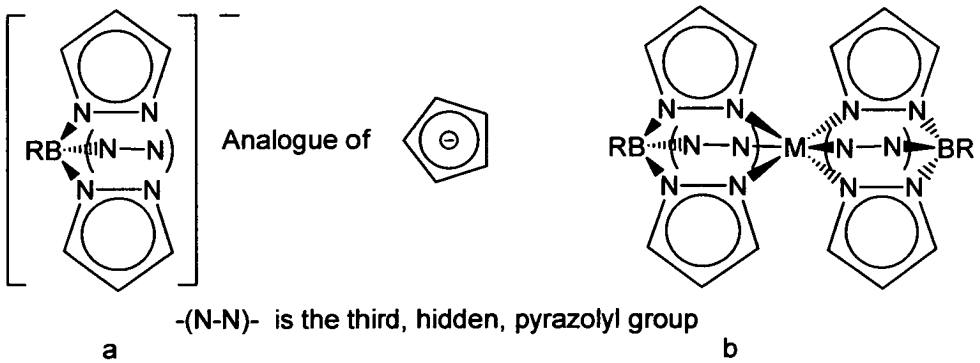

Figure 2.8 a) Tris(pyrazolyl)borate ion and relationship with cyclopentadienide ion. b) Chelate with a divalent transition metal.

One of the most important features of tris(1-pyrazolyl)borate ions is that they can be modified, by substitution in the 3-positions of the pyrazolyl ring, in order to introduce chiral environments for specific metals. This versatility in creating different steric environments around a metal is used to produce substantial changes in the chelate, since these groups lie on three sides and in close proximity to the co-ordinating metal.[1] Bulky substituents in the 3-position of the pyrazolyl ring do have a profound effect on the co-ordination chemistry of these ligands.[12] The formation of ML_2 complexes of polyfluoro- and polybrominated ligands (Figure 2.9) does not appear to be possible with the first-row transition-metal ions.[1] The co-ordination chemistry of most other tris(pyrazolyl)borate derivatives reported to date is dominated by the formation of ML_2 complexes.[1] With first-row transition-metal ions, the ligand $[HB(3\text{-}^tBupz)_3]^-$ appears to be a tetrahedral enforcer, leading to complexes with C_{3v} symmetry.[1,4] Ligands of intermediate steric requirements, with a 3-isopropyl group, show limited formation of ML_2 complexes and accessibility of the metal ion.[13,14]

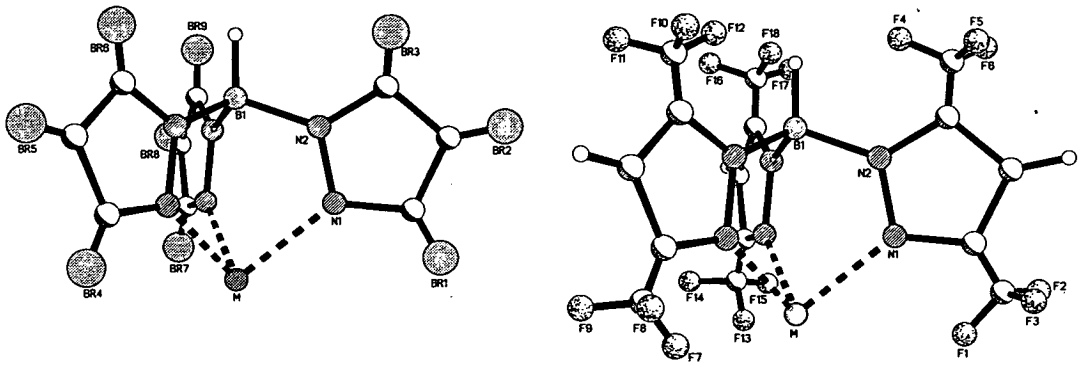

a b

Figure 2.9 a) Metal complex of hydrotris(3,4,5-tribromopyrazolyl)borate, b) Metal complex of hydrotris[3,5-bis(trifluoromethyl)pyrazolyl]borate.

2.2.4 Bis(pyrazolyl)borate and Tris(pyrazolyl)borate Chemistry

It can be seen from previous examples that several synthetic routes are available for the synthesis of bidentate and tridentate poly(pyrazolyl)borate ligands, where a wide variety of substituents could be used on carbon or boron atoms. Steric factors could be introduced in order to obtain chelate properties, but these are of greater significance in square-planar and tetrahedral chelates than in octahedral transition metal compounds.[2,4-7,9]

In general, since the first synthesis of bis-chelating dihydrobis-(pyrazoly)borates (Bp) and tris-chelating hydrotris(pyrazolyl)borates (Tp) by Trofimenko in 1966,[2] those ligands have found broad applications in co-ordination chemistry with nearly every metal of the periodic table.[1,4,6] Poly(pyrazolyl)borate ligands are also attractive for the synthesis of lanthanide complexes, especially those ligands with similar characteristics to those of cyclopentadienyl systems.[1,2,7,8]

2.2 Results

2.2.1 Reactivity of Potassium Dihydrobis(1-pyrazolyl)borate with MeMgCl (30 minute reaction)

Treatment of potassium of dihydrobis(1-pyrazolyl)borate,[2] $[K\{H_2B(pz)_2\}]$ (**1**), with an equimolar amount of MeMgCl in THF at room temperature was carried out, and the reaction was stopped after 30 minutes. After subsequent removal of the solvent in *vacuum* and extraction from ether, a colourless oil was obtained. The colourless oil was quite soluble in most solvents (benzene, ether, THF and toluene), but turned to an insoluble white suspension after 45 minutes. The NMR spectra of the colourless oil were investigated and show the formation of a possible monomeric species of $[\{H_2B(pz)_2\}Mg(Me)THF]$ (**2**) (Figure 2.10).

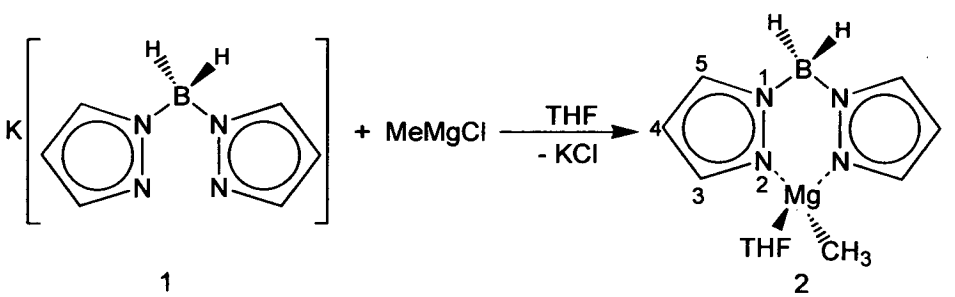

1 2

Figure 2.10 Reactivity of 1 and MeMgCl (30 minutes reaction).

The ^1H NMR spectrum of **2** shows a shift to downfield for H5 and H3 doublets at δ 7.62 and 7.18, while the H4 triplet is present at δ 6.12. The signal for Mg-Me in the ^1H NMR places a characteristic upfield value at δ -0.68. The solvated monomer displays the equivalent THF signals at δ 3.62 and 1.81 (Figure 2.11).

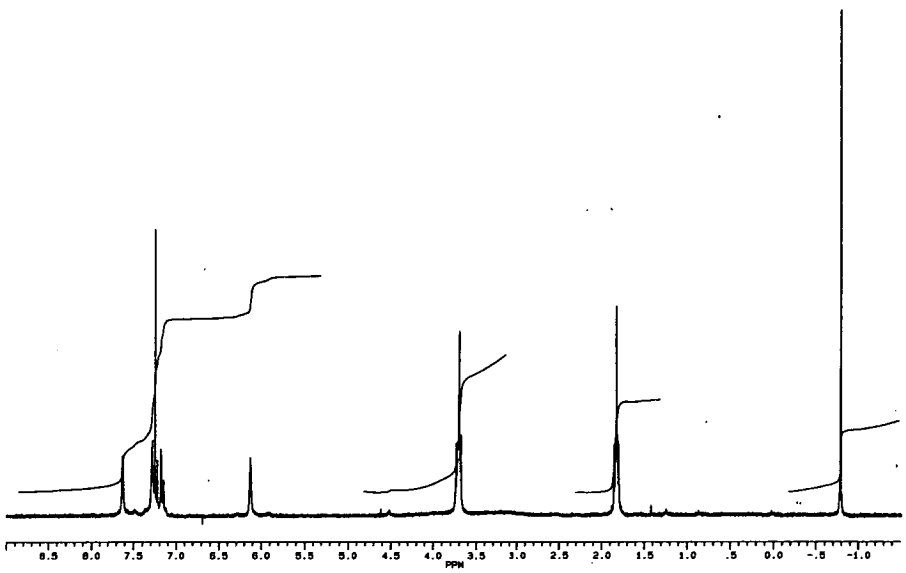

Figure 2.11 ^{1}H NMR spectrum in benzene-d_6 of 2.

The ^{13}C NMR of **2** shows downfield shifts of C3, C5 and C4 to δ 141.53, 128.30 and 104.37, whilst a singlet Mg-Me peak is also observed at chemical shift δ -11.62 (Figure 2.12). Two resonances at δ 67.30 and 25.10 are assignable to THF solvated. Due to the insolubility, air and moisture-sensitive nature of the final product no further analysis could be done.

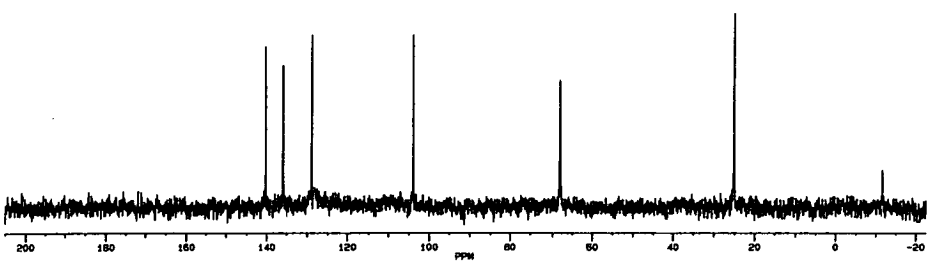

Figure 2.12 ^{13}C NMR spectrum in benzene-d_6 of 2.

2.2.2 Reactivity of Potassium Dihydrobis(1-pyrazolyl)borate with MeMgCl (3 hours reaction)

A second treatment of **1** with an equimolar amount of MeMgCl in THF at room temperature was carried out, and the reaction was stopped after 3 hours. The suspension was filtered, and extraction from diethyl ether produced a white powder

which followed by re-crystallisation from diethyl ether gave colourless crystals of $[\{H_2B(pz)_2\}Mg(THF)(\mu\text{-}Cl)_2Mg(THF)_2\{(pz)_2BH_2\}]$ (**3**). The NMR spectra show only one type of pyrazolyl group at room temperature, indicating a rapid inversion of the co-ordinated $[H_2B(pz)_2]^-$ ligand. The ^1H NMR spectrum of **3** indicates that the upfield singlet peak for Mg-Me is not present (Figure 2.13). Two multiplets at δ 3.71 and 1.84 indicate the presence of co-ordinated THF. The ^1H NMR spectrum places the H5 and H3 doublets at δ 7.65 and 7.26, whilst the H4 triplet is observed at δ 6.18. The ^{13}C NMR gives two sets of signals at δ 67.80 and 24.60 which are assigned to the THF solvated, while C3, C5 and C4 are placed at δ 141.20, 136.10 and 104.30, respectively (Figure 2.14).

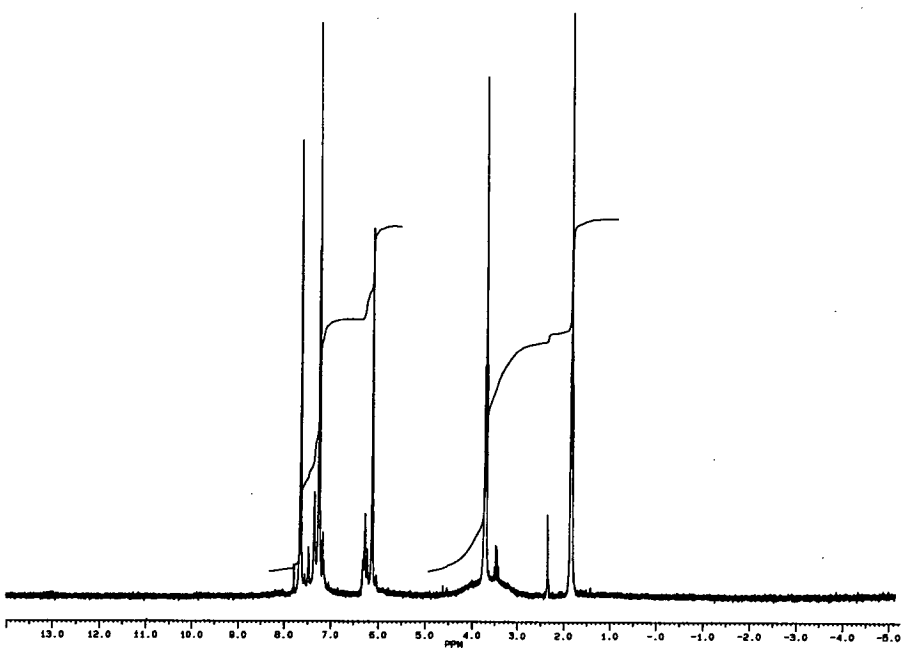

Figure 2.13 ^1H NMR spectrum in $CDCl_3$ of 3.

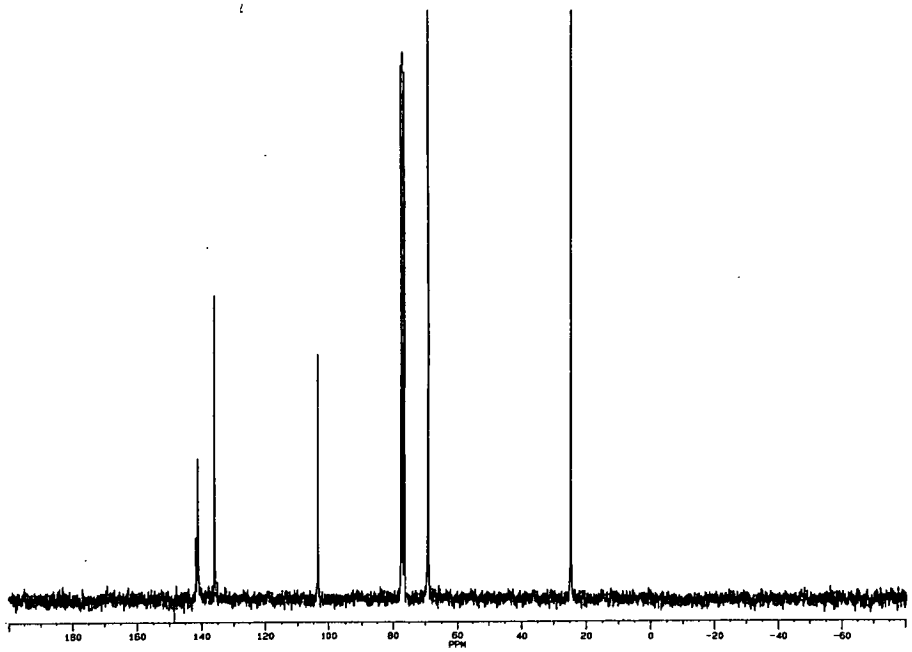

Figure 2.14 ^{13}C NMR spectrum in $CDCl_3$ of 3.

The X-ray crystal structure of **3** reveals a bridged halide dimer complex, and the structure is illustrated in Figure 2.15. The two pyrazolyl ligands present a "boat or scorpionate" conformation and both of them co-ordinate in κ2 fashion. The first magnesium centre [Mg(1)] shows an octahedral geometry which is bonded through both nitrogen and chloride atoms. The axial co-ordination sites are occupied by oxygen atoms of two distorted THF molecules. In contrast, the second magnesium centre [Mg(2)] possesses a distorted square-pyramidal geometry which is bonded through both nitrogen and chlorine atoms. The solvent THF occupies the axial positions.

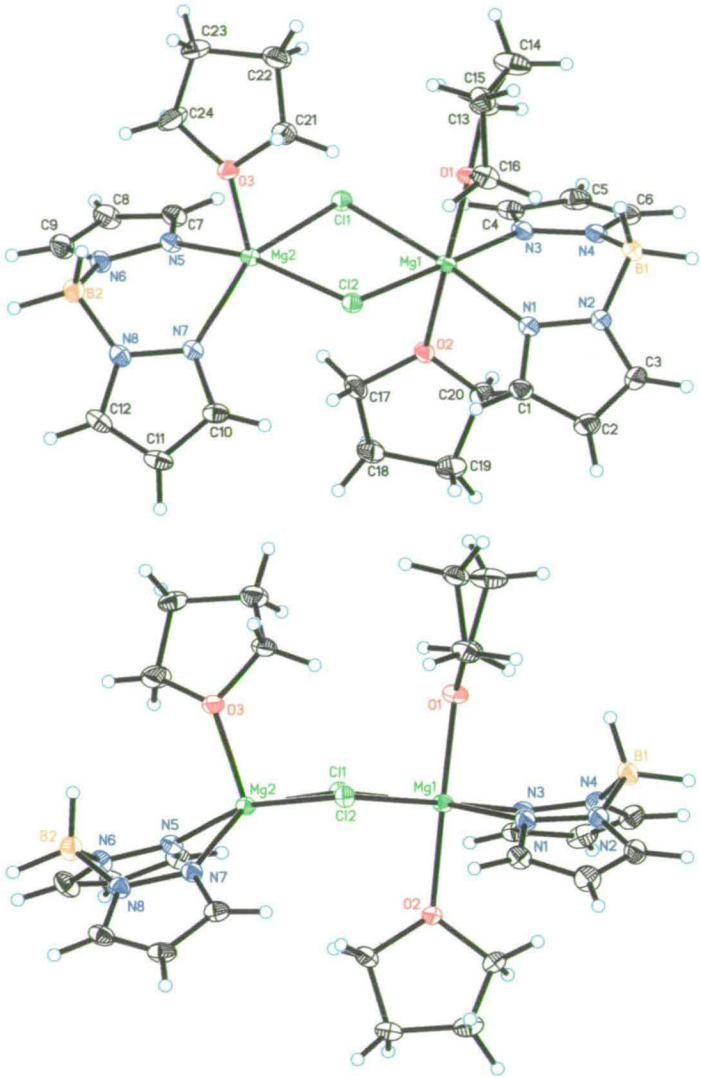

Figure 2.15 Crystallographic structure of 3 with two different orientations. Displacement ellipsoids are shown at the 50% probability level.

The formation of this species may be explained by a disproportionation of the Grignard reagent and the simple model of the Schlenk equilibrium involved, according to Figure 2.16. The solvation of the Grignard reagent and its association are predominantly by halide rather than carbon bridges of monomeric complexes. In addition, a large solvent effect is present during the reaction (especially when strong donor solvents such as THF or ether are used).

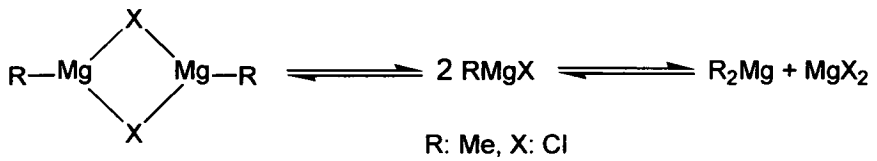

Figure 2.16 Schlenk equilibrium for dissociation of the Grignard reagent.

The Mg-N bond distances of 2.1350(18) and 2.1298(17) Å (for the hexa-coordinate magnesium atom), 2.1312(18) and 2.1394(17) Å (for the penta-coordinate magnesium atom) are typical σ-bonding distances for similar magnesium complexes.[21-25] Both distorted THF molecules on the six-coordinate magnesium atom are situated at very similar Mg-O distances 2.0924(15) and 2.1482(15) Å, respectively. The THF solvates produce an octahedral magnesium, and this could also be explained by the high electronegativity and low steric demand of the dihydrobis(1-pyrazolyl)borate group. The steric effect of the disordered THF molecules from the octahedral magnesium make higher co-ordination for the five-coordinate magnesium quite difficult. Moreover, the electron requirement for [Mg(2)] produces a distorted square-pyramidal geometry, where a strong Mg-O bond of 2.0206(15) Å is present (a strong Mg-O bond has a length around 2.0 Å, whilst a very weak Mg-O interaction is around 2.7 Å). Finally, the two chloride atoms bridge the metals forming a "square" Mg_2Cl_2 core, where the Mg-Cl-Mg angles are 94.05(3) and 94.55(3) Å and the Cl-Mg-Cl angles are 84.08(3) and 85.99(3) Å, respectively. Selected bond lengths and angles are shown in Table 2.1.

Table 2.1 Selected bond distances (Å) and angles (°) for 3.

Cl(1)-Mg(1)	2.5231(8)	Cl(1)-Mg(2)	2.4580(8)	Cl(2)-Mg(1)	2.4934(8)
Cl(2)-Mg(2)	2.4680(8)	Mg(1)-O(1)	2.0924(15)	Mg(1)-N(3)	2.1298(17)
Mg(1)-N(1)	2.1350(18)	Mg(1)-O(2)	2.1482(15)	Mg(2)-O(3)	2.0206(15)
Mg(2)-N(5)	2.1312(18)	Mg(2)-N(7)	2.1394(17)	N(1)-N(2)	1.366(2)
N(2)-B(1)	1.556(3)	N(3)-N(4)	1.365(2)	N(4)-B(1)	1.555(3)
N(5)-N(6)	1.368(2)	N(6)-B(2)	1.550(3)	N(7)-N(8)	1.367(2)
N(8)-B(2)	1.550(3)				

Mg(2)-Cl(1)-Mg(1)	94.05(3)	Mg(2)-Cl(2)-Mg(1)	94.55(3)
O(1)-Mg(1)-N(3)	91.16(6)	O(1)-Mg(1)-N(1)	93.08(6)
N(3)-Mg(1)-N(1)	90.35(7)	O(1)-Mg(1)-O(2)	178.10(6)
N(3)-Mg(1)-O(2)	87.02(6)	N(1)-Mg(1)-O(2)	87.49(6)
O(1)-Mg(1)-Cl(2)	90.18(5)	N(3)-Mg(1)-Cl(2)	176.84(6)
N(1)-Mg(1)-Cl(2)	92.43(5)	O(2)-Mg(1)-Cl(2)	91.60(5)
O(1)-Mg(1)-Cl(1)	91.17(5)	N(3)-Mg(1)-Cl(1)	93.03(5)
N(1)-Mg(1)-Cl(1)	174.51(5)	O(2)-Mg(1)-Cl(1)	88.37(5)
Cl(2)-Mg(1)-Cl(1)	84.08(3)	O(3)-Mg(2)-N(5)	97.98(6)

O(3)-Mg(2)-N(7)	115.68(7)	N(5)-Mg(2)-N(7)	87.14(7)
O(3)-Mg(2)-Cl(1)	96.05(5)	N(5)-Mg(2)-Cl(1)	90.59(5)
N(7)-Mg(2)-Cl(1)	148.21(5)	O(3)-Mg(2)-Cl(2)	99.17(5)
N(5)-Mg(2)-Cl(2)	162.77(6)	N(7)-Mg(2)-Cl(2)	86.93(5)
Cl(1)-Mg(2)-Cl(2)	85.99(3)	N(2)-N(1)-Mg(1)	122.58(13)
N(1)-N(2)-B(1)	121.54(16)	N(4)-N(3)-Mg(1)	123.60(13)
N(3)-N(4)-B(1)	122.89(17)	N(8)-N(7)-Mg(2)	121.62(12)
N(6)-N(5)-Mg(2)	121.48(13)	N(7)-N(8)-B(2)	120.87(16)
N(5)-N(6)-B(2)	121.62(16)	N(4)-B(1)-N(2)	109.57(17)
N(6)-B(2)-N(8)	108.15(17)		

2.2.3 Reactivity of Potassium Dihydrobis(1-pyrazolyl)borate with MeMgCl (10 hours reaction)

A third treatment of **1** with an equimolar amount of MeMgCl in THF at room temperature was carried out, and the reaction was stopped after 10 hours. KCl was filtered off, and extraction from diethyl ether produced a white powder which, followed by re-crystallisation from diethyl ether, formed colourless crystals of $[\{H_2B(pz)_2\}_2Mg(THF)]$ (**4**). The NMR spectra were investigated and show only one type of pyrazolyl group at room temperature, indicating a rapid inversion of the co-ordinated $[H_2B(pz)_2]^-$ ligand. Two resonances in the ^1H NMR at δ 3.70 and 1.85 indicate the presence of THF solvated. The ^1H NMR spectrum of **4** places the H5 and H3 doublets at δ 7.65 and 7.34, whilst the H4 triplet is observed at δ 6.32, respectively (Figure 2.17). The ^{13}C NMR spectrum gives two sets of signals at δ 67.80 and 26.10 which are assigned to the THF solvated, whilst C3, C5 and C4 are also placed at δ 141.35, 136.10 and 103.70, respectively (Figure 2.18). The ^{13}C NMR (DEPT; $\theta=135^o$) spectrum shows correspondence signals; positive C3, C5 and C4 atoms are observed and negative values for the set of peaks for the THF solvated (Figure 2.18).

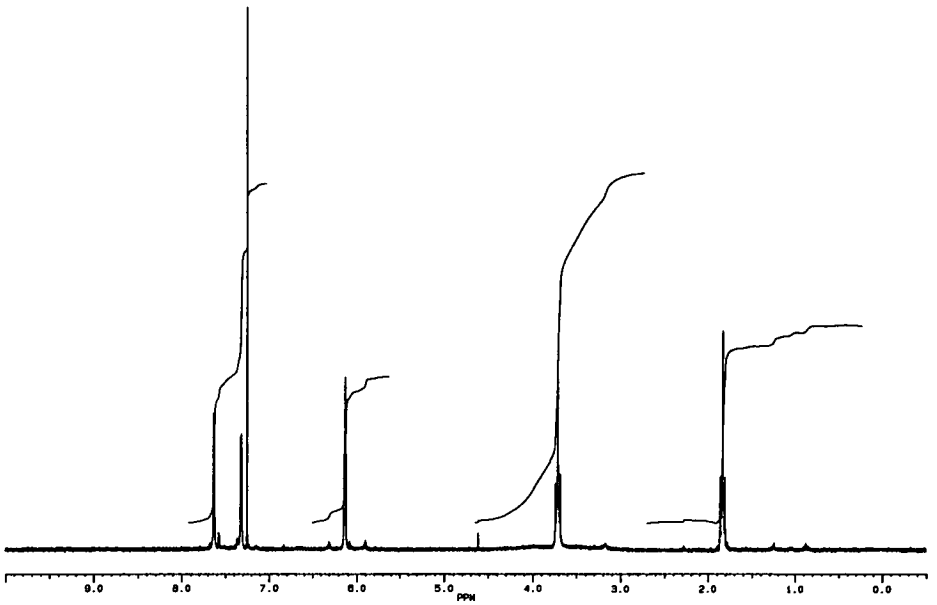

Figure 2.17 ^{1}H NMR spectrum in $CDCl_3$ of 4.

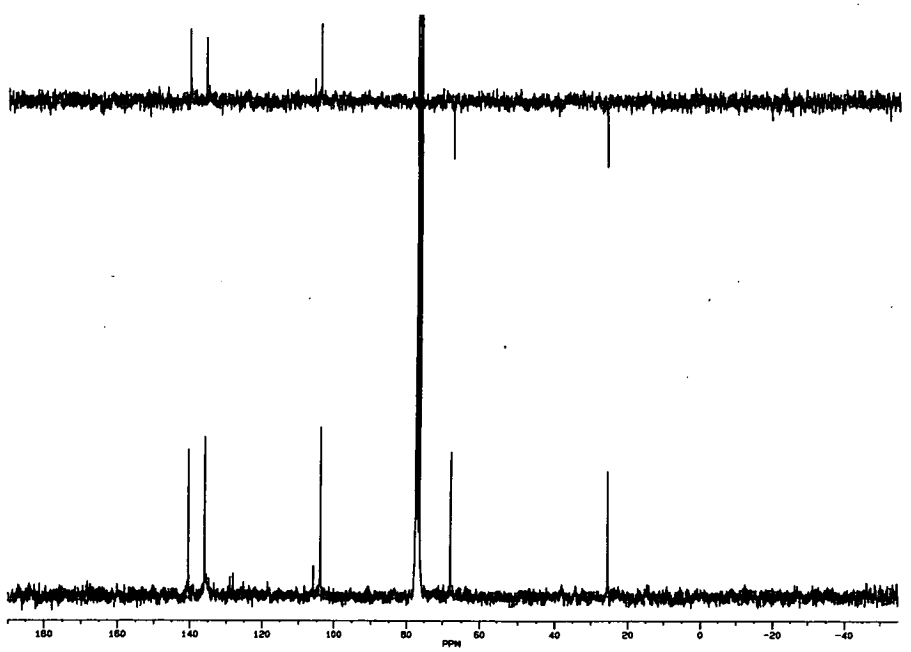

Figure 2.18 ^{13}C NMR spectrum in $CDCl_3$ of 4.

The X-ray crystal structure of **4** reveals a square-pyramidal geometry around the magnesium atom (Figure 2.19). The dihydrobis(1-pyrazolyl)borate ligands (in a "boat or scorpionate" form) act as bidentate chelates forming the basal plane and the THF solvent occupies the axial position.

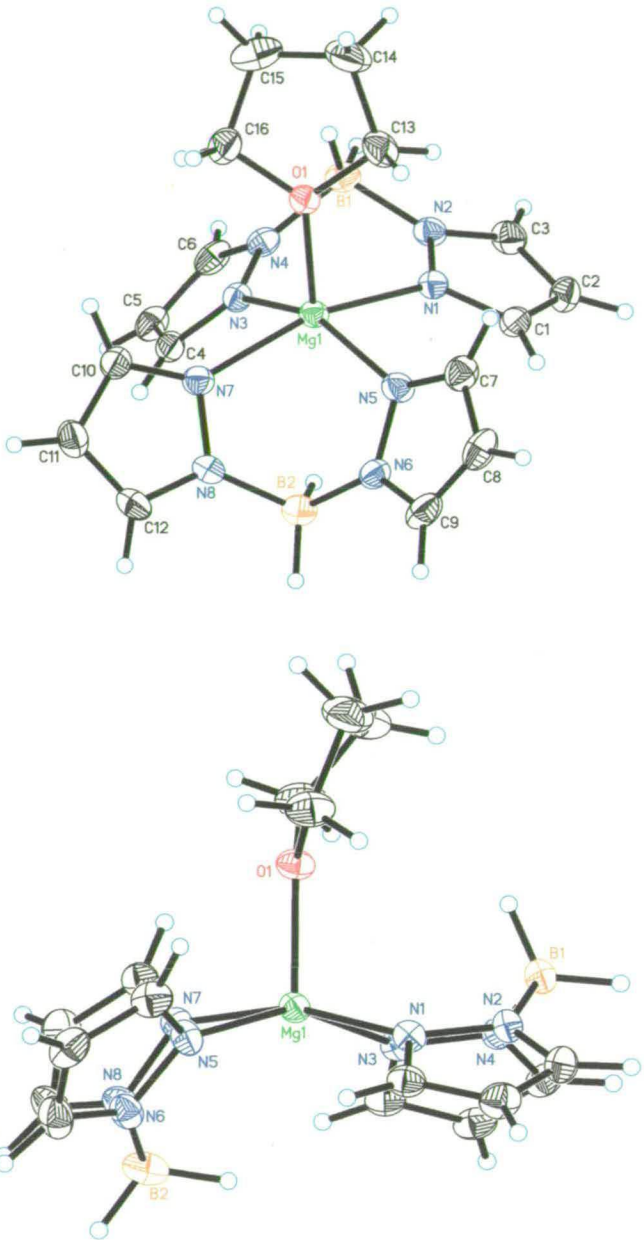

Figure 2.19 Crystallographic structure of 4 with different orientations. Displacement ellipsoids are shown at the 50% probability level.

Analogous to the complex **3**, the Mg-N distances 2.1435(19), 2.1206(19), 2.1467(19) and 2.1643(19) Å are typical of σ-bonding. The strong Mg-O interaction of 2.0238(16) Å agrees well with previously reported values.[21-26] The formation of

the square-pyramidal magnesium complex could also be explained on the basis of the Schlenk equilibrium explained in Figure 2.16. The dissociation should take place by the formation of a monomeric magnesium complex which reacts quickly with the excess ligand present and the final product is obtained according to Figure 2.20. Selected bond lengths and angles are shown in Table 2.2.

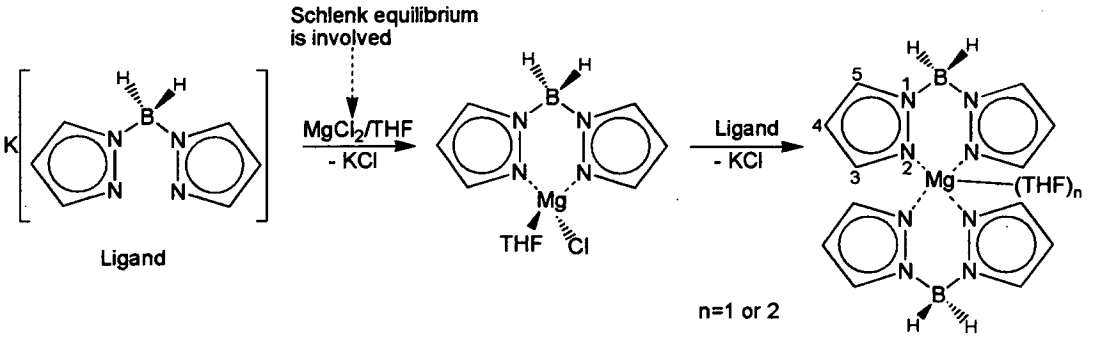

Figure 2.20 Dissociation of the Grignard reagent and monomeric reactivity with the ligand.

Table 2.2 Selected bond distances (Å) and angles (°) for 4.

Mg(1)-O(1)	2.0238(16)	Mg(1)-N(3)	2.1206(19)	Mg(1)-N(1)	2.1435(19)
Mg(1)-N(5)	2.1467(19)	Mg(1)-N(7)	2.1643(19)	N(1)-N(2)	1.367(2)
N(2)-B(1)	1.555(3)	N(3)-N(4)	1.367(2)	N(4)-B(1)	1.546(3)
N(5)-N(6)	1.356(2)	N(6)-B(2)	1.541(4)	N(7)-N(8)	1.362(2)
N(8)-B(2)	1.543(4)				

O(1)-Mg(1)-N(3)	106.49(7)	O(1)-Mg(1)-N(1)	98.59(7)
N(3)-Mg(1)-N(1)	87.54(7)	O(1)-Mg(1)-N(5)	99.52(7)
N(3)-Mg(1)-N(5)	153.99(8)	N(1)-Mg(1)-N(5)	88.95(7)
O(1)-Mg(1)-N(7)	98.16(7)	N(3)-Mg(1)-N(7)	88.62(7)
N(1)-Mg(1)-N(7)	163.23(8)	N(5)-Mg(1)-N(7)	87.37(7)
N(1)-N(2)-B(1)	120.85(18)	N(4)-N(3)-Mg(1)	122.86(13)
N(3)-N(4)-B(1)	120.86(18)	N(6)-N(5)-Mg(1)	113.83(13)
C(9)-N(6)-N(5)	109.1(2)	N(5)-N(6)-B(2)	118.7(2)
N(8)-N(7)-Mg(1)	113.86(13)	N(7)-N(8)-B(2)	118.08(19)
N(4)-B(1)-N(2)	107.89(19)	N(6)-B(2)-N(8)	107.8(2)

2.2.4 Reactivity of Potassium Dihydrobis(1-pyrazolyl)borate with MeMgCl (1-3 days reaction)

Several treatments of **1** with an equimolar amount of MeMgCl in THF at room temperature were carried out, and the reactions were stopped between 1 and 3 days. For every reaction KCl was removed, and extraction from diethyl ether produced a white powder which, followed by re-crystallisation from diethyl ether,

produced colourless crystals of the bis-THF complex $[\{H_2B(pz)_2\}_2Mg(THF)_2]$ (**5**). The synthesis of **5** by treatment with AllylMgCl in THF was also achieved. The NMR spectra were recorded and show similar spectra for all the obtained complexes, analogous to previous reactions (Figure 2.17 and 2.18). One type of pyrazolyl group at room temperature is shown, indicating a rapid inversion of the co-ordinated $[H_2B(pz)_2]^-$ ligand. In the ^1H NMR spectrum of **5**, two singlets at δ 3.70 and 1.83 indicate the presence of co-ordinated THF. The doublet signals at δ 7.65 and 7.28 are assigned as H5 and H3, whilst a triplet at δ 6.18 is assigned as H4 (Figure 2.21). The ^{13}C NMR spectrum gives two sets of signals at δ 68.30 and 25.10 which are also assigned to the THF solvate, whilst C3, C5 and C4 are placed at δ 142.01, 136.50 and 104.22, respectively (Figure 2.22).

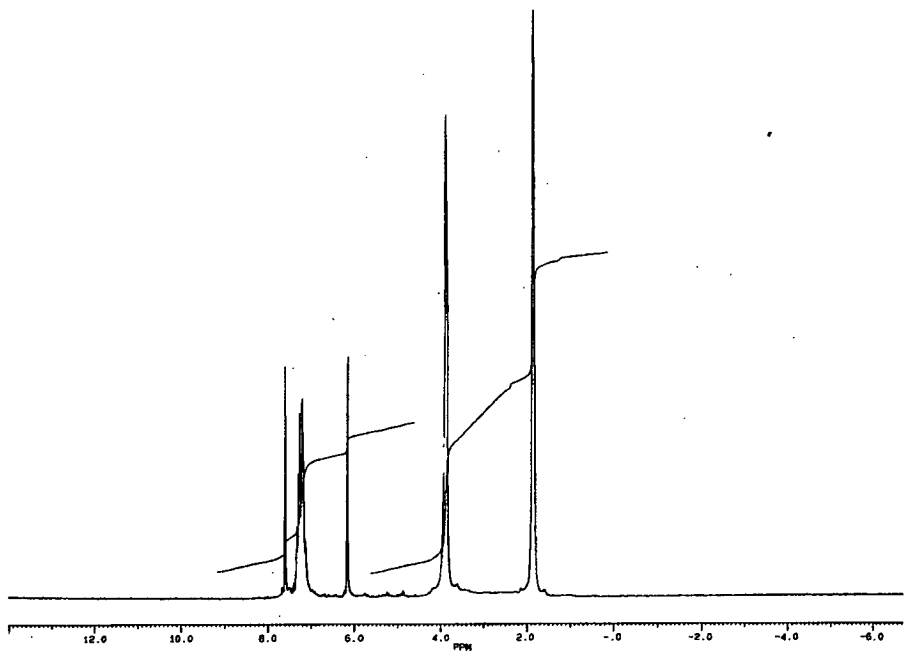

Figure 2.21 ^1H NMR spectrum in $CDCl_3$ of 5.

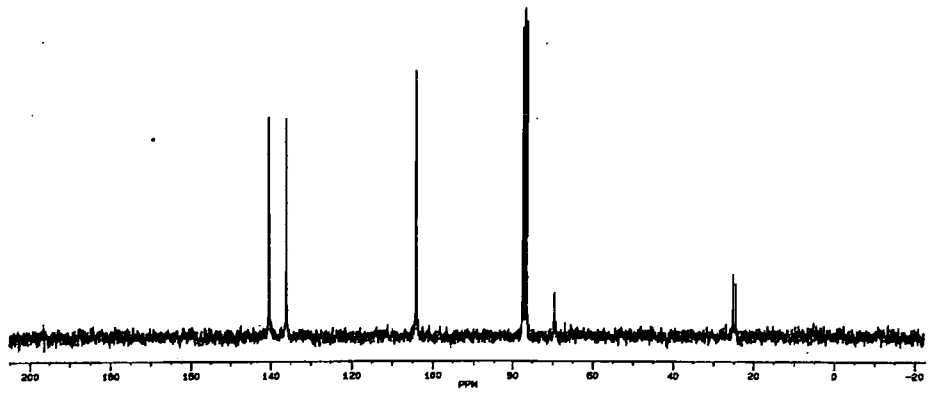

Figure 2.22 ^{13}C NMR spectrum in $CDCl_3$ of 5.

The X-ray crystal structure of **5** reveals a monomeric complex (Figure 2.23), with an octahedral geometry around the magnesium atom. The axial co-ordination sites are occupied by the oxygen atoms of two THF molecules. The magnesium complex contains a two-fold axis perpendicular to the O(1)-Mg-O(2) axis. The $[H_2B(pz)_2]^-$ ligands are co-ordinating in κ2 fashion, and the Mg-N distances of 2.1960(14) and 2.1908(13) Å in the chelated ligands are typical σ-bonding distances. The THF molecules are disordered having two conformations with occupancies of 50% each. The longer bond length observed for Mg-O of 2.17351(12) Å is due to the "pushing-pulling" effect over the magnesium atom for each THF molecule. The "pushing-pulling" effect makes a more regular octahedral structure, where the THF solvents are nearly perpendicular to the magnesium-nitrogen atom plane, with angles of 90.61(4) and 89.39(4)° for N-Mg-O, respectively. Selected bond lengths and angles are shown in Table 2.3.

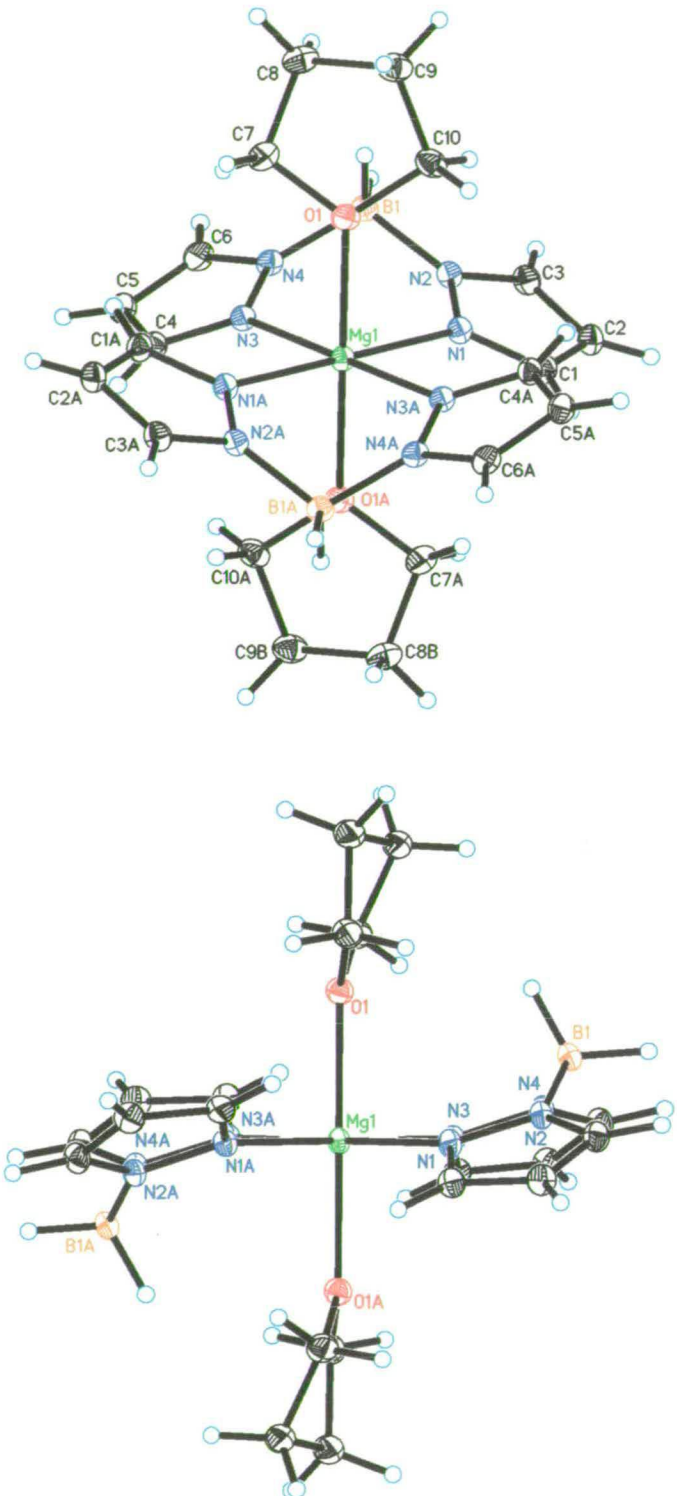

Figure 2.23 Crystallographic structure of 5 with different orientations. Displacement ellipsoids are shown at the 50% probability level.

Table 2.3 Selected bond distances (Å) and angles (°) for 5. Symmetry transformations used to generate equivalent atoms: #1 -x+1,-y+1,-z+1.

Mg(1)-O(1)	2.1735(12)	Mg(1)-O(1)#1	2.1735(12)	Mg(1)-N(1)#1	2.1908(13)
Mg(1)-N(1)	2.1908(13)	Mg(1)-N(3)#1	2.1960(14)	Mg(1)-N(3)	2.1960(14)
N(1)-N(2)	1.3670(15)	N(2)-B(1)	1.549(2)	N(3)-N(4)	1.3643(15)
N(4)-B(1)	1.5493(19)				

O(1)-Mg(1)-O(1)#1	180.000(1)	O(1)-Mg(1)-N(1)#1	89.39(4)
O(1)#1-Mg(1)-N(1)#1	90.61(4)	O(1)-Mg(1)-N(1)	90.61(4)
O(1)#1-Mg(1)-N(1)	89.39(4)	N(1)#1-Mg(1)-N(1)	180.0
O(1)-Mg(1)-N(3)#1	90.63(4)	O(1)#1-Mg(1)-N(3)#1	89.37(4)
N(1)#1-Mg(1)-N(3)#1	88.23(6)	N(1)-Mg(1)-N(3)#1	91.77(6)
O(1)-Mg(1)-N(3)	89.37(4)	O(1)#1-Mg(1)-N(3)	90.63(4)
N(1)#1-Mg(1)-N(3)	91.77(6)	N(1)-Mg(1)-N(3)	88.23(6)
N(3)#1-Mg(1)-N(3)	180.0	N(2)-N(1)-Mg(1)	122.47(9)
N(1)-N(2)-B(1)	123.21(11)	N(4)-N(3)-Mg(1)	122.26(8)
N(3)-N(4)-B(1)	123.83(11)		

2.2.5 Reactivity of Potassium Dihydrobis(1-pyrazolyl)borate with ($PhCH_2$)MgCl

Reaction of **1** with an equimolar amount of ($PhCH_2$)MgCl in THF at room temperature was carried out, and the reaction was stopped after 1 hour. KCl was filtered off, and extraction from diethyl ether produced a colourless oil. NMR spectra show formation of a possible monomeric magnesium species containing one co-ordinated THF molecule (Figure 2.24). The ^{1}H NMR spectrum of [{$H_2B(pz)_2$}Mg(CH_2Ph)THF] (**6**) places the H5 and H3 doublets at δ 7.64 and 7.32, respectively, whilst the H4 triplet is placed at δ 6.14. The significant peak for the co-ordinated Mg-CH_2- gives a characteristic upfield value at δ 1.12, while the upfield aromatic *m*-C_6H_5, *o*-C_6H_5 and *p*-C_6H_5 resonances are placed at δ 7.28, 7.12 and 6.75, respectively. Two signals at δ 3.73 and 1.85 are assignable to the THF solvated (Figure 2.25). The ^{13}C NMR spectrum of **6** shows downfield shifts for C3, C5 and C4 at δ 142.10, 136.10 and 104.30, respectively. The Mg-CH_2- shifts to δ 22.10, whilst the *ipso*-C_6H_5, *m*-C_6H_5, *o*-C_6H_5 and *p*-C_6H_5 downfield aromatic peaks are observed at δ 148.10, 128.70, 126.12 and 113.80, respectively (Figure 2.26). Two sets of signals at δ 67.20 and 25.30 are assigned to the THF solvated. Attempts were made to crystallise the colourless oil, but only the bis-ligand complex (**5**) was obtained.

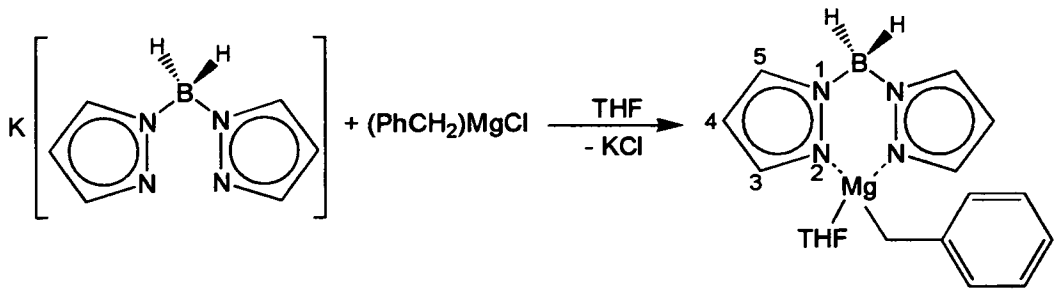

Figure 2.24 Reactivity of 1 and $(PhCH_2)MgCl$ (1 hour reaction).

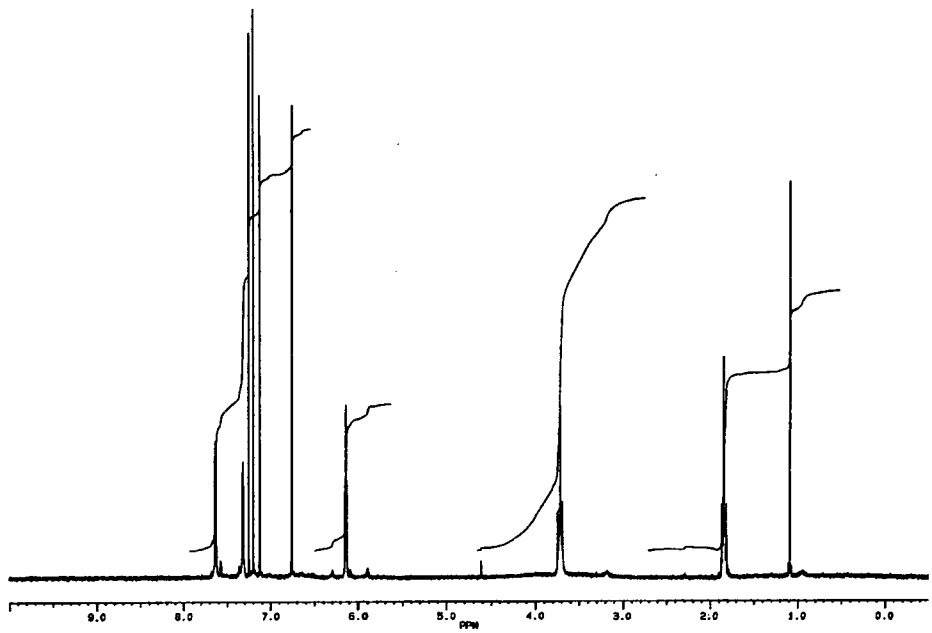

Figure 2.25 ^1H NMR spectrum in $CDCl_3$ of 6.

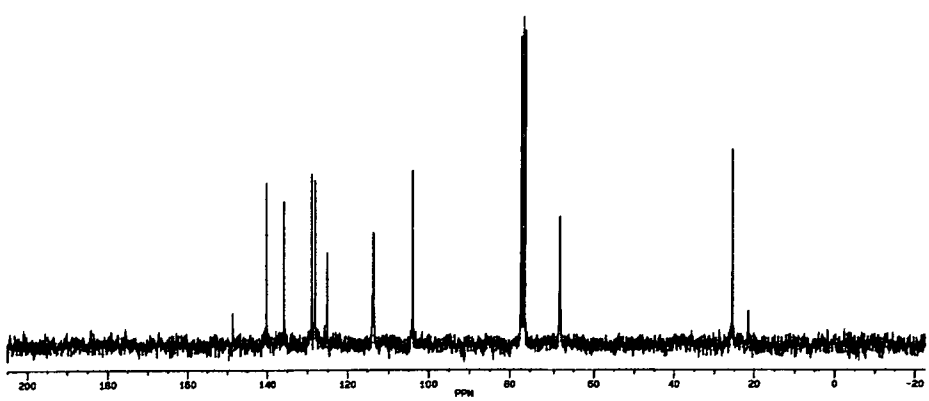

Figure 2.26 ^{13}C NMR spectrum in $CDCl_3$ of 6.

2.2.6 Reaction of $(PhCH_2)MgCl$ Grignard Reagent with Crude Potassium Dihydrobis(1-pyrazolyl)borate

Although crude **1** has been suitable for reactions with transition-metal ions,[1] its purification requires a difficult process. In some cases KBH_4 is still present, and the final product needs several steps to be obtained completely pure.

The reaction of crude **1** with an equimolar amount of $(PhCH_2)MgCl$ Grignard reagent in THF at room temperature was carried out for 1 hour, after which the reaction was stopped and KCl removed. Extraction from diethyl ether produced a colourless oil. NMR spectra mainly show the formation of **5** (Figure 2.21 and 2.22). Although, the structure of **5** was identified using X-ray crystallography, a few crystals of $[\{H_2B(pz)_2\}Mg(THF)_3][B(CH_2Ph)_4]$ (**7**) were also isolated (Figure 2.27), which could not be characterised by NMR spectra. The small amount of KBH_4 in the crude **1** is also soluble in THF, but should react easily with the $(PhCH_2)MgCl$ Grignard reagent, according to Figure 2.28. Comins and Herrick have reported reduction of esters at –20 °C by adding mixtures of $LiBH_4$ (**I**) and BuMgCl (**II**), but no reactivity between **I** and **II** was reported.[26] In addition, it is possible that reduction might occur faster than the addition of Grignard reagent. However, it is possible that at room temperature the substitution should take an important role in order to produce reactivity between KBH_4 and $(PhCH_2)MgCl$.

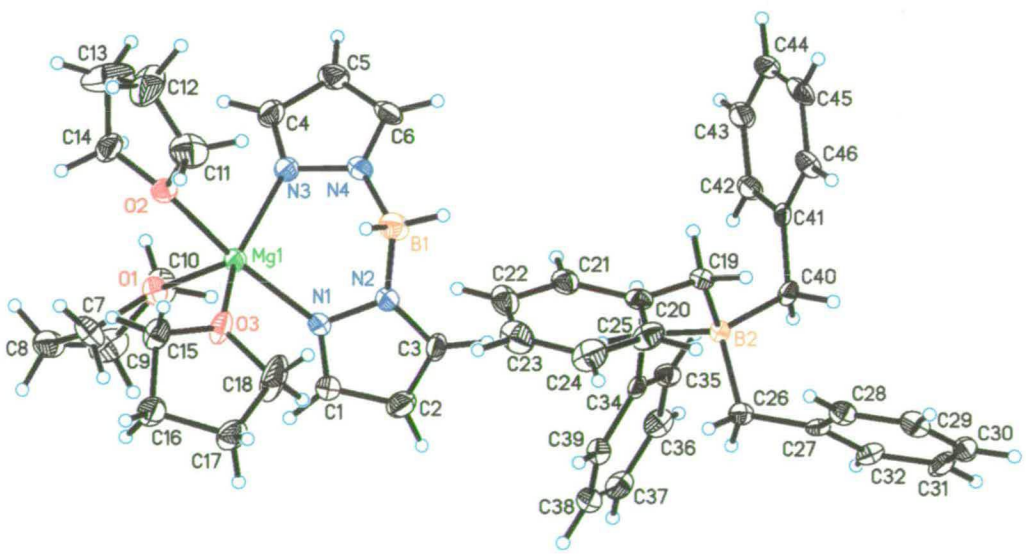

Figure 2.27 Crystallographic structure of 7. Displacement ellipsoids are shown at the 50% probability level.

$$[K\{H_2B(pz)_2\}] + KBH_4 \xrightarrow{(PhCH_2)MgCl/THF} [\{H_2B(pz)_2\}Mg(THF)_3][B(CH_2Ph)_4] + KCl$$

Figure 2.28 Reactivity of crude 1 and $(PhCH_2)MgCl$ Grignard reagent.

The X-ray crystal structure of **7** reveals a distorted square-pyramidal monomeric magnesium centre. Significant bond lengths and angles are shown in Table 2.4. The ligand acts in a κ2 fashion and scorpionate form, where the magnesium-nitrogen bond lengths of 2.093(5) and 2.125(4) Å are comparable to previous results (**3-5**). The three disordered THF molecules interacting with magnesium atom rotate freely to produce unremarkable shorter Mg-O bond lengths of 2.002(3), 2.037(3) and 2.058(3) Å, respectively. The counter ion $[B(CH_2Ph)_4]^-$ satisfies the electron needs of the magnesium cation. The boron atom centre shows a tetrahedral geometry, where the B-C bond lengths are 1.673(5), 1.654(5), 1.669(5) and 1.663(5) Å.

Table 2.4 Selected bond distances (Å) and angles (°) for 7.

Mg(1)-O(1)	2.009(3)	Mg(1)-O(3)	2.038(3)	Mg(1)-O(2)	2.063(3)
Mg(1)-N(1)	2.105(3)	Mg(1)-N(3)	2.129(3)	N(1)-N(2)	1.352(4)
N(2)-B(1)	1.541(6)	N(3)-N(4)	1.350(4)	N(4)-B(1)	1.547(6)
B(2)-C(26)	1.654(5)	B(2)-C(40)	1.663(5)	B(2)-C(33)	1.669(5)
B(2)-C(19)	1.673(5)				
O(1)-Mg(1)-O(3)		103.07(12)	O(1)-Mg(1)-O(2)		92.07(11)
O(3)-Mg(1)-O(2)		86.63(11)	O(1)-Mg(1)-N(1)		96.87(12)
O(3)-Mg(1)-N(1)		91.70(12)	O(2)-Mg(1)-N(1)		171.06(13)
O(1)-Mg(1)-N(3)		105.89(12)	O(3)-Mg(1)-N(3)		150.79(14)
O(2)-Mg(1)-N(3)		88.54(12)	N(1)-Mg(1)-N(3)		88.65(12)
N(4)-B(1)-N(2)		108.2(3)	C(26)-B(2)-C(40)		110.6(3)
C(26)-B(2)-C(33)		108.4(3)	C(40)-B(2)-C(33)		110.8(3)
C(26)-B(2)-C(19)		112.0(3)	C(40)-B(2)-C(19)		107.7(3)
C(33)-B(2)-C(19)		107.2(3)			

2.2.7 Reactivity of KBH_4 with $(PhCH_2)MgCl$ Grignard Reagent- Formation of a Novel Polymeric Potassium Salt

In order to investigate the reactivity of KBH_4 with Grignard reagents, a treatment of potassium borohydride with $(PhCH_2)MgCl$ Grignard reagent (1:4 molar ratio) in THF was undertaken, and its reaction produced a fast evolution of hydrogen. Subsequent removal of the solvent in *vacuum*, extraction from ether and

crystallisation from toluene produced colourless crystals of $K[B(CH_2Ph)_4]$ (**8**). The NMR spectra show one type of benzyl group at room temperature (Figure 2.29). The ^1H NMR spectrum of **8** places the -CH_2- upfield singlet at δ 1.99 while the aromatic hydrogen atoms for *m*-C_6H_5, *o*-C_6H_5 and *p*-C_6H_5 are assigned to resonances at δ 7.24, 7.18 and 6.89, respectively (Figure 2.30). ^{13}C NMR spectrum shows downfield aromatic resonances correspondening to *ipso*-C_6H_5, *m*-C_6H_5, *o*-C_6H_5 and *p*-C_6H_5 at δ 157.80, 127.90, 126.30 and 115.40, respectively, while the upfield -CH_2- is placed at δ 22.90 (Figure 2.31). The ^{11}B NMR spectrum contains an intense singlet at δ -12.53.

$$KBH_4 + 4\ (PhCH_2)MgCl \xrightarrow{THF} K[B(CH_2Ph)_4] + H_2 + \text{unknown Mg species}$$

Figure 2.29 Reactivity of KBH_4 and $(PhCH_2)MgCl$ Grignard reagent.

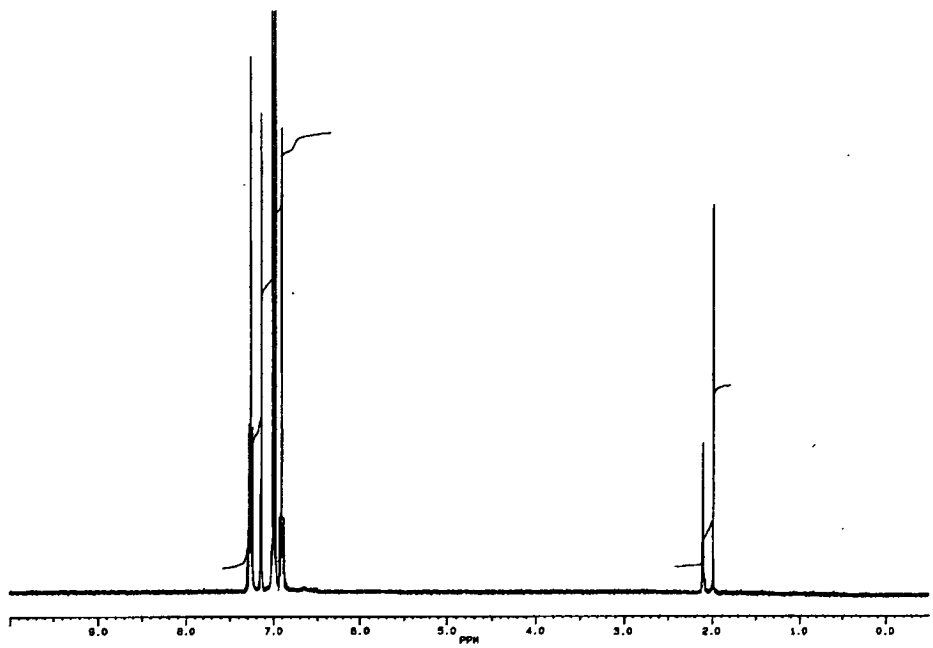

Figure 2.30 ^1H NMR spectrum in toluene-d_8 of 8.

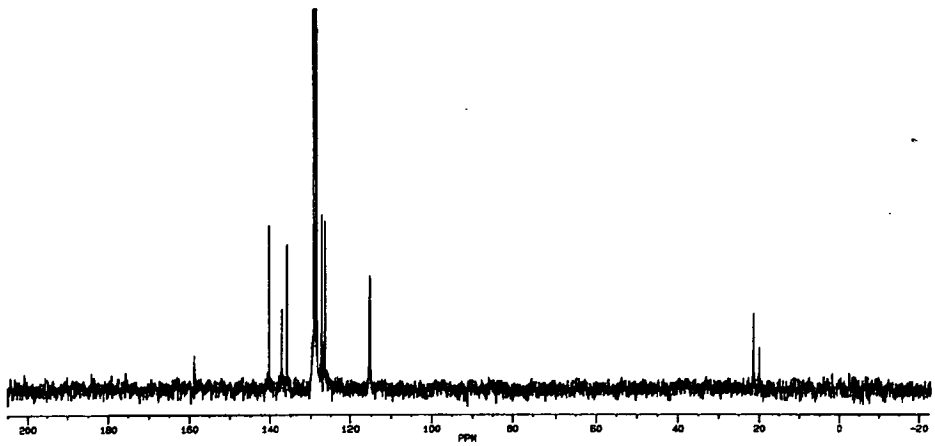

Figure 2.31 ^{13}C NMR spectrum in toluene-d_8 of 8.

X-ray crystallography of the structure was conducted revealing a novel polymeric structure for **8** illustrated in Figure 2.32. The high diffusive electron density of the phenyl rings permits $(\eta^6\text{-}C_6H_5)\cdots K^+$ interactions which are not orthogonal to the metal-to-ring axis. The easy solvation of the potassium ion induces second interactions such as $(\eta^2\text{-}C_6H_5)\cdots K^+$, which occur between the potassium ion and the Cα and Cβ atoms from the aromatic groups. In addition, unusual interactions $CH_2\cdots K^+$ are identified and also explained by the solvation effect on the potassium ion.

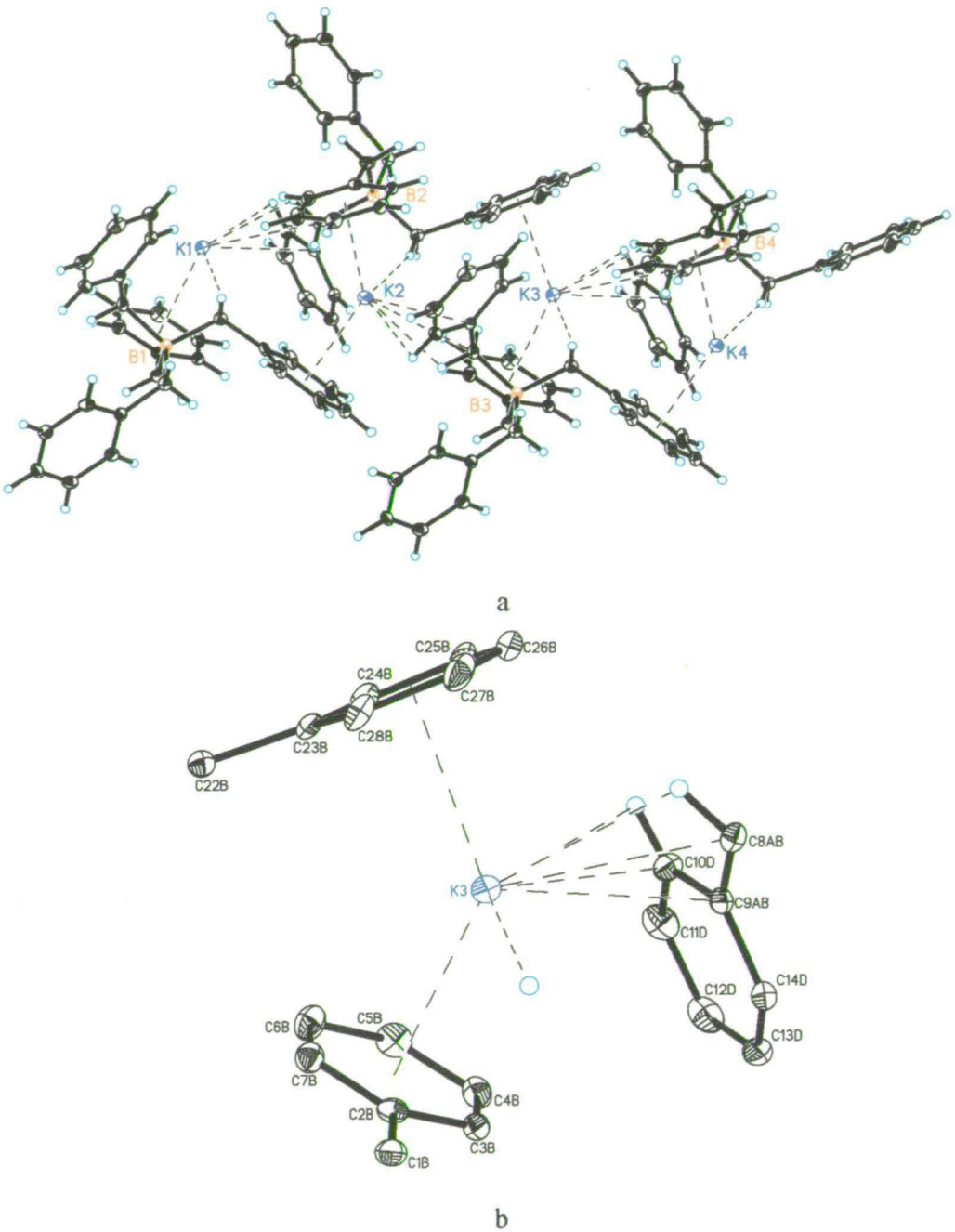

Figure 2.32 Crystallographic structure of 8: Polymeric view (a) and core (b). Displacement ellipsoids are shown at the 50% probability level.

Similar research carried out by Armstrong *et al.*[27] indicates that $(PhCH_2)_2N^-$ ligands are susceptible to competitive interactions of CH units with a Li ion, suggested by a high electron demand from the Li. In addition, the charge on the

amide N could be delocalizated when the benzyl group is orientated towards the metal atom. The explanation given by Armstrong *et al.*[27] can be exemplified using Figure 2.33, where if N presents a single lone pair of electrons, the torsion angle between N-CH_2-Cα-Cβ would be more than 90°, and the lone pair position should be situated in a non-interactive position with the benzyl unit (Figure 2.33a). If there is a negative charge on the atom close to the CH_2, however, the torsion angle between N-CH_2-Cα-Cβ could be closer to 90°, and the two lone pairs could be orientated towards the aromatic ring belonging to the benzyl unit (Figure 2.33b). A negative charge on the nitrogen atom could produce a dipolar moment towards the aromatic group, resulting in a charge concentration over the CH_2. The partial negative charge on the CH_2 group suggests the possibility of an interaction with the metal, as demonstrated by Barr *et al.*[28]

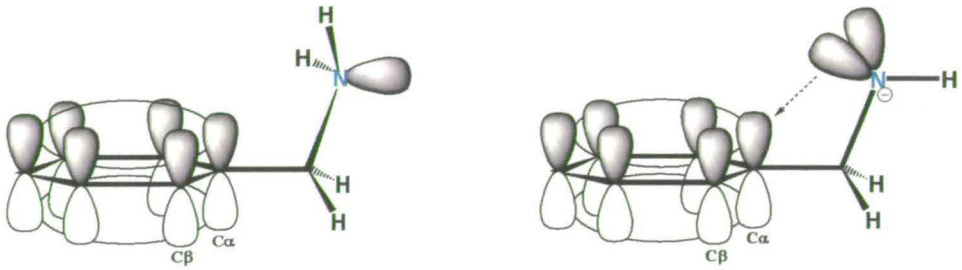

Figure 2.33 Possible interaction and transference of charge: (a) one lone pair of electrons; (b) two lone pairs of electrons.

It is believed that K···benzyl interactions may be responsible for the changed state of association of the K ions themselves, and could cause the much closer approach of the benzyl units to the K atoms in Figure 2.32, which in turn, sterically necessitates expansion to a large ring system. *Ab initio* calculations on $K[B(CH_2Ph)_4]$ monomer using extended Hückel values and the analysis of Mulliken population for assigning charges have been undertaken. Mulliken population analysis is an arbitrary scheme for assigning charges, and due to the electron density, a quantum mechanism is not observable; such schemes are ultimately arbitrary. The boron atom is a significant site of negative charge (-0.65), but this atom also transfers charge to the aromatic group by the closeness to it. The increase of polarity towards the benzyl groups could be illustrated by a strong dipole moment (12.11 Debye). The charge

transference process from the boron atom to the benzyl group produces a high accumulation of charge around the CH_2 groups, and this effect is represented by a negative charge on each CH_2 group (-0.69). Moreover, the electronic requirement of the K (0.91) atom is satisfied by the formation of a polymeric association suggesting the stability of the polymeric complex.

Analysis of the structure **8** shows (η^6-C_6H_5)···K^+ distances that range from 3.204(3) Å to 3.308(3) Å (the η^6 hapticity suggests that the cone angle is 134.51°) while those (η^2-C_6H_5)···K^+ have values of 3.179(3) Å (for Cα) and 3.084(3) Å (for Cβ). Longer K···CH_2 bond distances of 3.309(3) Å represent a genuine bending of the benzyl groups towards the K atoms, and it has been proposed that these kinds of K···CH interactions may contribute significantly to the stereochemistry and bonding of the K-alkyl. Evidence for intramolecular K···H interaction has also been proposed, as contributing significantly to the stereochemistry and bonding of the compound, with K···H of 2.956 Å (HCβ), 2.819 Å (HCH intermolecular), and 2.385 Å (HCH close to Cα). Selected bond distances and angles are provided in Table 2.5.

Table 2.5 Selected bond distances (Å) and angles (°) for 8. Symmetry transformations used to generate equivalent atoms: #1 -x+1,y+1/2,-z+1; #2 -x+1,y-1/2,-z+1.

K(1)-C(2)	3.248(3)	K(1)-C(3)	3.204(3)	K(1)-C(4)	3.177(3)
K(1)-C(5)	3.161(3)	K(1)-C(6)	3.173(3)	K(1)-C(7)	3.207(3)
K(1)-C(9)#1	3.179(3)	K(1)-C(10)#1	3.084(3)	K(1)-C(23)#2	3.183(3)
K(1)-C(24)#2	3.122(3)	K(1)-C(25)#2	3.207(3)	K(1)-C(28)#2	3.235(3)
B(1)-C(1)	1.655(4)	B(1)-C(8)	1.666(4)	B(1)-C(15)	1.665(4)
B(1)-C(22)	1.668(4)	C(8)-K(1)#2	3.309(3)	C(9)-K(1)#2	3.179(3)
C(10)-K(1)#2	3.084(3)	C(23)-K(1)#1	3.183(3)	C(24)-K(1)#1	3.122(3)
C(25)-K(1)#1	3.207(3)	C(26)-K(1)#1	3.308(3)	C(27)-K(1)#1	3.306(3)
C(28)-K(1)#1	3.235(3)				
C(1)-B(1)-C(8)		108.65(19)	C(15)-B(1)-C(8)		112.7(2)
C(1)-B(1)-C(15)		107.03(19)	C(1)-B(1)-C(22)		112.4(2)
C(15)-B(1)-C(22)		107.38(19)	C(8)-B(1)-C(22)		108.7(2)

D-H...A	d(D-H)	D(H...A)	d(D...A)	<(DHA)
C(22)-H(22A)...K(1)	0.97	2.82	3.761(3)	164.0
C(8)-H(8A)...K(1)	0.97	3.36	4.196(3)	145.3

2.2.8 Analysis of [K{$H_2B(pz)_2$}] Ligand

Bis(pyrazolyl)borate has been previously compared to β-diketonate, and Cp or Cp*, to tris(pyrazolyl)borate,[1] but very little information has been available regarding their solid-state structures. Although such comparisons have been considered, they fail to provide an understanding of the close relationship between bis- and tris(pyrazolyl)borates. The present study could explain the close relationship between the bis(pyrazolyl)borate and tris(pyrazolyl)borate with Cp.

Observation of the different resonance structures for bis(pyrazolyl)borate (Figure 2.34) could neutralise the negative charge on the boron atom by a positive charge on the closest nitrogen atom. In addition, both bis- and tris(pyrazolyl)borate are used as potassium complexes, and the potassium atom, which has huge electron demands, could help us to understand three kind of interactions for poly(pyrazolyl)borates.

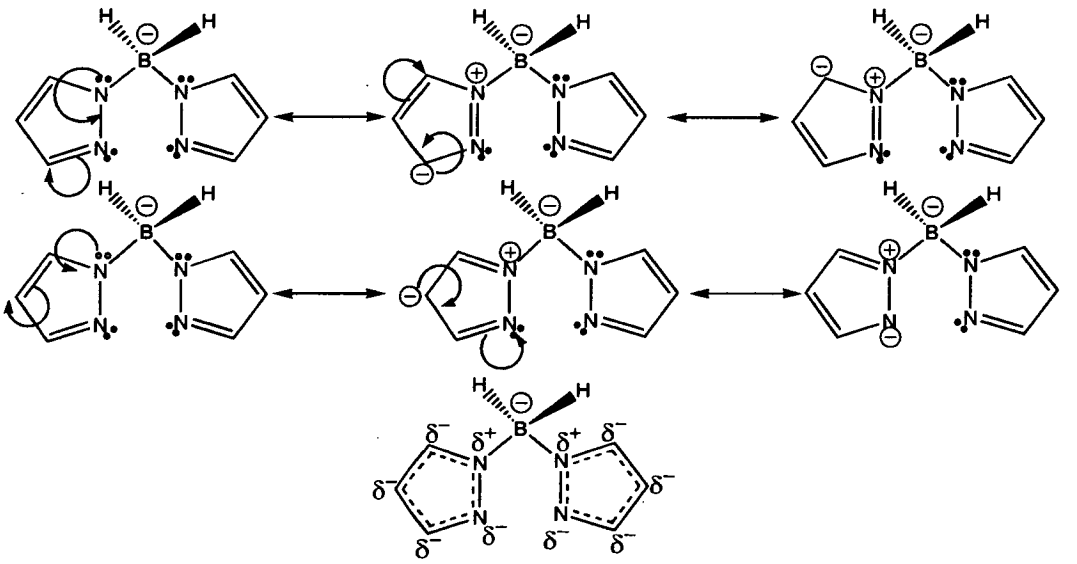

Figure 2.34 Delocalization of charge around the rings of a bis(pyrazolyl)borate ion.

Firstly, observation of the bis(pyrazolyl)borate resonance structures suggest σ-bonding interactions with the potassium atom in a κ2 fashion co-ordination (Figure 2.35a). Secondly, delocalization of the lone paired electrons around the five membered ring makes partial negative charges for their atoms possible, even the

closest nitrogen atom to the boron shows a concentration of charge when holding its lone pair electrons. Moreover, the disposition of both rings to hold charges makes (η^5-pyrazole)···K interactions possible by π-bonding contacts (Figure 2.35b). Thirdly, an inductive effect from the boron atom towards their hydrogen atoms may produce a concentration of charge on each hydrogen atom, and this could also induce interactions with the metal. The inductive effect with the metal is well known as a μ_2 donor (bridging hydride), and is illustrated in Figure 2.35c. Finally, there could be an excellent delocalization of electrons around rings and localization of the lone pair electrons on nitrogen atoms in the same magnitude or order, making possible three kinds of interactions simultaneously, according to Figure 2.35d.

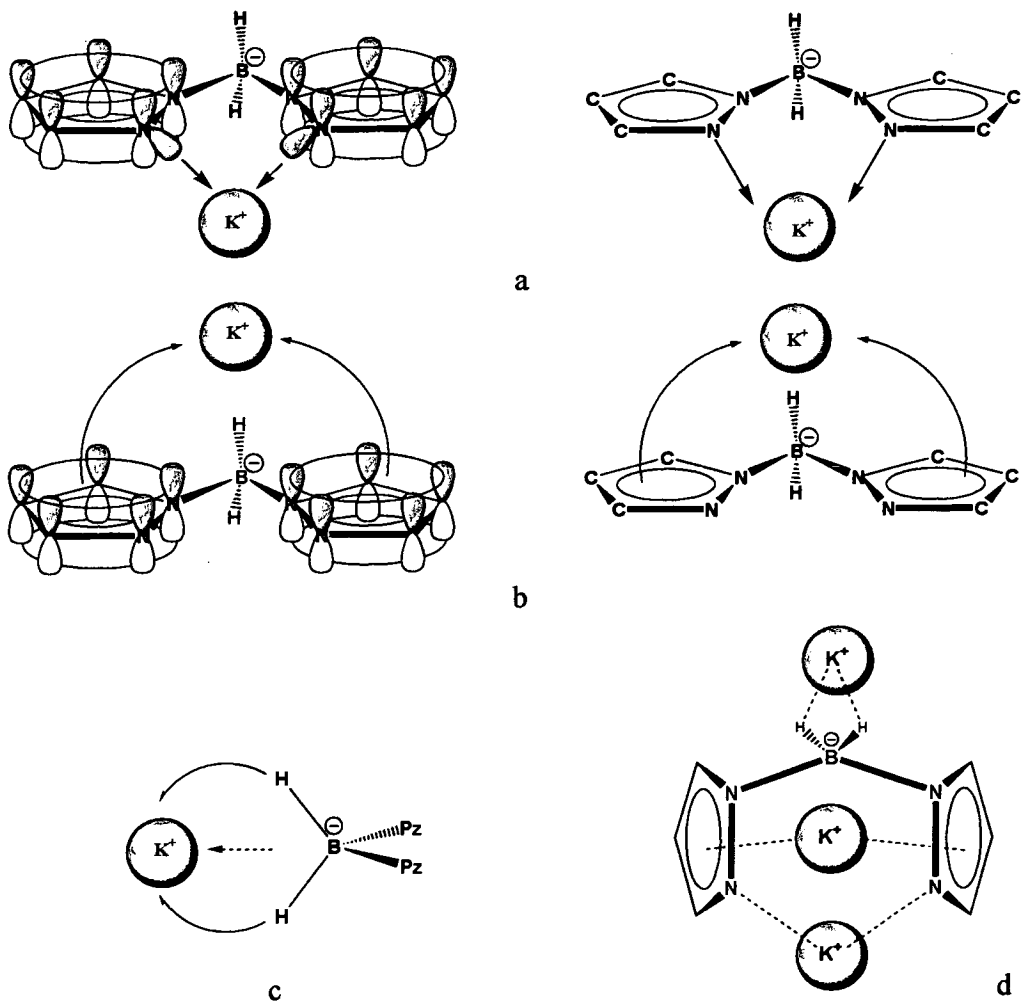

Figure 2.35 Possible interactions between the bis(pyrazoly)borate and potassium: (a) σ, (b) η^5, (c) μ_2 donor and (d) all of three. Hydrogen atoms have been omitted for clarity.

Tris(pyrazolyl)borate, which shows similar resonance structures to bis(pyrazolyl)borate (Figure 2.36), produces a much stronger delocalization of charge using its three rings. This, however, may change according to the metal used for the interaction.

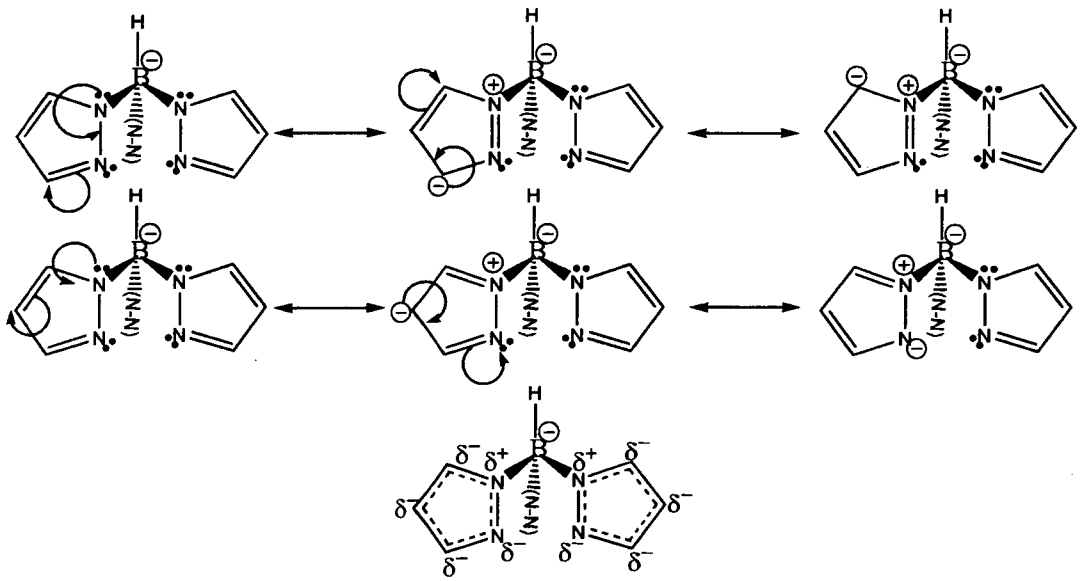

Figure 2.36 Delocalization of charge around the rings of a tris(pyrazolyl)borate ion.

Comparing potassium bis(pyrazolyl)borate and potassium tris(pyrazolyl)borate, it can be seen that in both complexes similar interactions to those illustrated in Figure 2.35 are present. In the tripodal ligand, the charge will be much better delocalized around three rings than around two rings, and each ring could act like a potential η^5-pyrazol donor, according to the relationship named by Trofimenko.[1] In addition, interactions between the potassium atom and the ligand in a κ3 fashion also occur. Finally, the bridging of the hydride to the potassium atom (μ-BH)···K could occur (Figure 2.37).

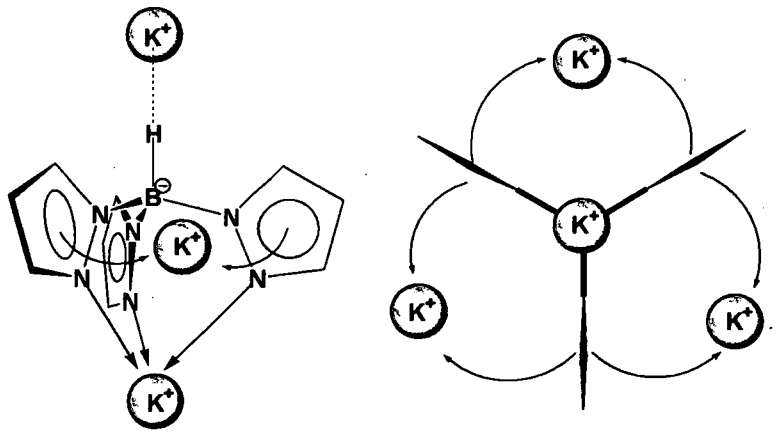

Figure 2.37 Possibility of interaction between the tris(pyrazoly)borate and potassium: η^5 and μ_2 and donor σ.

Dias *et al.*[16,29] have reported σ-bonding interactions between potassium ion and fluorinated poly(pyrazolyl)borate ligands, whilst (μ-BH)···K interactions have been only observed for bis(pyrazolyl)borate ligands. Hu and Gorun[30], however, have reported a novel η^5-coordination mode of tri(pyrazolyl)borate ligands, where one ring acts not only as a σ-N donor but also as an η^5-pyrazole π donor.

The X-ray crystal structure analysis for **1** was conducted, and the structure is illustrated in Figure 2.38. The polymeric structure suggests a high charge delocalization by (η^5-pyrazole)-K^+ interactions and σ-bonding in a κ2 fashion. Also, the bridging of the hydride to the potassium atom (μ-BH_2)···K is also present, where two hydrogen atoms of the BH_2 group co-ordinate through a μ-interaction to two different potassium atoms. A monomeric structure could suggest an electron deficient potassium atom, however, in a polymeric structure the electron requirement of the potassium atom is satisfied by its multiple interactions. There could be some difficulty in determining which of the resonance structures predominates over the rest, because they all show similar importance. Using magnesium, however, which is smaller than potassium, the predominant co-ordinating resonance structure shows a κ2 pattern, with σ-bonding interactions with the magnesium atom.

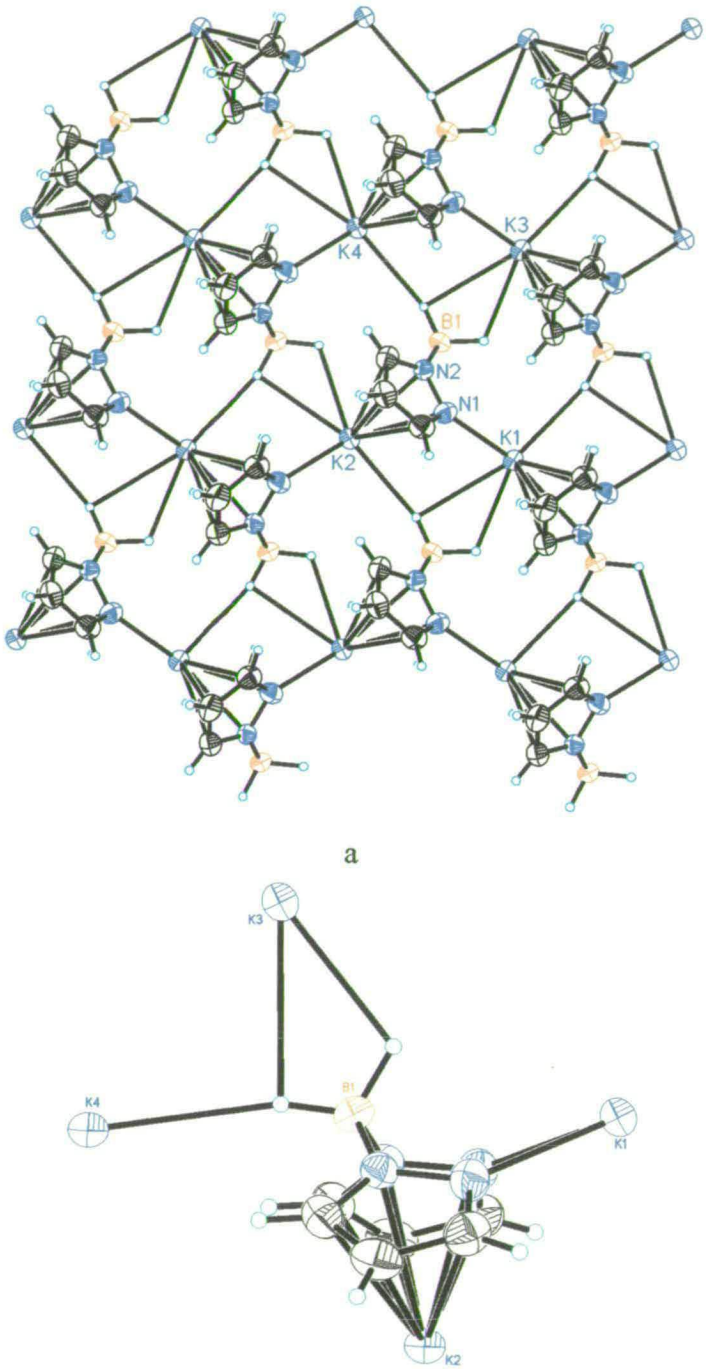

Figure 2.38 Crystallographic structure of 1: Polymeric view (a) and core (b). Displacement ellipsoids are shown at the 50% probability level.

Analysis of the structure shows values for (η^5-pyrazole)-K^+ distances between 3.026-3.500 Å (with an average of 3.215 Å). When (η^5-pyrazole)-K^+

contacts in Tp^{CF_3,CH_3} (3.355 Å) and (η^5-indol)-K^+ (3.640 Å)[30] are compared with (η^5-pyrazole)-K^+ contacts from potassium bis(pyrazolyl)borate, the relative average distance suggests a stronger π-bond with the potassium atom for the latter. In addition, 3.215 Å shows a stronger interaction than other reported (η^6-arene)-K^+ contacts (Figure 2.32). The σ-bonding interactions with the potassium atom have shorter contacts, with an average value of 2.786 Å, whilst K···H contacts are slightly shorter than π-interactions providing extra stability to the polymeric complex (2.820 Å). The polymeric structure shows that the ring planes of the (η^5-pyrazole) are not orthogonal to the metal-to-ring axis, and the η^5 hapticity in Figure 2.38 suggests that the cone angle is 98.13°, compared to 180° for Tp's and 100° for Cp.[30] More information and significant distances and angles are listed in Table 2.6.

Table 2.6 Selected bond distances (Å) and angles (°) for 1. Symmetry transformations used to generate equivalent atoms: #1 -x+1,-y+1,z-1/2; #2 x,-y+1,z-1/2; #3 -x+1,y,z; #4 -x+1,-y+1,z+1/2; #5 -x+1,-y,z-1/2.

K^+ σ interactions					
K(1)-N(1)$^{\#1}$	2.786(17)	K(1)-N(1)$^{\#2}$	2.786(17)	N(1)$^{\#1}$-K(1)-N(1)$^{\#2}$	71.72(6)
K^+ π interactions					
K(1)-N(1)	3.101(19)	K(1)-N(2)	3.026(19)	N(1)$^{\#3}$-K(1)-N(1)	63.51(6)
K(1)-C(1)	3.350(19)	K(1)-C(2)	3.475(19)	N(2)$^{\#3}$-K(1)-N(2)	50.20(6)
K(1)-C(3)	3.273(2)			C(1)$^{\#3}$-K(1)-C(1)	109.75(7)
K^+···(μ-BH_2) interactions					
K(1)-B(1)	3.346(4)	K(1)-H(1)	2.72(3)	N(2)-N(1)-K(1)$^{\#4}$	122.77(9)
K(1)-H(2)	3.04(3)	H(2)-K(1)$^{\#2}$	2.820	N(2)$^{\#5}$-B(1)-K(1)	124.15(12)

2.3 Conclusions

The main interest in preparing magnesium complexes is to investigate their effectiveness as ethene polymerisation catalysts. Originally, we assumed we would form a magnesium alkyl complex similar to [{$H_2B(pz)_2$}MgR] (R: alkyl), a three co-ordinate monomer. Potassium dihydrobis(1-pyrazolyl)borate ligand has been tested and different novel complexes prepared and characterised. The high delocalization of charge around each ring of pyrazole makes several alternatives of co-ordination possible (Figure 2.39a). In addition, reactivity of the ligand with magnesium-like atom suggests co-ordination using its resonance structure with a partial negative charge on each terminal nitrogen atom (Figure 2.39b).

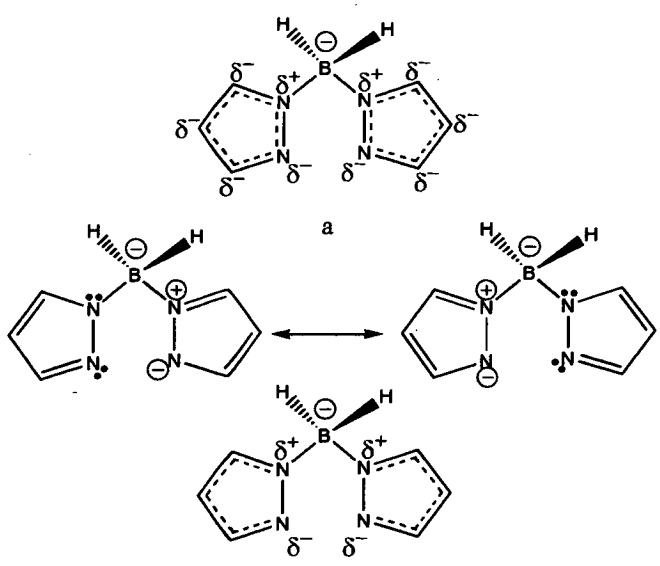

a

b

Figure 2.39 (a) High charge delocalized for 1; (b) Preference of co-ordination by partial negative charges on the terminal nitrogen atoms.

Co-ordination numbers of five or six for magnesium could be facilitated by the relatively high electronegativity and the low steric demand of the dihydrobis(1-pyrazolyl)borate group. In addition, a higher delocalization of π-electrons around the pyrazolyl borate ligand contributes to a partial formal bond with a magnesium atom. The charge transfer from the ligand has the effect of neutralising the formal Mg^{2+}

charge, and this effect does not produce zwitterionic complexes, according to Figure 2.40.

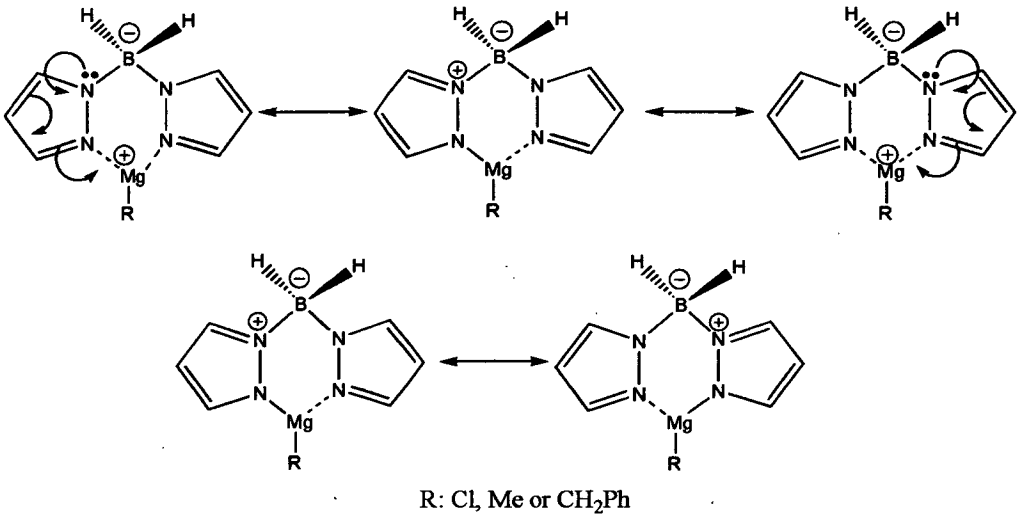

Figure 2.40 Partial formal Mg-N bond by movement of π-electrons around the pyrazole rings toward the magnesium atom.

It is important to point out that the formation of complexes such as $[\{H_2B(pz)_2\}Mg(R)THF]$ (R: Me or CH_2Ph) could take place at the beginning of each reaction (every reaction was done using a 1:1 molar ratio), but the unreacted ligand is always present which could react with the reactive $[\{H_2B(pz)_2\}MgR]$ complex and produce the predominant $[\{H_2B(pz)_2\}_2Mg(THF)_2]$ bis-chelate complex (Figure 2.41). Disproportionation of the Grignard reagent by the Schlenk equilibrium suggests a solvation and association, by which $MgCl_2$ is formed in solution, and associations by μ-bridging halide predominate.

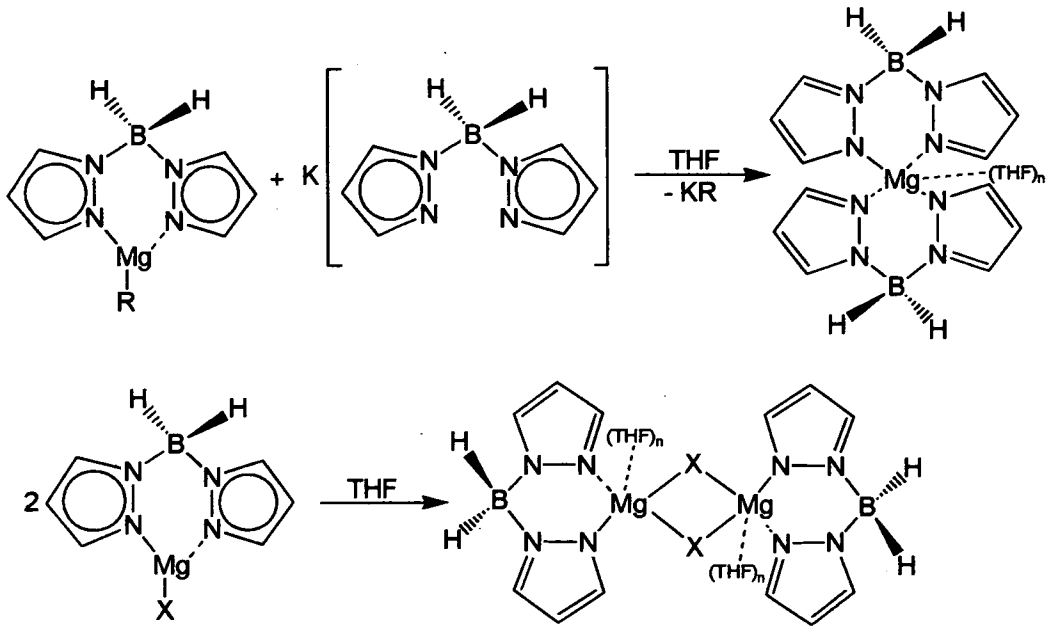

Figure 2.41 Association of [{$H_2B(pz)_2MgR$] (R: Me, CH_2Ph; X: Cl).

2.4 Experimental

2.4.1 General Procedures

All manipulations were carried out under nitrogen atmosphere using standard Schlenk and cannula techniques or in a conventional nitrogen-filled glove-box (Saffron Scientific), fitted with oxygen and water scavenging columns. Solvents were refluxed over an appropriate drying agent, and distilled and degassed prior to use. Solvents and reagents where commercially available were bought from Aldrich, Acros or Fischer, with the exception of NMR solvents which were purchased from Goss Scientific. Diethyl ether, toluene, hexane, benzene and THF were all distilled from Na/benzophenone under a nitrogen atmosphere. NMR solvents were degassed using three freeze-pump-thaw cycles and stored over 4 Å molecular sieves.

2.4.2 Instrumentation

Elemental analyses were performed by sealing aluminium capsules containing approximately 1 mg of compound under nitrogen in the glove box, and performed using a Perkin-Elmer 2400 CHN Analyser. The NMR spectra were recorded on Bruker AC 250 MHz and Varian Gemini 200 MHz spectrometers. Infrared spectra were obtained using a Perkin-Elmer 1600 Paragon Series FT-IR spectrometer as potassium bromide discs or as liquid thin films. Electron impact (EI) mass spectra were obtained either on a Finnigan MAT 4600 quadrupole spectrometer or on a Kratos MS50TC spectrometer. Fast atom bombardment (FAB) mass spectra were obtained on a MS50TC spectrometer. ^{1}H and ^{13}C NMR spectra were referenced to TMS and ^{11}B NMR spectra were referenced to $BF_3(Et_2O)$.

2.4.3 Synthesis

$[K\{H_2B(pz)_2\}]$ (1)

A mixture of finely divided potassium borohydride of (3.851 g, 71 mmol) and pyrazole (9.667 g, 142 mmol) were placed together into a flask which was connected

by a 50 cm air condenser to a volumetric device, and then placed into an oil bath resting on a heating and stirring plate. The oil bath was heated to 90 °C and the mixture was allowed to melt with stirring. Hydrogen evolution started at this point, and continued briskly as the potassium borohydride dissolved. The melt temperature was raised gradually to maintain a steady yet controlled evolution of hydrogen but kept below 125 °C. When the total amount of hydrogen had evolved, the melt was clear or contained a few undissolved potassium borohydride particles. These were removed mechanically, and the still-hot mixture was stirred for about five minutes and filtered hot. The solid was washed over a funnel with warm hexane (two portions of 150 cm^3), and 10.127 g (54.42 mmol, 76% yield) was obtained. Colourless crystals were gown from a concentrated THF solution at room temperature.

IR(KBr): ν(BH) at 2432.5 and 2402.0 cm^{-1}. ^1H NMR (DMSO/ppm): δ 7.30 (d, *H*5), δ 7.20 (d, *H*3), δ 5.84 (t, *H*4). ^{13}C NMR (DMSO/ppm): δ 137.78 (*C*3), δ 133.52 (*C*5), δ 102.49 (*C*4). ^{11}B NMR (DMSO/ppm): δ -5.51. M.p. 171-172 °C

Empirical formula	$C_6H_8BKN_4$	β/ °	90
Formula weight	186.07	γ/ °	90
Crystal system	Orthorhombic	Volume/ $Å^3$	878.1(9)
Space group	$Cmc2_1$	Z	4
a/ Å	17.167(5)	Z'	0.5
b/ Å	5.843(5)	Density calc./ Mgm^{-3}	1.408
c/ Å	8.754(5)	μ(Mo-K)/ mm^{-1}	0.551
α/ °	90		

Data were collected on a Bruker SMART APEX diffractometer[31] equipped with an Oxford Cryosystems low-temperature device at 150 K and using an colourless plate oil-coated crystal[32] of dimension 0.20 x 0.05 x 0.03 mm^3. The initial unit cell was indexed using a least-squares analysis of a random set of reflections collected from three series of 0.3° wide ω-scans, 10 s per frame, and 25 frames per series that were well distributed in reciprocal space. Data frames were collected [Mo Kα = 0.71073 Å] with 0.3° wide ω-scans, 10 s per frame and 600 frames per series. Three complete series were collected at varying φ angles (φ=0, 90, 180°). The crystal to detector distance was 6.0 cm, this providing a set of $4.00 \leq 2\theta \leq 52.78$. A total of 2522 reflections were collected and integrated using SAINT,[33] whilst absorption correction was applied using SADABS[34] with 928 unique [R(int)=0.0204]. System

symmetry, systematic absences and intensity statistics indicated the unique orthorhombic space group $Cmc2_1$. The structure was determined by direct methods with the location of nearly all of the non-hydrogen atoms using the program SHELXS[35] and refined by full-matrix least-squares on F^2 using SHELXL.[36] All non-hydrogen atoms were refined anisotropically, while hydrogen atoms were placed in calculated positions, constrained to ride on their carbon atoms with group U_{iso} values assigned ($U_{iso}(H)= 1.20U_{iso}$). Hydrogen atoms on B were located from the difference map and the positions and the isotropic thermal parameters were refined. The final structure was refined to convergence [$\Delta/\sigma \leq 0.001$] with R(F) = 0.0237 (for 928 data with F>4σF), GOF = 1.004 and *w*R2 = 0.0564 (all data). [$R1 = \Sigma|F_O - F_C|/\Sigma|F_O|$, $wR2 = \{[\Sigma w(F_O^2 - F_C^2)^2]/\Sigma wF_O^4\}^{0.5}$, $w = 1/[\sigma^2(F_O^2) + (xP)^2 + yP]$, $P = (F_O^2+2F_C^2/3)$]. The largest difference between peaks and holes in the final difference map was 0.268 and –0.172 eÅ^{-3}.

[{$H_2B(pz)_2$}Mg(Me)THF] (2)

[K{$H_2B(pz)_2$}] (1.000 g, 5.358 mmol) was dissolved in THF (5 cm^3) and MeMgCl (1.8 cm^3, 3.0 M in THF, 5.358 mmol) was added with stirring at room temperature for 30 minutes. The solvent and volatile components were removed under *vacuum*, diethyl ether added (10 cm^3) and KCl removed under a nitrogen atmosphere through Celite 521. The solvent was removed under *vacuum* and a colourless oil was obtained (3.59 mmol, 67% yield). The final colourless oil turned into an insoluble suspension after 45 minutes and no further analysis could be done.

IR(KBr): ν(BH) at 2409.8 and 2388.5 cm^{-1}. ^{1}H NMR (benzene-d_6/ppm): δ 7.68 (d, *H*5), 7.18 (d, *H*3), 6.12 (t, *H*4), 3.72 (m, THF), 1.83 (m, THF), -0.68 (s, Mg-CH_3). ^{13}C NMR (benzene-d_6/ppm): δ 141.53 (*C*3), 128.30 (*C*5), 104.37 (*C*4), 67.30 (THF), 25.10 (THF), -11.62 (Mg-CH_3). ^{11}B NMR (benzene-d_6/ppm): δ -6.51.

[{$H_2B(pz)_2$}Mg(THF)(μ-Cl)$_2$Mg(THF)$_2${(pz)$_2BH_2$}] (3)

[K{$H_2B(pz)_2$}] (1.000 g, 5.358 mmol) was dissolved in THF (5 cm^3) and MeMgCl (1.8 cm^3, 3.0 M in THF, 5.358 mmol) was added with stirring at room

temperature, for three hours. The solvent and volatile components were removed under *vacuum*, diethyl ether added (10 cm^3) and the suspension was filtered under a nitrogen atmosphere through Celite 521. The final solution was concentrated (5 cm^3) and left at room temperature for two days to give colourless crystals suitable for analysis (1.69 mmol, 63% yield). Due to the air- and moisture- sensitive nature of the final product, reliable microanalysis was not possible.

IR(KBr): ν(BH) at 2409.8 and 2388.5 cm^{-1}. ^1H NMR ($CDCl_3$/ppm): δ 7.65 (d, *H*5), 7.26 (d, *H*3), 6.18 (t, *H*4), 3.71 (m, THF), 1.84 (m, THF). ^{13}C NMR ($CDCl_3$/ppm): δ 141.20 (*C*3), 136.10 (*C*5), 104.30 (*C*4), 67.80 (THF), 24.60 (THF). ^{11}B NMR ($CDCl_3$/ppm): δ -6.51.

Empirical formula	$C_{24}H_{40}B_2Cl_2Mg_2N_8O_3$	β/ °	99.319(3)
Formula weight	629.78	γ/ °	90
Crystal system	Monoclinic	Volume/ $Å^3$	3195.8(9)
Space group	$P2_1/n$	Z	4
a/ Å	15.119(3)	Z'	1
b/ Å	13.862(2)	Density calc./ Mgm^{-3}	1.309
c/ Å	15.453(3)	μ (Mo-K)/ mm^{-1}	0.282
α/ °	90		

Data were collected on a Bruker SMART APEX diffractometer[31] equipped with an Oxford Cryosystems low-temperature device at 150 K and using an colourless plate oil-coated crystal[32] of dimension 0.40 x 0.20 x 0.10 mm^3. The initial unit cell was indexed using a least-squares analysis of a random set of reflections collected from three series of 0.3° wide ω-scans, 10 s per frame, and 25 frames per series that were well distributed in reciprocal space. Data frames were collected [Mo Kα = 0.71073 Å] with 0.3° wide ω-scans, 10 s per frame and 600 frames per series. Three complete series were collected at varying φ angles (φ=0, 90, 180°). The crystal to detector distance was 6.0 cm, this providing a set of $3.50 \leq 2\theta \leq 52.70$. A total of 38688 reflections were collected and integrated using SAINT,[33] whilst absorption correction was applied using SADABS[34] with 7862 unique [R(int)=0.0513]. System symmetry, systematic absences and intensity statistics indicated the unique monoclinic space group $P2_1/n$. The structure was determined by direct methods with the location of nearly all non-hydrogen atoms using the program SHELXS[35] and refined by full-matrix least-squares on F^2 using SHELXL.[36] All non-hydrogen atoms

were refined anisotropically, while hydrogen atoms were placed in calculated positions, constrained to ride on their carbon atoms with group U_{iso} values assigned ($U_{iso}(H)= 1.20U_{iso}$). Hydrogen atoms on B were located from the difference map and the positions and the isotropic thermal parameters were refined. The final structure was refined to convergence [$\Delta/\sigma \leq 0.001$] with R(F) = 0.0544 (for 7862 data with F>4σF), GOF = 1.089 and *w*R2 = 0.1339 (all data). [$R1 = \sum|F_O - F_C|/\sum|F_O|$, $wR2 = \{[\sum w(F_O^2 - F_C^2)^2]/\sum wF_O^4\}^{0.5}$, $w = 1/[\sigma^2(F_O^2) + (xP)^2 + yP]$, $P = (F_O^2+2F_C^2/3)$]. The largest difference between peaks and holes in the final difference map was 0.535 and –0.264 eÅ^{-3}.

[{$H_2B(pz)_2$}$_2$Mg(THF)] (4)

[K{$H_2B(pz)_2$}] (1.000 g, 5.358 mmol) was dissolved in THF (5 cm^3) and MeMgCl (1.8 cm^3, 3.0 M in THF, 5.358 mmol) was added with stirring at room temperature for ten hours. The solvent and volatile components were removed under *vacuum*, diethyl ether added (10 cm^3) and KCl was removed by filtration under a nitrogen atmosphere through Celite 521. The final solution was concentrated (5 cm^3) and left at room temperature for two days to give colourless crystals suitable for X-ray analysis (1.82 mmol, 68% yield). Due to the air- and moisture- sensitive nature of the final product, reliable microanalysis was not possible.

IR(KBr): ν(BH) at 2410.2 and 2390.1 cm^{-1}. ^{1}H NMR ($CDCl_3$/ppm): δ 7.65 (d, *H*5), 7.34 (d, *H*3), 6.32 (t, *H*4), 3.70 (m, THF), 1.85 (m, THF). ^{13}C NMR ($CDCl_3$/ppm): δ 141.35 (*C*3), 136.10 (*C*5), 103.70 (*C*4), 67.80 (THF), 26.10 (THF). ^{11}B NMR ($CDCl_3$/ppm): δ -6.30.

Empirical formula	$C_{18}H_{24}B_2MgN_8O$	β/ °	97.4100(10)
Formula weight	390.36	γ/ °	107.9090(10)
Crystal system	Triclinic	Volume/ Å^3	2070.1(2)
Space group	P$\bar{1}$	Z	4
a/ Å	9.9508(6)	Z'	2
b/ Å	10.7407(6)	Density calc./ Mgm^{-3}	1.253
c/ Å	20.9957(12)	μ (Mo-K)/ mm^{-1}	0.109
α/ °	99.1370(10)		

Data were collected on a Bruker SMART APEX diffractometer[31] equipped with an Oxford Cryosystems low-temperature device at 150 K and using an colourless plate oil-coated crystal[32] of dimension 0.09 x 0.07 x 0.03 mm^3. The initial unit cell was indexed using a least-squares analysis of a random set of reflections collected from three series of 0.3° wide ω-scans, 10 s per frame, and 25 frames per series that were well distributed in reciprocal space. Data frames were collected [Mo Kα = 0.71073 Å] with 0.3° wide ω-scans, 10 s per frame and 600 frames per series. Four complete series were collected at varying ϕ angles (ϕ=0, 90, 120, 180°). The crystal to detector distance was 6.0 cm, this providing a set of $2.00 \leq 2\theta \leq 52.78$. A total of 17258 reflections were collected and integrated using SAINT,[33] whilst absorption correction was applied using SADABS[34] with 8384 unique [R(int)=0.0314]. System symmetry, systematic absences and intensity statistics indicated the unique triclini space group Pī. The structure was determined by direct methods with the location of nearly all non-hydrogen atoms using the program SHELXS[35] and refined by full-matrix least-squares on F^2 using SHELXL.[36] All non-hydrogen atoms were refined anisotropically, while hydrogen atoms were placed in calculated positions, constrained to ride on their carbon atoms with group U_{iso} values assigned ($U_{iso}(H)= 1.20U_{iso}$). Hydrogen atoms on B were located from the difference map and the positions and the isotropic thermal parameters were refined. The final structure was refined to convergence [$\Delta/\sigma \leq 0.001$] with R(F) = 0.0499 (for 8384 data with $F>4\sigma F$), GOF = 0.968 and *w*R2 = 0.1249 (all data). [$R1 = \Sigma|F_O - F_C|/\Sigma|F_O|$, $wR2 = \{[\Sigma w(F_O^2 - F_C^2)^2]/\Sigma wF_O^4\}^{0.5}$, $w = 1/[\sigma^2(F_O^2) + (xP)^2 + yP]$, $P = (F_O^2+2F_C^2/3)$]. The largest difference between peaks and holes in the final difference map was 0.302 and –0.300 $eÅ^{-3}$.

[{$H_2B(pz)_2$}$_2$Mg(THF)$_2$] (5)

a) Using MeMgCl. Several samples of [K{$H_2B(pz)_2$}] (1.000 g, 5.358 mmol) were each dissolved in THF (5 cm^3) and for every reaction, MeMgCl (1.8 cm^3, 3.0 M in THF, 5.358 mmol) was added with stirring at room temperature. The reactions were allowed to stir between 1 and 3 days. The solvent and volatile components were removed under *vacuum*, diethyl ether added (10 cm^3) and KCl was removed by

filtration under a nitrogen atmosphere through Celite 521 for each reaction. The final solutions were concentrated (5 cm^3) and left at room temperature for two days to give colourless crystals suitable for X-ray analysis (1.92 mmol, 72% yield). Due to the air- and moisture- sensitive nature of the final product, reliable microanalysis was not possible.

b) Using AllylMgCl. $K[H_2B(pz)_2]$ (1.000 g, 5.358 mmol) was dissolved in THF (10 cm^3) and AllylMgCl (2.7 cm^3, 2.0 M in THF, 5.358 mmol) was dropped at room temperature. The reaction was stirred for one hour, solvent and volatile components were removed under *vacuum* and diethyl ether (10 cm^3) was added. The final suspension was filtered (KCl was removed under a nitrogen atmosphere using Celite 521), concentrated (5 cm^3) and crystallised at room temperature for one day to give colourless crystals suitable for X-ray analysis (1.91 mmol, 72% yield).

IR(KBr): ν(BH) at 2410.2 and 2390.1 cm^{-1}. ^1H NMR ($CDCl_3$/ppm): δ 7.65 (d, *H*5), 7.28 (d, *H*3), 6.18 (t, *H*4), 3.70 (m, THF), 1.83 (m, THF). ^{13}C NMR ($CDCl_3$/ppm): δ 142.01 (*C*3), 136.50 (*C*5), 104.22 (*C*4), 68.30 (THF), 25.10 (THF). ^{11}B NMR ($CDCl_3$/ppm): δ -6.30.

Empirical formula	$C_{20}H_{32}B_2MgN_8O_2$	β/ °	109.329(3)
Formula weight	462.47	γ/ °	105.568(3)
Crystal system	Triclinic	Volume/ $Å^3$	1199.2(4)
Space group	$P\bar{1}$	Z	2
a/ Å	9.4171(19)	Z'	1
b/ Å	10.936(2)	Density calc./ Mgm^{-3}	1.281
c/ Å	13.013(3)	μ (Mo-K)/ mm^{-1}	0.108
α/ °	94.069(3)		

Data were collected on a Bruker SMART APEX diffractometer[31] equipped with an Oxford Cryosystems low-temperature device at 150 K and using an colourless plate oil-coated crystal[32] of dimension 0.10 x 0.11 x 0.14 mm^3. The initial unit cell was indexed using a least-squares analysis of a random set of reflections collected from three series of 0.3° wide ω-scans, 10 s per frame, and 25 frames per series that were well distributed in reciprocal space. Data frames were collected [Mo Kα = 0.71073 Å] with 0.3° wide ω-scans, 10 s per frame and 600 frames per series. Four complete series were collected at varying ϕ angles (ϕ=0, 90, 120, 180°). The crystal to detector distance was 6.0 cm, this providing a set of $3.36 \leq$

$2\theta \leq 57.90$. A total of 10757 reflections were collected and integrated using SAINT,[33] whilst absorption correction was applied using SADABS[34] with 5640 unique [R(int)= 0.0222]. System symmetry, systematic absences and intensity statistics indicated the unique triclinic space group $P\bar{1}$. The structure was determined by direct methods with the location of nearly all non-hydrogen atoms using the program SHELXS[35] and refined by full-matrix least-squares on F^2 using SHELXL.[36] All non-hydrogen atoms were refined anisotropically, while hydrogen atoms were placed in calculated positions, constrained to ride on their carbon atoms with group U_{iso} values assigned ($U_{iso}(H)= 1.20U_{iso}$). Hydrogen atoms on B were located from the difference map and the positions and the isotropic thermal parameters were refined. The final structure was refined to convergence [$\Delta/\sigma \leq 0.001$] with R(F) = 0.04279 (for 5640 data with $F>4\sigma F$), GOF = 0.9728 and *w*R2 = 0.1084 (all data). [$R1 = \Sigma|F_O - F_C|/\Sigma|F_O|$, $wR2 = \{[\Sigma w(F_O^2 - F_C^2)^2]/ \Sigma w F_O^4\}^{0.5}$, $w = 1/[\sigma^2(F_O^2) + (xP)^2 + yP]$, $P = (F_O^2+2F_C^2/3)$]. The largest difference between peaks and holes in the final difference map was 0.296 and -0.319 eÅ^{-3}.

[{$H_2B(pz)_2$}Mg(CH_2Ph)(THF)] (6)

[K{$H_2B(pz)_2$}] (1.000 g, 5.358 mmol) was dissolved in THF (5 cm^3) and ($PhCH_2$)MgCl (2.7 cm^3, 2.0 M in THF, 5.358 mmol) was added dropwise at room temperature. The reaction was stirred for one hour, solvent and volatile components were removed under *vacuum* and diethyl ether (10 cm^3) was added. The final suspension was filtered under a nitrogen atmosphere and KCl removed through Celite 521. The solvent was removed under *vacuum* and toluene (10 cm^3) was added. The clear solution was concentrated (5 cm^3) and a colourless oil was obtained (2.84 mmol, 53% yield).

IR: ν(BH) at 2409.8 and 2388.5 cm^{-1}. ^{1}H NMR ($CDCl_3$/ppm): δ 7.64 (d, *H*5), 7.32 (sd *H*3), 7.28 (s, *m*-C_6H_5), 7.12 (s, *o*-C_6H_5), 6.75 (s, *p*-C_6H_5), 6.14 (t, *H*4), 3.73 (m, THF), 1.85 (m, THF), 1.12 (s, Mg-CH_2-). ^{13}C NMR ($CDCl_3$/ppm): δ 142.10 (C3), 136.10 (C5), 104.30 (C4), 67.20 (THF), 25.30 (THF), 22.10 (Mg-CH_2-). ^{11}B NMR ($CDCl_3$/ppm): δ -6.51.

$[\{H_2B(pz)_2\}Mg(THF)_3][B(CH_2Ph)_4]$ (7)

$[K\{H_2B(pz)_2\}]$ (1.000 g, 5.358 mmol) was dissolved in THF (5 cm^3) and $(PhCH_2)MgCl$ (10.8 cm^3, 2.0 M in THF, 21.432 mmol) was added dropwise at room temperature. The reaction was stirred for one hour, solvent and volatile components were removed under *vacuum* and diethyl ether (10 cm^3) was added. The final suspension was filtered under a nitrogen atmosphere and KCl removed through Celite 521. The solvent was removed under *vacuum* and toluene (10 cm^3) added. The clear solution was concentrated (5 cm^3) and crystallised at room temperature for two days to give colourless crystals suitable for X-ray analysis (2.46 mmol, 46% yield). Due the air- and moisture-sensitive nature of the final product, it could not be characterised using NMR spectra.

Empirical formula	$C_{46}H_{60}B_2MgN_4O_3$	β/ °	111.012(5)
Formula weight	762.91	γ/ °	90
Crystal system	Monoclinic	Volume/ $Å^3$	4381(2)
Space group	P $2_1/c$	Z	4
a/ Å	12.567(5)	Z'	1
b/ Å	23.718(5)	Density calc./ Mgm^{-3}	1.157
c/ Å	15.746(5)	μ (Mo-K)/ mm^{-1}	0.084
α/ °	90		

Data were collected on a Bruker SMART APEX diffractometer[31] equipped with an Oxford Cryosystems low-temperature device at 150 K and using an colourless plate oil-coated crystal[32] of dimension 0.22 x 0.20 x 0.10 mm^3. The initial unit cell was indexed using a least-squares analysis of a random set of reflections collected from three series of 0.3° wide ω-scans, 10 s per frame, and 25 frames per series that were well distributed in reciprocal space. Data frames were collected [Mo Kα = 0.71073 Å] with 0.3° wide ω-scans, 10 s per frame and 600 frames per series. Three complete series were collected at varying ϕ angles (ϕ=0, 90, 180°). The crystal to detector distance was 6.0 cm, this providing a set of $3.46 \leq 2\theta \leq 52.82$. A total of 24664 reflections were collected and integrated using SAINT,[33] whilst absorption correction was applied using SADABS[34] with 8966 unique [R(int)= 0.0747]. System symmetry, systematic absences and intensity statistics indicated the unique monoclinic space group $P2_1/c$. The structure was determined by direct methods with the location of nearly all non-hydrogen atoms using the program

SHELXS[35] and refined by full-matrix least-squares on F^2 using SHELXL.[36] All non-hydrogen atoms were refined anisotropically, while hydrogen atoms were placed in calculated positions, constrained to ride on their carbon atoms with group U_{iso} values assigned ($U_{iso}(H)= 1.20U_{iso}$). Hydrogen atoms on B were located from the difference map and the positions and the isotropic thermal parameters were refined. The final structure was refined to convergence [$\Delta/\sigma \leq 0.001$] with R(F) = 0.0956 (for 8966 data with F>4σF), GOF = 1.083 and *w*R2 = 0.1949 (all data). [$R1 = \Sigma|F_O - F_C|/\Sigma|F_O|$, $wR2 = \{[\Sigma w(F_O^2 - F_C^2)^2]/\Sigma wF_O^4\}^{0.5}$, $w = 1/[\sigma^2(F_O^2) + (xP)^2 + yP]$, $P = (F_O^2+2F_C^2/3)$]. The largest difference between peaks and holes in the final difference map was 0.356 and -0.271 eÅ^{-3}.

K[B(CH$_2$Ph)$_4$] (8)

Potassium borohydride (0.200 g, 3.71 mmol) was dissolved in THF (15 cm^3) at room temperature and (PhCH$_2$)MgCl (7.4 cm^3, 2.0 M in THF, 14.84 mmol) was added dropwise. After stirring for one hour the solution was filtered and the solvent and volatile components were removed under *vacuum*. The final product was dissolved in toluene (10 cm^3) and the solution was concentrated (5 cm^3) under *vacuum*. Crystallisation at room temperature produced colourless crystal of the final product (2.22 mmol, 60% yield).

^{1}H NMR (toluene-d$_8$/ppm): δ 7.24 (t, 8H, *m*-C$_6H_5$), 7.18 (d, 8H, *o*-C$_6H_5$), 6.89 (t, 4H, *p*-C$_6H_5$), 1.99 (s, 8H, -CH$_2$). ^{13}C NMR (toluene-d$_8$/ppm): δ 157.80 (*ipso-C*), 127.90 (*m*-C$_6$H$_5$), 126.30 (*o*-C$_6$H$_5$), 115.40 (*p*-C$_6$H$_5$), 22.90 (-CH$_2$C$_6$H$_5$). ^{11}B NMR (toluene-d$_8$/ppm): δ -12.53. Elemental analysis for C$_{28}$H$_{28}$BK: Expected: 81.13%C; 6.82%H. Found: 79.94%C; 6.80%H.

Ab initio calculations were obtained from the Gaussian 98[37] package at 6-311G** basis set, and by using the atomic co-ordinates from crystal structure data.

Empirical formula	$C_{28}H_{28}BK$	β/ °	103.002(5)
Formula weight	414.41	γ/ °	90
Crystal system	Monoclinic	Volume/ Å^3	1108.9(9)
Space group	$P2_1$	Z	2
a/ Å	10.057(5)	Z'	1
b/ Å	9.681(5)	Density calc./ Mgm^{-3}	1.241
c/ Å	11.689(5)	μ (Mo-K)/ mm^{-1}	0.252

α/ °	90	

Data were collected on a Bruker SMART APEX diffractometer[31] equipped with an Oxford Cryosystems low-temperature device at 150 K and using an colourless plate oil-coated crystal[32] of dimension 0.24 x 0.20 x 0.12 mm^3. The initial unit cell was indexed using a least-squares analysis of a random set of reflections collected from three series of 0.3° wide ω-scans, 10 s per frame, and 25 frames per series that were well distributed in reciprocal space. Data frames were collected [Mo Kα = 0.71073 Å] with 0.3° wide ω-scans, 10 s per frame and 600 frames per series. Three complete series were collected at varying ϕ angles (ϕ=0, 90, 180°). The crystal to detector distance was 6.0 cm, this providing a set of $3.48 \leq 2\theta \leq 52.78$. A total of 6292 reflections were collected and integrated using SAINT,[33] whilst absorption correction was applied using SADABS[34] with 3839 unique [R(int)= 0.0285]. System symmetry, systematic absences and intensity statistics indicated the unique monoclinic space group $P2_1$. The structure was determined by direct methods with the location of nearly all non-hydrogen atoms using the program SHELXS[35] and refined by full-matrix least-squares on F^2 using SHELXL.[36] All non-hydrogen atoms were refined anisotropically, while hydrogen atoms were placed in calculated positions, constrained to ride on their carbon atoms with group U_{iso} values assigned ($U_{iso}(H)= 1.20U_{iso}$). Hydrogen atoms on B were located from the difference map and the positions and the isotropic thermal parameters were refined. The final structure was refined to convergence [$\Delta/\sigma \leq 0.001$] with R(F) = 0.0423 (for 3839 data with $F>4\sigma F$), GOF = 1.074 and *w*R2 = 0.0878 (all data). [$R1 = \Sigma|F_O - F_C|/\Sigma|F_O|$, $wR2 = \{[\Sigma w(F_O^2 - F_C^2)^2]/\Sigma wF_O^4\}^{0.5}$, $w = 1/[\sigma^2(F_O^2) + (xP)^2 + yP]$, $P = (F_O^2+2F_C^2/3)$]. The largest difference between peaks and holes in the final difference map was 0.239 and -0.232 $eÅ^{-3}$.

2.5 References

1 S. Trofimenko, *Chem. Rev.*, **1993**, *93*, 943.

2 S. Trofimenko, *J. Am. Chem. Soc.*, **1966**, *88*, 1842.

3 L. H. Toporcer, R. E. Dessy and W. I. Green, *J. Am. Chem. Soc.*, **1965**, *87*, 1237.

4 S. Trofimenko, *J. Am. Chem. Soc.*, **1967**, *89*, 3165.

5 S. Trofimenko, *J. Am. Chem. Soc.*, **1967**, *89*, 3170.

6 S. Trofimenko, *Chem. Rev.*, **1967**, *89*, 4948.

7 S. Trofimenko, *J. Am. Chem. Soc.*, **1967**, *89*, 3904.

8 S. Trofimenko, *Chem. Rev.*, **1972**, *72*, 503.

9 S. Trofimenko, *J. Am. Chem. Soc.*, **1967**, *89*, 6288.

10 S. Trofimenko, *J. Am. Chem. Soc.*, **1969**, *91*, 3183.

11 A. Rheingold, C. Incarvito and S. Trofimenko, *Inorg. Chem.*, **2000**, *39*, 5569.

12 S. Trofimenko, J. C. Calabrese and J. S. Thompson, *Inorg. Chem.*, **1987**, *26*, 1507.

13 S. Trofimenko, J. C. Calabrese, P. J. Domaille and J. S. Thompson, *Inorg. Chem.*, **1989**, *28*, 1091.

14 S. Trofimenko, J. C. Calabrese, P. J. Domaille and G. J. Long, *Inorg. Chem.*, **1991**, *30*, 2795.

15 A. Rheingold, L. M. Liable-Sands, C. L. Incarvito and S. Trofimenko, *J. Chem. Soc., Dalton Trans.*, **2002**, 2297.

16 H. V. Dias and J. D. Gorden, *Inorg. Chem.*, **1996**, *35*, 318.

17 C. K. Chang and F. Ebina, *J. Chem. Soc., Chem. Commun.*, **1981**, 778.

18 M. Díaz-Requejo, T. Belderrain, C. Nicasio, S. Trofimenko and P. Pérez, *J. Am. Chem. Soc.*, **2002**, *124*, 896.

19 N. J. Curtis and R. S. Brown, *Can. J. Chem.*, **1985**, *59*, 65.

20 B. Kaptein, L. Wang-Griffin, G. Barf and R. M. Kellog, *J. Chem. Soc., Chem. Commun.*, **1987**, 1457.

21 R. Han, A. Looney and G. Parkin, *J. Am. Chem. Soc.*, **1989**, *111*, 7276.

22 H. Viebrock and E. Weiss, *J. Organomet. Chem.*, **1994**, *464*, 121.

23 B. Srinivas, C. Chang-Cheng, C. Chau-Han, M. Y. Chian, C. I-Ting, Y. Wang and G. Lee, *J. Chem. Soc., Dalton Trans.*, **1997**, 957.

24 P. J. Bailey, C. M. E. Dick, S. Fabre and S. Parsons, *J. Chem., Soc. Dalton Trans.*, **2000**, 1655.

25 P. J. Bailey, R. A. Coxall, C. M. E. Dick, S. Fabre and S. Parsons, *Organometallics*, **2001**, *20*, 798.

26 D. Comins and J. Herrick, *Tetrahedron Letters*, **1984**, *25*, 1321.

27 D. R. Armstrong, R. Mulvey, G. Walker, D. Barr, R. Snaith, W. Clegg and D. Reed, *J. Chem. Soc. Dalton Trans.*, **1988**, 617.

28 D. Barr, W. Clegg, R. Mulvey and R. Snaith, *J. Chem. Soc., Chem. Commun.*, **1984**, 287.

[29] V. R. Dias, H. Lu, R. Ratcliff and S. Bott, *Inorg. Chem.*, **1995**, *34*, 1975.

[30] Z. Hu and S. M. Gorun, *Inorg. Chem.*, **2001**, *40*, 667.

[31] Bruker. *SMART*. Bruker-AXS, Madison, Wisconsin, USA, **2001**.

[32] D. Stalke and T. Kottke, *J. Appl. Crystallogr.*, **1993**, *26*, 615.

[33] Bruker. *SAINT*. Bruker-AXS, Madison, Wisconsin, USA, **2002**.

[34] G. M. Sheldrick, *SADABS*. Version 2.06. University of Gottingen, Germany, **2001**.

[35] G. M. Sheldrick, *SHELXS97*. University of Gottingen, Germany, **1997**.

[36] G. M. Sheldrick, *SHELXL97*. University of Gottingen, Germany, **1997**.

[37] Gaussian 98, Revision A.11. M. J. Frisch, G. W. Trucks, H. B. Schlegel, G. E. Scuseria, M. A. Robb, J. R. Cheeseman, V. G. Zakrzewski, J. A. Montgomery, R. E. Stratmann, J. C. Burant, S. Dapprich, J. M. Millam, A. D. Daniels, K. N. Kudin, M. C. Strain, O. Farkas, J. Tomasi, V. Barone, M. Cossi, R. Cammi, B. Mennucci, C. Pomelli, C. Adamo, C. Cliord, J. Ochterski, G. A. Petersson, P. Y. Ayala, Q. Cui, K. Morokuma, D. K. Malick, A. D. Rabuck, K. Raghavachari, J. B. Foresman, J. Cioslowski, J. V. Ortiz, B. B. Stefanov, G. Liu, A. Liashenko, P. Piskorz, I. Komaromi, R. Gomperts, R. L. Martin, D. J. Fox, T. Keith, M. A. Al-Laham, C. Y. Peng, A. Nanayakkara, C. Gonzalez, M. Challacombe, P. M. W. Gill, B. F. G. Johnson, W. Chen, M. W. Wong, J. L. Andres, M. Head-Gordon, E. S. Replogle and J. A. Pople, Gaussian Inc., Pittsburgh PA, **2001**.

Chapter 3:

New Borate Centred Ligands for Zwitterionic Metal Complexes

3.1 Introduction

The present investigation is an attempt to synthesise novel monoanionic bidentate nitrogen donor ligands, in order to generate a range of zwitterionic mono-alkyl magnesium complexes (Figure 3.1).

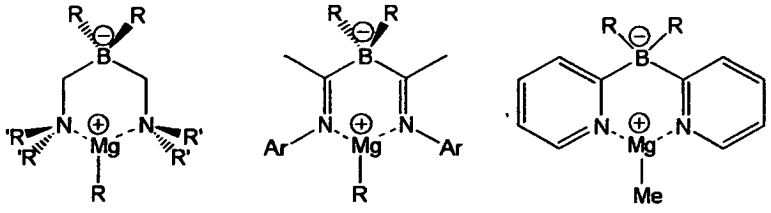

Figure 3.1 Zwitterionic mono-alkyl magnesium complexes proposed.

Three different borate centred ligands have been suggested for zwitterionic magnesium complexes. Firstly, the proposed novel ligands of $[R_2B(CH_2NEt_2)_2]^-$ (R: Me or Ph) could be synthesised from a reductive carbon cleavage of (phenylthiomethyl)amines (Section 3.1.1) and further treatment with R_2BX (R: Me or Ph; X: Br or Cl). The zwitterionic mono-alkyl magnesium complexes should be obtained by the treatment of $[\{R_2B(CH_2NEt_2)_2]\}Li]$ with the respective Grignard reagent (Figure 3.2).

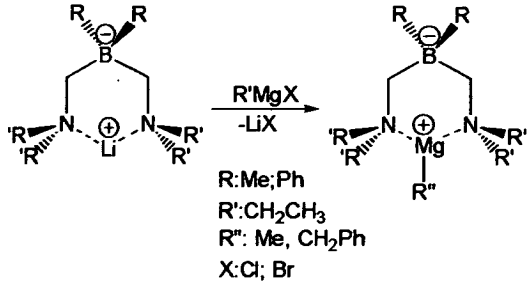

Figure 3.2 Zwitterionic mono-alkyl magnesium complexes proposed.

Secondly, the proposed novel ligand $[R_2B\{C(Me)NAr\}_2]^-$ (R: Me or Ph) could be synthesised by using the appropriate lithium isonitrile compound (Section 3.1.2) and further treatment with R_2BX (R: Me or Ph; X: Br or Cl). The zwitterionic

mono-alkyl magnesium complexes should be obtained after the treatment of $[R_2B\{C(Me)NAr\}_2]^-$ with the respective Grignard reagent (Figure 3.3).

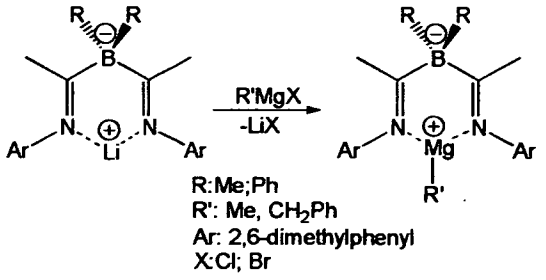

Figure 3.3 Zwitterionic mono-alkyl magnesium complexes proposed.

Thirdly, synthesis and chemistry of pyridyl borate ligands could be undertaken (Section 3.1.3). The complex of $[\{R_2B(2\text{-py})\}_2Li]$ should be synthesised from the reaction between a solution of R_2BX with a solution of 2-lithiopyridine. In addition, zwitterionic mono-alkyl magnesium complexes (Figure 3.4) could be compared with the bis(pyridyl)borate ligands which do not provide zwiterionic complexes. Finally, alkene polymerisation should be tested for the mono-alkyl magnesium zwitterionic complexes obtained (Figure 3.4).

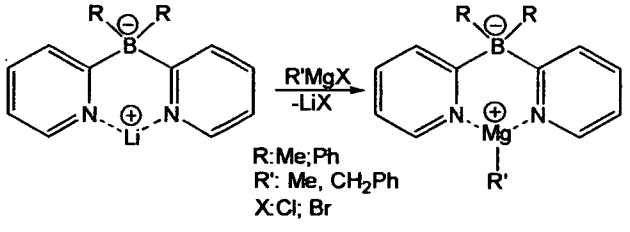

Figure 3.4 Zwitterionic mono-alkyl magnesium complexes proposed.

3.1.1 Reductive Carbon-Sulfur Bond Cleavage

Active hydrogen compounds react with formaldehyde and a primary or secondary amine to yield compounds called Mannich bases.[1] The Mannich reaction apparently proceeds through a variety of mechanisms depending on the reactants and the conditions that are employed. One mechanism that appears to operate in neutral or acidic media involves (step 1, Figure 3.5) an initial reaction of the secondary

amine with formaldehyde to yield an iminium ion and (step 2, Figure 3.5) subsequent reaction of the iminium ion with the enol form of the active hydrogen compound.[1,2]

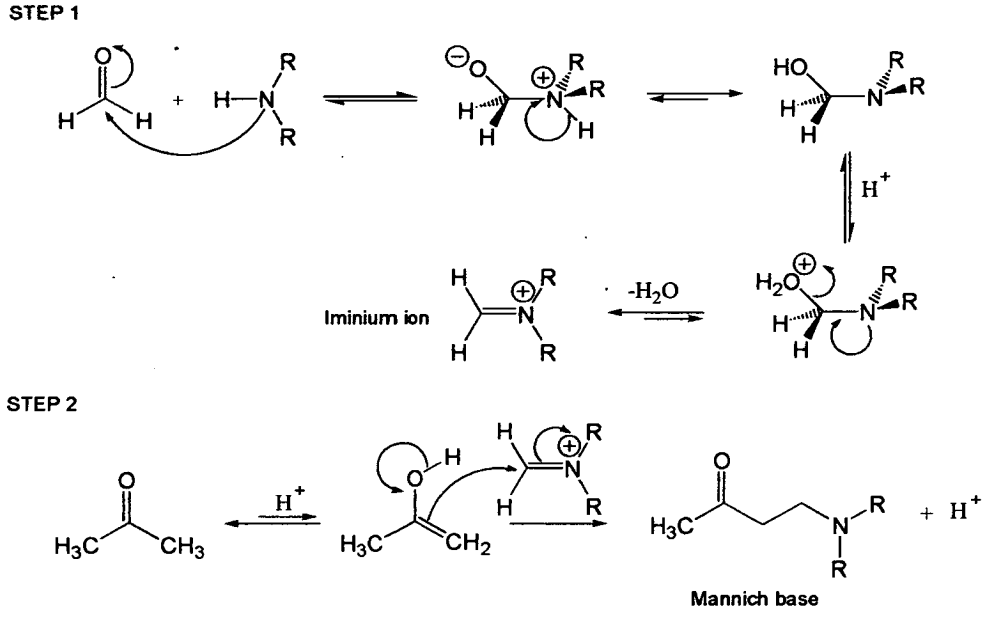

Figure 3.5 Mechanism of the Mannich reaction.

The overall result of the Mannich reaction is to replace an α–hydrogen atom of a ketone with a [CH_2NR_2] group. Utilisation of an arenethiol in this kind of reaction could theoretically lead to compounds of the same chemical class or to Mannich bases of the type produced with phenols, but Grillot *et al.*[3] have shown that aryl dialkylaminomethyl sulfides are ordinarily formed. Investigation of the reaction of iminium ion with thiophenols suggests formation of aryl dialkylaminomethyl sulfides, according to the reaction illustrated in Figure 3.6.[3] Thiols are related structurally to hydrogen sulfide, R or Ar having replaced one of the hydrogen atoms, while sulfur compounds containing HS groups are generally more acidic than their oxygen analogs: H_2S > H_2O > RSH > ROH > ArSH > ArOH; CH_3COSH > CH_3COOH.[2] Thiophenols thus behave like aliphatic mercaptans and not like phenols which undergo Mannich reactions.[4] The formation of aryl dialkylaminomethyl sulfides may suggest the mechanism illustrated in Figure 3.6 in which the iminium ion was used to produce the condensation of thiophenols.

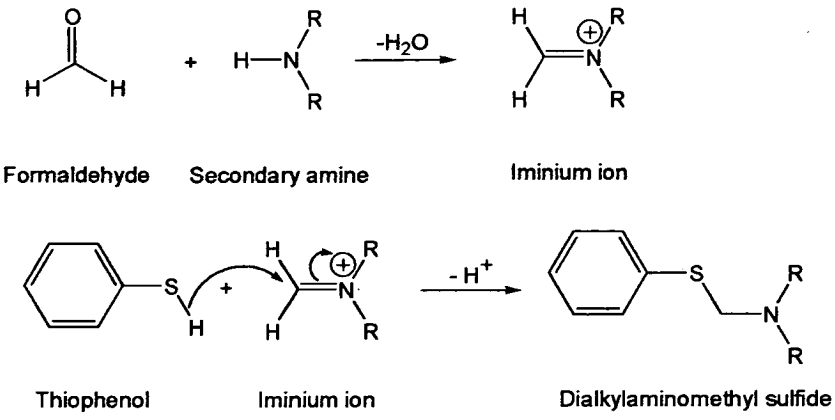

Figure 3.6 Mechanism for the synthesis of dialkylaminomethyl sulfide using the iminium ion.

3.1.1.1 Arene-Catalysed Lithiation Reactions

The importance of organolithium intermediates in synthetic organic chemistry has been proved by their versatility as a source of carbanionic species.[4] Sometimes the incompatibility between the functional group and the carbon-lithium bond is problematic but this can often be overcome by lithiation at low temperatures.[4-6] In many cases, this process does not work using lithium metal and it is necessary to activate the metal in order to get the desired lithiation.[4,7-9] During the last decade, two powerful methodologies have been developed in order to activate lithium: a) the use of certain aromatic compounds, called lithium-arenes or lithium arenides,[8] b) the use of a sub-stoichiometric (catalytic) amount of the same arene,[10,11] naphthalene and 4,4'-di-*tert*-butylbiphenyl (reagent of Freeman) being the most commonly used (Figure 3.7).[12] Both methods have been extensively applied in order to prepare organolithium reagents from non-halogenated material,[8] and for functionalised organolithium compounds, by halogen-lithium exchange or by ring opening of heterocycles.[13] Finally, both methods offer the advantage of improved chemical stability of the hydrocarbon by generating polylithiated species and the activation of transition metals, especially nickel.[14]

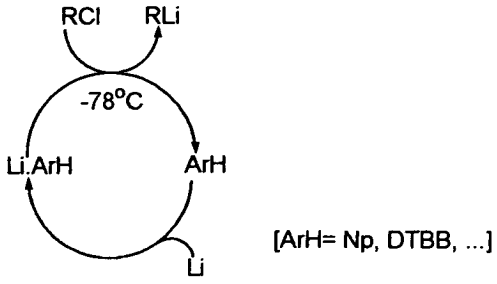

Figure 3.7 The arene-catalysed lithiation.

The use of stoichiometric amounts of arene in reactions can give similar or better yields in which the reaction times are far shorter.[8] Moreover, lithium dissolves when stirred with an ethereal solution of electron acceptor arene producing a deep green or blue colour of the radical anion.[12] The arene-catalysed lithiated reactions with the substrate to be lithiated can be followed from the beginning when the colour disappears and then when the mixture becomes coloured again when the substrate has been consumed.[8]

3.1.1.2 Reductive Carbon-Sulfur Cleavage of (Phenylthiomethyl)-amines

Reduction of (phenylthiomethyl)amines with a solution of lithium naphthalide ($LiC_{10}H_8$) under Barbier type reaction conditions (lithiation in the presence of the electrophile) gives the corresponding (lithiomethyl)amine, illustrated in Figure 3.8.[7,15]

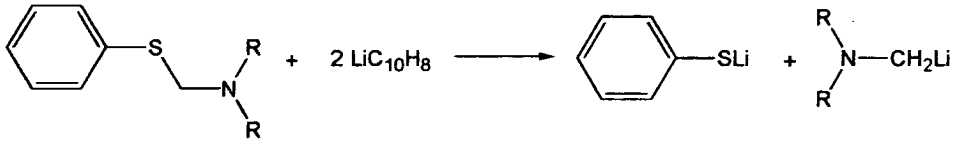

Figure 3.8 Reduction of (phenylthiomethyl)amine in presence of lithium naphthalide.

In most of these kinds of reactions, THF is used as solvent, and of course the cleavage reaction must be carried out at low enough temperatures in order to prevent organolithium loss by THF cleavage.[7,15] It is probable that the cleavage is controlled

by thermodynamic rather than kinetic factors where PhS- is a better leaving group than Ph- (Figure 3.9a).[7] Moreover, the accumulation of phenyl groups in the sulfide molecule increases the ease of cleavage of the sulfides.[8,15] In addition, using amines where the R groups present steric problems (di-isopropyl or biphenyl group) the reaction will behave differently (Figure 3.9b).[15]

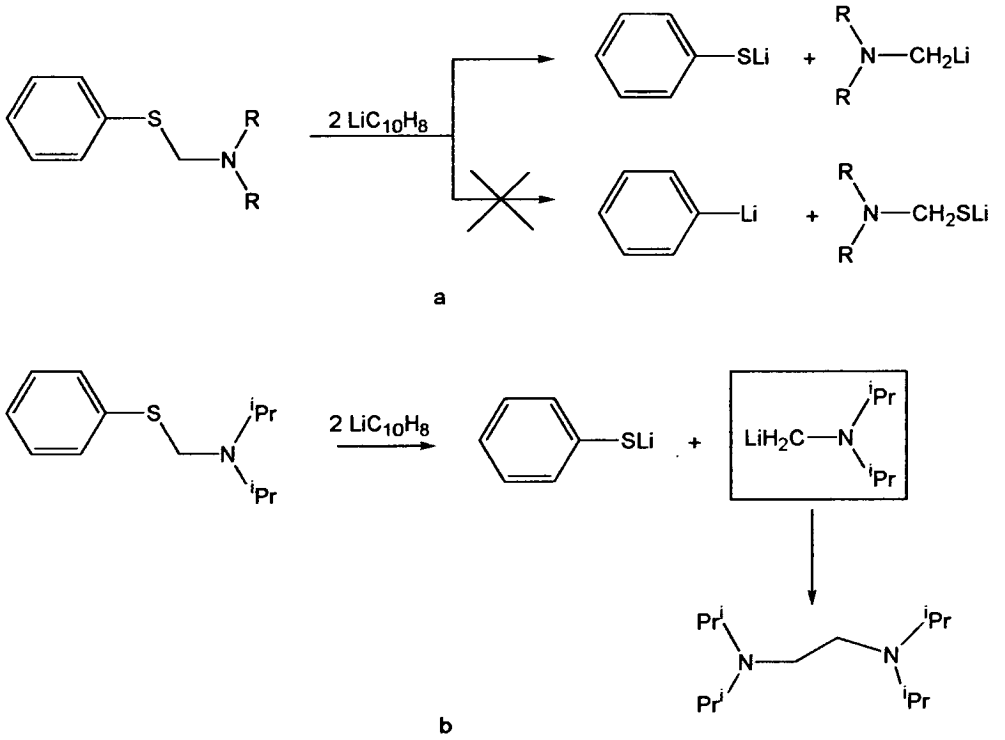

Figure 3.9 a) Thermodynamic cleavage of (phenylthiomethyl)amine; b) Using amines with steric problems.

Although the preparations of most multimetalated, non-stabilised (lithiomethyl)amines are under investigation, the reaction of the lithiated complexes with different electrophiles (Me_3SiCl or Et_2CO) under Barbier type reaction conditions can be used to produce synthesis of multimetalated systems where the expected diols or disilylated compounds are obtained.[7,8,15]

3.1.2 Reactivity of Isonitriles

Isonitriles possessing α–hydrogens tend to undergo deprotonation by organolithium compounds, rather than addition to the isonitrile-group. In the absence

of α-hydrogens, however, isonitriles show carbene-like reactivity, giving lithioimines; subsequent reaction with electrophiles produces imine derivatives, which may be desired in their own right or may be hydrolysed to the corresponding carbonyl compounds (Figure 3.10).[16]

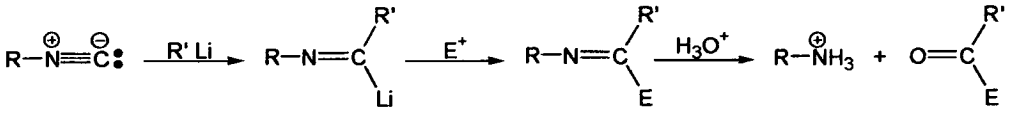

Figure 3.10 Imine and carbonyl derived from the lithiated aldimine.

The most convenient isonitrile for preparing aldimines is 1,1,3,3,-tetramethylbutylisonitrile, where organolithium is added and then the reaction mixture quenched with H_2O to produce the expected aldimine,[17] according to Figure 3.11. Although several studies using organolithium and Grignard reagents with isonitriles have been reported,[16,17] the Grignard reagents produce lower yields of aldehydes and α–keto acids than lithium aldimine reagents.[16]

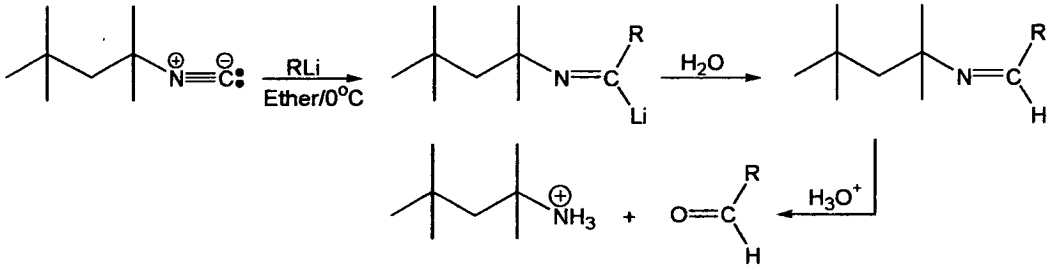

Figure 3.11 Imine and carbonyl derived from 1,1,3,3-tetramethylbutylisonitrile.

Moreover, several isonitriles can be used to produce the respective aldimine, but the α–carbon must not have more than one aromatic group in order to prevent oligomerization by an isonitrile-lithium exchange reaction (Figure 3.12).[16,18] Furthermore, the effect of the organolithium reagent is important, and primary or secondary aliphatic lithium reagents react quite well with most of the isonitrile used.[16] In some cases a high yield of aldimine can be obtained by using a tertiary organolithium reagent, but even when the requirement of low temperature is used, most of the reactions produce changes in the equilibrium and a mixture of products from further reaction of the initially formed aldimine is detected.[16]

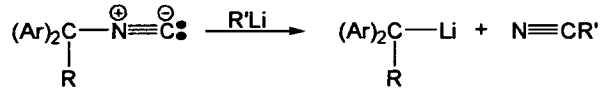

Figure 3.12 Lithiation effect of isonitrile with more than one aromatic group.

Finally, electrophilic reagents such as trimethylsilyl chloride or dimethylphenylsilyl chloride may give information about lithium aldimines, but their hydrolysis to produce aldehydes is thought to present some steric problems.[19]

3.1.3 Boron Pyridyl Chemistry

Since Trofimenko reported the first boron-pyrazole ligands they have proved to be very important chelates for metal complexes and their use as catalysts has increased.[20] There are numerous examples of the uses of poly-pyrazolylborate ligands in the context of transition metal chemistry.[20] It is only much more recently, however, that the pyrazolylborate chemistry of *s*- and *p*-block elements has begun to flourish. Moreover, poly(1-pyrazolyl)borates present a high electron delocalization around their pyrazolyl rings, whilst the magnesium complexes show charge transfer from the ligands to the metal where the neutralisation of charges is evident by the positive charge on nitrogen atoms (Figure 3.13).

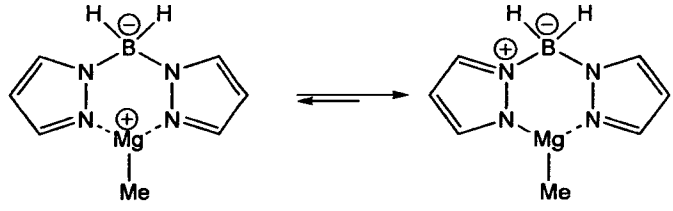

Figure 3.13 Equilibrium of resonance structures of [H_2B(pz)MgMe].

Polypyridyl borate ligands are of interest in co-ordination chemistry, due to the fact that their electronic and steric properties are similar to poly(1-pyrazolyl)borates, but they differ significantly in their ability to delocalize charges (Figure 3.14). Using pyridyl groups, the charge on the metal cannot be delocalized through the ligand to be located adjacent to the boron as is the case for pyrazolyl donors, and the final complex will consequently show zwitterionic properties.

Substituents at position 3- could improve the protecting environment to the metal centre, but bulky groups could overprotect the metal during substrate binding in catalytic processes.

Figure 3.14 Equilibrium of resonance structures of bis(pyridyl)borate ligands.

Preparation of hydrogen dimethylbis(pyridyl)borate, however, could involve complicated steps, and the reaction has to be done at a low enough temperature in order to prevent formation of dimers analogous to pyrazabole complexes (Figure 3.15).[21]

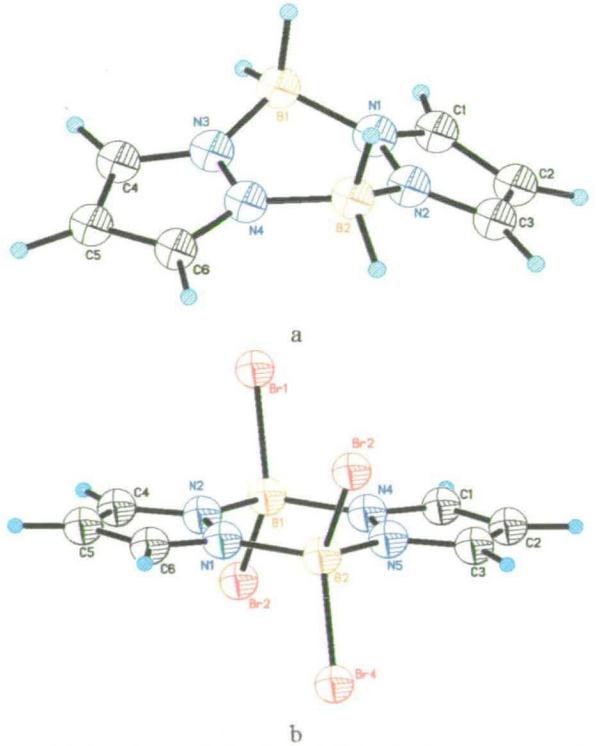

Figure 3.15 a) Pyrazobole; b) 4,4,8,8-tetrabromopyrazabole.

Hodgkins *et al.*[22] have synthesised bis(pyridyl)borate complexes using transition metals, $[\{Me_2B(2\text{-py})\}_2M]$ (M: Cu; Zn), but they have also confirmed

isomeric compounds analogous to pyrazabole by NMR spectroscopic analysis, according to Figure 3.16. However, the synthesis of novel hydrogen diphenylbis(pyridyl)borate and its magnesium complexes will be a challenging experience.

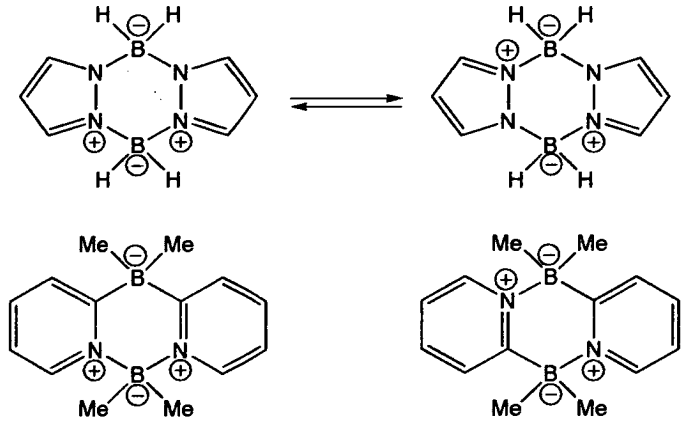

Figure 3.16 Resonance structures of pyrazobole and the 2-pyridyl analogues of pyrazoboles.

3.2 Results

3.2.1 Reductive Carbon-Sulfur Bond Cleavage and Reaction with $Me_2Si(Ph)Cl$

Carbon-sulfur cleavage of $PhSCH_2NEt_2$ (**9**) by lithium/naphthalene in the presence of $Me_2(Ph)SiCl$ has been tested in order to establish the formation of the desired intermediate lithiate $LiCH_2NEt_2$. The reaction must be carried out at a low enough temperature (-78 °C) in order to prevent $LiC_{10}H_8$ loss by reaction with solvent THF (Figure 3.17), while unknown products can be obtained when the temperature is not appropriate during the reaction. The naphthalene remaining in the final solution can be removed by sublimation under *vacuum* at 60 °C, and further distillation permits the isolation of pure colourless oil of $Et_2NCH_2Si(Ph)Me_2$ (**10**), which was fully characterised by NMR spectra.

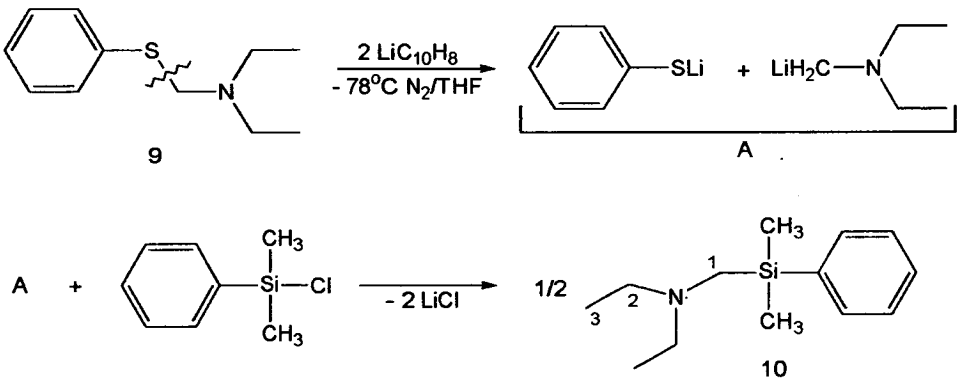

Figure 3.17 Carbon-sulphur cleavage of 9 and its reactivity with $Me_2(Ph)SiCl$.

The ^1H NMR spectrum of **10** places the downfield multiplet signals for the aromatic hydrogen atoms at δ 7.34, whilst a singlet for the H1 atoms is placed at δ 4.66 (Figure 3.18). Upfield, a quartet and a triplet signal at δ 2.45 and 0.94 are assigned to H2 and H3, while the characteristic peak for Si-CH_3 is located at δ 0.34. The ^{13}C NMR spectrum shows a downfield shift of the aromatic carbons at δ 133.40 (*ipso*-C_6H_5), δ 128.31 (*m*-C_6H_5), δ 127.45 (*o*-C_6H_5) and δ 126.31 (*p*-C_6H_5) (Figure 3.19). However, the co-ordinated Si-CH_3 resonances are placed at δ -0.18, whilst C1, C2 and C3 are observed at δ 49.43, δ 44.83 and δ 12.24, respectively.

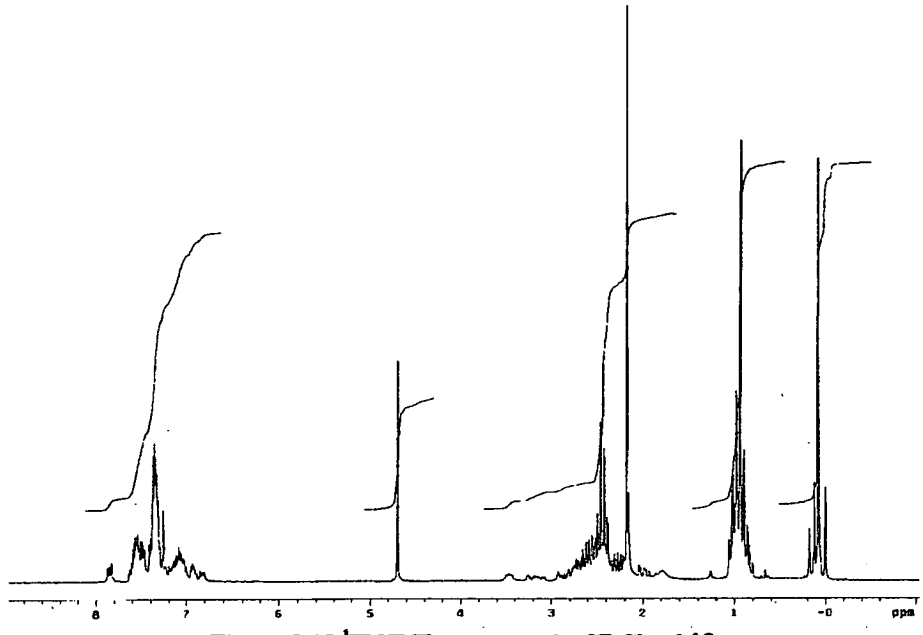

Figure 3.18 ^{1}H NMR spectrum in $CDCl_3$ of 10.

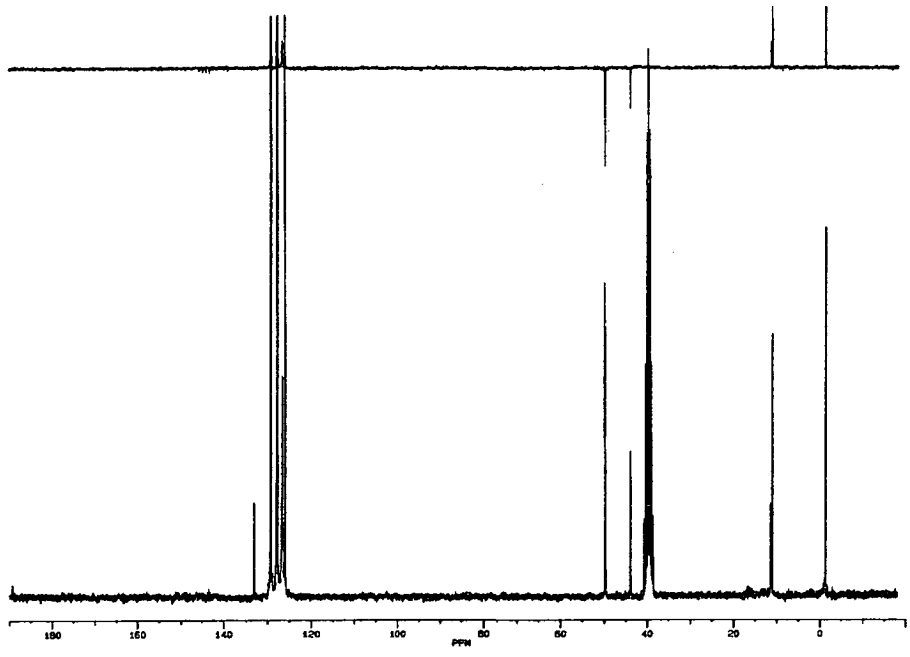

Figure 3.19 ^{13}C NMR spectrum in $CDCl_3$ 10.

3.2.2 Reductive Carbon-Sulfur Bond Cleavage and Reaction with Ph_2BCl

The outcome of the reaction with $Me_2(Ph)SiCl$ indicated the clean formation of $LiCH_2NEt_2$ and the synthesis of the desired ligand was therefore attempted (Figure 3.20). A carbon-sulfur cleavage reaction of **9** was treated with an equimolar amount of Ph_2BCl (**11**) at -78 °C, and the reaction was stopped after 24 hours. The unreactive naphthalene was removed under *vacuum* at 60 °C, in order to prevent thermal decomposition of the final product, but in some cases naphthalene remained in the final solution, according to NMR spectra. The extraction using hexane/ether permitted the isolation of two white powders. Although the extraction from ether represented the desired borate ligand of $[\{Ph_2B(CH_2NEt_2)_2\}Li(THF)]$ (**12**) (according to NMR spectra), it was not possible to improve the obtained yield of about 3 %. Perhaps, the different steps needed to purify the ligand give a very bad yield, making it difficult to use the ligand to prepare further transmetallation complexes.

The ^1H NMR spectrum of **12** indicates the downfield multiplet peak for aromatic hydrogen atoms at δ 7.28, whilst two singlets at δ 3.60 and 1.75 indicate the presence of co-ordinated THF (Figure 3.21). The signals for H1, H2 and H3 are placed at δ 3.37, 2.42 and 0.92, respectively. The ^{13}C NMR gives two sets of signals at δ 69.85 and 26.21 which are assigned to the THF solvated, whilst the aromatic carbon atoms are placed at δ 137.66 (*ipso*-C_6H_5), δ 131.60 (*m*-C_6H_5), δ 128.95 (*o*-C_6H_5), δ 127.77 (*p*-C_6H_5), respectively (Figure 3.22). The C2 and C3 are assigned upfield at δ 62.82 and 12.61, whilst C1 is located at δ 45.9. The ^{11}B NMR spectrum shows a single peak for the boron atom at δ -14.09 (Figure 3.23).

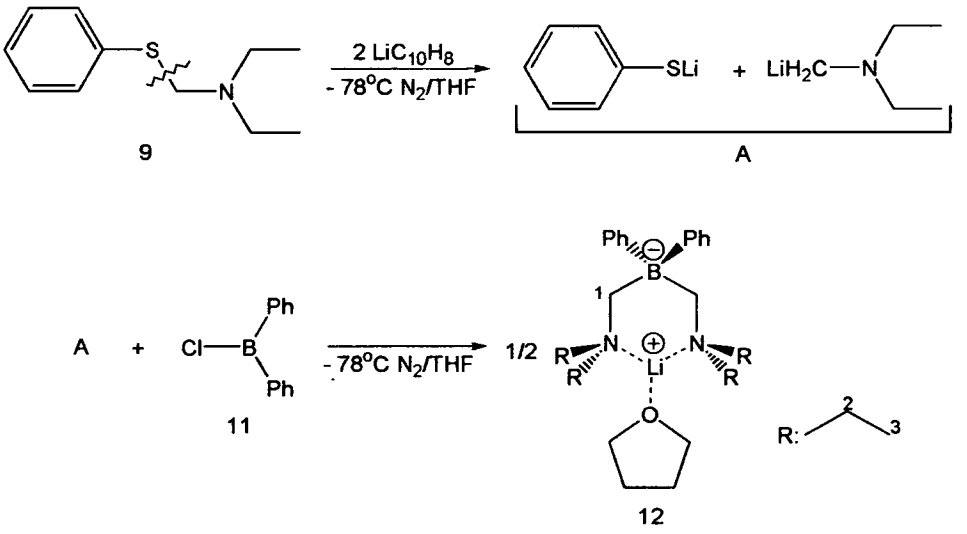

Figure 3.20 Carbon-sulfur cleavage of 9 and its reactivity with 11.

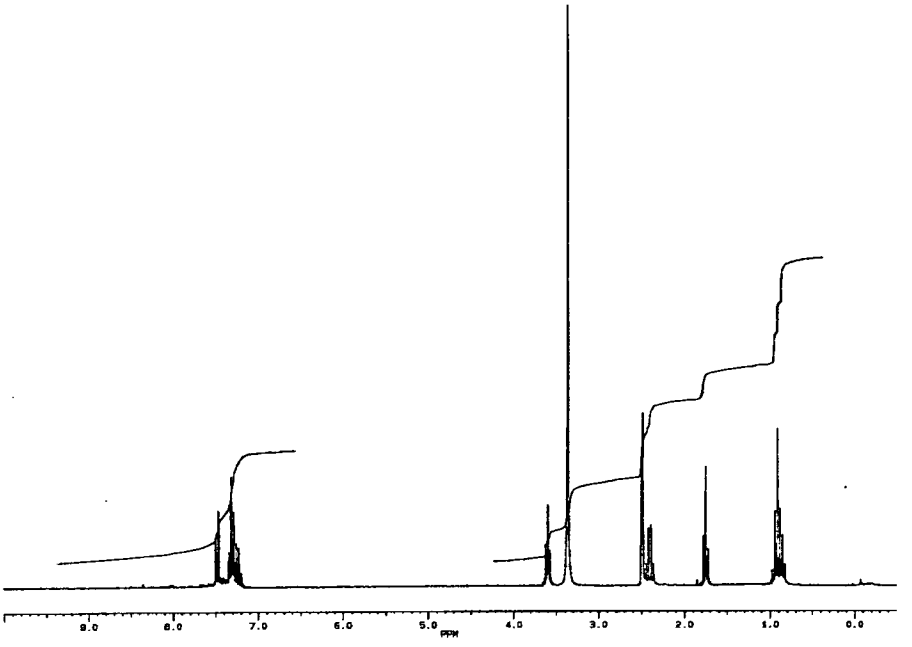

Figure 3.21 ^{1}H NMR spectrum in DMSO-d_6 of 12.

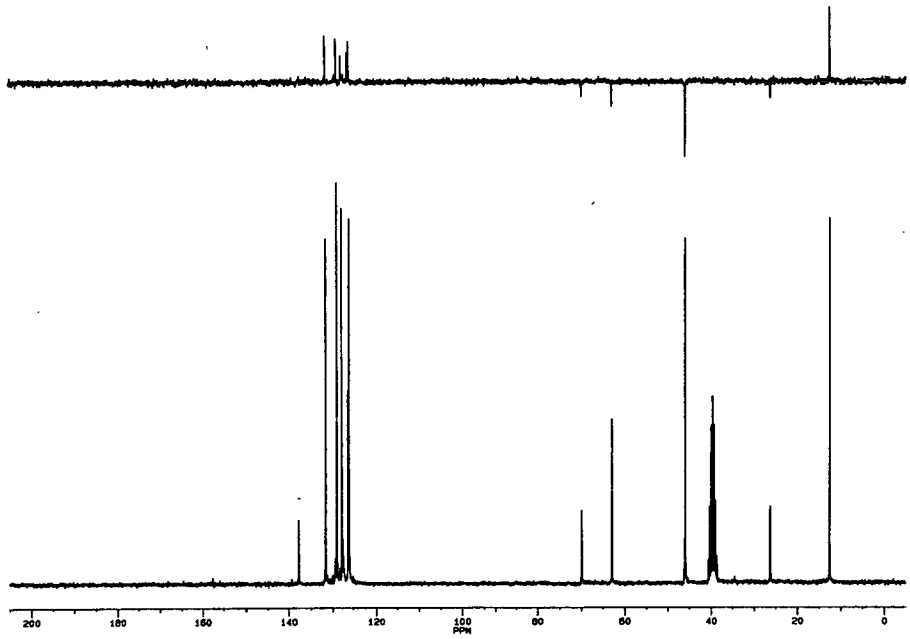

Figure 3.22 ^{13}C NMR spectrum in DMSO-d_6 of 12.

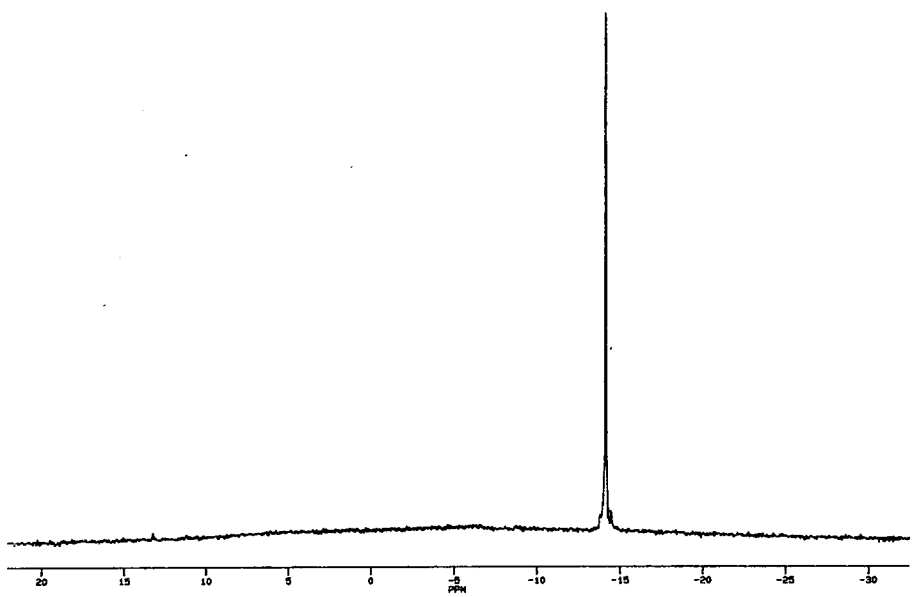

Figure 3.23 ^{11}B NMR spectrum in DMSO-d_6 of 12.

3.2.3 Reactivity of the Alkylated 2,6-Dimethylphenyl Isonitrile with Me_3SiCl

Treatment of 2,6-dimethylphenyl isonitrile, [ArNC] (Ar: 2,6-dimethylphenyl), with an equimolar amount of MeLi in Et_2O at –78 °C was carried out, and the obtained lithiated compound [ArNC(Me)Li] (Ar: 2,6-dimethylphenyl) (**13**) was treated with an equimolar amount of Me_3SiCl at –78 °C. KCl was filtered off, and extraction from diethyl ether resulted in the formation of two products, according to Figure 3.24. The alkylation of the 2,6-dimethylphenylisonitrile using MeLi produced better results than using ^{n}BuLi or *sec*-BuLi. Although the requirement of low temperature and the stoichiometric amount of methyllithium to produce the alkylation were taken under consideration to avoid the formation of a dimer, the reaction already described permitted the isolation of [ArNC(Me)$SiMe_3$] (**14**) as an orange oil and [ArNC(Me)C{$Si(Me)_3$}NAr] (Ar: 2,6-dimethylphenyl) (**15**) as an orange solid.

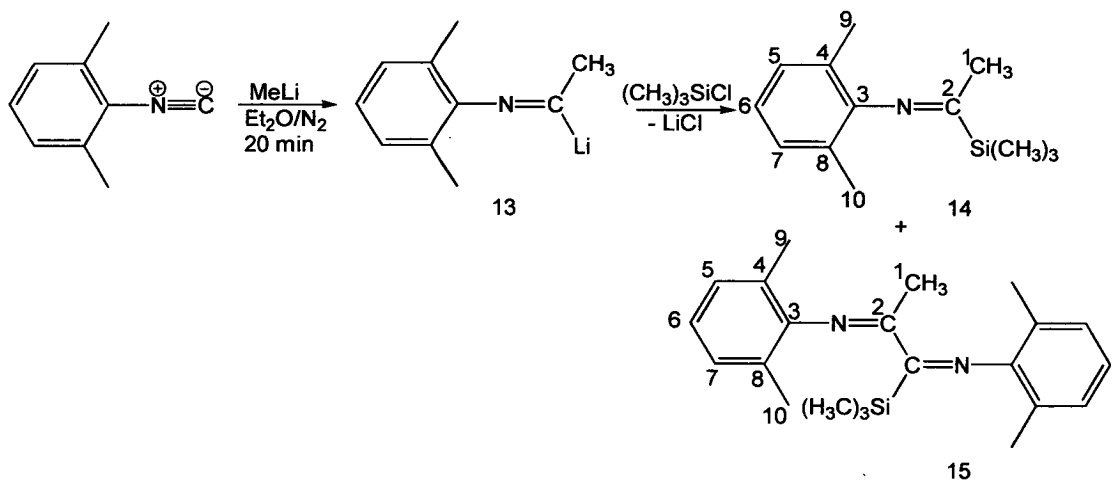

Figure 3.24 Reaction of 13 with Me_3SiCl: a) 14; b) 15.

The most reasonable interpretation of these results is that the solution of the lithium aldimine **13** may further react with an excess of 2,6-dimethylphenyl isonitrile to form a new lithium aldimine dimer of [ArNC(Me)C{Li}NAr] (Ar: 2,6-dimethylphenyl), which may react again with the respective electrophilic reagent (Me_3SiCl) to give the final product of **15**, according to the mechanism explained in

Figure 3.25. The NMR spectra of the orange oil and the orange crystals were investigated and show both products in Figure 3.24.

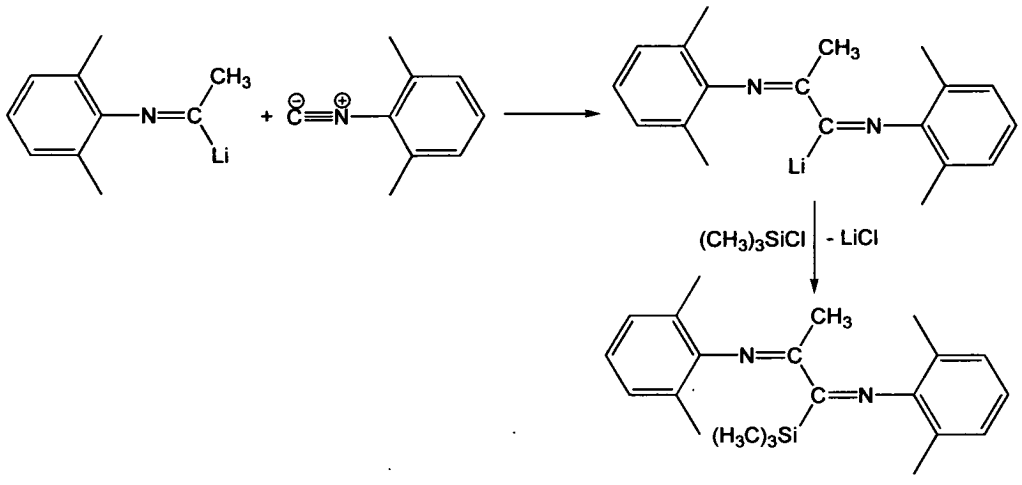

Figure 3.25 Reaction suggested for the formation of 15.

The ^{1}H NMR spectrum of **14** shows a shift to downfield for H5 and H6 as a multiplet at δ 6.90, whilst the equivalent H9 and H10 give raise to a singlet at δ 1.98 (Figure 3.26). The hydrogen atoms H1 are placed at δ 0.22, whilst the significant peak for the co-ordinated Si-CH_3 in the ^{1}H NMR spectrum gives a characteristic upfield value at δ 0.18. The ^{13}C NMR spectrum provides the aromatic carbon signals at δ 147.70, 126.80, 124.89 and 123.28, whilst the co-ordinated α-carbon C2 is placed at δ 152.10 (Figure 3.27). The co-ordinated C1, C9 and C10 show shifts to downfield at δ 18.30 and 17.11, respectively, whilst Si-CH_3 is characteristically placed upfield at δ 0.12.

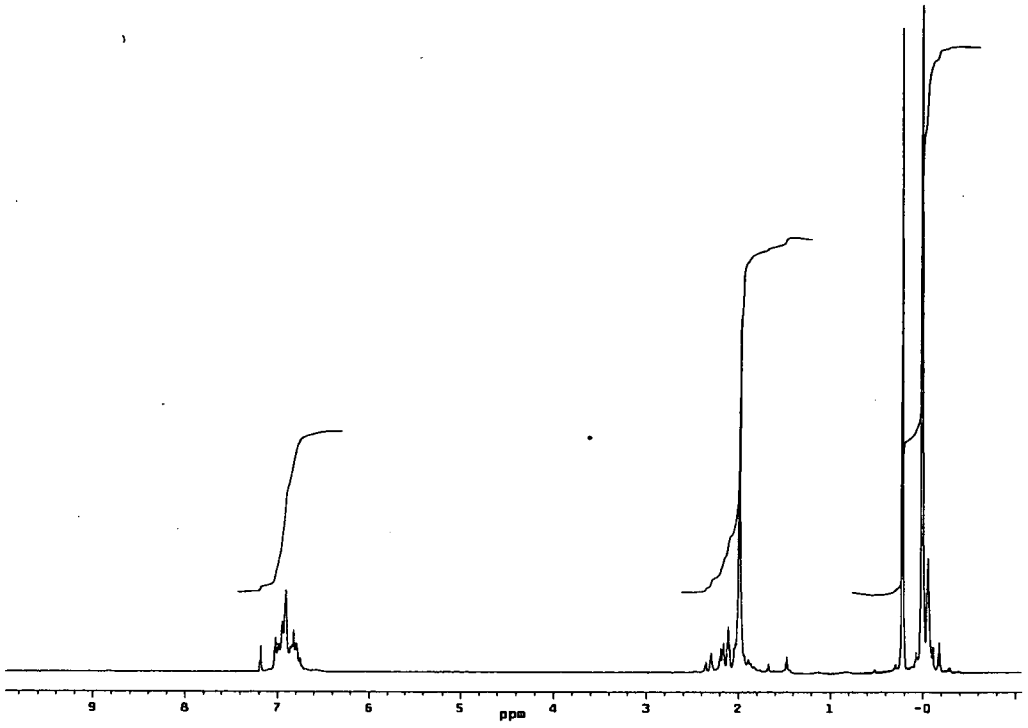

Figure 3.26 ^{1}H NMR spectrum in $CDCl_3$ of 14.

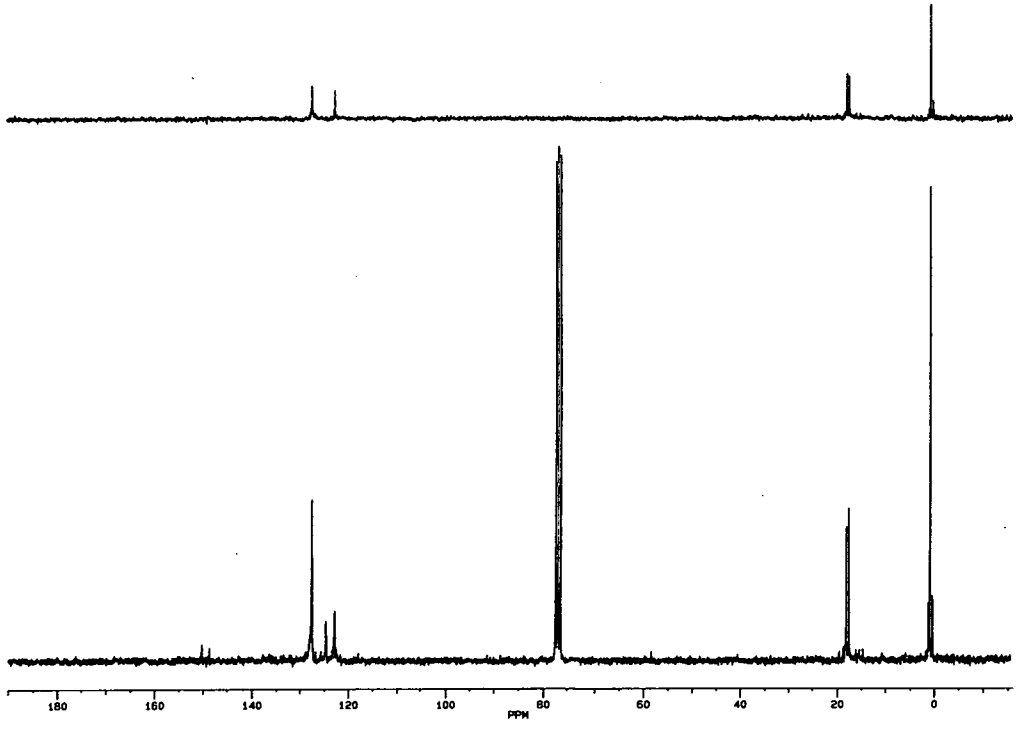

Figure 3.27 ^{13}C NMR spectrum in $CDCl_3$ of 14.

The NMR spectra of **15** are analogous to **14**. The ^{1}H NMR spectrum places downfield H5 and H6 as a multiplet at δ 6.80, whilst the equivalent H9 and H10 give a singlet at δ 1.90 (Figure 3.28). The hydrogen atoms H1 are placed at δ 1.60, whilst the significant peak for the co-ordinated Si-CH_3 in the ^{1}H NMR occurs at a characteristic upfield value at δ 0.10. The ^{13}C NMR spectrum gives signals for the C3, C5, C4 and C6 at δ 147.35, 126.80, 124.89 and 123.28, whilst the co-ordinated α-carbon C2 is placed at δ 149.10 (Figure 3.29). The co-ordinated C1, C9 and C10 show shifts to downfield at δ 15.05 and 14.88, respectively, whilst Si-CH_3 is characteristically upfield at δ 0.10.

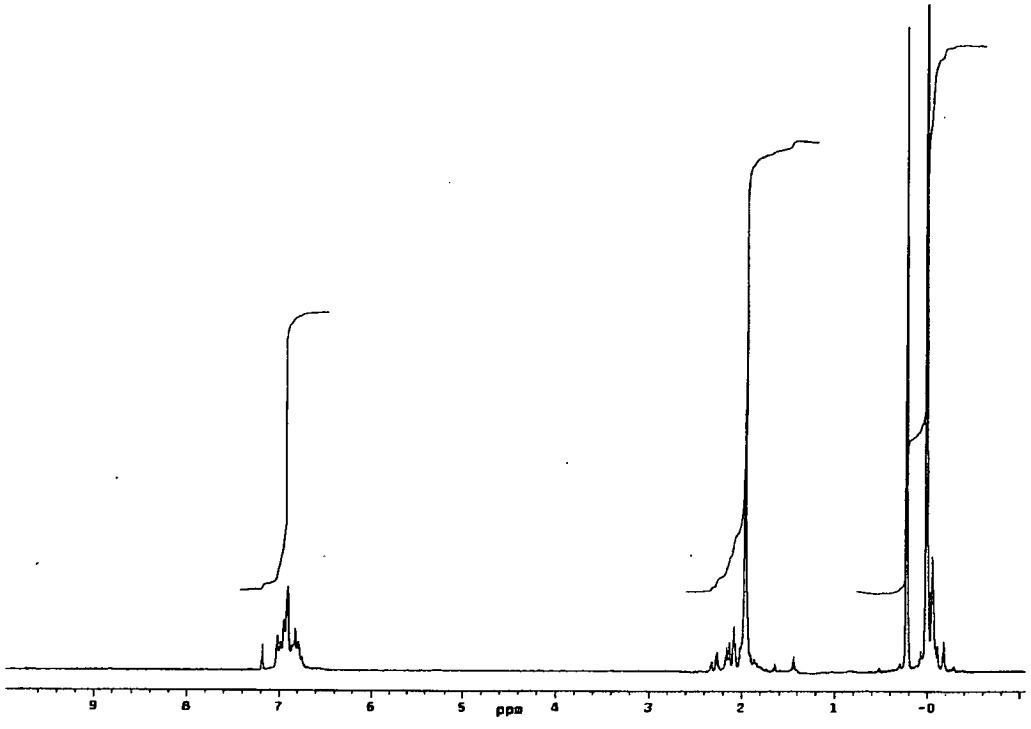

Figure 3.28 ^{1}H NMR spectrum in $CDCl_3$ of 15.

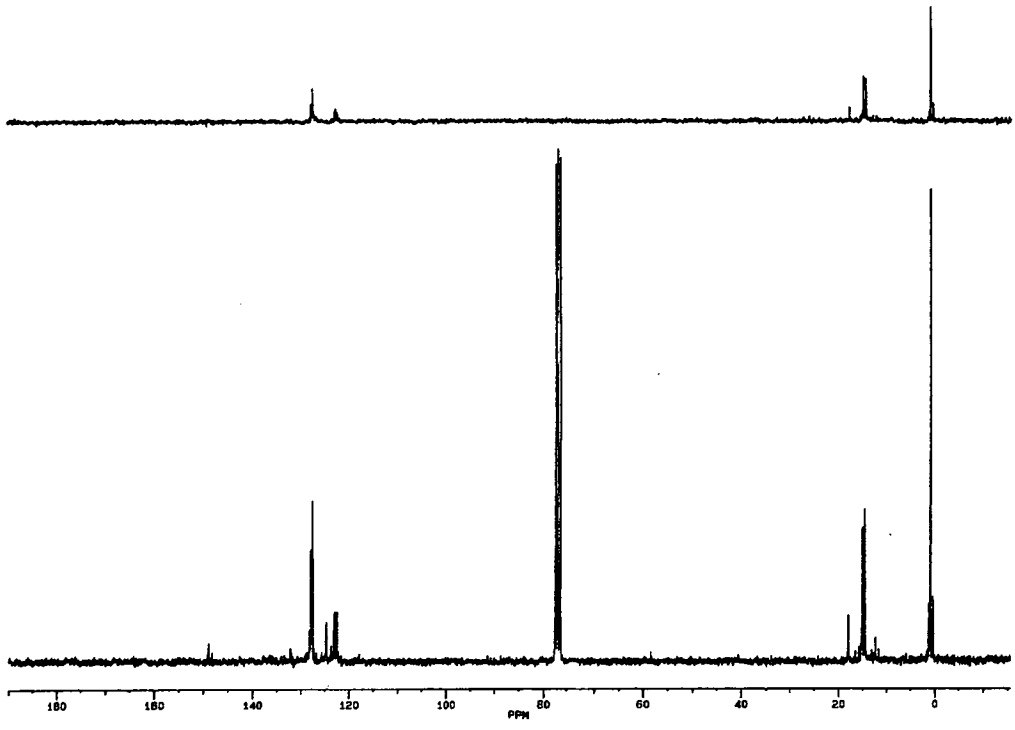

Figure 3.29 ^{13}C NMR spectrum in $CDCl_3$ of 15.

The X-ray structure of **15** is shown in Figure 3.30. Significant bond lengths and angles are provided in Table 3.1. The silicon atom has Si-C bond lengths of 1.858(4), 1.854(6) and 1.862(5) Å, whilst the bond length of the α-C is 1.929(5) Å. The methyl carbon atom bonded to the second α-carbon is situated at 1.509(6) Å. The two α-carbon atoms show a trigonal geometry, and both are situated in the same plane, where the geometry for Si(1)-N(1)-C(1)-N(2) is almost planar with a deviation of 9.25° from the plane. The bulky silicon atom occupies alternate positions with C(1) and between both phenyl groups. Finally, the N-(α-C) bond lengths of 1.287(5) and 1.283(5) Å are typical of this kind of interaction.

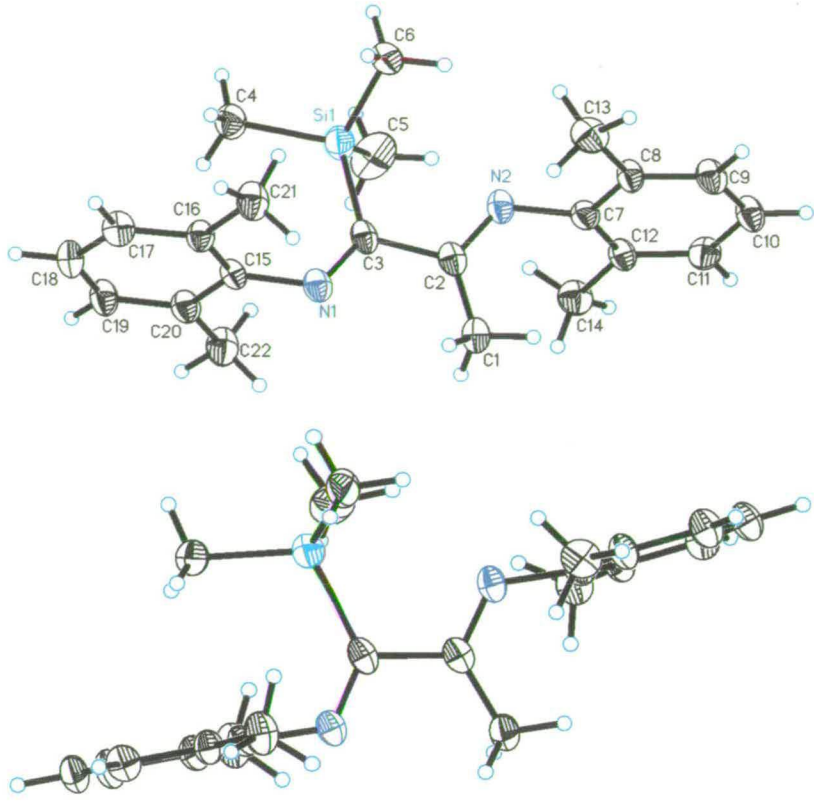

Figure 3.30 Crystallographic structure of 15 with different orientations. Displacement ellipsoids are shown at the 50 % probability level.

Table 3.1 Selected bond distances (Å), angles and torsion (°) for 15.

Si(1)-C(3)	1.929(5)	Si(1)-C(4)	1.858(5)	Si(1)-C(5)	1.854(6)
Si(1)-C(6)	1.862(5)	N(1)-C(3)	1.287(5)	N(1)-C(15)	1.427(6)
N(2)-C(2)	1.283(5)	N(2)-C(7)	1.414(6)	C(1)-C(2)	1.509(6)
C(3)-N(1)-C(15)	122.0(4)	C(2)-N(2)-C(7)	123.2(4)		
N(2)-C(2)-C(1)	125.9(4)	N(2)-C(2)-C(3)	114.1(4)		
C(1)-C(2)-C(3)	119.9(4)	N(1)-C(3)-C(2)	113.7(4)		
N(1)-C(3)-Si(1)	129.9(4)	C(2)-C(3)-Si(1)	116.4(3)		
C(7)-N(2)-C(2)-C(1)	-0.7(7)	C(7)-N(2)-C(2)-C(3)	179.1(4)		
C(15)-N(1)-C(3)-C(2)	179.6(4)	C(15)-N(1)-C(3)-Si(1)	-0.4(6)		
N(2)-C(2)-C(3)-N(1)	-170.7(4)	C(1)-C(2)-C(3)-N(1)	9.1(6)		
N(2)-C(2)-C(3)-Si(1)	9.4(5)	C(1)-C(2)-C(3)-Si(1)	-170.8(3)		

3.2.4 Reactivity of the Alkylated 2,6-Dimethylphenyl Isonitrile with $Me_2(Ph)SiCl$

Reactions of the lithiated isonitrile ligand **13** with a more bulky electrophile, such as $Me_2(Ph)SiCl$, can avoid byproducts and dimeric or polymeric compounds (Figure 3.31). Although using $Me_2(Ph)SiCl$ gives one product, the yield is also reduced by this reagent. When $Ph_2(Me)SiCl$ is used no product is obtained. The ^1H

NMR spectrum of [ArNC(Me)Si(Ph)Me_2] (Ar: 2,6-dimethylphenyl) (**16**) was conducted and shows an aromatic proton shifted downfield at δ 7.34, whilst H9 and H10 are placed at δ2.45. The resonance of hydrogen atoms attached to C1 is located at δ 0.98, whilst that of co-ordinated Si-CH_3 is placed at δ 0.34 (Figure 3.32).

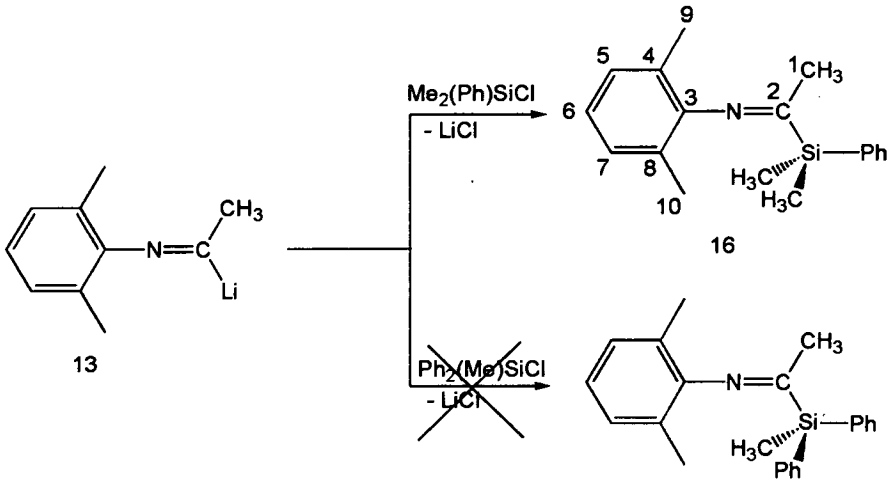

Figure 3.31 Reaction of 13 with: a) Me_2(Ph)SiCl; b) Ph_2(Me)SiCl.

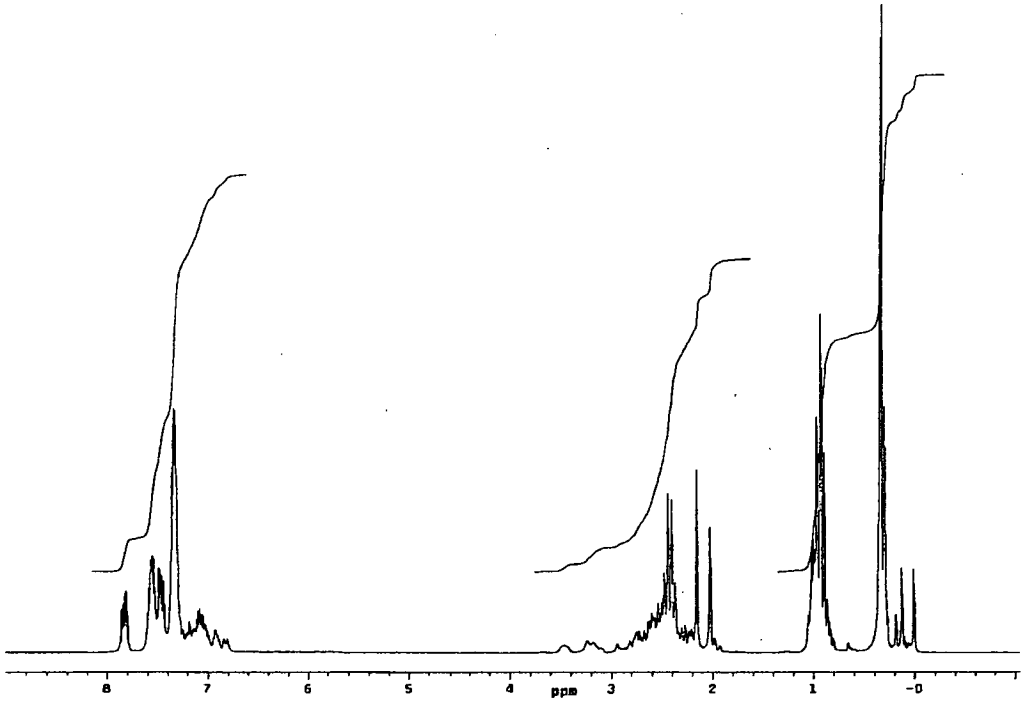

Figure 3.32 ^{1}H NMR spectrum in $CDCl_3$ of 16.

3.2.5 Reactivity of the Alkylated 2,6-Dimethylphenyl Isonitrile with Ph_2BCl

Reaction of lithium aldimine **13** with Ph_2BCl (**11**) (2:1 molar ratio) under similar conditions (Figure 3.33) was undertaken in order to obtain the ligand proposed, but was unsuccessful. In addition, there was no interaction between the **11** and **13** at different conditions, according to NMR spectroscopy. The only product following the reaction given in Figure 3.33 was a new isonitrile tetramer $[\{ArNC(Me)CNAr\}_2]_2$ (Ar: 2,6-dimethylphenyl) (**17**) (Figure 3.34).

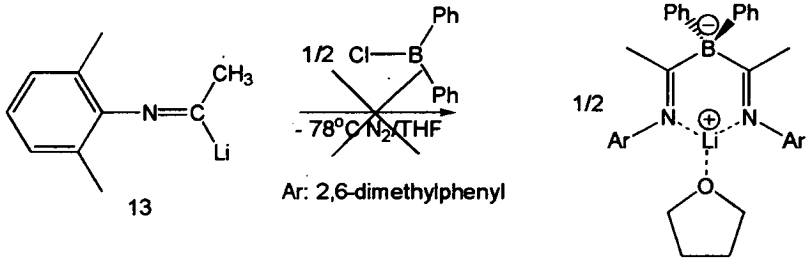

Figure 3.33 Suggested reactivity between 13 and 11.

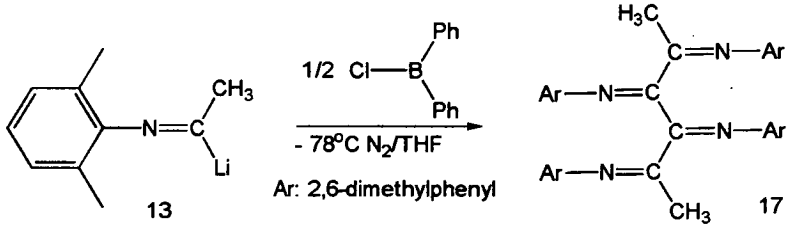

Figure 3.34 Reactivity of 13 with 11.

The ^1H NMR spectrum of **17** places a downfield multiplet signal belonging to the aromatic hydrogen atoms at δ 6.84, whilst the upfield singlet for H9 and H10 is placed at δ 3.21. The significant peak for hydrogen atoms H1 are located at δ 1.15 (Figure 3.35). The ^{13}C NMR spectrum shows a downfield shift for C3, C5 and C4 at downfield δ 142.10, 136.10 and 104.30, respectively. The resonance of Ar-CH_3 shifted to δ 31.72, whilst that of CH_3–(α-C) is shifted to δ 15.05, respectively (Figure 3.36).

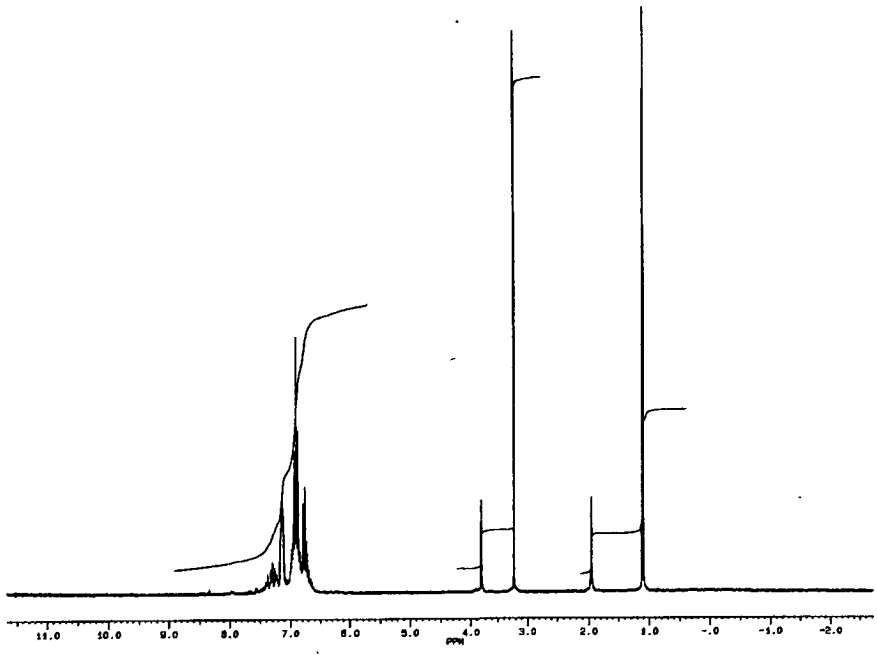

Figure 3.35 ^{1}H NMR spectrum in THF-d_8 of 17.

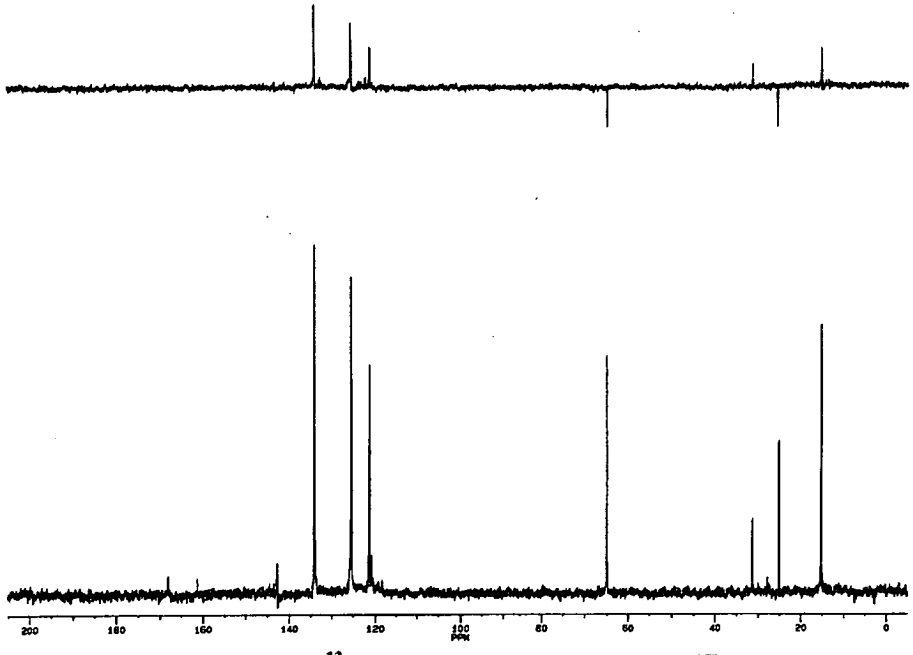

Figure 3.36 ^{13}C NMR spectrum in THF-d_8 of 17.

The X-ray crystal structure of **17** reveals a tetrameric compound (Figure 3.37) where C3 and C22 may represent the core of the molecule. Similar groups are situated in alternate positions in order to prevent high repulsion between them. Significant bond lengths and angles are shown in Table 3.2. Methyl groups bonded to

α-carbon atoms are situated at 1.501(3) Å, and the N-(α-C) bond lengths of 1.272(2) and 1.269(2) Å agree with this type of interaction but with shorter distances than in Figure 3.30. The α-carbon atoms C3 and C22 are connected to each other at 1.493(3) Å, whilst C2-C3 and C22-C21 bond lengths are 1.507(2) Å.

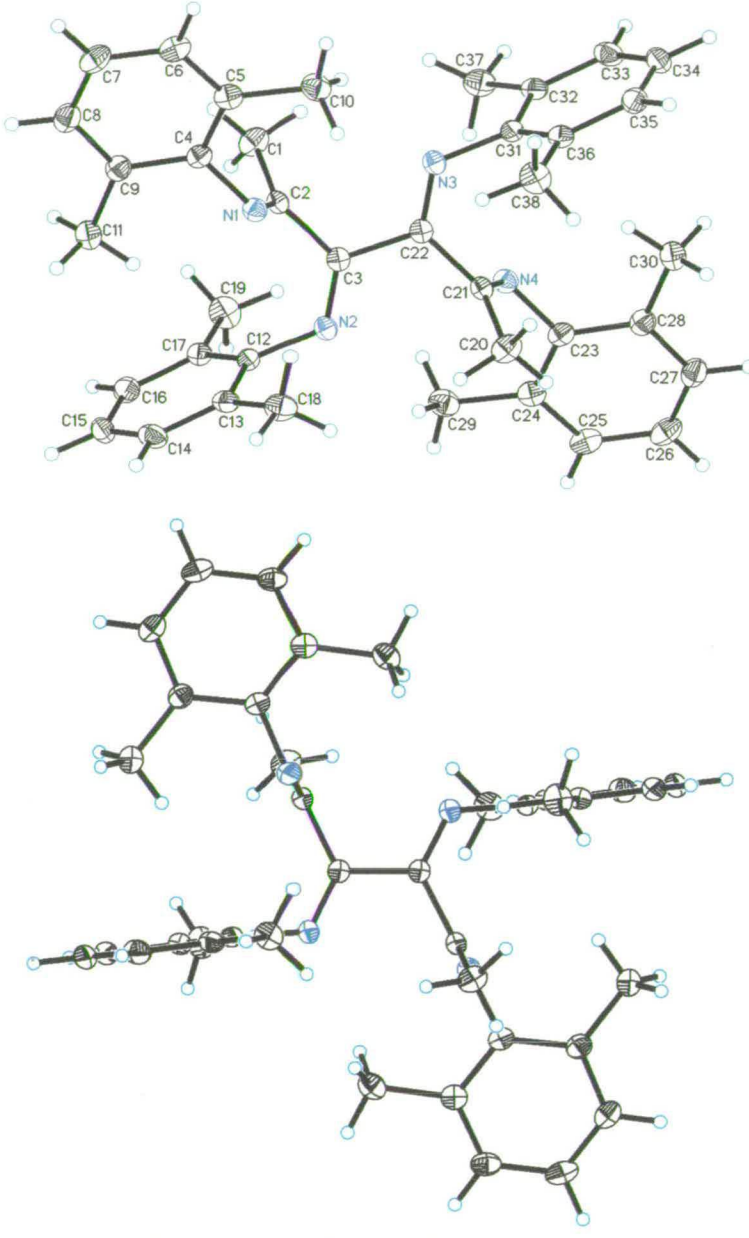

Figure 3.37 Crystallographic structure of 17 with different orientations. Displacement ellipsoids are shown at the 50% probability level.

Table 3.2 Selected bond distances (Å), angles and torsion (°) for 17. Symmetry transformations used to generate equivalent atoms: #1 -x+1,-y+1,-z+1.

N(1)-C(2)	1.269(2)	N(1)-C(4)	1.431(2)	N(2)-C(3)	1.272(2)
N(2)-C(12)	1.427(2)	C(1)-C(2)	1.501(3)	C(2)-C(3)	1.507(2)
C(3)-C(3)#1	1.493(3)				
C(2)-N(1)-C(4)	119.84(15)	C(3)-N(2)-C(12)	121.44(14)		
N(1)-C(2)-C(1)	126.69(16)	N(1)-C(2)-C(3)	115.96(15)		
C(1)-C(2)-C(3)	117.33(16)	N(2)-C(3)-C(3)#1	117.49(18)		
N(2)-C(3)-C(2)	126.60(15)	C(4)-N(1)-C(2)-C(1)	-0.9(3)		
C(4)-N(1)-C(2)-C(3)	177.62(14)	C(12)-N(2)-C(3)-C(3)#1	-179.95(17)		
C(12)-N(2)-C(3)-C(2)	-0.1(3)	N(1)-C(2)-C(3)-N(2)	77.2(2)		
C(1)-C(2)-C(3)-N(2)	-104.2(2)	N(1)-C(2)-C(3)-C(3)#1	-103.0(2)		
C(1)-C(2)-C(3)-C(3)#1	75.7(2)				

A possible explanation for this unexpected result could be that a single electron is transferred between two different lithiated species, according to the scheme shown in Figure 3.38. In addition, organolithium reagents are known to react quite well with oxidizing reagents to form unexpected radical intermediates which can then abstract hydrogen from the solvent or react with other ligands remaining in the same reaction.[7,23] Although, the conditions for the reaction of [ArNC] (Ar: 2,6-dimethylphenyl) with MeLi were one to one equivalent to an excess of MeLi to prevent a possible dimerization, the products were always the same (**17**). As suggested in Figure 3.38, the high reactivity of the lithium aldimine with the still unreactive isonitrile could produce the new lithium aldimine **III**, which suggests two reasonable routes for reaching the final product **17**. The route **A** involves an attraction by coupling (**IVA**) between two lithiated species of **III** to form **17**. Alternatively, the second route **B**, involves the attraction brought on by the transference of electrons (**IVB**) between two lithiated species of **IV** and an excess of unreactive [ArNC] (Ar: 2,6-dimethylphenyl) to produce **17**.

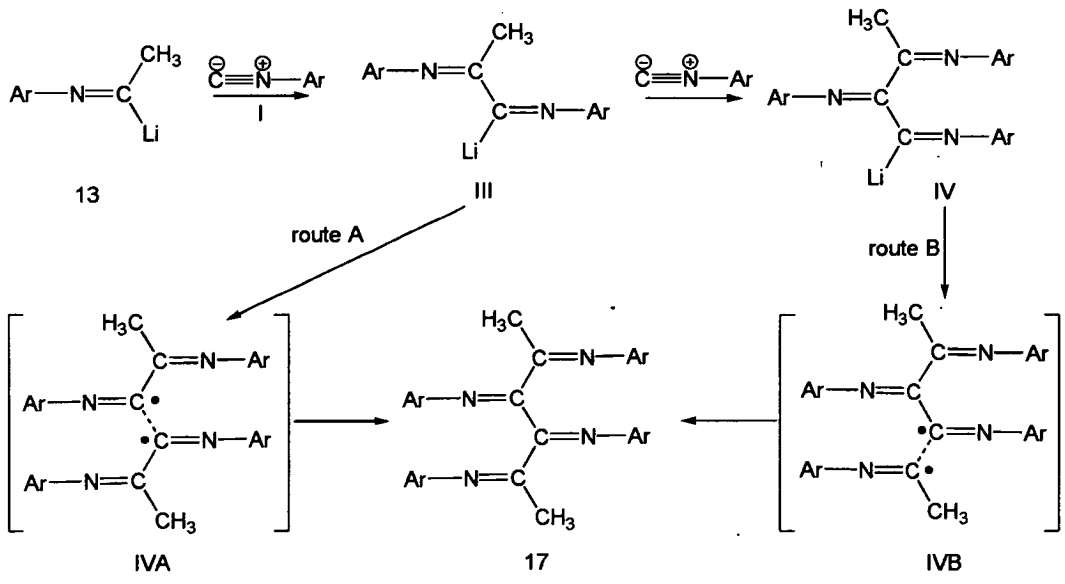

Figure 3.38 Reaction suggested for the formation of 17.

Moreover, the unreactive isonitrile reagent may react with the new lithium aldimine formed, producing a large polymeric product, according to the scheme shown in Figure 3.39. It is important to note that without the presence of Ph_2BCl (**11**) the tetramer was not formed, thus this electrophilic reagent may be acting as a catalyst producing a short chain of product.

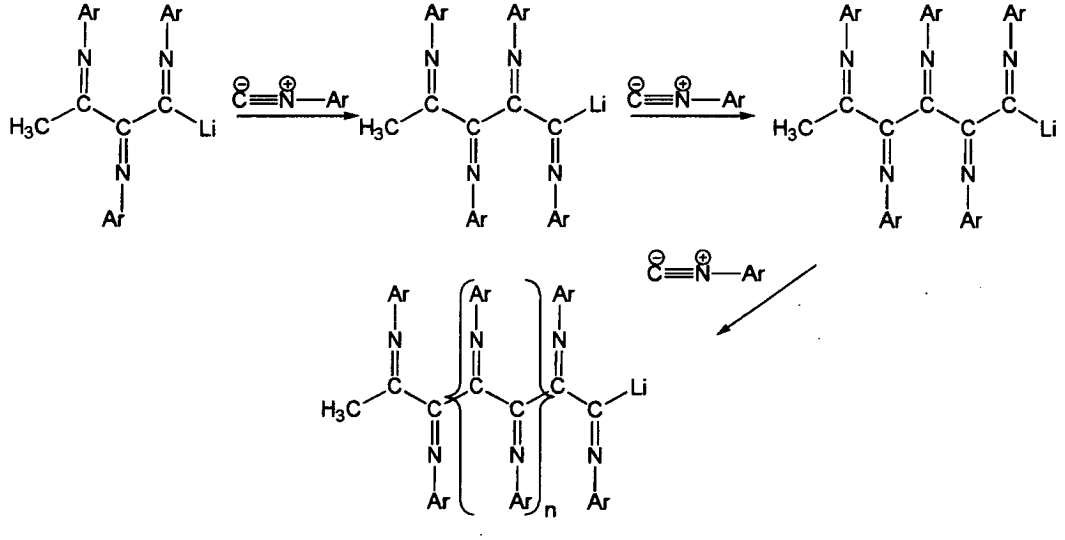

Figure 3.39 Reaction suggested for the formation of a polymer from 13.

3.2.6 Reactivity of the 1,1,3,3-Tetramethylbutyl Isonitrile with Me_3SiCl

Treatment of 1,1,3,3-tetramethylbutylisonitrile, [TMBuNC], with different organolithium reagents (MeLi, ^{n}BuLi, *sec*-BuLi) did not produce a satisfactory lithiation of the α–carbon. Only ^{n}BuLi produced a good yield of lithiated aldimine [TMBuNC(Bu)Li] (**18**) and further reactivity with a reagent such as Me_3SiCl gave a yellow oil of [TMBuNC(Bu)$SiMe_3$] (**19**), according to Figure 3.40. No activity activity, however, was detected when other electrophilic reagents, such as $Ph_2(Me)SiCl$ or Ph_2BCl (**11**) were used. The ^{1}H NMR spectrum of **19**, gives a mutiplet signal for all the methyl hydrogen atoms at δ 1.27, whilst the CH_2 multiple signals are placed at δ 0.88. The characteristic peak for the hydrogen atoms from the Si-CH_3 is located upfield at δ 0.07 (Figure 3.41). The ^{13}C NMR (DEPT; θ=135°) spectrum shows α–carbon (C1) at downfield chemical shift of δ 158.62 (no signal), whilst C2, C3, C4, C5 and C6 shifted to δ 61.30 (no signal), δ 58.22 (negative signal), δ 60.02 (no signal), δ 32.51 (positive signal) and δ 32.01 (positive signal), respectively. The upfield butyl signals for CH_2 and CH_3 carbon atoms are also placed at δ 29.31 (negative signal), 23.80 (negative signal) and 13.70 (positive signal), respectively. The co-ordinated Si-CH_3 are placed at δ 0.90 (positive signal) (Figure 3.42).

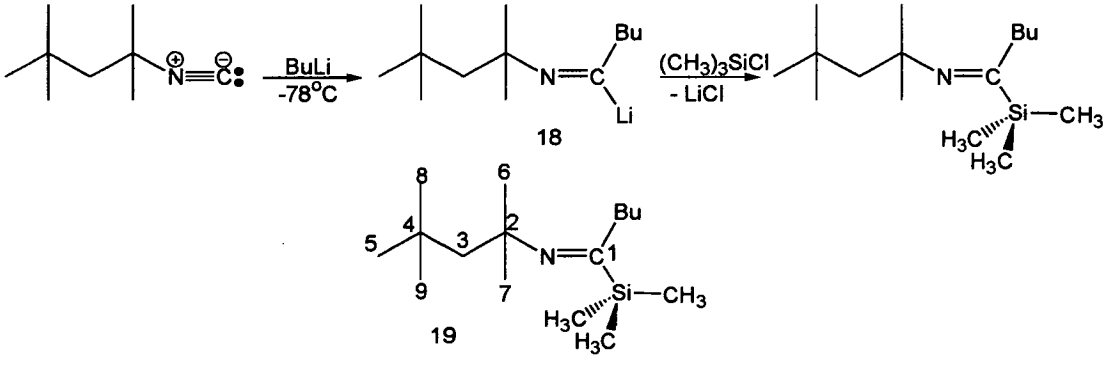

Figure 3.40 Reaction of 18 with Me_3SiCl.

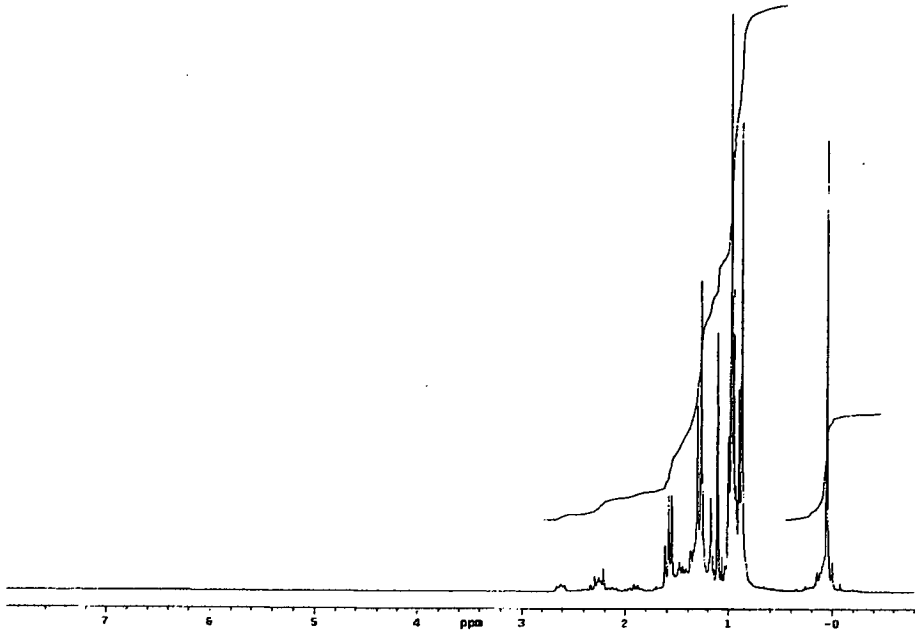

Figure 3.41 ^{1}H NMR spectrum in $CDCl_3$ of 19.

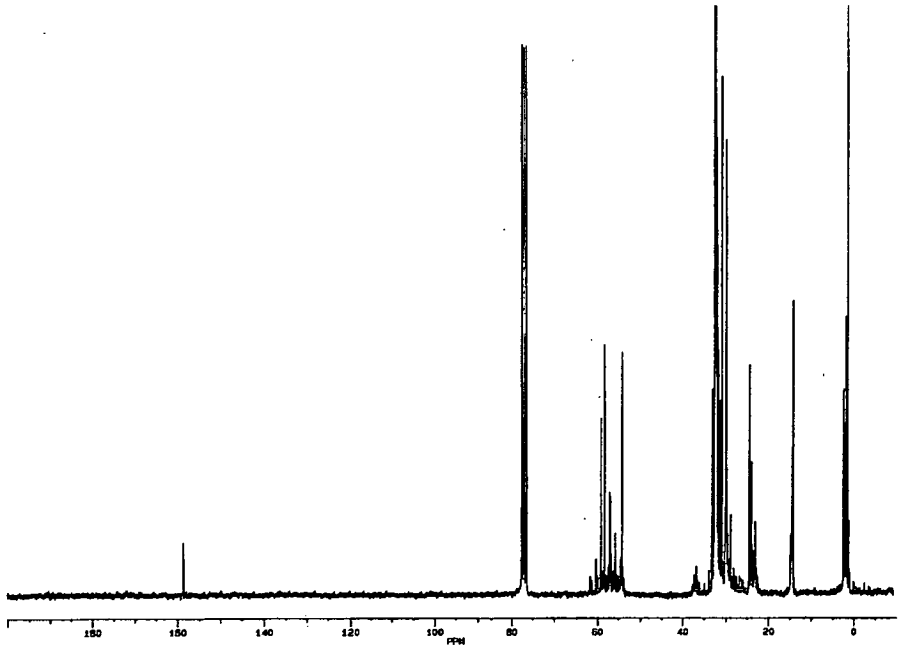

Figure 3.42 ^{13}C NMR spectrum in $CDCl_3$ of 19.

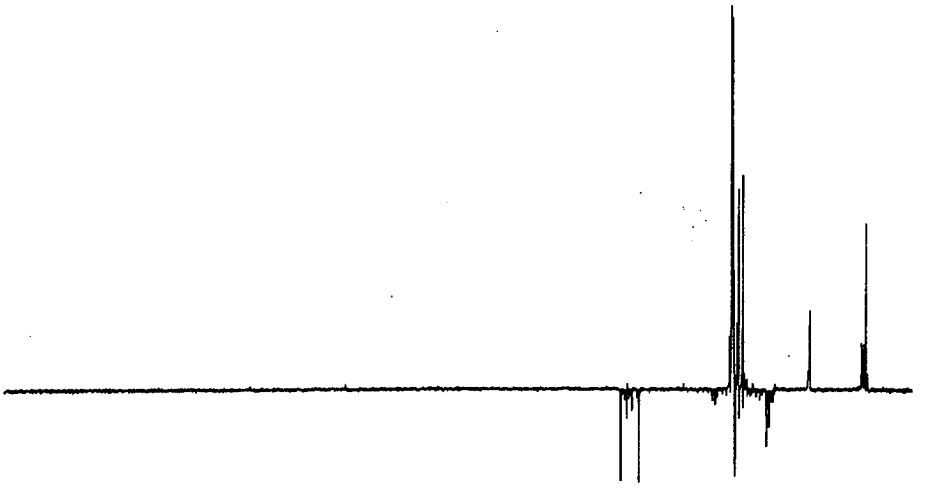

Figure 3.42 (Continued) ^{13}C NMR (DEPT;θ=135°) spectrum in $CDCl_3$ of 19.

3.2.7 Synthesis of Hydrogen Dimethylbis(2-pyridyl)borate and Isomeric Products

Reaction of 2-lithiopyridine with half an equivalent of dimethylboron bromide (**20**) in diethyl ether at –78 °C, resulted satisfactorily in the formation of lithiated dimethylbis(2-pyridyl)borate, [{$Me_2B(2\text{-}py)_2$}Li] (**21**), as shown in Figure 3.43. After an acidic treatment of **21** hydrogen dimethylbis(2-pyridyl)borate, [$Me_2B(2\text{-}py)_2(H)$] (**22**), was obtained in 62% yield. Colourless crystals of **22** suitable for X-ray analysis were grown from a concentrated hexane solution at –20 °C.

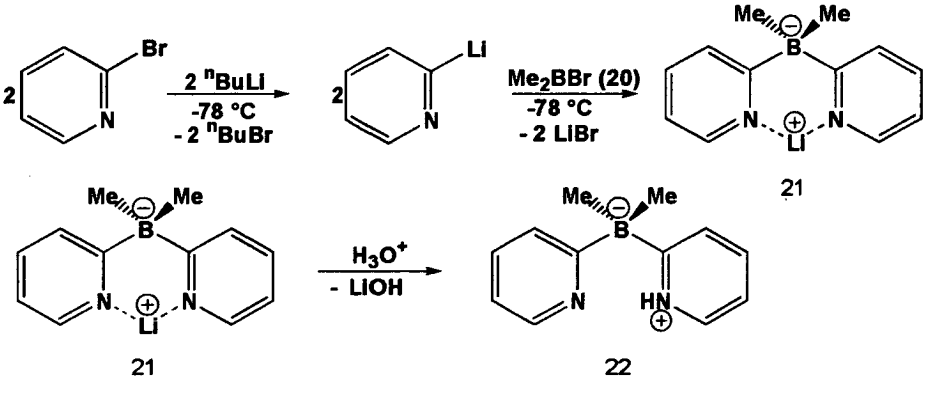

Figure 3.43 Synthesis of 22.

The ^1H NMR spectrum of **22** gives consistent downfield peaks for the pyridyl ring at δ 8.40, 7.87, 7.70 and 7.19, while a singlet signal at δ 18.54 is assigned to the

nitrogen bonded proton (Figure 3.44). In the upfield region a triplet signals is assigned to the dimethylborate protons at δ 0.14. The ^{13}C NMR (DEPT; θ=135°) spectrum shows a shift of pyridyl ring resonances to downfield at δ 188.40 (no signal), 141.87 (positive signal), 136.10 (positive signal), 130.62 (positive signal) and 120.01 (positive signal), while dimethylborate carbons are presented at upfield δ 13.74 (positive signal) (Figure 3.45). The ^{11}B NMR spectrum of **22** shows a characteristic sharp singlet at δ -18.28 (Figure 3.46).

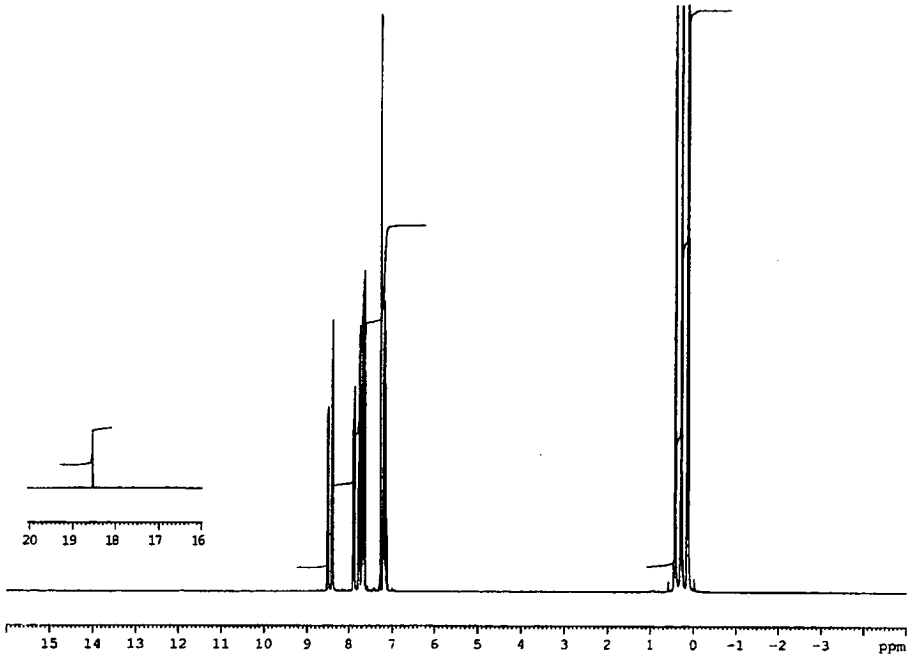

Figure 3.44 ^1H NMR spectrum in $CDCl_3$ of 22.

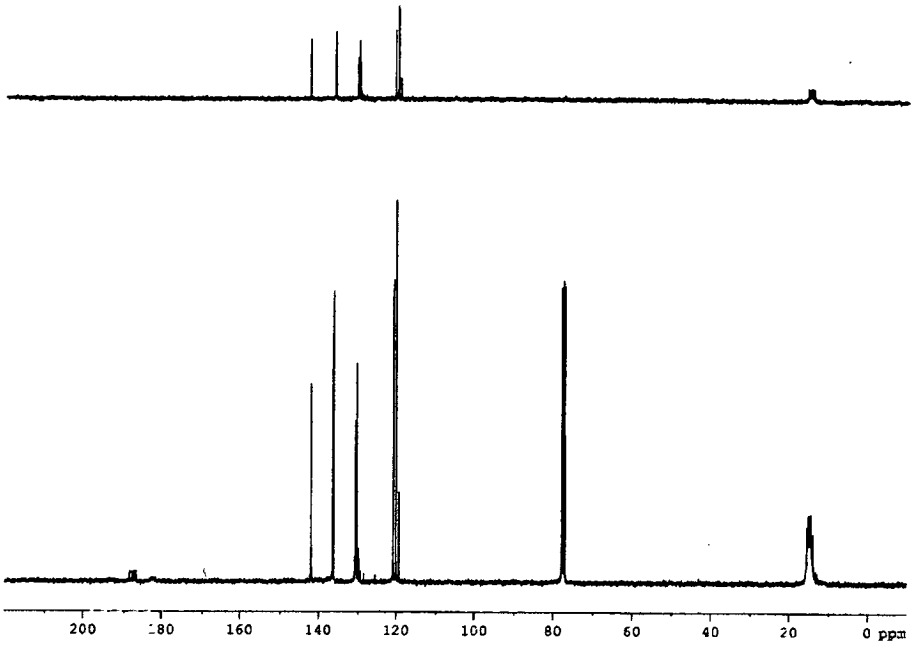

Figure 3.45 ^{13}C NMR spectrum in $CDCl_3$ of 22.

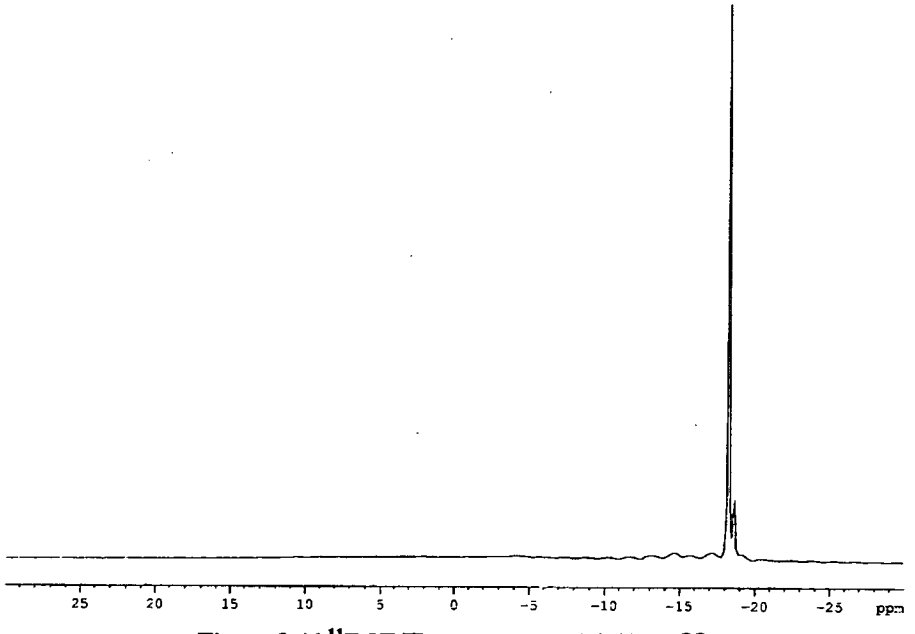

Figure 3.46 ^{11}B NMR spectrum in $CDCl_3$ of 22.

The X-ray crystal structure of **22** reveals a tetrahedral boron centre, with both pyridyl rings situated in the same plane (Figure 3.47). The B-C(aromatic) bond lengths are 1.632(3) and 1.631(2) Å, whilst both methyl carbon atoms are placed at 1.637(2) Å from the tetrahedral boron atom. Strong intramolecular hydrogen bonding makes molecules of **22** planar (except for the methyl group atoms) and appears to

account for the fact that this compound has few acid properties. In addition, the aromaticity provides extra stability of a favourable planar symmetry structure. Selected bond lengths and angles are shown in Table 3.3.

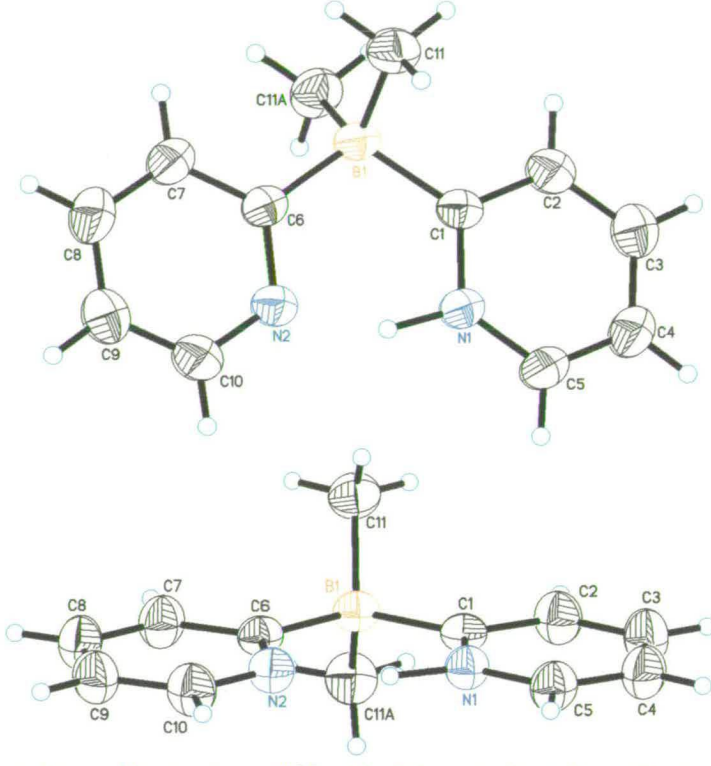

Figure 3.47 Crystallographic structure of 22 with different orientations. Displacement ellipsoids are shown at the 50% probability level.

Table 3.3 Selected bond distances (Å) and angles (°) for 22. Symmetry transformations used to generate equivalent atoms: #1 x,-y+1/2,z.

C(1)-N(1)	1.344(3)	C(1)-B(1)	1.632(3)	N(1)-C(5)	1.340(3)
C(6)-N(2)	1.346(3)	C(6)-B(1)	1.631(3)	N(2)-C(10)	1.340(3)
B(1)-C(11)	1.637(2)	B(1)-C(11)#1	1.637(2)		

N(1)-C(1)-C(2)	115.2(2)	N(1)-C(1)-B(1)	121.0(2)
N(1)-C(5)-C(4)	121.2(2)	C(1)-B(1)-C(11)#1	107.50(13)
C(1)-B(1)-C(11)	107.50(13)	C(2)-C(1)-B(1)	123.8(2)
C(5)-N(1)-C(1)	123.6(2)	C(6)-B(1)-C(1)	112.8(2)
C(6)-B(1)-C(11)	109.31(12)	C(6)-B(1)-C(11)#1	109.31(12)
C(7)-C(6)-B(1)	121.6(2)	C(10)-N(2)-C(6)	120.7(2)
N(2)-C(10)-C(9)	123.5(2)	N(2)-C(6)-B(1)	121.5(2)
C(11)#1-B(1)-C(11)	110.4(2)		

D-H...A	d(D-H)	d(H...A)	d(D...A)	<(DHA)
N(1)-H(1N)...N(2)	1.085(2)	1.59(2)	2.606(15)	153.6(12)

The synthesis of **22** involved several steps where even with the use of a stoichiometric amount of a strong Lewis acid (Me_2BBr) and the low temperatures employed the formation of compounds analogous to the pyrazoboles were also obtained (Figure 3.48). Moreover, it is important to point out that during the reaction the main product was obtained *via* the intermediate borate **21**, suggesting that the formation of dimethylboronium bis(2-pyridyl)borate (**23**) is preferred over the dimeric dimethyl(2-pyridyl)borane (**24**). Although the isomeric compounds **23** and **24** were not separated, they were identified by NMR spectroscopy and the first X-ray crystallographic structure was resolved.

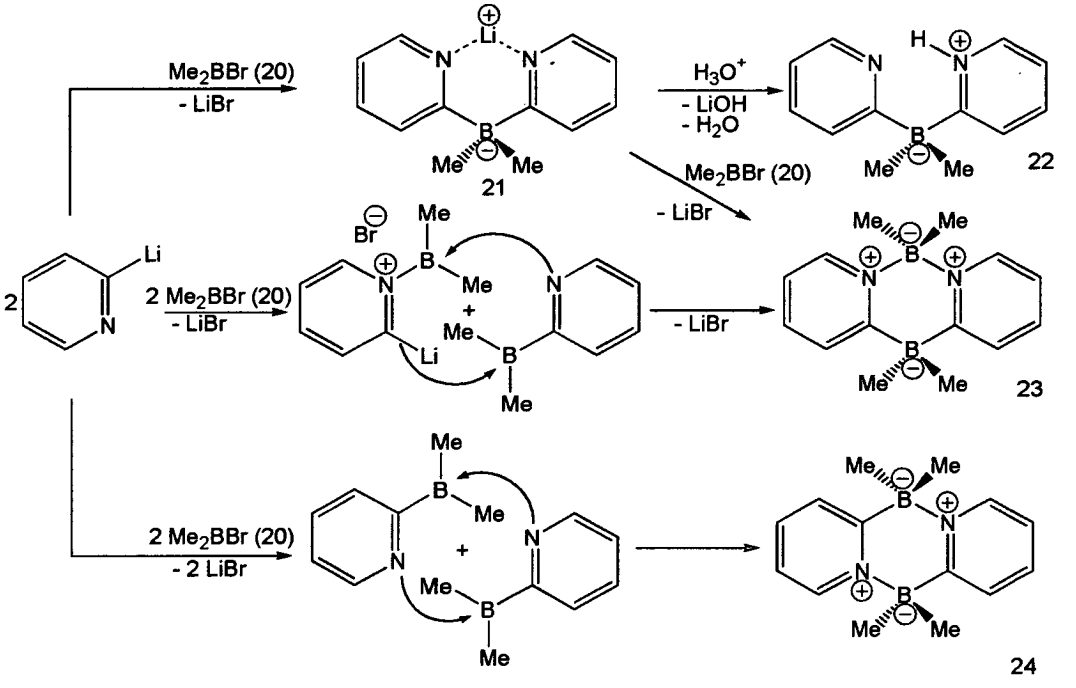

Figure 3.48 Mechanism suggested for the formation of 23 and 24.

The ^1H NMR spectrum for the isomers (**23**, **24**) shows downfield peaks consistent with shifts for pyridyl rings between δ 8.44 and 7.15, while in the upfield region triplet signals are assigned to the protons of the dimethylborate units at δ 0.21 and 0.06 (Figure 3.49). The ^{13}C NMR spectrum shows a shift of the pyridyl rings to downfield between δ 188.39 and 120.00, while the dimethylborate carbon atoms are observed upfield at δ 14.86 (Figure 3.50). The ^{11}B NMR spectrum of the isomer mixture gives two sharp singlets at δ 6.39 and −14.29 for **23**, and one singlet for **24**

at δ -1.85 (Figure 3.51). The ^{11}B NMR spectrum indicates the presence of **23** and **24** in an approximate ratio of 4:1

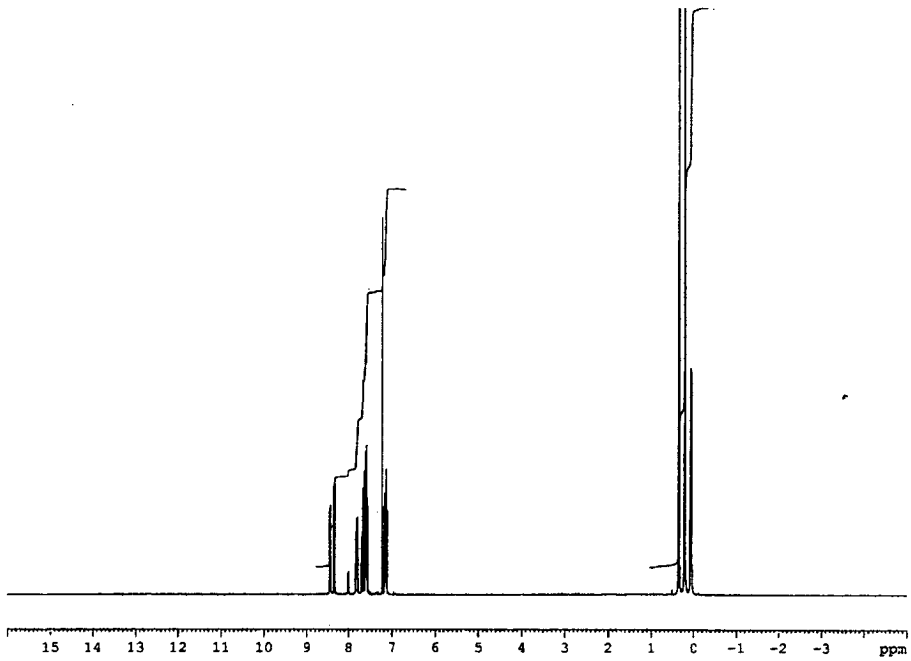

Figure 3.49 ^{1}H NMR spectrum in $CDCl_3$ of 23 and 24.

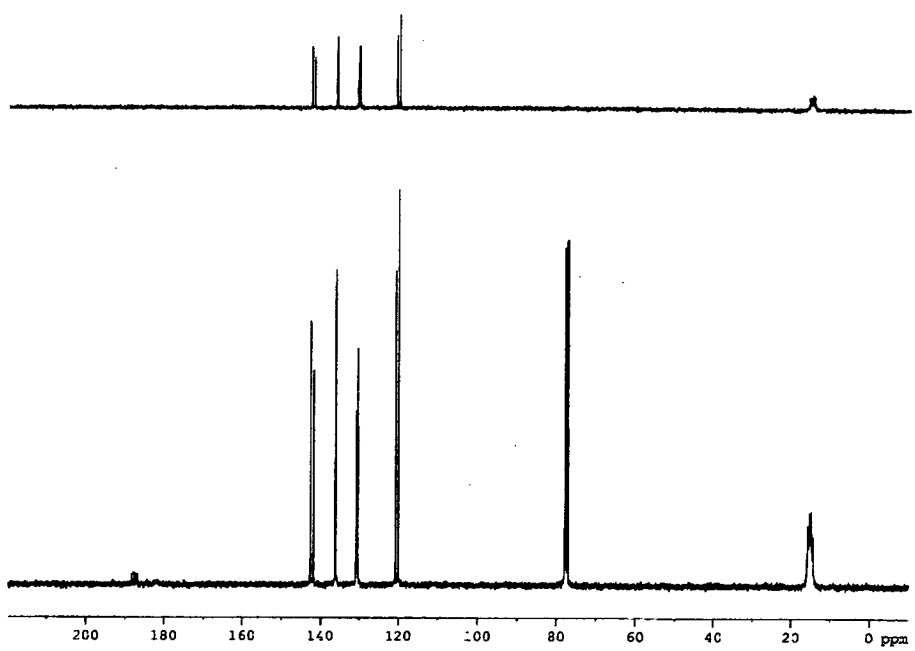

Figure 3.50 ^{13}C NMR spectrum in $CDCl_3$ of 23 and 24.

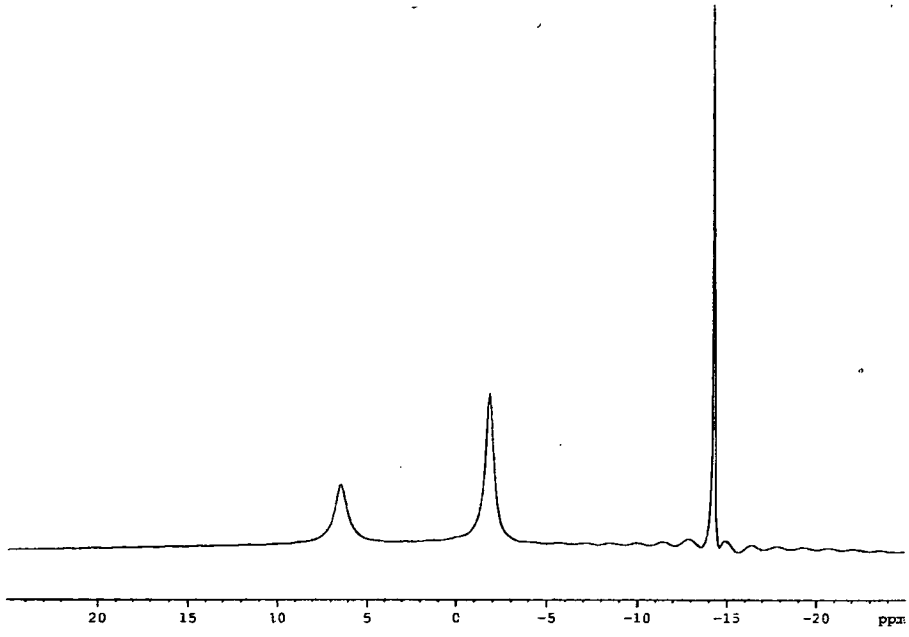

Figure 3.51 ^{11}B NMR spectrum in $CDCl_3$ of 23 and 24.

The X-ray data reveals a structure containing a disordered nitrogen atom, which is modelled as nitrogen and carbon atoms (in the ratio 80:20 over two positions with a common boron-position). The disorder observed in the crystallographic structure suggests the presence of both **23** (Figure 3.52) and **24** within the crystal (Figure 3.53). This result is confirmed by the ^{11}B NMR spectrum. The crystal structure reveals two tetrahedral boron atom centres, and both pyridyl rings are situated on the same plane. The B-C(aromatic) bond lengths are 1.619(7) Å, whilst both methyl atoms are placed at 1.603(8) and 1.642(8) Å from the tetrahedral boron atom. Selected bond lengths and angles are shown in Table 3.4.

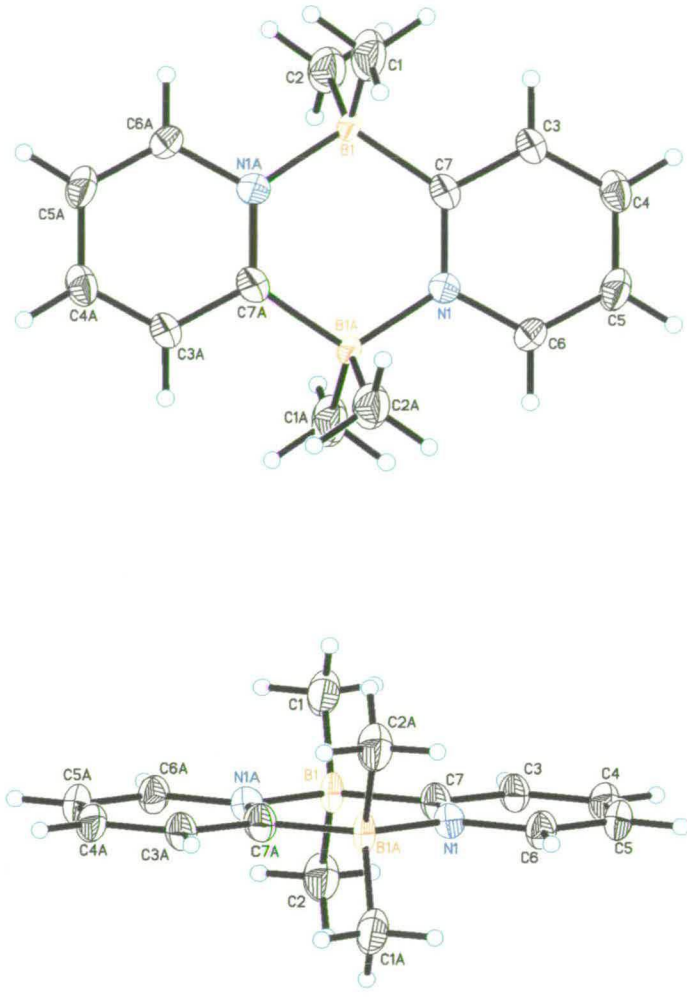

Figure 3.52 Crystallographic structure of 23 with different orientations. Displacement ellipsoids are shown at the 50% probability level.

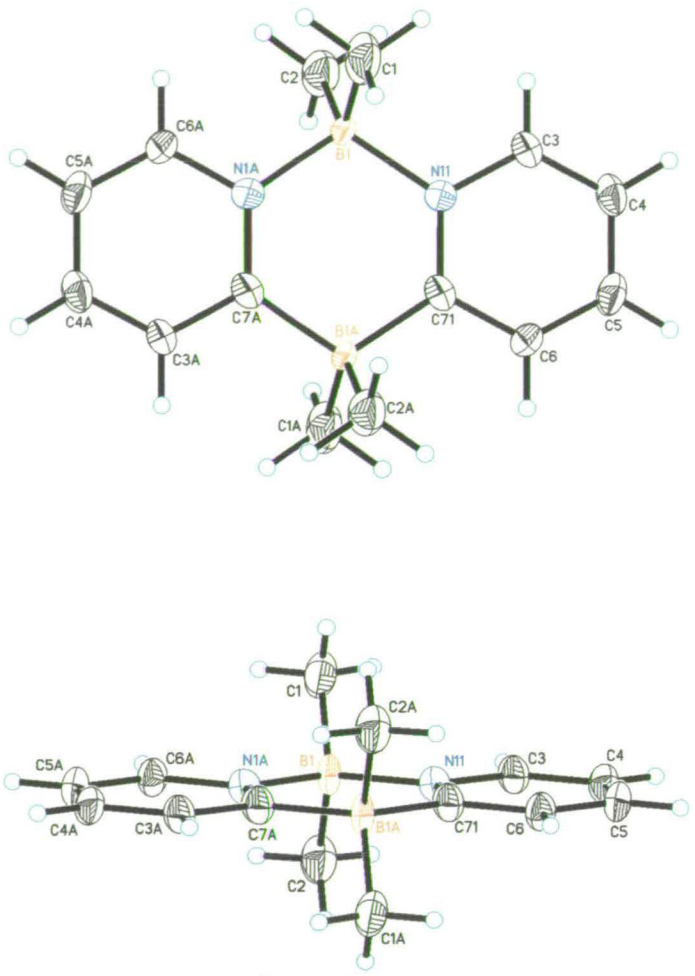

Figure 3.53 Crystallographic structure of 24 with different orientations. Displacement ellipsoids are shown at the 50% probability level.

Table 3.4 Selected bond distances (Å) and Angles (°) for 23 and 24. Symmetry transformations used to generate equivalent atoms: $^{\#1}$ -x+1,-y+1,-z.

C(1)-B(1)	1.603(8)	C(2)-B(1)	1.642(8)	B(1)-C(71)$^{\#1}$	1.612(6)
B(1)-N(1)$^{\#1}$	1.612(6)	B(1)-C(7)	1.619(7)	C(6)-N(1)	1.389(6)
N(1)-C(7)	1.351(7)	N(1)-B(1)$^{\#1}$	1.612(6)		
C(1)-B(1)-C(71)$^{\#1}$	108.6(4)		C(1)-B(1)-N(1)$^{\#1}$	108.6(4)	
C(1)-B(1)-C(7)	108.6(4)		C(71)$^{\#1}$-B(1)-C(7)	111.2(4)	
N(1)$^{\#1}$-B(1)-C(7)	111.2(4)		C(71)$^{\#1}$-B(1)-C(2)	108.1(4)	
N(1)$^{\#1}$-B(1)-C(2)	108.1(4)		C(7)-N(1)-C(6)	118.3(4)	
C(7)-N(1)-B(1)$^{\#1}$	124.4(4)		C(6)-N(1)-B(1)$^{\#1}$	117.3(4)	
N(1)-C(7)-B(1)	124.4(4)				

3.2.8 Reactivity of Lithium Dimethylbis(2-pyridyl)borate with MeMgCl

Different reactions have been undertaken using the lithium salt of the ligand **21** with an equimolar amount of MeMgCl at room temperature. Subsequent removal of the solvent in *vacuum* and extraction from ether, gives a partially insoluble white powder (no crystals could be obtained). The NMR spectra of the white powder were investigated and show the possible formation of a monomeric zwitterionic complex [{$Me_2B(2\text{-}py)_2$}Mg(Me)THF] (**25**) in 63 % yield (Figure 3.54).

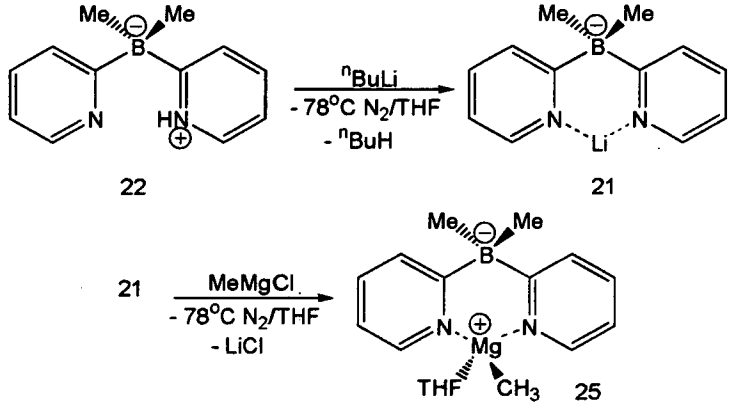

Figure 3.54 Synthesis of 25.

The ^{1}H NMR spectrum of **25** shows the expected 2-pyridyl pattern; with doublets at δ 8.61 and 7.81, and triplets at δ 7.66 and 7.29, respectively (Figure 3.55). A broad upfield singlet at δ 1.17 is located for the hydrogen atoms in the methyl groups bonded to the boron atom. The significant peak for the co-ordinated Mg-CH_3 in the ^{1}H NMR gives a characteristic value at δ –1.38. In addition, the co-ordination of magnesium atom is supported by the presence of two upfield singlet signals for solvated THF at δ 3.63 and 1.78, respectively. The ^{13}C NMR gives the downfield signal for the pyridyl carbon atoms bonded to the boron atom at 183.80, whilst the typical 2-pyridyl pattern is observed at δ 141.03, 136.21, 131.14 and 121.15 (Figure 3.56). The solvated monomer gives the equivalent THF signals at δ 67.12 and 23.30, respectively.

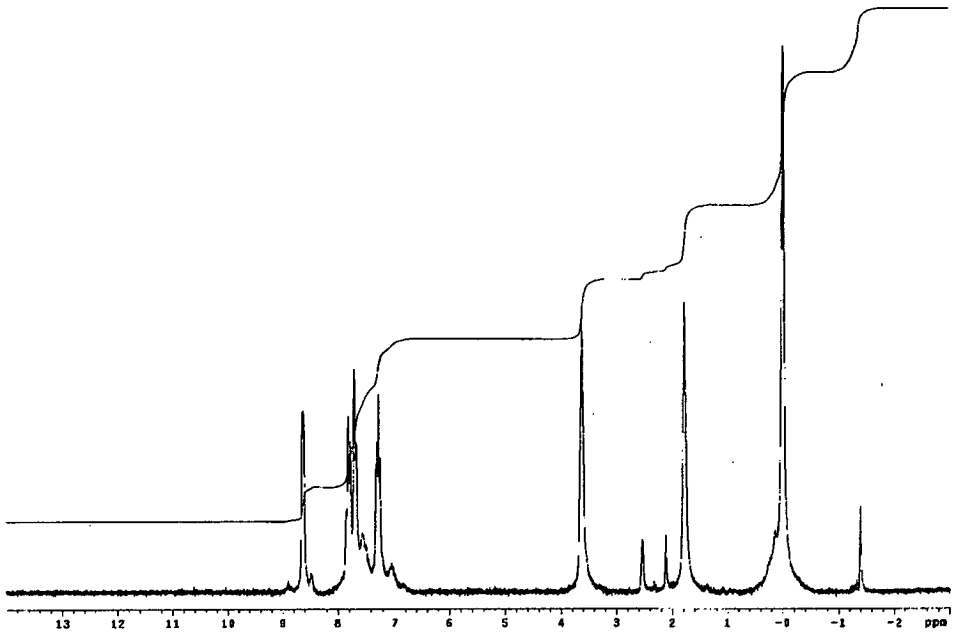

Figure 3.55 ^{1}H NMR spectrum in toluene-d_8 of 25.

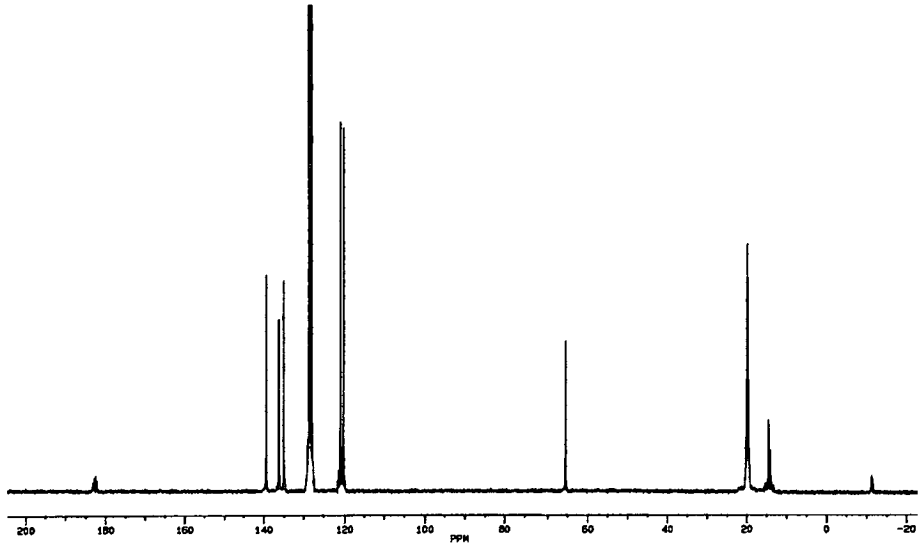

Figure 3.56 ^{13}C NMR spectrum in toluene-d_8 of 25.

3.2.9 Reactivity of Lithium Dimethylbis(2-pyridyl)borate with MeMgBr, ($PhCH_2$)MgCl and AllylMgCl

A solution of **21** was treated with a stoichiometric amount of MeMgBr in THF at room temperature. Subsequent removal of the solvent in *vacuum* and extraction from ether produced [{$Me_2B(2\text{-}py)_2$}$_2$Mg] (**26**) as a white powder. The

colourless crystals of **26** were grown from a concentrated solution of toluene at room temperature. The NMR spectra of the white powder were investigated and show only one type of pyridyl goup at room temperature, indicating a rapid inversion of the co-ordinated $[Me_2B(2\text{-}py)_2]^-$ ligand. The characteristic methyl groups bonded to the boron atom were not observed, while no THF· solvated signals were detected by NMR spectra. The X-ray crystallographic structure, however, revealed that a bischelated magnesium complex is obtained, as shown in Figure 3.57.

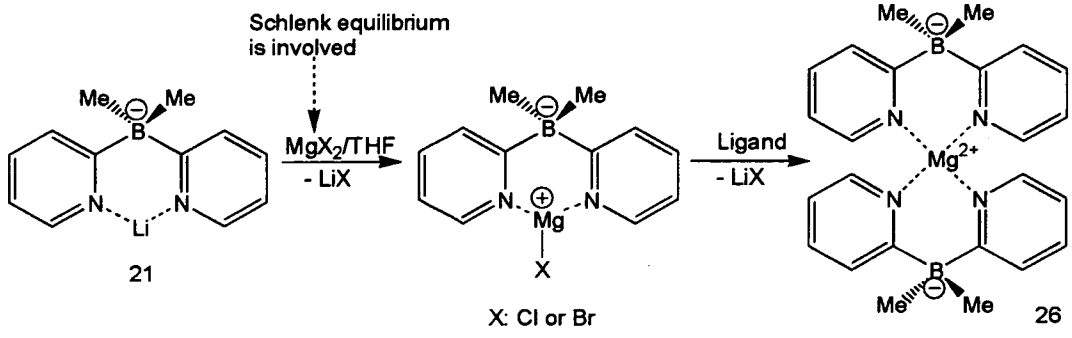

Figure 3.57 Synthesis of 26.

The ^1H NMR spectrum of $[\{Me_2B(2\text{-}py)_2\}_2Mg]$ (**26**) shows doublets at δ 8.73 and 8.32, whilst triplets at δ 7.84 and 7.07 for the expected 2-pyridyl groups are observed. Two singlets for the methyl hydrogen atoms bonded to the boron atom are shifted downfield to δ 0.61 and 0.08 (Figure 3.58). The ^{13}C NMR spectrum gives five sets of signals at 182.82, 139.46, 136.23, 128.17 and 120.83 which are assigned to the 2-pyridyl pattern, whilst the methyl carbon atoms are placed at the upfield frequency of δ 14.28 (Figure 3.59). Similar results were obtained when $(PhCH_2)MgCl$ and AllylMgCl were used (other Grignard reagents gave insoluble oils).

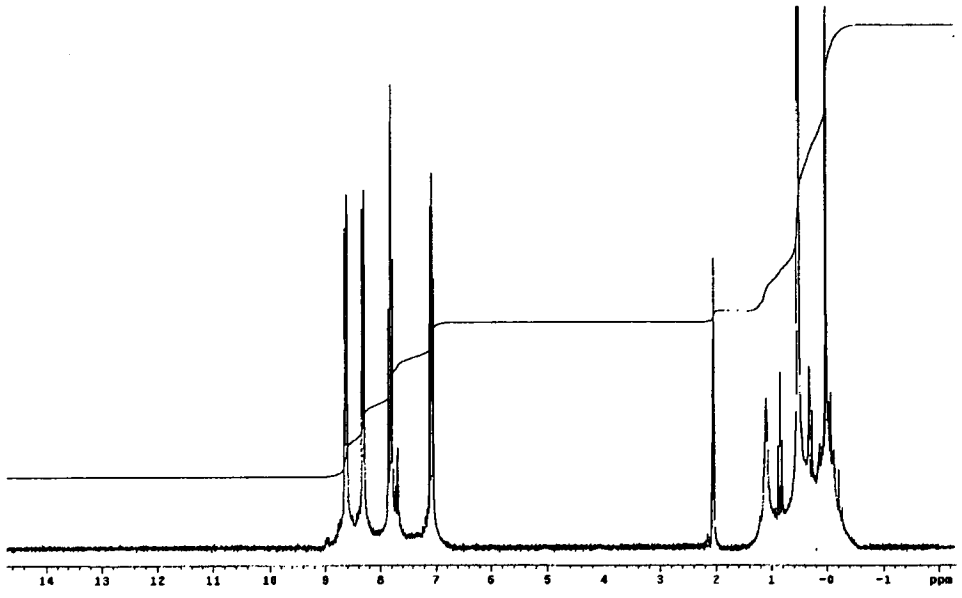

Figure 3.58 ^{1}H NMR spectrum in toluene-d_8 of 26.

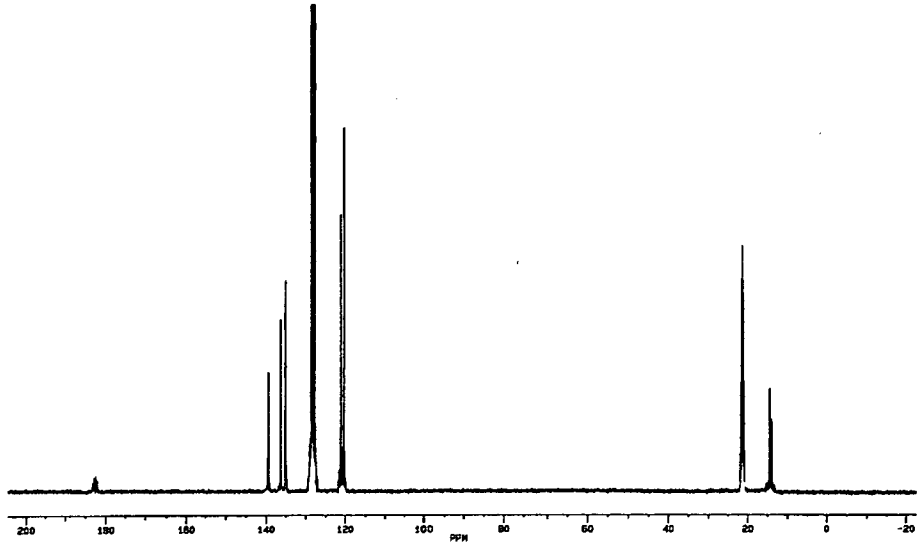

Figure 3.59 ^{13}C NMR spectrum in toluene-d_8 of 26.

The X-ray crystal structure of **26** reveals a tetrahedral geometry around the magnesium atom (Figure 3.60). The $[Me_2B(2\text{-py})]^-$ ligand acts as a bidentate chelate in a κ2 donor fashion to the magnesium atom. The boat conformation gives Mg-N bond lengths of 2.1023(18), 2.1191(18), 2.1301(18) and 2.1019(18) Å, whilst the interactions are typical σ-bonding distances. The B-CH_3 bond lengths are 1.652(2)

and 1.647(2) Å which are longer than corresponding bonds in **22**, **23** and **24** respectively. Selected bond lengths and angles are shown in Table 3.5.

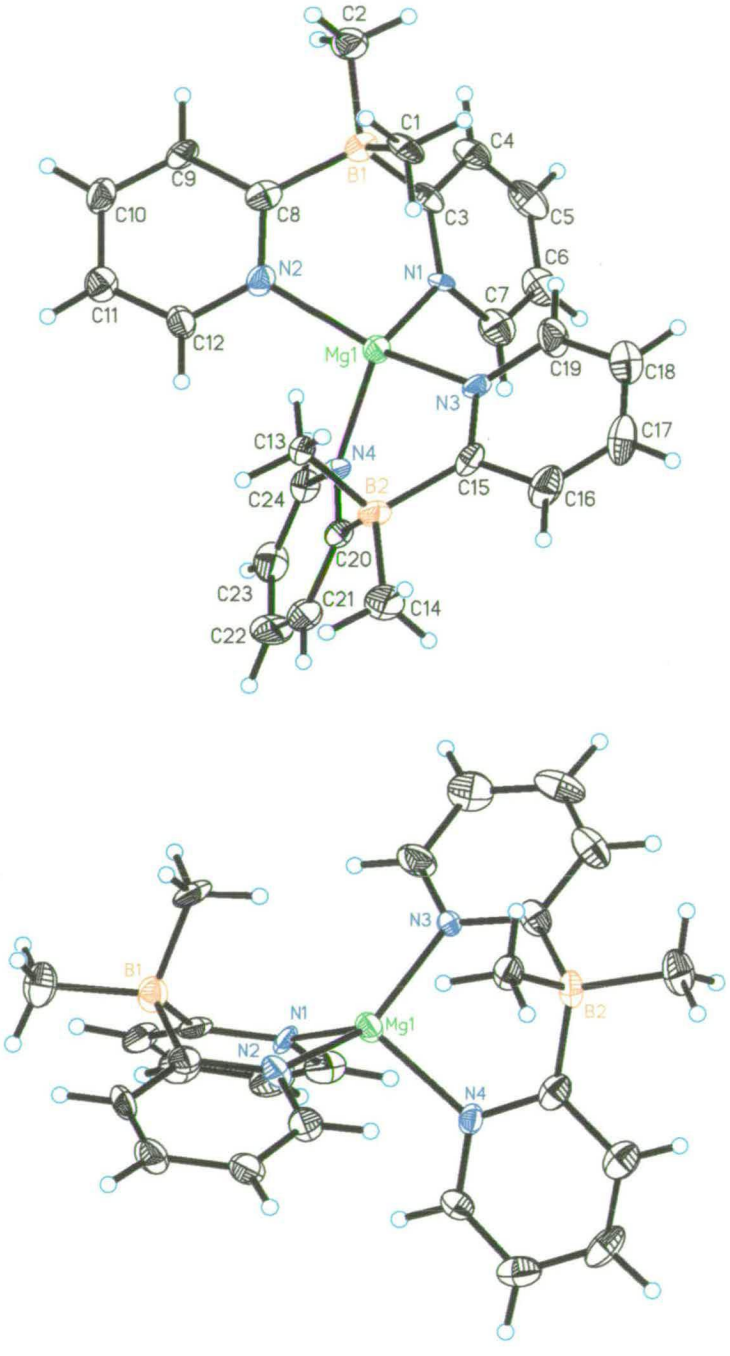

Figure 3.60 Crystallographic structure of 26 with different orientations. Displacement ellipsoids are shown at the 50% probability level.

Table 3.5 Selected bond distances (Å) and Angles (°) for 26.

Mg(1)-N(1)	2.1023(18)	Mg(1)-N(2)	2.1191(18)	Mg(1)-N(3)	2.1301(18)
Mg(1)-N(4)	2.1019(18)	N(1)-C(3)	1.322(3)	N(1)-C(7)	1.388(2)
N(2)-C(8)	1.359(3)	N(2)-C(12)	1.359(3)	N(3)-C(15)	1.336(3)
N(3)-C(19)	1.365(2)	N(4)-C(20)	1.385(3)	N(4)-C(24)	1.352(3)
C(1)-B(1)	1.652(2)	C(2)-B(1)	1.647(2)	C(3)-B(1)	1.661(2)
C(8)-B(1)	1.629(2)	C(13)-B(2)	1.613(2)	C(14)-B(2)	1.622(2)
C(15)-B(2)	1.642(2)	C(20)-B(2)	1.637(2)		
N(1)-Mg(1)-N(2)		96.57(6)	N(1)-Mg(1)-N(3)		102.61(5)
N(1)-Mg(1)-N(4)		114.65(7)	N(2)-Mg(1)-N(3)		143.47(6)
N(2)-Mg(1)-N(4)		102.68(6)	N(3)-Mg(1)-N(4)		97.16(6)
N(1)-C(3)-B(1)		117.29(5)	N(2)-C(8)-B(1)		119.16(5)
N(3)-C(15)-B(2)		120.48(5)	N(4)-C(20)-B(2)		120.68(5)
Mg(1)-N(1)-C(3)		122.14(5)	Mg(1)-N(1)-C(7)		117.00(7)
Mg(1)-N(2)-C(8)		119.09(5)	Mg(1)-N(2)-C(12)		119.43(5)
Mg(1)-N(3)-C(15)		119.66(3)	Mg(1)-N(3)-C(19)		119.67(5)
Mg(1)-N(4)-C(20)		117.00(7)	Mg(1)-N(4)-C(24)		121.00(5)

3.2.10 Synthesis of Hydrogen Diphenylbis(2-pyridyl)borate

Reaction of 2-lithiopyridine with one half equivalent of diphenylboron bromide (**27**) in Et_2O at –78 °C, resulted satisfactorily in the formation of lithiated diphenylbis(2-pyridyl)borate, [{$Ph_2B(2\text{-}py)_2$}Li(THF)] (**28**), as shown in Figure 3.61. After an acidic treatment of **28** the ligand, hydrogen diphenylbis(2-pyridyl)borate, [$Ph_2B(2\text{-}py)_2(H)$] (**29**), was obtained in 62 % yield. Crystals suitable for X-ray analysis were grown from a concentrated toluene solution of **29** at room temperature.

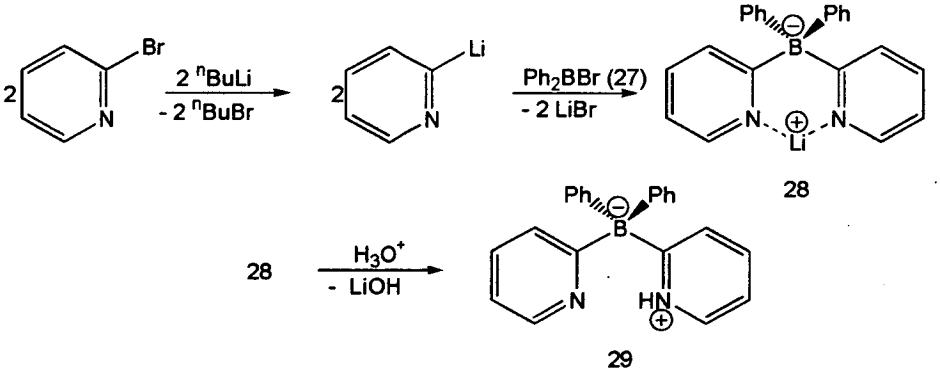

Figure 3.61 Synthesis of 29.

The ^1H NMR spectrum of **29** gives downfield peaks from the aromatic rings at δ 7.48, 7.21, 7.17 and 7.14, whilst a singlet signal at δ 11.83 is assigned to the nitrogen bonded proton (Figure 3.62). The ^{13}C NMR spectrum shows a downfield

shift of aromatic carbon atoms at δ 188.40, 138.86, 136.25, 127.11 and 123.51 (Figure 3.63). The ^{11}B NMR spectrum of **29** shows a characteristic sharp singlet at δ -13.81 (Figure 3.64).

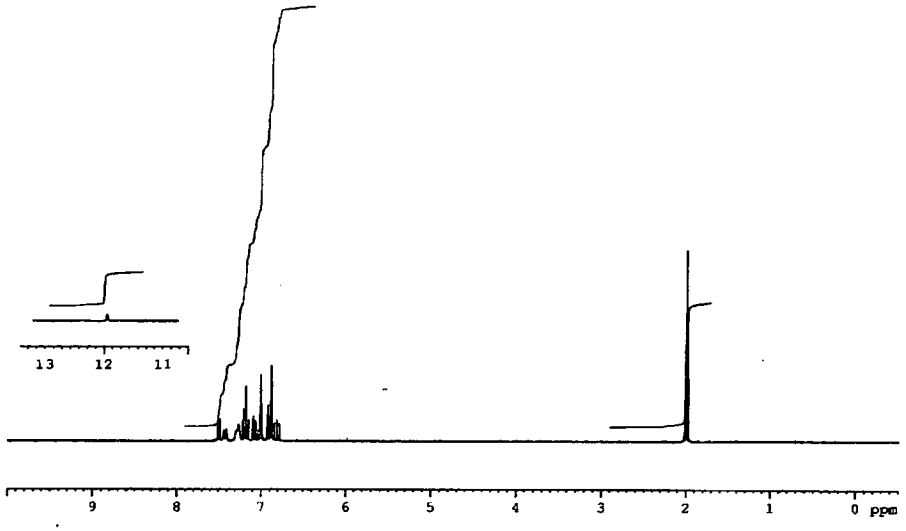

Figure 3.62 ^{1}H NMR spectrum in toluene-d_8 of 29.

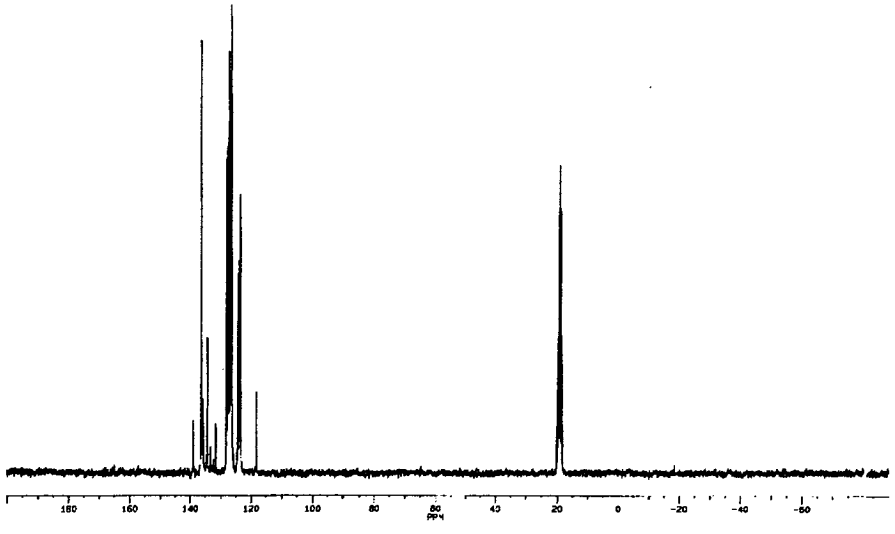

Figure 3.63 ^{13}C NMR spectrum in toluene-d_8 of 29.

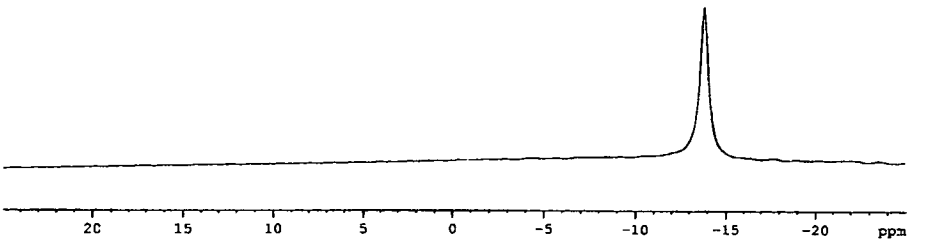

Figure 3.64 ^{11}B NMR spectrum in toluene-d_8 of 29.

The X-ray crystal structure of **29** reveals a tetrahedral boron centre, where both pyridyl rings are situated almost in the same plane (Figure 3.65). The B-C bond lengths are 1.6396(19), 1.64002(19), 1.6459(19) and 1.6353(19) Å, which are longer than distances in the similar hydrogen dimethylbis(2-pyridyl)borate ligand. Phenyl groups produce a steric repulsion between them and the pyridyl groups, affecting the B-C distances. Intramolecular hydrogen bonding between N atoms are observed, whilst the steric effect makes both pyridyl groups slightly out of the plane. Selected bond lengths and angles are shown in Table 3.6.

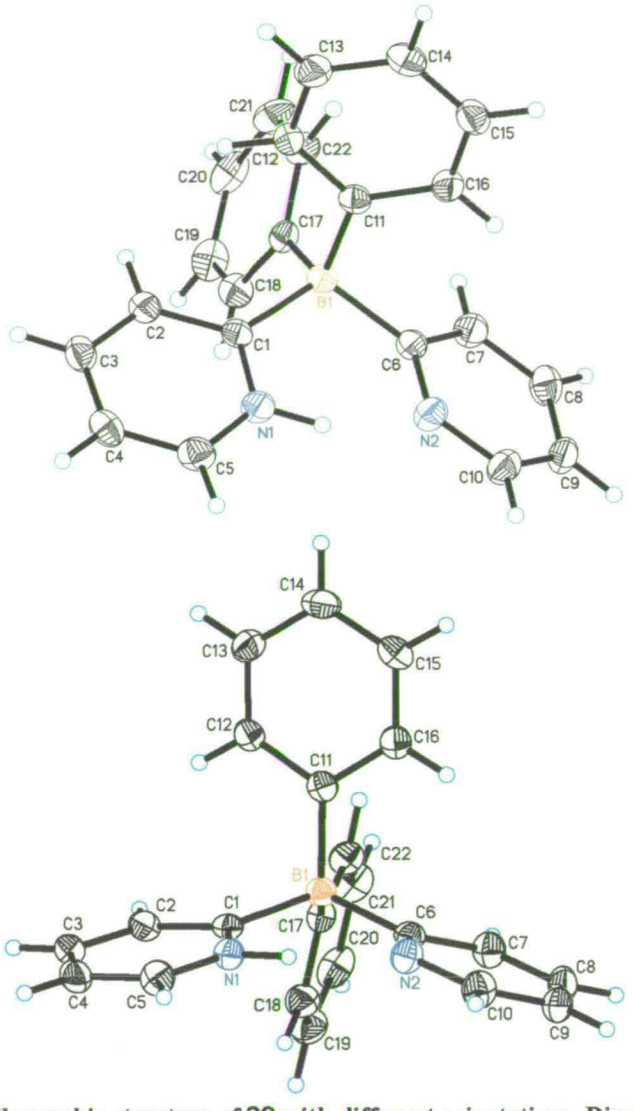

Figure 3.65 Crystallographic structure of 29 with different orientations. Displacement ellipsoids are shown at the 50% probability level.

Table 3.6 Selected bond distances (Å) and angles (°) for 29.

N(1)-C(1)	1.3500(17)	N(1)-C(5)	1.3493(18)	N(2)-C(10)	1.3471(18)
N(2)-C(6)	1.3577(17)	B(1)-C(1)	1.6396(19)	B(1)-C(6)	1.6402(19)
B(1)-C(11)	1.6459(19)	B(1)-C(17)	1.6353(19)		

C(1)-N(1)-H(1N)	113.1(12)	C(5)-N(1)-C(1)	125.22(12)
C(5)-N(1)-H(1N)	121.6(12)	C(10)-N(2)-C(6)	119.81(12)
C(17)-B(1)-C(1)	109.23(11)	C(17)-B(1)-C(6)	108.79(10)
C(1)-B(1)-C(6)	111.35(11)	C(17)-B(1)-C(11)	111.68(11)
C(1)-B(1)-C(11)	106.01(10)	C(6)-B(1)-C(11)	109.77(11)
N(2)-C(6)-B(1)	119.28(11)		

D-H...A	d(D-H)	d(H...A)	d(D...A)	<(DHA)
N(1)-H(1N)...N(2)	0.96	1.78	2.6443(17)	147.3(17)

NMR spectra were recorded during most of the steps during the synthesis of hydrogen diphenylbis(2-pyridyl)borate, but no evidence was found for the formation of dimeric cyclic structures as observed when using Me_2BCl. The synthesis of **29** was also achieved with Ph_2BCl (**11**).

3.2.11 Reactivity of Lithium Diphenylbis(2-pyridyl)borate with MeMgCl

A solution of **29** was treated with a stoichiometric amount of ^{n}BuLi in diethyl ether at – 78 °C (Figure 3.66). The ^{1}H NMR spectrum of **28** no longer showed a downfield signal at δ 11.83 for the nitrogen bonded proton, whilst the lithium atom co-ordination is suggested by the upfield signals for the THF solvated at δ 3.47 and 1.61, respectively (Figure 3.67). A further transmetallation reaction was performed by using a stoichiometric amount of MeMgCl at room temperature, and an extraction with ether gave a colourless oil. NMR spectra of the colourless oil were recorded, showing the possible formation of a monomeric zwitterionic complex [{$Ph_2B(2\text{-}py)_2$}Mg(Me)THF] (**30**).

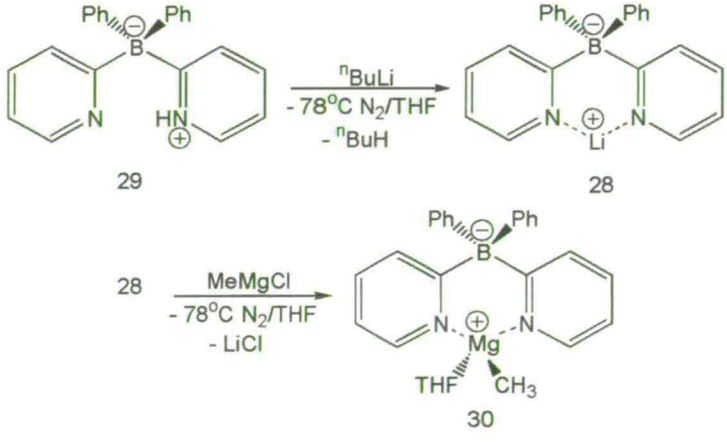

Figure 3.66 Synthesis of the 28 and 30.

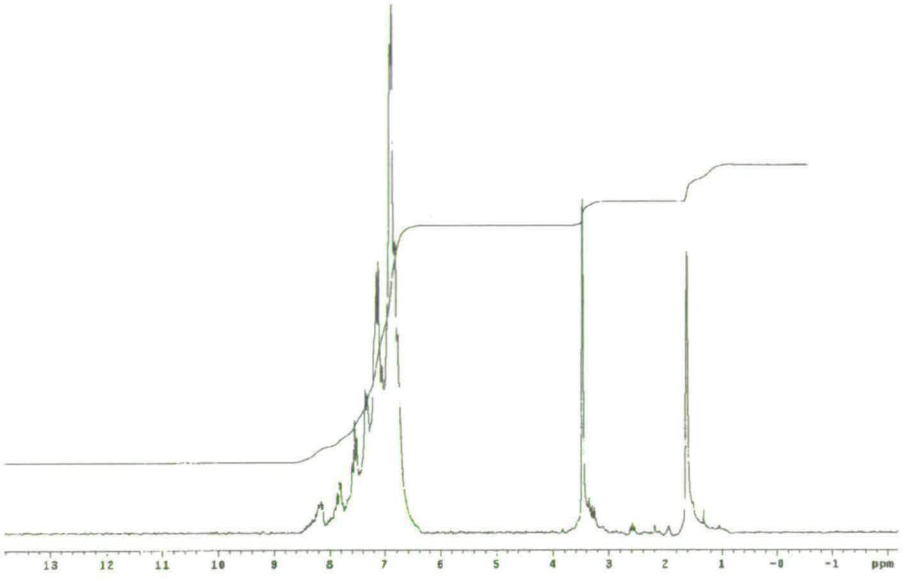

Figure 3.67 ^{1}H NMR spectrum in toluene-d_8 of 28.

In order to get better results from the ^{1}H NMR spectrum of **30**, two separate experiments were conducted by using toluene-d_8 and THF-d_8, respectively. Using the toluene, the aromatic protons are located at δ 7.32, 7.29 and 7.13 (Figure 3.68). The magnesium co-ordination is verified by the upfield peaks for the THF solvated at δ 3.16 and 1.99, whilst the methyl carbon atom bonded to magnesium is placed at δ -1.05. However, using THF the aromatic protons are placed at δ 7.76, 7.58 and 7.49, respectively (Figure 3.69). The magnesium co-ordination is verified by the upfield peaks for the THF solvated at δ 3.76 and 1.90, while the methyl carbon atom bonded to magnesium atom is placed at δ -1.55. The ^{13}C NMR spectrum gives signals at δ 140.44, 136.25 and 123.51 which are assigned to the aromatic ring (Figure 3.70). The magnesium co-ordination shows the upfield methyl carbon atom signal at δ -16.30, whilst the THF solvated peaks are placed at frequency of δ 68.02 and 23.12, respectively.

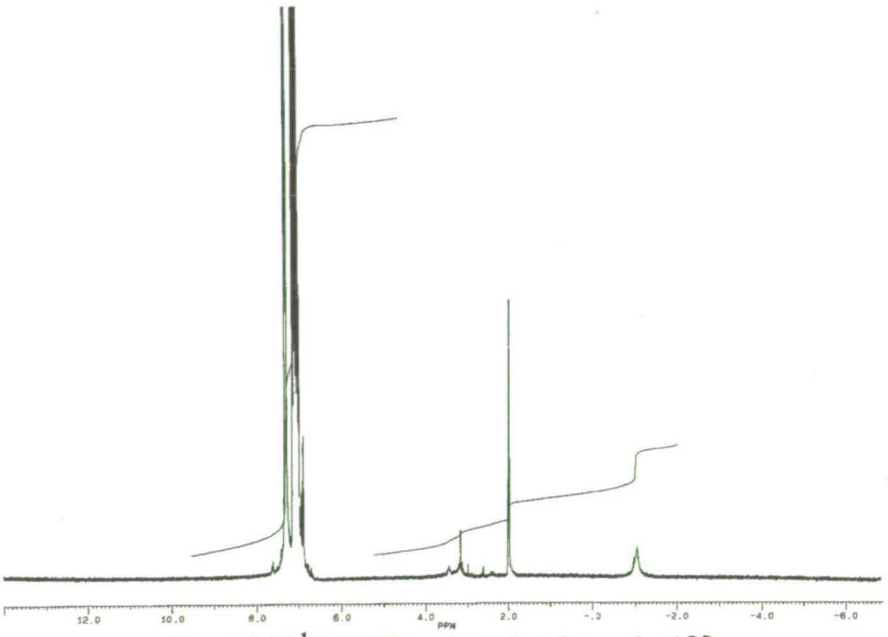

Figure 3.68 ^{1}H NMR spectrum in toluene-d_8 of 30.

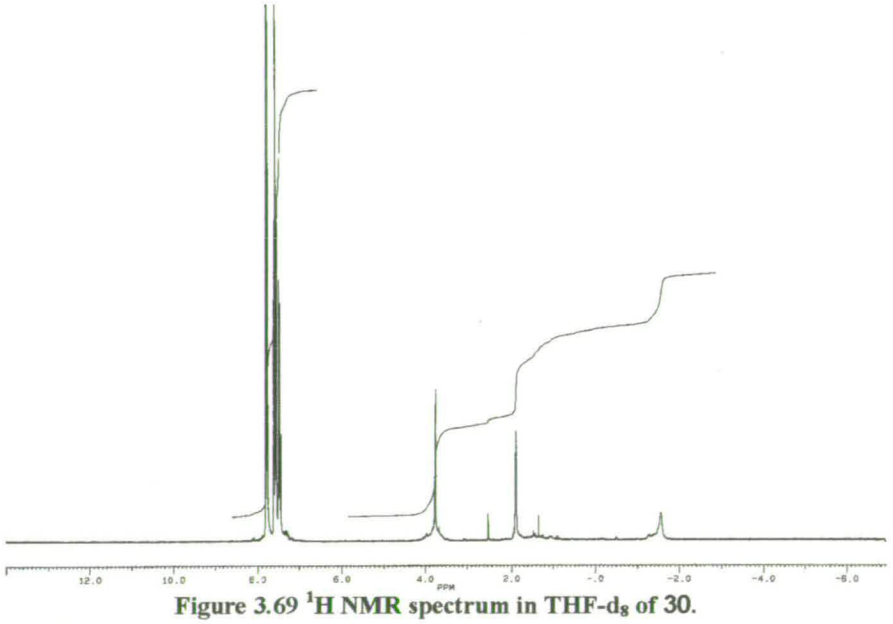

Figure 3.69 ^{1}H NMR spectrum in THF-d_8 of 30.

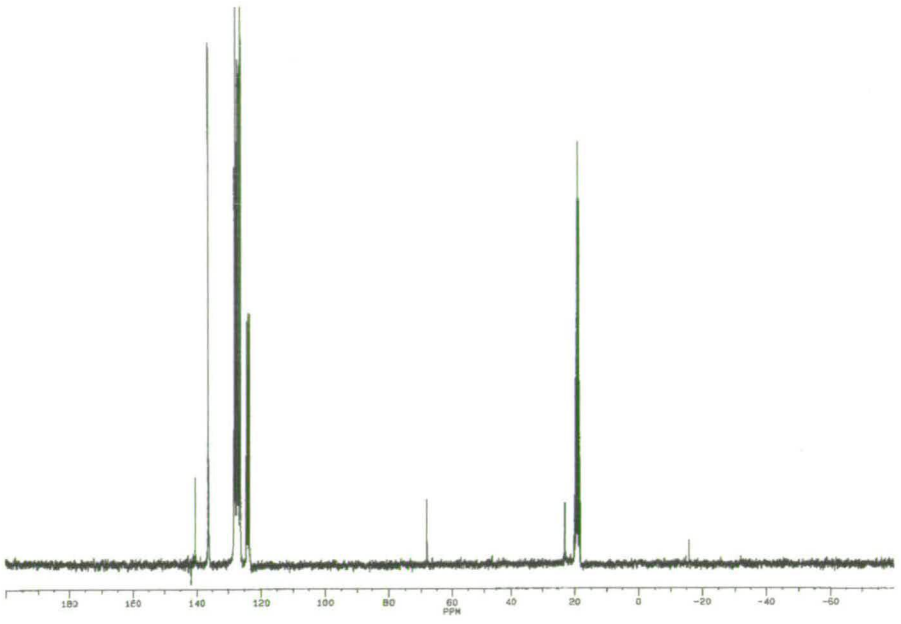

Figure 3.70 ^{13}C NMR spectrum in toluene-d_8 of 30.

3.3 Conclusions

The main interest for this chapter was to investigate the reactivity of reductive carbon-sulfur cleavages and the α-addition to isonitrile ligands, for the preparation of new boron centred nitrogen donor chelating ligands to provide zwitterionic complexes.

The reductive carbon-sulphur cleavage of (phenylthiomethyl)amine was tested and its reactivity investigated. The naphthalene-catalysed lithiation provides a powerful methodology for the synthesis of very reactive organolithium intermediates. The stoichiometric amount of naphthalene with lithium gives excellent results when (phenylthiomethyl)amine is used, and its effectiveness is represented by the reactivity of different electrophiles. A catalytic amount of naphthalene used to activate the lithium did not react successfully with the (phenylthiomethyl)amine and the yields were relatively low during the reaction time. Barbier-type reaction conditions have been performed in the presence of different electrophilic reagents [$Me_2(Ph)SiCl$ or $Ph_2(Me)SiCl$], and this method has been effective in some cases, especially for $Me_2(Ph)SiCl$. The separation and purification of products from the naphthalene remaining in solution presents a serious problem, and no product can be obtained until all the naphthalene is removed under mild conditions.

(Phenylthiomethyl)amine using naphthalene-catalysed lithiation and in the presence of Ph_2BCl (**11**) produces a complicated reaction, where the lithiated species shows a low reactivity with the respective electrophile. The malodorous reaction mixture presents problems for product isolation due to the presence of naphthalene and thiophenol in the reaction. It could be suggested that the low reactivity of **11** with the lithiated reagent would induce the THF solvent to produce extensive enolization of $LiCH_2NEt_2$ during the reaction. Moreover, due to the complicated isolation of naphthalene, the products can produce unknown species by simple reactions with perhaps the unreacted lithium-naphthalene in solution. In addition, if the reactivity of Ph_2BCl with the $LiCH_2NEt_2$ is low, this could be due to a high reactivity of the PhSLi which competes for the electrophilic reagent.

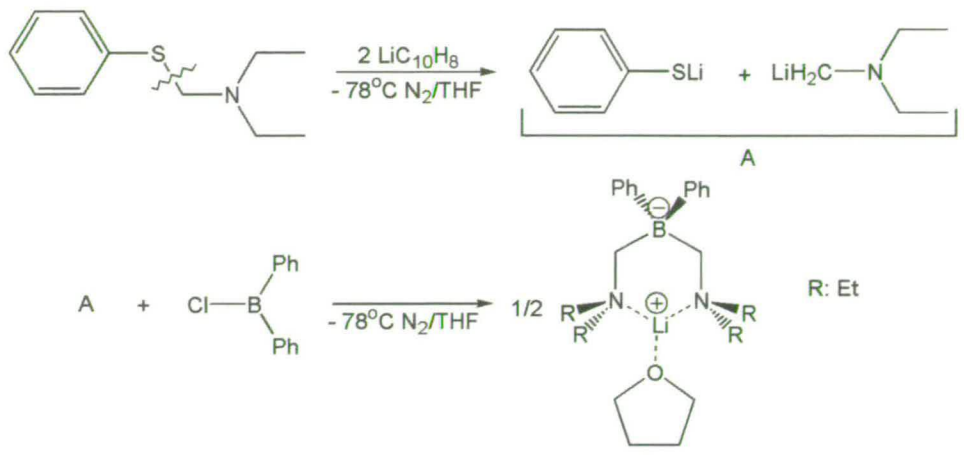

Figure 3.20 Carbon-sulfur cleavage of 9 and its reactivity with 11.

Finally, although the expected ligand [{$Ph_2B(CH_2NEt_2)_2$}Li(THF)] (**12**) was synthesised (Figure 3.20), according to NMR spectroscopy, the yield was too poor for the conduction of further transmetallation reactions. Attempts to produce more ligand were not fruitful due the large amount of naphthalene involved in the reaction.

The reactivity of isonitriles with organolithium reagents gives the respective α-alkylation, which can be verified by reaction with electrophilic reagents [Me_3SiCl or $Me_2(Ph)SiCl$]. The temperature at which the reaction is conducted is one of the most important factors, and in order to prevent polymerisation or dimerisation it must be lower than –70 °C. The methylation and protonation of the α–carbon of 2,6-dimethylphenyl isonitrile are produced when the isonitrile ligand is treated with MeLi and then quenched in water. The resulting product is of a high quality, and the quenching process may help to prevent side products when the lithiated aldimines remain unreacted. The use of an electrophilic reagent, however, such as Me_3SiCl gives the expected product, but a dimer species is also present, even when a low temperature is used. Moreover, when the electrophilic reagent has one or more phenyl groups, the possibility of obtaining side products is reduced. In contrast, the yield can also be affected in the same way (no products could be isolated for the $Ph_2(Me)SiCl$ reagent).

According to NMR spectroscopy, there was no reaction when **11** was used with the lithiated aldimine under any of the conditions employed. The product obtained, however, suggests a high rate of transference of electrons between lithiated

complexes during the reaction, whilst the electrophilic reagent, **11**, could help to stabilise short chains of isonitrile additions (acting as a catalyst).

The reactivity of [{$Me_2B(2\text{-}py)_2$}Li] (**21**) or [{$Ph_2B(2\text{-}py)_2$}Li(THF)] (**28**) has been tested in the presence of different Grignard reagents, but unfortunately, suitable X-ray quality crystals of the probable zwitterionic complexes could not be obtained. Most of the possible complexes were characterised by NMR spectroscopy, except bischelate complexes obtained when **21** and the respective Grignard reagents were used. Perhaps the geometry for both 2-pyridyl rings in the $[Me_2B(2\text{-}py)_2]^-$ ion could help to produce bischelate complexes, where each methyl group bonded to the boron atom does not produce a strong steric (protecting) effect over the magnesium atom (Figure 3.71). In addition, it is probable that bischelate complexes are formed when the Schlenk equilibrium is favourable towards the magnesium chloride ($MgCl_2$), whilst the zwitterionic complex could react immediately with a further ligand to produce a bischelate complex (Figure 3.72). Moreover, according to the NMR spectroscopy no decomposition of the powders was observed at any time.

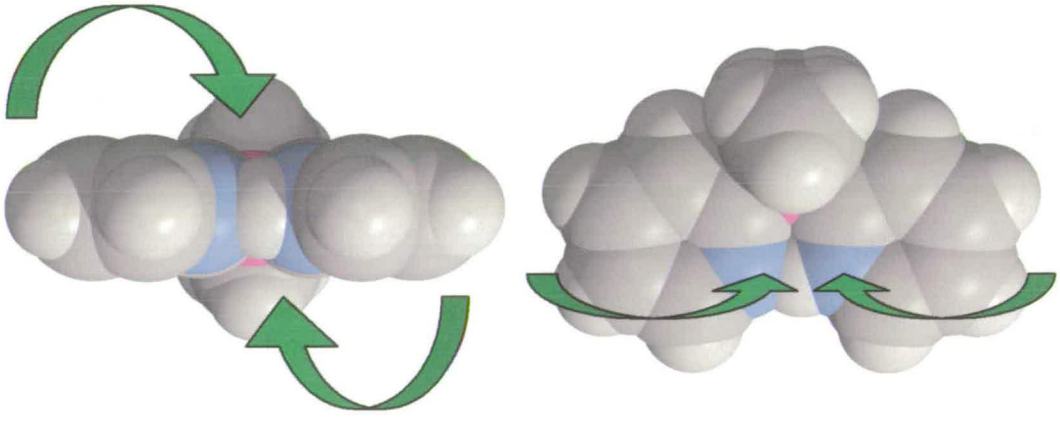

Figure 3.71 Space-filling molecular model for 22. The green arrows represent possible attacks of MeLi reagent.

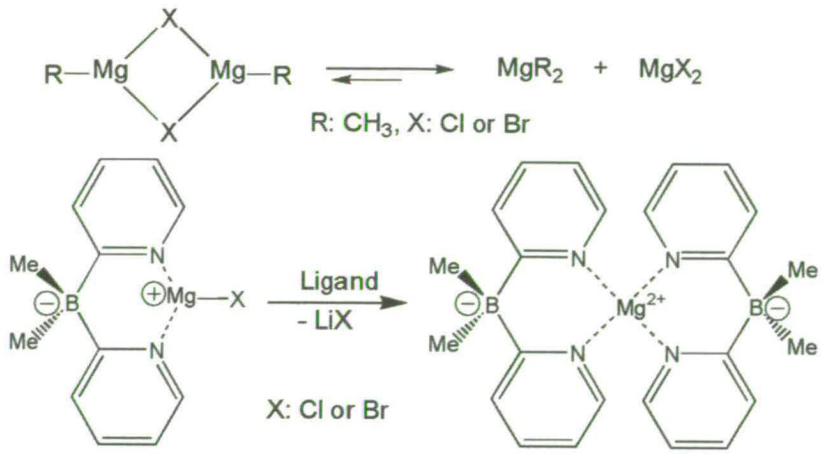

Figure 3.72 Schlenk equilibrium for dissociation of the Grignard reagent.

The reactivity of [{$Ph_2B(2\text{-}py)_2$}Li(THF)] (**28**) with any Grignard reagent showed similar results to its analogue dimethylbis(2-pyridyl)borate, where according to the NMR spectroscopy, zwitterionic complexes [LMg(Me)THF] were obtained. Perhaps the two phenyl groups bonded to the boron atom may protect the magnesium atom centre and also avoid the formation of bischelate complexes (Figure 3.73). NMR spectroscopy did not show signs of decomposition of the oils obtained.

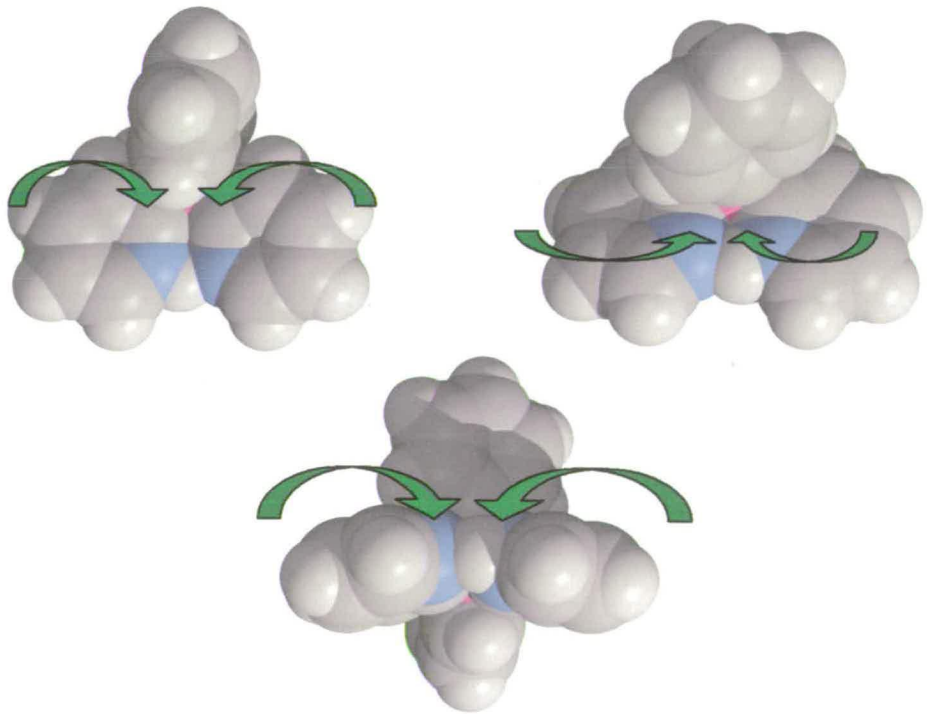

Figure 3.73 Space-filling molecular model for 29. The green arrows represent possible attacks of MeLi.

3.4 Experimental

3.4.1 General Procedures

All manipulations were carried out under a nitrogen atmosphere using standard Schlenk and cannula techniques or in a conventional nitrogen-filled glove-box (Saffron Scientific), fitted with oxygen and water scavenging columns. Solvents were refluxed over an appropriate drying agent, and distilled and degassed prior to use. Solvents and reagents where commercially available were bought from Aldrich, Acros or Fischer, with the exception of NMR solvents which were purchased from Goss Scientific. Diethyl ether, toluene, hexane, benzene and THF were all distilled from Na/benzophenone under a nitrogen atmosphere. NMR solvents were degassed using three freeze-pump-thaw cycles and stored over 4 Å molecular sieves.

3.4.2 Instrumentation

Elemental analyses were performed by sealing aluminium capsules containing approximately 1 mg of compound under nitrogen in the glove box, and performed using a Perkin-Elmer 2400 CHN Analyser. The NMR spectra were recorded on Bruker AC 250 MHz and Varian Gemini 200MHz spectrometers. Infrared spectra were obtained using a Perkin-Elmer 1600 Paragon Series FT-IR spectrometer as potassium bromide discs or as liquid thin films. Electron impact (EI) mass spectra were obtained either on a Finnigan MAT 4600 quadrupole spectrometer or on a Kratos MS50TC spectrometer. Fast atom bombardment (FAB) mass spectra were obtained on a MS50TC spectrometer. ^{1}H and ^{13}C NMR spectra were referenced to TMS and ^{11}B NMR spectra were referenced to $BF_3(Et_2O)$.

3.4.3 Synthesis

$PhSCH_2NEt_2$ (9)[15]

The diethylamine (18.89 cm^3, 0.182 mol) was added dropwise to an equimolar quantity of thiophenol (19.07 cm^3, 0.182 mol), maintaining the

temperature below 20 °C. An equimolar quantity of formaldehyde (14.29 cm^3, 0.182 mol) was added to this mixture, and the temperature was raised to 80 °C for two hours. Upon cooling, the oils were extracted with ether (100 cm^3), and the solution was dried over magnesium sulphate. The solution was filtered off , and the solvent and volatile components were removed under *vacuum* to produce a colourless oil. A final distillation was done at 112 °C under *vacuum* (5 mmHg) (145.30 mmol, 81.0% yield).

^{1}H NMR ($CDCl_3$/ppm): δ 7.40 (m, 5H, C_6H_5), 4.60 (s, 2H, CH_2), 2.62 (q, 4H, CH_2), 0.97 (t, 6H, CH_3). ^{13}C NMR ($CDCl_3$/ppm): δ 134.81 (*ipso*-C_6H_5), 132.63 (*m*-C_6H_5), 128.67 (*o*-C_6H_5), 126.28 (*p*-C_6H_5), 63.25 (CH_2), 46.94 (CH_2), 13.24 (CH_3). EIMS(*m/z*): 194, 109 [M-N(C_2H_5)$_2$]. B.p. 110-112°C. Elemental analysis for $C_{11}H_{17}NS$: Expected: C, 67.64; H, 8.77; N, 7.17. Found: C, 67.12; H, 8.61; N, 7.02.

$Et_2NCH_2Si(Ph)Me_2$ (10)

To a fresh solution of lithium naphthalide from lithium granules (0.081 g, 11.70 mmol) and naphthalene (1.500 g, 11.70 mmol) in THF (25 cm^3) at -78 °C was added $PhSCH_2NEt_2$ (1.137 g, 5.58 mmol) pre-cooled to the same temperature. After 30 minutes, $Me_2(Ph)SiCl$ (1.997 g, 11.70 mmol) in hexane (10 cm^3) was added dropwise during the next 30 minutes. The mixture was warmed to room temperature and stirred for 24 hours. The mixture was then filtered, and the solvent and volatile components were removed under *vacuum*. The remaining naphthalene was removed by steam distillation under *vacuum* at 60 °C. The product was extracted with diethyl ether (two portions of 20 cm^3). The solvent was removed under *vacuum* to give a colourless oil as a final product (5.87 mmol, 60% yield).

^{1}H NMR ($CDCl_3$/ppm): δ 7.34 (m, 5H, C_6H_5), 4.66 (s, 2H, CH_2-Si), 2.45 (q, 4H, CH_2-N), 0.94 (t, 6H, CH_3), 0.34 (s, 6H, Si-CH_3). ^{13}C NMR ($CDCl_3$/ppm): δ 133.40 (*ipso*-C_6H_5), 128.31 (*m*-C_6H_5), 127.45 (*o*-C_6H_5), 126.31 (*p*-C_6H_5), 49.43 (CH_2), 44.83 (CH_2), 12.24 (CH_3), -0.18 (CH_3). EIMS(*m/z*): 221. Elemental analysis for $C_{13}H_{23}NSi$: Expected: C, 70.52; N, 10.47; N, 6.33. Found: C, 69.68; H, 9.95; N, 6.21.

Ph_2BCl (11)[24]

a) **$PhBCl_2$.**[24] Boron trichloride (8.50 cm^3, 1.0 M in hexanes, 8.53 mmol) was added to a suspension of tetraphenyltin (9.720 g; 2.28 mmol) in dichloromethane as the solvent (50 cm^3) at –84 °C (slush bath of ethyl acetate/liquid nitrogen). The mixture was allowed to warm, and between 0 and 5 °C a violent reaction occurred. Solvent and volatile components were removed under *vacuum* and were trapped at –84 °C. Distillation of the residue afforded the final product (6.16 mmol; 90% yield).

IR: ν(B-C_6H_5) at 1224.6 and 907.1 cm^{-1}; ν(B-Cl) at 546.2 cm^{-1}. ^1H NMR ($CDCl_3$/ppm): δ 7.40 (d, 5H). ^{13}C NMR ($CDCl_3$/ppm): δ 126.50. EIMS(*m/z*): $C_6H_5BCl_2$: 158, M-Cl: 123. B.p 65-70 °C/12 mmHg. FABMS(*m/z*): $C_6H_5SnCl_3$ (M^+): 303. B.p. 129-130 °C/12 mmHg.

b) **Ph_3B**. Boron trichloride (40.0 cm^3, 1.0 M in hexanes, 40.00 mmol) was dissolved in hexane (50 cm^3) and pre-cooled at –78 °C. To this solution, phenyllithium (71.1 cm^3, 1.80 M in hexanes, 128.00 mmol) was dropped slowly via syringe at –78 °C. The mixture was left to warm to room temperature overnight. The final solution was filtered off and the LiCl removed. Solvent and volatile components were removed under *vacuum*, and the final residue was distilled at low pressure to obtain a pure product (25.60 mmol, 64% yield).

^1H NMR ($CDCl_3$/ppm): δ 7.48 (d, 15H). ^{13}C NMR ($CDCl_3$/ppm): δ 126.92. EIMS (*m/z*): 242. B.p. 155-166 °C/10 mmHg.

c) **Ph_2BCl.**[24] Triphenyl borane (5.000 g, 20.9 mmol) was covered with dichlorophenylborane (3.970 g, 30.0 mmol) in a dry nitrogen atmosphere. The mixture was slowly heated to reflux over a period of three hours, and the temperature was maintained for about 15 minutes. A distillation of the reaction product under *vacuum* gave the final product (32.19 mmol, 77% yield).

IR: ν(B-C_6H_5) at 1223.3 and 904.1 cm^{-1}; ν(B-Cl) at 544.5 cm^{-1}. ^1H NMR ($CDCl_3$/ppm): δ 7.38 (d, 10H). ^{13}C NMR ($CDCl_3$/ppm): δ 126.55. EIMS(*m/z*): 200. B.p. 106-108 °C (3-5mmHg).

[{$Ph_2B(CH_2NEt_2)_2$}Li(THF)] (12)

To a freshly prepared solution of lithium naphthalide from lithium granules (0.070 g, 9.98 mmol) and naphthalene (1.279 g, 9.98mmol) in THF (25 cm^3) at -78 °C was added $PhSCH_2NEt_2$ (1.946 g, 9.98 mmol) in THF (10 cm^3) pre-cooled to the same temperature. After 30 minutes, Ph_2BCl (1.000 g, 4.49 mmol) in hexane (10 cm^3) was added dropwise during 30 minutes. The mixture was warmed to room temperature and stirred for 24 hours. The mixture was then filtered, and the solvent and volatile components were removed under *vacuum*. The remaining naphthalene was removed by steam distillation under *vacuum* at 60 °C. The product was extracted with diethyl ether (two portions of 20 cm^3). The solvent was removed under *vacuum* to give a white solid as the final product (0.22 mmol, 2.70% yield).

^1H NMR (DMSO/ppm): δ 7.28 (m, 10H, C_6H_5), 3.60 (t, 4H, THF), 3.37 (s, 4H, N-CH_2-), 2.42 (q, 8H, -CH_2-N), 1.75 (t, 4H, THF), 0.92 (t, 12H, CH_3-). ^{13}C NMR (DMSO/ppm): δ 137.66 (*ipso*-C_6H_5), 131.60 (*m*-C_6H_5), 128.95 (*o*-C_6H_5), 127.77 (*p*-C_6H_5), 69.85 (THF), 62.84 (N-CH_2), 45.90 (N-CH_2), 26.21 (THF), 12.61 (CH_3-). ^{11}B NMR (DMSO/ppm): δ -14.09. FABMS (*m/z*): 343 (M^+).

[ArNC(Me)Li] (13), [ArNC(Me)$SiMe_3$] (14) and [ArNC(Me)$Si(Me)_3$CNAr] (Ar: 2,6-dimethylphenyl) (15)

A solution of 2,6-dimethylphenyl isonitrile (0.260 g, 1.910 mmol) in diethyl ether (10 cm^3) was treated with MeLi (1.20 cm^3, 1.6 M in hexanes, 1.910 mmol) at –78 °C to provide (**13**). After 30 minutes, Me_3SiCl (0.24 cm^3, 1.91 mmol) was dropped via syringe at -78 °C and the mixture was allowed to warm to room temperature overnight. The solution was filtered under a nitrogen atmosphere and the LiCl removed by filtration through Celite 521. The solvent and volatile components were removed under *vacuum* to provide two products: a) An orange liquid **14** (1.28 mmol, 65% yield). b) Orange solid **15** (0.50 mmol, 25% yield). Orange crystals were grown from a concentrated ether solution at room temperature.

(a) IR(KBr): ν(C=N) at 1641.1 and 1577.4 cm^{-1}. ^1H NMR ($CDCl_3$/ppm): δ 6.90 (m, 3H), 1.98 (s, 6H), 0.22 (s, 3H), 0.18 (s, 9H). ^{13}C NMR ($CDCl_3$/ppm): δ 152.10 (C), 147.70 (*ipso*-C_6H_5), 126.80 (*m*-C_6H_5), 124.89 (*o*-C_6H_5), 123.28 (*p*-C_6H_5),

18.30 (CH_3), 17.11 (CH_3), 0.12 (Si-CH_3). EIMS (*m/z*): 220. Elemental analysis for $C_{13}H_{21}NSi$: Expected: C, 71.15; H, 9.66; N, 6.38. Found: C, 70.84; H, 9.51; N, 6.31. (b): IR(KBr): ν(C=N) at 1651.1 and 1587.4 cm^{-1}. ^1H NMR ($CDCl_3$/ppm): δ 6.80 (m, 6H), 1.90 (m, 12H), 1.60 (s, 3H), 0.10 (m, 9H). ^{13}C NMR ($CDCl_3$/ppm): δ 149.10 (C), 147.35 (*ipso*-C_6H_5), 126.80 (*m*-C_6H_5), 124.89 (*o*-C_6H_5), 123.28 (*p*-C_6H_5), 15.05 (CH_3), 14.88 (CH_3), 0.10 (Si-CH_3). EIMS (*m/z*): 351. Elemental analysis for $C_{22}H_{30}N_2Si$: Expected: C, 79.29; H, 8.64; N, 7.99. Found: C, 77.55; H, 8.31; N, 7.80.

Empirical formula	$C_{22}H_{30}N_2Si$	β/ °	92.692(8)
Formula weight	350.57	γ/ °	90
Crystal system	Monoclinic	Volume/ $Å^3$	2105.82(12)
Space group	$P2_1/n$	Z	4
a/ Å	8.159(5)	Z'	1
b/ Å	12.612(8)	Density calc./ Mgm^{-3}	1.106
c/ Å	20.486(12)	μ (Mo-K)/ mm^{-1}	0.118
α/ °	90		

Data were collected on a Bruker SMART APEX diffractometer[25] equipped with an Oxford Cryosystems low-temperature device at 150 K and using an orange plate oil-coated crystal[26] of dimension 0.18 x 0.16 x 0.09 mm^3. The initial unit cell was indexed using a least-squares analysis of a random set of reflections collected from three series of 0.3° wide ω-scans, 10 s per frame, and 25 frames per series that were well distributed in reciprocal space. Data frames were collected [Mo Kα = 0.71073 Å] with 0.3° wide ω-scans, 10 s per frame and 600 frames per series. Three complete series were collected at varying ϕ angles (ϕ=0, 90, 180°). The crystal to detector distance was 6.0 cm, this providing a set of $3.80 \leq 2\theta \leq 52.86$. A total of 11186 reflections were collected and integrated using SAINT,[27] while absorption correction was applied using SADABS[28] with 4258 unique [R(int)=0.1222]. System symmetry, systematic absences and intensity statistics indicated the unique monoclinic space group $P2_1/n$. The structure was determined by direct methods with the location of nearly all non-hydrogen atoms using the program SHELXS[29] and refined by full-matrix least-squares on F^2 using SHELXL.[30] All non-hydrogen atoms were refined anisotropically, while hydrogen atoms were placed in calculated positions, constrained to ride on their carbon atoms with group U_{iso} values assigned ($U_{iso}(H) = 1.20U_{iso}$). The final structure was refined to convergence [$\Delta/\sigma \leq 0.001$]

with R(F) = 0.0775 (for 4258 data with F>4σF), GOF = 1.002 and *w*R2 = 0.1839 (all data). [$R1 = \Sigma|F_o - F_c|/\Sigma|F_o|$, $wR2 = \{[\Sigma w(F_o^2 - F_c^2)^2]/\Sigma wF_o^4\}^{0.5}$, $w = 1/[\sigma^2(F_o^2) + (xP)^2 + yP]$, $P = (F_o^2+2F_c^2/3)$]. The largest difference between peak and hole in the final difference map, 0.351 and –0.271 eÅ^{-3}.

[ArNC(Me)Si(Ph)Me$_2$] (Ar: 2,6-dimethylphenyl) (16)

A solution of 2,6-dimethylphenyl isonitrile (0.260 g, 1.910 mmol) in diethyl ether (10 cm^3) was treated with MeLi (1.20 cm^3, 1.6 M in hexanes, 1.910 mmol) at –78 °C. After 30 minutes, $Me_2(Ph)SiCl$ (0.32 cm^3, 1.91 mmol) was added dropwise via syringe at -78 °C and the mixture was allowed to warm to room temperature overnight. The solution was filtered under nitrogen atmosphere and the LiCl removed by filtration through Celite 521. The solvent and volatile components were removed under *vacuum* to give a yellow oil as final product (1.05 mmol, 55% yield).

IR(KBr): ν(C=N) at 1641.1 and 1577.4 cm^{-1}. ^{1}H NMR ($CDCl_3$/ppm): δ 7.34 (m, 8H), 2.45 (m, 6H), 0.98 (m, 3H), 0.34 (s, 6H). ^{13}C NMR ($CDCl_3$/ppm): δ 156.30 (C), 150.63 (*ipso*-C_6H_5), 144.38 (*ipso*-C_6H_5), 133.80 (*m*-C_6H_5), 131.04 (*o*-C_6H_5), 129.31 (*p*-C_6H_5), 127.83 (*m*-C_6H_5), 126.41 (*o*-C_6H_5), 124.77 (*p*-C_6H_5), 18.23 (CH_3), 17.81 (CH_3), 0.11 (Si-CH_3). EIMS (*m/z*): 281. Elemental analysis for $C_{18}H_{23}NSi$: Expected: C, 76.81; H, 8.24; N, 4.98. Found: C, 76.02; H, 8.01; N, 4.77.

[{ArNC(Me)CNAr}$_2$] (Ar: 2,6-dimethylphenyl) (17)

A solution of 2,6-dimethylphenyl isonitrile (1.000g, 7.62 mmol) in diethyl ether (10 cm^3) was treated with MeLi (4.8 cm^3, 1.6 M in hexanes, 7.64 mmol) at -78°C. After 10 minutes, a solution of Ph_2BCl (52.49 mg, 3.81 mmol) in hexane (10 cm^3) was added dropwise within 30 minutes and the solution was allowed to warm to room temperature overnight. The solution was filtered, and the solvent and volatile components were removed under *vacuum*. The final product was extracted from ether, and crystallised from dimethylformamide to give yellow crystals suitable for X-ray analysis.

IR(KBr): ν(C=N) at 1643.3 and 1578.4 cm^{-1}. ^1H NMR (THF-d_8/ppm): δ 6.84 (m, 12H), 3.21 (s, 24H), 1.15 (s, 6H). ^{13}C NMR (THF-d_8/ppm): δ 168.30 (C), 162.01 (C), 143.25 (*ipso*-C_6H_5), 134.10 (*m*-C_6H_5), 126.21 (*o*-C_6H_5), 121.77 (*p*-C_6H_5), 31.72 (CH_3), 15.05 (CH_3). EIMS (*m/z*): 555, 539 (M-CH_3). Elemental analysis for $C_{38}H_{42}N_4$: Expected: C, 82.27; H, 7.63; N, 10.10. Found: C, 81.07; H, 7.14; N, 9.97.

Empirical formula	$C_{19}H_{21}N_2$	β/ °	93.508(8)
Formula weight	277.38	γ/ °	90
Crystal system	Monoclinic	Volume/ $Å^3$	1581.4(15)
Space group	$P2_1/c$	Z	4
a/ Å	8.524(5)	Z'	0.5
b/ Å	24.123(13)	Density calc./ Mgm^{-3}	1.165
c/ Å	7.706(4)	μ (Mo-K)/ mm^{-1}	0.068
α/ °	90		

Data were collected on a Bruker SMART APEX diffractometer[25] equipped with an Oxford Cryosystems low-temperature device at 150 K and using a yellow plate oil-coated crystal[26] of dimension 0.18 x 0.14 x 0.10 mm^3. The initial unit cell was indexed using a least-squares analysis of a random set of reflections collected from three series of 0.3° wide ω-scans, 10 s per frame, and 25 frames per series that were well distributed in reciprocal space. Data frames were collected [Mo Kα = 0.71073 Å] with 0.3° wide ω-scans, 10 s per frame and 600 frames per series. Three complete series were collected at varying ϕ angles (ϕ=0, 90, 180°). The crystal to detector distance was 6.0 cm, this providing a set of $3.38 \leq 2\theta \leq 52.90$. A total of 8898 reflections were collected and integrated using SAINT,[27] while absorption correction was applied using SADABS[28] with 3232 unique [R(int)=0.0204]. System symmetry, systematic absences and intensity statistics indicated the unique triclinic space group $P2_1/c$. The structure was determined by direct methods with the location of nearly all non-hydrogen atoms using the program SHELXS[29] and refined by full-matrix least-squares on F^2 using SHELXL.[30] All non-hydrogen atoms were refined anisotropically, while hydrogen atoms were placed in calculated positions, constrained to ride on their carbon atoms with group U_{iso} values assigned ($U_{iso}(H)$= $1.20U_{iso}$). The final structure was refined to convergence [$\Delta/\sigma \leq 0.001$] with R(F) = 0.0494 (for 3232 data with F>4σF), GOF = 0.956 and *w*R2 = 0.1279 (all data). [$R1 = \Sigma|F_O - F_C|/\Sigma|F_O|$, $wR2 = \{[\Sigma w(F_O^2 - F_C^2)^2]/\Sigma wF_O^4\}^{0.5}$, $w = 1/[\sigma^2(F_O^2) + (xP)^2 +$

y*P*], $P = (F_o^2+2F_c^2/3)$]. The largest difference between peaks and holes in the final difference map was 0.232 and –0.185 eÅ^{-3}.

[TMBuNC(Bu)Li] (18) and [TMBuNC(Bu)SiMe$_3$] (19)

A solution of 1,1,3,3-tetramethylbutyl isonitrile (0.200 g, 1.436 mmol) in diethyl ether (15 cm^3) was treated with ^{n}BuLi (0.90 cm^3, 1.6 M in hexanes, 1.436 mmol) at –78 °C. After 45 minutes, Me_3SiCl (0.15 cm^3, 1.436 mmol) was added dropwise via syringe at -78 °C and the mixture was allowed to warm to room temperature overnight. The solution was filtered under nitrogen atmosphere and the LiCl removed by filtration through Celite 521. The solvent and volatile components were removed under *vacuum* to give **19** as a yellow oil as final product (0.89 mmol, 62% yield).

IR(KBr): ν(C=N) at 1637.2 and 1566.7 cm^{-1}. ^{1}H NMR ($CDCl_3$/ppm): δ 1.27 (m, 8H), 0.88 (m, 18H), 0.07 (s, 9H). ^{13}C NMR ($CDCl_3$/ppm): δ 158.62 (C), 61.30 (C), 60.02 (C), 58.22 (CH_2), 54.03 (CH_2), 32.51 (CH_3), 32.01 (CH_3), 31.83 (CH_3), 29.31 (CH_2), 23.80 (CH_2), 13.70 (CH_3), 0.90 (Si-CH_3). FABMS (*m/z*): 268 (M^+). Elemental analysis for $C_{16}H_{35}NSi$: Expected: C, 71.30; H, 13.09; N, 5.20. Found: C, 70.01; H, 12.02; N, 5.00.

Me$_2$BBr (20)

Tetramethyltin (10.00 g; 55.40 mmol) was dropped into boron tribromide (5.28 cm^3, 55.40 mmol) at –50 °C (n-butylamine/liquid N_2) within one hour. The reaction was left to reach room temperature when there was an exothermic reaction. After reaching room temperature the reaction was refluxed for fifteen minutes to no more than 170 °C. The product was distilled at 30 °C (at 720 mmHg) to obtain the final product (26.87 mmol; 97% yield).

^{1}H NMR (benzene-d_6/ppm): δ 0.44 (s, 6H). ^{13}C NMR (benzene$_6$/ppm): δ 17.60. EIMS(*m/z*): C_2H_6BBr: 120. B.p 31 °C.

[{$Me_2B(2\text{-}py)_2$}Li] (21), [$Me_2B(2\text{-}py)_2(H)$] (22), Dimethylboronium Bis(2-pyridyl)borate (23) and Dimeric Dimethyl(2-pyridyl)borane (24)

A solution of 2-bromopyridine (18.41 g; 116.50 mmol) in diethyl ether (50 cm^3) at –78°C was added over a thirty minute period to a stirred solution of ^nBuLi (46.60 cm^3; 2.5 M in hexanes, 116.50 mmol) and diethyl ether (100 cm^3) at –78 °C under a nitrogen cover. After 10 minutes a solution of Me_2BBr (7.04 g; 58.25 mmol) in hexane (70 cm^3) was added for further a 30 minutes, and the solution became noticeably lighter in colour. Stirring was continued whilst the reaction mixture warmed to room temperature overnight. The brown solution obtained was filtered (**A**) whilst the remaining solution was stirred for one hour with activated charcoal and filtered again to provide the organic solution of [{$Me_2B(2\text{-}py)_2$}Li]. The organic solution was shaken with water (two portions of 50 cm^3 each), and the aqueous layer discarded (**B1**). The organic layer was shaken with acetic acid solution (three portions of 50 cm^3 each; 1.00 M), and the aqueous layer discarded (**B2**). The organic layer was evaporated to dryness (**C**). The combined aqueous layers, **B1** and **B2**, were made alkaline with sodium hydroxide (two portions of 40 cm^3 each; 6.0 M), and a yellowish solid was collected by filtration (**D**). The combined solids, **A** and **D**, were re-dissolved in hexane (100 cm^3), stirred with activated charcoal for one hour and was filtered. The solution was concentrated (to 40 cm^3) and left at –20 °C for five days to give colourless crystals of hydrogen dimethylbis(2-pyridyl)borate **22** suitable for analysis (72.23 mmol, 62% yield). A solution of **C** in diethyl ether (50 cm^3) was stirred with activated charcoal for one hour and then filtered off. The solution was concentrated (25 cm^3) and left at room temperature for two days to give colourless crystals of dimethylboronium bis(2-pyridyl)borate **23** and dimeric dimethyl(2-pyridyl)borane **24** suitable for analysis (11.65 mmol, 20% yield).

Hydrogen dimethylbis(2-pyridyl)borane (**22**). IR: ν(C=N-H) at 3059.7 cm^{-1}; ν(C=N) at 1591.3 cm^{-1}; ν(C=C) at 1476.4 cm^{-1}; ν(B-C) at 1428.7; ν(B-CH_3) at 728.3 cm^{-1}. ^1H NMR ($CDCl_3$/ppm): δ 18.54 (s, 1H, N*H*), 8.40 (d, 2H, C_5H_5N), 7.87 (d, 2H, C_5H_5N), 7.70 (t, 2H, C_5H_5N), 7.19 (t, 2H, C_5H_5N), 0.14 (t, 6H, CH_3). ^{13}C NMR ($CDCl_3$/ppm): δ 188.40 (q, C_5H_5N), 141.87 (s, C_5H_5N), 136.10 (s, C_5H_5N), 130.62 (t, C_5H_5N), 120.01 (q, C_5H_5N), 13.74 (q, CH_3). ^{11}B NMR ($CDCl_3$/ppm): δ -18.28. EIMS

(*m/z*): 198.3 (M^+), 197.2 (M^+-H), 120.1 (M^+-C_5H_4N). Elemental analysis for $C_{12}H_{15}N_2B$: Expected: C, 72.77; H, 7.63; N, 14.14. Found: C, 72.14; H, 7.58; N, 14.01.

Empirical formula	$C_{12}H_{15}N_2B$	β/ °	99.812(15)
Formula weight	198.07	γ/ °	90
Crystal system	Monoclinic	Volume/ Å^3	580.29(13)
Space group	P 2_1/m	Z	2
a/ Å	8.836(2)	Z'	1
b/ Å	7.1825(5)	Density calc./ Mgm^{-3}	1.134
c/ Å	9.2789(11)	μ (Mo-K)/ mm^{-1}	0.067
α/ °	90		

Data were collected on a Bruker SMART APEX diffractometer[25] equipped with an Oxford Cryosystems low-temperature device at 150 K and using an colourless plate oil-coated crystal[26] of dimension 0.23 x 0.12 x 0.11 mm^3. The initial unit cell was indexed using a least-squares analysis of a random set of reflections collected from three series of 0.3° wide ω-scans, 10 s per frame, and 25 frames per series that were well distributed in reciprocal space. Data frames were collected [Mo Kα = 0.71073 Å] with 0.3° wide ω-scans, 20 s per frame and 600 frames per series. Four complete series were collected at varying ϕ angles (ϕ=0, 90, 120, 180°). The crystal to detector distance was 6.0 cm, this providing a set of $4.22 \leq 2\theta \leq 52.10$. A total of 3502 reflections were collected and integrated using SAINT,[27] while absorption correction was applied using SADABS[28] with 878 unique [R(int)=0.0224]. System symmetry, systematic absences and intensity statistics indicated the unique monoclinic space group P 2_1/m. The structure was determined by direct methods with the location of nearly all non-hydrogen atoms using the program SHELXS[29] and refined by full-matrix least-squares on F^2 using SHELXL.[30] All non-hydrogen atoms were refined anisotropically, while hydrogen atoms were placed in calculated positions, constrained to ride on their carbon atoms with group U_{iso} values assigned (U_{iso}(H)= 1.20U_{iso}). Hydrogen atom on N was located from the difference map and the positions and the isotropic thermal parameters were refined. The final structure was refined to convergence [$\Delta/\sigma \leq 0.001$] with R(F) = 0.0322 (for 878 data with F>4σF), GOF = 1.096 and *w*R2 = 0.1032 (all data). [$R1 = \Sigma|F_O - F_C|/\Sigma|F_O|$, $wR2 = \{[\Sigma w(F_O^2 - F_C^2)^2]/\Sigma wF_O^4\}^{0.5}$, $w = 1/[\sigma^2(F_O^2) + (xP)^2 + yP]$, $P =$

($F_O^2+2F_C^2/3$)]. The largest difference between peak and hole in the final difference map, 0.212 and –0.125 eÅ^{-3}.

Dimethylboronium bis(2-pyridyl)borate(a) **23** and dimeric dimethyl(2-pyridyl)borane(b) **24** analysis. IR(a,b): ν(B-N) at 2412.1 cm^{-1}; ν(C=N) at 1591.3 cm^{-1}; ν(C=C) at 1476.4 cm^{-1}; ν(B-C) at 1428.7; ν(B-CH_3) at 728.3 cm^{-1}. ^{1}H NMR ($CDCl_3$/ppm): δ 8.44 (d, 2H, C_5H_4)(b), 8.34 (d, 2H, C_5H_5N)(a), 7.81 (t, 2H, C_5H_5N)(a), 7.71 (t, 2H, C_5H_5N)(b), 7.65 (t, 2H, C_5H_5N)(b), 7.63 (t, 2H, C_5H_5N)(a), 7.18 (d, 2H, C_5H_5N)(b), 7.15 (d, 2H, C_5H_5N)(a), 0.21 (s, 6H, CH_3)(a,b), 0.06 (s, 6H, CH_3)(a). ^{13}C NMR ($CDCl_3$/ppm): δ 188.39 (q, C_5H_5N)(a,b), 142.59 (s, C_5H_5N)(b), 141.87 (s, C_5H_5N)(a), 136.10 (t, C_5H_5N)(a,b), 130.62 (q, C_5H_5N)(b), 130.33 (q, C_5H_5N)(a), 120.70 (q, C_5H_5N)(b), 120.00 (q, C_5H_5N)(a), 14.86 (q, CH_3)(a,b). ^{11}B NMR ($CDCl_3$/ppm): δ 6.39(a), -1.85(b), -14.29(a). Elemental analysis for $C_{14}H_{20}N_2B_2$: Expected: C, 70.67; H, 8.47; N, 11.77. Found: C, 70.22; H, 8.36; N, 11.52.

Empirical formula	$C_{14}H_{20}N_2B_2$	β/ °	112.925(7)
Formula weight	237.94	γ/ °	90
Crystal system	Monoclinic	Volume/ Å^3	691.8(5)
Space group	P $2_1/c$	Z	2
a/ Å	8.536(4)	Z'	1
b/ Å	12.642(5)	Density calc./ Mgm^{-3}	1.142
c/ Å	6.961(3)	μ (Mo-K)/ mm^{-1}	0.065
α/ °	90		

Data were collected on a Bruker SMART APEX diffractometer[25] equipped with an Oxford Cryosystems low-temperature device at 150 K and using an colourless plate oil-coated crystal[26] of dimension 0.20 x 0.08 x 0.03 mm^3. The initial unit cell was indexed using a least-squares analysis of a random set of reflections collected from three series of 0.3° wide ω-scans, 10 s per frame, and 25 frames per series that were well distributed in reciprocal space. Data frames were collected [Mo Kα = 0.71073 Å] with 0.3° wide ω-scans, 10 s per frame and 600 frames per series. Three complete series were collected at varying ϕ angles (ϕ=0, 90, 180°). The crystal to detector distance was 6.0 cm, this providing a set of $3.22 \leq 2\theta \leq 57.58$. A total of 5340 reflections were collected and integrated using SAINT,[27] while absorption correction was applied using SADABS[28] with 1652 unique

[R(int)=0.0409]. System symmetry, systematic absences and intensity statistics indicated the unique monoclinic space group P $2_1/c$. The structure was determined by direct methods with the location of nearly all non-hydrogen atoms using the program SHELXS[29] and refined by full-matrix least-squares on F^2 using SHELXL.[30] All non-hydrogen atoms were refined anisotropically, while hydrogen atoms were placed in calculated positions, constrained to ride on their carbon atoms with group U_{iso} values assigned ($U_{iso}(H)= 1.20U_{iso}$). In the pyridyl ring the nitrogen and a carbon atom are disordered in the ratio of 80:20 over two positions with a common boron-position. The final structure was refined to convergence [$\Delta/\sigma \leq 0.001$] with R(F) = 0.0871 (for 1652 data with F>4σF), GOF = 1.198 and *w*R2 = 0.2216 (all data). [$R1 = \Sigma|F_O - F_C|/\Sigma|F_O|$, $wR2 = \{[\Sigma w(F_O^2 - F_C^2)^2]/\Sigma wF_O^4\}^{0.5}$, $w = 1/[\sigma^2(F_O^2) + (xP)^2 + yP]$, $P = (F_O^2+2F_C^2/3)$]. The largest difference between peak and hole in the final difference map, 0.412 and –0.125 eÅ^{-3}.

[{$Me_2B(2\text{-}py)_2$}Mg(Me)THF] (25)

To a solution of hydrogen dimethylbis(2-pyridyl)borate (0.581 g, 2.93 mmol) in THF (10 cm^3) was added ^{n}BuLi (1.17 cm^3, 2.5 M in hexanes, 2.93 mmol) at –78 °C. The mixture was allowed to warm to room temperature and stirred for 4 hours. At room temperature the orange/red solution obtained was treated with MeMgCl (0.98 cm^3, 3.0 M in THF, 2.93 mmol) and allowed to stir for 24 hours. The solvent and volatile components were removed under *vacuum*, diethyl ether added (10 cm^3) and the LiCl was filtered under nitrogen atmosphere using the Cannula technique. The solvent was removed again under *vacuum* to give a white powder which was quite insoluble in most of the organic solvents tested. NMR spectra were conducted in toluene after filtering the solution obtained (1.86 mmol, 63% yield, according to the NMR spectroscopy).

^{1}H NMR (toluene-d_8/ppm): δ 8.61 (d, 2H, C_5H_5N), 7.81 (d, 2H, C_5H_5N), 7.66 (t, 2H, C_5H_5N), 7.29 (t, 2H, C_5H_5N), 3.63 (m, THF), 1.78 (m, THF), 1.17 (s, 6H, CH_3), -1.38 (s, 3H, $MgCH_3$). ^{13}C NMR (toluene-d_8/ppm): δ 183.80 (q, C_5H_5N),

141.03 (s, C_5H_5N), 136.21 (s, C_5H_5N), 131.14 (t, C_5H_5N), 121.15 (q, C_5H_5N), 67.12 (THF), 23.30 (THF), 13.72 (q, CH_3), -17.30 (q, $MgCH_3$).

[{$Me_2B(2\text{-}py)_2$}$_2$Mg] (26)

A solution of hydrogen dimethylbis(2-pyridyl)borate (0.581 g, 2.93 mmol) in THF (10 cm^3) was treated with ^{n}BuLi (1.17 cm^3, 2.5 M in hexanes, 2.93 mmol) at –78 °C. The mixture was allowed to warm to room temperature and stirred for 4 hours. At room temperature the orange/red solution obtained was treated with MeMgBr (0.98 cm^3, 3.0 M in THF, 2.93 mmol) and stired for three days. The solvent and volatile components were removed under *vacuum*, diethyl ether added (10 cm^3) and LiBr was filtered under a nitrogen atmosphere using the Cannula technique. The solvent was removed again under *vacuum* to give a white powder which was quite insoluble in most of the organic solvents tested. NMR spectra were conducted in toluene after filtering the solution obtained. Crystallisation was achieved by dissolving the sample in hot toluene (10 cm^3), and filtering under a nitrogen atmosphere using the Cannula technique. The Schlenk was cooled down slowly and left for two months to give colourless crystals suitable for X-ray analysis (0.84 mmol; 57% yield). Similar results were obtained when BzMgCl or AllylMgCl were used (different Grignard reagents gave insoluble oils).

^{1}H NMR (toluene-d_8/ppm): δ 8.73 (d, 2H, C_5H_5N), 8.32 (d, 2H, C_5H_5N), 7.84 (t, 2H, C_5H_5N), 7.09 (t, 2H, C_5H_5N), 0.61 (s, 6H, CH_3), 0.08 (s, 6H, CH_3). ^{13}C NMR (toluene-d_8/ppm): δ 182.82 (q, C_5H_5N), 139.46 (s, C_5H_5N), 136.23 (s, C_5H_5N), 128.17 (t, C_5H_5N), 120.83 (q, C_5H_5N), 14.28 (q, CH_3). FABMS (*m/z*): 419 (M^+); 404 (M^+-CH_3).

Empirical formula	$C_{24}H_{28}N_4B_2Mg$	β/ °	74.00(2)
Formula weight	418.24	γ/ °	79.38(2)
Crystal system	Triclinic	Volume/ Å^3	4694.5(15)
Space group	P$\bar{1}$	Z	4
a/ Å	8.589(2)	Z'	1
b/ Å	8.967(5)	Density calc./ Mgm^{-3}	1.180
c/ Å	11.826(4)	μ (Mo-K)/ mm^{-1}	0.167
α/ °	85.3(5)		

Data were collected on a Bruker SMART APEX diffractometer[25] equipped with an Oxford Cryosystems low-temperature device at 150 K and using an colourless plate oil-coated crystal[26] of dimension 0.22 x 0.14 x 0.12 mm^3. The initial unit cell was indexed using a least-squares analysis of a random set of reflections collected from three series of 0.3° wide ω-scans, 10 s per frame, and 25 frames per series that were well distributed in reciprocal space. Data frames were collected [Mo Kα = 0.71073 Å] with 0.3° wide ω-scans, 10 s per frame and 600 frames per series. Four complete series were collected at varying ϕ angles (ϕ=0, 90, 120, 180°). The crystal to detector distance was 6.0 cm, this providing a set of $4.44 \leq 2\theta \leq 50.10$. A total of 3314 reflections were collected and integrated using SAINT,[27] while absorption correction was applied using SADABS[28] with 3008 unique [R(int)=0.0588]. System symmetry, systematic absences and intensity statistics indicated the unique triclinic space group P $\bar{1}$. The structure was determined by direct methods with the location of nearly all non-hydrogen atoms using the program SHELXS[29] and refined by full-matrix least-squares on F^2 using SHELXL.[30] All non-hydrogen atoms were refined anisotropically, while hydrogen atoms were placed in calculated positions, constrained to ride on their carbon atoms with group U_{iso} values assigned ($U_{iso}(H)= 1.20U_{iso}$). Hydrogen atom on N was located from the difference map and the positions and the isotropic thermal parameters were refined. The final structure was refined to convergence [$\Delta/\sigma \leq 0.001$] with R(F) = 0.0432 (for 3008 data with F>4σF), GOF = 1.008 and *w*R2 = 0.0689 (all data). [$R1 = \Sigma|F_O - F_C|/\Sigma|F_O|$, $wR2 = \{[\Sigma w(F_O^2 - F_C^2)^2]/\Sigma wF_O^4\}^{0.5}$, $w = 1/[\sigma^2(F_O^2) + (xP)^2 + yP]$, $P = (F_O^2+2F_C^2/3)$]. The largest difference between peak and hole in the final difference map, 0.455 and –0.325 $eÅ^{-3}$.

Ph_2BBr (27)

Boron tribromide (10.30 cm^3, 107.40 mmol) was added to tetraphenyltin (22.95 g; 53.70 mmol) at –78 °C. The suspension was allowed to warm to 20 °C (the reaction became more reactive and exothermic). Once the temperature reached 20 °C the suspension was refluxed at 250 °C for three hours. After distillation

between 80 – 140 °C (at 10 mmHg) $SnBr_4$ is obtained, while between 154 - 160°C (at 10 mmHg) diphenylboron bromide was obtained (77.33 mmol; 72% yield).

IR: ν(B-C_6H_5) at 1223.8 and 900.2 cm^{-1}; ν(B-Br) at 543.2 cm^{-1}. ^1H NMR ($CDCl_3$/ppm): δ 7.39 (d, 5H). ^{13}C NMR ($CDCl_3$/ppm): δ 126.30. EIMS(*m/z*): $C_{12}H_{10}BBr$: 244, M-Br: 164. B.p 154-160 °C/10 mmHg.

[{$Ph_2B(2\text{-}py)_2$}Li(THF)] (28) and [$Ph_2B(2\text{-}py)_2(H)$] (29)

a) [{$Ph_2B(2\text{-}py)_2$}Li(THF)]. A solution of hydrogen diphenyl(2-pyridyl)borane (0.500 g, 1.55 mmol) in diethyl ether (10 cm^3) was treated with ^{n}BuLi (0.97 cm^3, 1.6 M in hexanes, 1.55 mmol) at –78 °C. The mixture was allowed to warm to room temperature and stirred overnight. The solvent and volatile components were removed under *vacuum* to give a yellow solid which was washed with cold hexane (20 cm^3). The final yellow powder was filtered under a nitrogen atmosphere using the Cannula technique. NMR spectra were conducted in toluene after filtering the solution obtained (1.364 mmol, 88% yield; according to the NMR spectroscopy).

^1H NMR (toluene-d_8/ppm): δ 8.15-6.84 (brm, Ar); 3.47 (s, THF); 1.61 (m, THF).

b) [$Ph_2B(2\text{-}py)_2(H)$]. A solution of 2-bromopyridine (10.32 g; 65.32 mmol) in diethyl ether (75 cm^3) at –78°C was added over a period of thirty minutes period to a stirred solution of ^{n}BuLi (26.20 cm^3; 2.5 M in hexanes, 65.32 mmol) and diethyl ether (100 cm^3) at –78 °C under a nitrogen cover. After 10 minutes a solution of Ph_2BBr (8.00 g; 32.66 mmol) in hexane (70 cm^3) was added over a further 30 minute period, and the solution became noticeably in lighter colour. Stirring was continued whilst the reaction mixture warmed to room temperature overnight. The brown solution obtained was filtered, stirred for one hour with activated charcoal and then filtered again to provide the organic solution of [{$Ph_2B(2\text{-}Py)_2$}Li]. The organic solution was shaken with water (two portions of 50 cm^3 each), and the aqueous layer separated (**A1**). The organic layer was shaken with acetic acid solution (three portions of 50 cm^3 each; 1.00 M), and the aqueous layer separated (**A2**). The organic layer was evaporated to dryness (**B**). The combined aqueous layers, **A1** and **A2**,

were made alkaline with sodium hydroxide (two portions of 40 cm^3 each; 6.0 M), and the yellowish solid obtained was filtered off (**C**). The combined solids, **A** and **C**, were re-dissolved in hexane (100 cm^3), stirred with activated charcoal for one hour and filtered. The solution was concentrated (to 40 cm^3) and left at –20°C for three days to give colourless crystals of hydrogen diphenylbis(2-pyridyl)borate suitables for analysis (18.29 mmol, 56% yield).

IR: ν(C=N-H) at 3035.4 cm^{-1}; ν(C=N) at 1563.0 cm^{-1}; ν(C=C) at 1479.1 cm^{-1}; ν(B-C) at 1427.0; ν(B-C_6H_6) at 734.8 cm^{-1}. ^{1}H NMR (toluene-d_8/ppm): δ 11.83 (s, 1H, N*H*), 7.48 (d, 2H, Ar), δ 7.21 (t, 4H, Ar), 7.17 (t, 4H, Ar), 7.14 (t, 2H, Ar). ^{13}C NMR (toluene-d_8/ppm): δ 188.40 (C-Ar), 138.86 (C-Ar), 136.25 (C-Ar), 127.11 (C-Ar), 123.51 (C-Ar), 119.20 (C-Ar). ^{11}B NMR (toluene-d_8/ppm): δ -13.81. EIMS (*m/z*): 323 (M^+), 244 (M^+-C_5H_4NH). Elemental analysis for $C_{22}H_{19}N_2B$: Expected: C, 82.01; H, 5.94; N, 8.69. Found: C, 89.82; H, 5.90; N, 8.55.

Empirical formula	$C_{22}H_{19}N_2B$	β/°	87.673(2)
Formula weight	322.20	γ/°	80.1310(10)
Crystal system	Triclinic	Volume/ Å^3	879.39(13)
Space group	P $\bar{1}$	Z	2
a/ Å	9.0834(8)	Z'	1
b/ Å	9.4879(8)	Density calc./ Mgm^{-3}	1.216
c/ Å	10.4124(9)	μ (Mo-K)/ mm^{-1}	0.071
α/ °	84.461(2)		

Data were collected on a Bruker SMART APEX diffractometer[25] equipped with an Oxford Cryosystems low-temperature device at 150 K and using an colourless plate oil-coated crystal[26] of dimension 0.12 x 0.09 x 0.06 mm^3. The initial unit cell was indexed using a least-squares analysis of a random set of reflections collected from three series of 0.3° wide ω-scans, 10 s per frame, and 25 frames per series that were well distributed in reciprocal space. Data frames were collected [Mo Kα = 0.71073 Å] with 0.3° wide ω-scans, 20 s per frame and 600 frames per series. Four complete series were collected at varying ϕ angles (ϕ=0, 90, 120, 180°). The crystal to detector distance was 6.0 cm, this providing a set of $4.00 \leq 2\theta \leq 52.88$. A total of 4725 reflections were collected and integrated using SAINT,[27] while absorption correction was applied using SADABS[28] with 3312 unique [R(int)=0.0113]. System symmetry, systematic absences and intensity statistics

indicated the unique triclinic space group $P\bar{1}$. The structure was determined by direct methods with the location of nearly all non-hydrogen atoms using the program SHELXS[29] and refined by full-matrix least-squares on F^2 using SHELXL.[30] All non-hydrogen atoms were refined anisotropically, while hydrogen atoms were placed in calculated positions, constrained to ride on their carbon atoms with group U_{iso} values assigned ($U_{iso}(H) = 1.20U_{iso}$). Hydrogen atom on N was located from the difference map and the positions and the isotropic thermal parameters were refined. The final structure was refined to convergence [$\Delta/\sigma \leq 0.001$] with R(F) = 0.0439 (for 3312 data with F>4σF), GOF = 1.096 and *w*R2 = 0.1077 (all data). [$R1 = \Sigma|F_O - F_C|/\Sigma|F_O|$, $wR2 = \{[\Sigma w(F_O^2 - F_C^2)^2]/\Sigma wF_O^4\}^{0.5}$, $w = 1/[\sigma^2(F_O^2) + (xP)^2 + yP]$, $P = (F_O^2+2F_C^2/3)$]. The largest difference between peak and hole in the final difference map, 0.312 and –0.175 eÅ^{-3}.

[{$Ph_2B(2\text{-}py)_2$}Mg(Me)THF] (30)

A solution of hydrogen diphenyl(2-pyridyl)borane (0.500 g, 1.55 mmol) in diethyl ether (10 cm^3) was treated with ^{n}BuLi (0.97 cm^3, 1.6 M in hexanes, 1.55 mmol) at –78 °C. The mixture was allowed to warm to room temperature and stirred overnight. At room temperature the orange/red solution obtained was treated with MeMgCl (0.52 cm^3, 3.0 M in THF, 1.55 mmol) and allowed to stir overnight. The solution was filtered under a nitrogen atmosphere using the Cannula technique. The solvent was removed again under *vacuum* to give a colourless oil which was quite insoluble in most of the organic solvents used. The NMR spectra were conducted in toluene after filtering the solution obtained (0.70 mmol, 45% yield; according to the NMR spectroscopy).

^{1}H NMR (toluene-d_8/ppm): δ 7.32 (d, 8H, Ar), 7.29 (m, 4H, Ar), δ 7.13 (m, 6H, Ar), 3.16 (s, THF), 1.99 (m, THF), -1.05 (br, 3H, MgCH_3). ^{13}C NMR (toluene-d_8/ppm): δ 140.44 (*o*-C_5H_5N), 136.25 (*p*-C_6H_5N), 123.51 (*m*-C_6H_5N), 68.02 (THF), 23.12 (THF), -16.30 (MgCH_3). ^{1}H NMR (THF-d_8/ppm): δ 7.76 (d, 8H, Ar), 7.58 (m, 4H, Ar), 7.49 (m, 6H, Ar), 3.76 (s, THF), 1.90 (m, THF), -1.55 (br, 3H, MgCH_3).

3.5 References

1 J. D. Roberts and M. Caserio, *Modern Organic Chemistry,* W.A. Benjamin, INC, New York, **1987**, 51.

2 F. G. Bordwell, *Organic Chemistry*, The MacMillan Company, New York, **1969**, 296.

3 G. F. Grillot, H. R. Felton, B. R. Garret, H. Greeberg, R. Green, R. Cementi and M. Moskowitz, *J. Am. Chem. Soc.*, **1954**, *76*, 3969.

4 C. G. Screttas and M. M. Screttas, *J. Org. Chem.*, **1978**, *43*, 1064.

5 D. Guijarro and M. Yus, *Tetrahedron Lett.*, **1994**, *35*, 2965.

6 E. Alonso, D. Guijarro and M. Yus, *Tetrahedron*, **1995**, *51*, 2699.

7 M. Yus, *Chem. Soc. Rev.*, **1996**, 155.

8 a) C. Gómez, F. Huerta and M. Yus, *Tetrahedron Lett.*, **1997**, *38*, 687; b) F. Foubelo, A. Gutierrez and M. Yus, *Tetrahedron Lett.*, **1997**, *38*, 4837; c) I. Gómez, E. Alonso, D. Ramon and M. Yus, *Tetrahedron*, **2000**, *56*, 4043; d) M. Yus, D. Ramon and I. Gómez, *J. Organomet. Chem.*, **2002**, *21*, 663.

9 M. Yus, C. Gómez and P. Candela, *Tetrahedron*, **2002**, *58*, 6207.

10 D. Ramón and M. Yus, *Eur. J. Org. Chem.*, **2000**, 225.

11 M. Yus, R. Herrera and A. Guijarro, *Tetrahedron Lett.*, **2001**, *42*, 3455.

12 C. Gómez, S. Ruiz and M. Yus, *Tetrahedron Lett.*, **1998**, *39*, 397.

13 M. Yus and F. Foubelo, *Rev. Heteroatom. Chem.*, **1997**, *17*, 73.

14 F. Foubelo and M. Yus, *Trends Org. Chem.*, **1998**, *7*, 1.

15 C. Strohmann and C. Bors, *Angew. Chem. Int. Ed. Engl.*, **1996**, *35*, 2378.

16 G. Niznik, W. Morrinson and H. Walborsky, *J. Org. Chem.*, **1974**, *39*, 600; b) N. Hirowatari and H. Waborsky, *J. Org. Chem.*, **1974**, *39*, 604; c) G. Niznik and H. Walborsky, *J. Org. Chem.*, **1974**, *39*, 608; d) M. Periasamy and H. Walborsky, *J. Org. Chem.*, **1974**, *39*, 611; e) H. Walborsky and P. Roman, *J. Org. Chem.*, **1975**, *43*, 731.

17 H. Walborsky, W. Morrison and G. Niznik, *J. Am. Chem. Soc.*, **1970**, *92*, 6675.

18 H. Walborsky, G. Niznik and M. Periasamy, *Tetrahedron Lett.*, **1971**, *22*, 4965.

19 a) J. Barluenga, F. Foubelo, F. Fañanás and M. Yus, *Tetrahedron Lett.*, **1988**, *29*, 2859; b) Y. Ito, H. Imai, T. Matsuura and T. Saegusa, *Tetrahedron Lett.*, **1984**, *25*, 3091.

20 S. Trofimenko, *Chem. Rev.*, 1972, *72*, 497.

21 E. Hanecker, T. G. Hodgkins, K. Niedenzu and H. Nöth, *Inorg. Chem.*, **1985**, *24*, 459-462.

22 a) T. Hodgkins, *Inorg. Chem.*, **1993**, *32*, 6115; T. Hodgkins and D. Powell, *Inorg. Chem.*, **1996**, *35*, 2140.

23 N. Holy, *Chem. Rev.*, **1974**, *74*, 260.

24 a) K. Niendenzu, *Organometal. Chem. Rev.*, **1966**, *1*, 305; b) J. Burch, W. Gerrard, M. Horwarth and E. Mooney, *J. Chem. Soc.*, **1960**, 4916; c) E. Abel, S. Dandegaonker, W. Gerrard and M. Lappert, *J. Chem. Soc.*, **1956**, 4697.

[25] Bruker. *SMART*. Bruker-AXS, Madison, Wisconsin, USA, **2001**.

[26] D. Stalke and T. Kottke, *J. Appl. Crystallogr.*, **1993**, 26, 615.

[27] Bruker. *SAINT*. Bruker-AXS, Madison, Wisconsin, USA, **2002**.

[28] G. M. Sheldrick, *SADABS*. Version 2.06. University of Gottingen, Germany, **2001**.

[29] G. M. Sheldrick, *SHELXS97*. University of Gottingen, Germany, **1997**.

[30] G. M. Sheldrick, *SHELXL97*. University of Gottingen, Germany, **1997**.

Chapter 4:

Evidence for a Borene Carbene Analogue

4.1 Introduction

4.1.1 Background

The present investigation is an attempt to explore the chemistry of boron supported by the β-diketiminate ligand. The use of β-diketiminate ligands has several attractive features, including the tuneability possible in both Ar and R and variable bonding modes ranging from purely σ to a combination of σ and π donation depending on the steric environment and the electron demand at the boron atom. The exploration of the synthesis and structural elucidation of borane complexes supported by β-diketiminate ligands has been proposed (Figure 4.1).

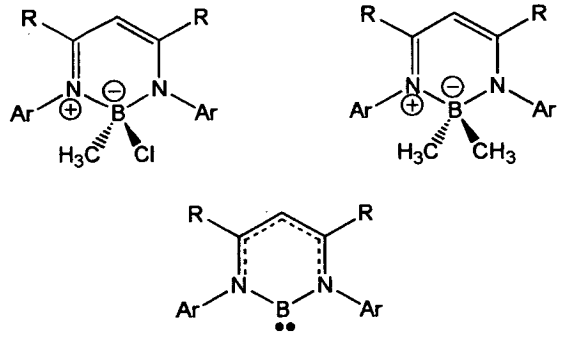

Figure 4.1 Desired boron methyl, dimethyl β-diketiminate and borane carbene analogue.

The conjugated, monoanionic, β-difunctional ligand represented by Figure 4.2, shows one of the most fundamental chelating systems in co-ordination chemistry.[1] One of its principal advantages is the flexibility of synthesis such that a wide variety of terminal substituents R and R′ and donor atoms or groups X and Y may be easily incorporated, producing stereochemical and electronic changes.[1,2] The chemistry of β-difunctional ligands with X: N, S and NR (R= H, aromatic, alkyl) has been recently studied, and some properties of their bis-chelate systems have been elucidated.[3]

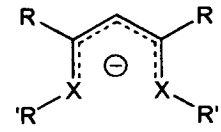

R: Me or ^{t}Bu; R': Ar
X: S, N

Figure 4.2 Anionic chelating nitrogen donor dikitiminato.

Complexes of β-difunctional ligands with transition metals or with main group alkyl compounds hold considerable scientific and economic importance for polymerisation catalysis.[4] The synthesis of β-diketiminato ligands by condensation reactions between primary amines and 2,4-pentadione has been known for many years,[5] and the ligand can be represented either by a rapid tautomeric conversion or by a symmetrically hydrogen-bonded structure (Figure 4.3). Equivalent observations have been reported by Brasen and Dorman,[6,7] where the dipole moment can be attributed to an aromatic six-π-electron system corresponding to a structure of C_{2v} symmetry.

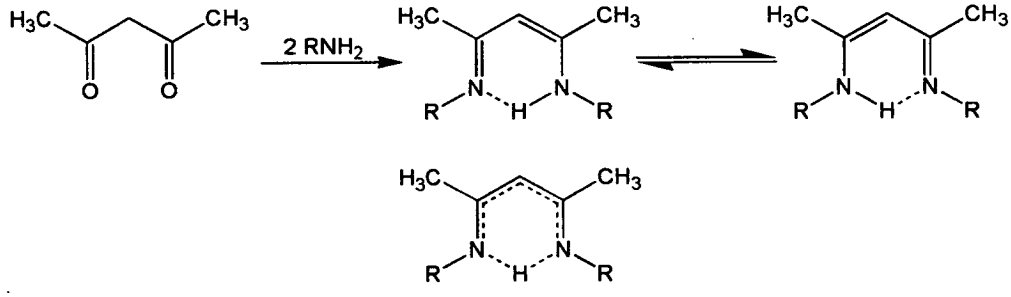

Figure 4.3 Synthesis of β-diketiminate system, and the suggested tautomeric species.

One importance of cationic metal complex species has emerged in the generation of possible main group and lanthanide complexes for ethylene polymerisation catalysis, prepared by a transmetallation of the lithium salts (Figure 4.4a).[8] In addition, these ligands have been applied successfully to the stabilisation of low-coordinate, and low oxidation state main group metal complexes, whilst their potassium salts exist as polymers associated *via* the potassium ion.[9] Neutral dialkyl compounds require prior activation *via* alkide abstraction with a Lewis acid in order to attain olefin polymerisation activity (Figure 4.4b).[9] The synthesis and reactions of

diketiminates of some alkali metals, including their role in preparing unusual transition metal and main group complexes, has been reviewed by Lappert *et al.*[10] The complexation of magnesium species by using β-diketiminate ligands has attracted increasing attention, where the polymerisation activity by such main group metal complexes has been tested (Figure 4.4c).[11,12] Moreover, zinc complexes of β-diketiminato ligands have shown to be highly active catalysts for the living stereoselective polymerisation of lactide to produce poly(lactic acid), whilst the activity of zinc complexes for copolymerisation reactions of CO_2 and epoxides has yielded good conversion.[13] The ligands that offer steric protection of the metal centre, however, often block the metal from the interesting intermolecular reactivity expected from the unusual orbital structure of the low-coordinate metal.[14,15] The steric protection even stabilises highly electronically unsaturated organometallic complexes, and thus it has been possible to synthesise the first three-coordinate methyl complexes of the transition metals (Figure 4.4d).[16]

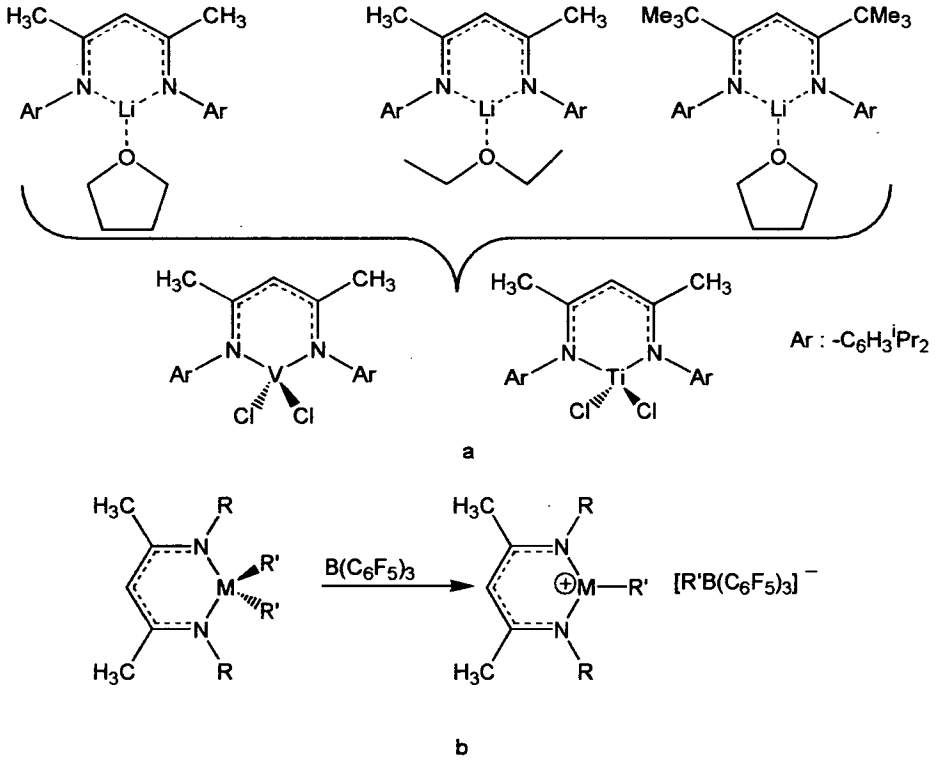

Figure 4.4 a) β-diketiminate transition metal complexes prepared from the lithiated ligand; b) activation of a neutral metal complex for olefin polymerisation.

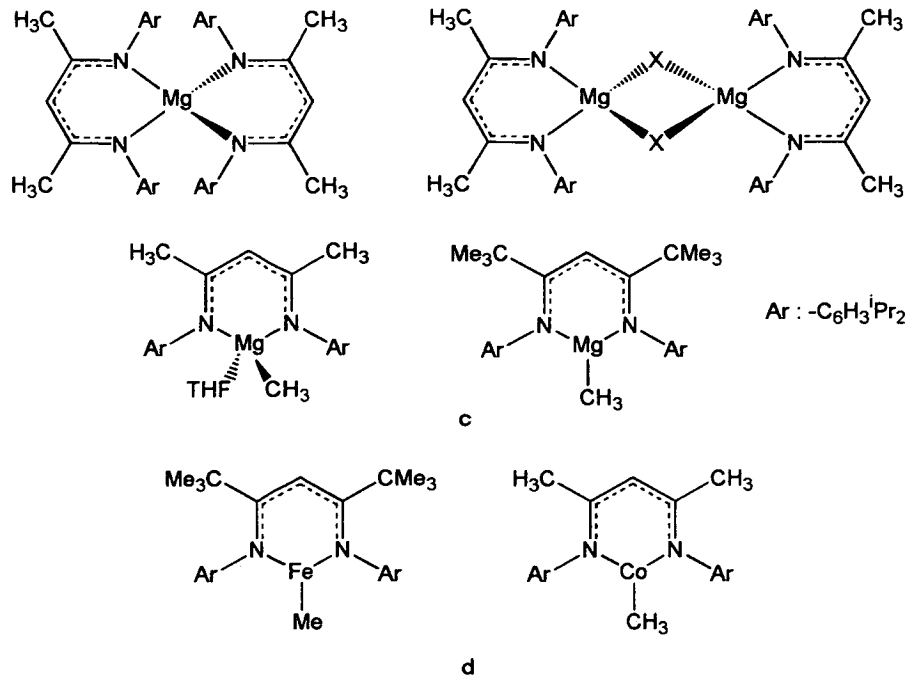

Figure 4.4 (Continued) c) β-diketiminate magnesium complexes; d) the first two three co-ordinate methyl complexes of transition metals.

In polymerisation catalysis, main-group compounds play important roles as activators in the generation of cationic transition-metal alkyl species that polymerise α-olefins.[14] There is an extensive chemistry of species with bonding between heavier group 13 elements and nitrogen,[17] while such compounds are of interest because they are isoelectronic to the corresponding carbon group 14 element derivatives, which permits interesting comparisons of properties.[18] The stability of the group 13 alkyl cations will depend on the ancillary ligand set and the choice of counteranion, and this was recently shown to be the case in main-group systems as reported by Coles and Jordan for the polymerisation of ethylene by cationic aluminium species.[19] It is apparent that the steric properties of the ligand play a key role in determining the stability of the main group complexes, and the easy synthesis of β-diketiminate ligands make them alternative candidates in stoichiometric and catalytic applications.[20]

4.1.2 Evidence for Group 13 "Carbene Analogue"

A number of interesting aluminium and gallium β-diketiminato complexes have been synthesised and fully characterised by using the precursor $AlCl_3$ or $GaCl_3$.[21] Further reduction of aluminium complexes with potassium metal can give the two-coordinate, low-valence aluminium(I) derivatives which may be considered as carbene analogues.[22] Neutral, molecular derivatives of low-valence gallium usually exist as Ga-Ga bonded tetramers or hexamers of formula $(GaR)_4$ or $(GaR)_6$, which may dissociate to the monomers (GaR) in either vapour of solution phase.[23] The low-valence gallium derivatives can be obtained by using "GaI" followed by reduction with potassium, according to Figure 4.5.[23]

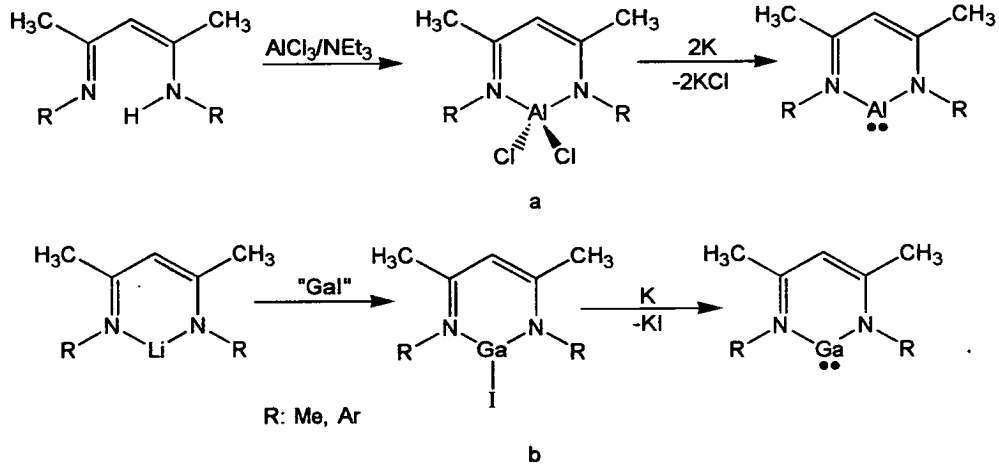

Figure 4.5: Synthesis of low-valence aluminium (a) and gallium (b) carbene analogues.

Analogous low valent compounds of silicon, germanium, aluminium and gallium are also well known whilst the absence of the isoelectronic boron compound has motivated scientists to look for the still unknown boranide anion.[23,24] Quantum chemical calculations have investigated the bonding features of this kind of compound, and it has been predicted to be a stable species.[24] Reactivity of BF_3 with the β-diketiminate ligands has been tested to form a six-membered heterocyclic complex.[25] Further methylation can produce the expected boron complex, where methyl substitution of the remaining fluoride ligands is observed (Figure 4.6). Lothar *et al.*[26] have examined a reduction of 2-bromo-1,3,2-diazaborole using alkali metals,

and the formation of dimer complexes suggest an intermediate radical reaction, according to Figure 4.7.

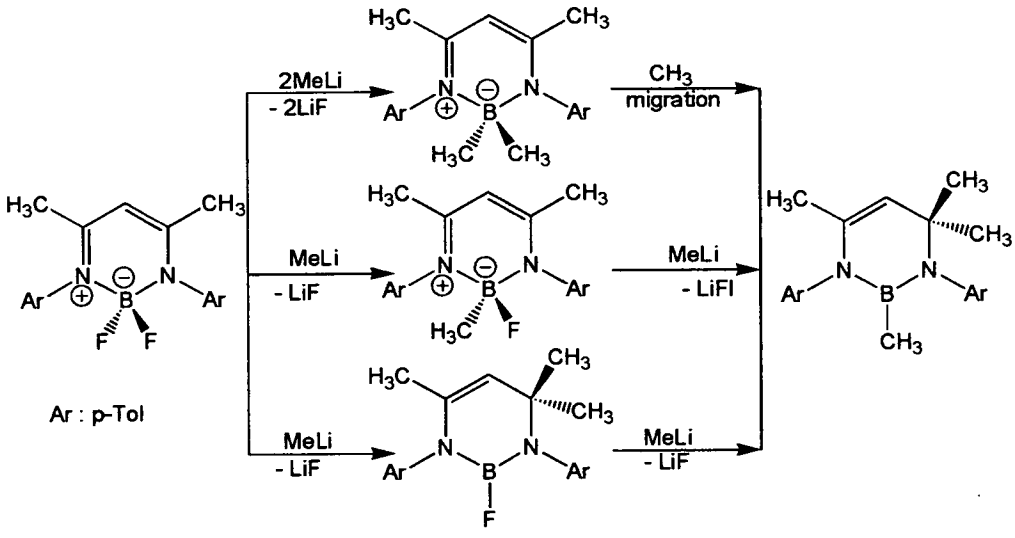

Figure 4.6 β-Diketiminate boron complexes and evidences of methyl migration.

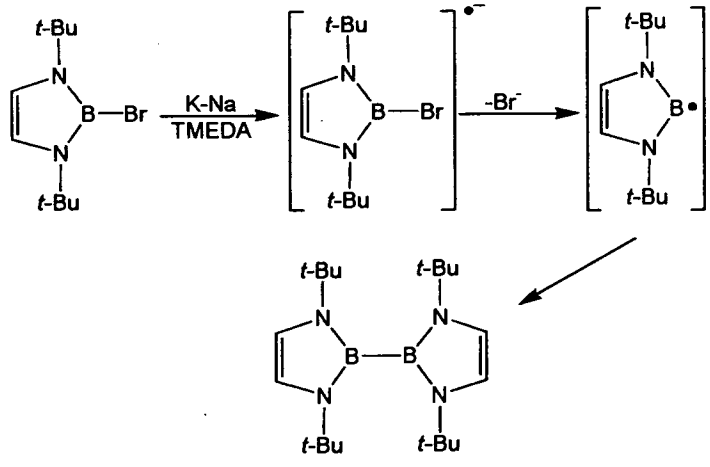

Figure 4.7 K-Na reduction of 2-bromo-1,3,2-diazoborole.

4.2 Results

4.2.1 Reactivity of Lithium β-Diketiminate with BCl_3

Treatment of [HC(MeCNAr')$_2$Li] (Ar'=2,6-diisopropylphenyl) (**32**) with an equimolar amount of BCl_3 in diethyl ether at –78 °C was carried out, and the reaction stopped after leaving overnight. The suspension was filtered off and subsequent removal of the solvent in *vacuum* and extraction with ether, resulted in the formation of [HC(MeCNAr')$_2$BCl$_2$] (**33**) as an orange oil (Figure 4.8). Satisfactory NMR spectra were obtained, but elemental analysis (CHN) and mass spectra could not be obtained due to the reactivity of the sample. The ^{1}H NMR spectrum of **33** suggests a monomeric structure which is consistent with the multiplet downfield peaks of the aromatic ring are centred at δ 7.15, whilst the γ–C*H* singlet is shifted to δ 5.40. The isopropyl hydrogen atoms are placed in the region of δ 3.32, 1.35 and 1.17, whilst the singlet of the methyl hydrogen atoms is placed at δ 2.14 (Figure 4.9). The ^{13}C NMR spectrum shows the characteristic downfield resonances of aromatic carbon atoms between δ 161.0 and 94.70, whilst the non-aromatic carbon atoms are assigned to the upfield region between δ 28.52 and 20.01 (Figure 4.10). The ^{11}B NMR spectrum of **33** is consistent with a characteristic tetrahedral boron centre, where a broad peak is placed at δ 4.90 (Figure 4.11).

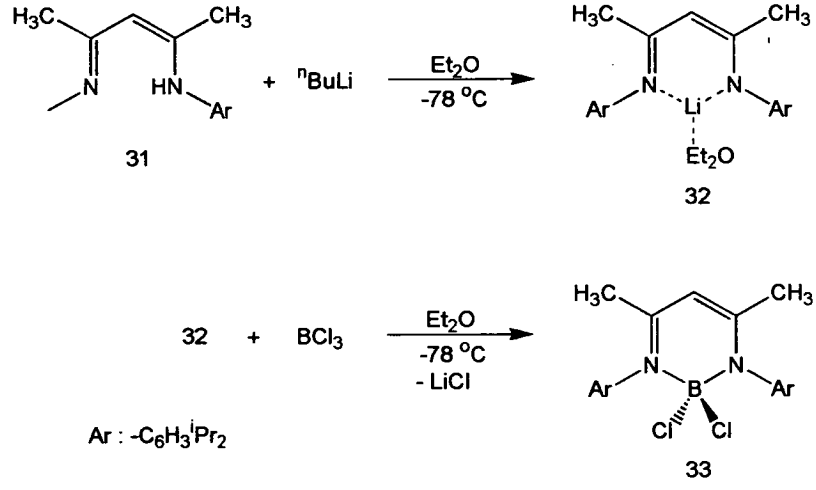

Figure 4.8 Reactivity of 32 with BCl_3.

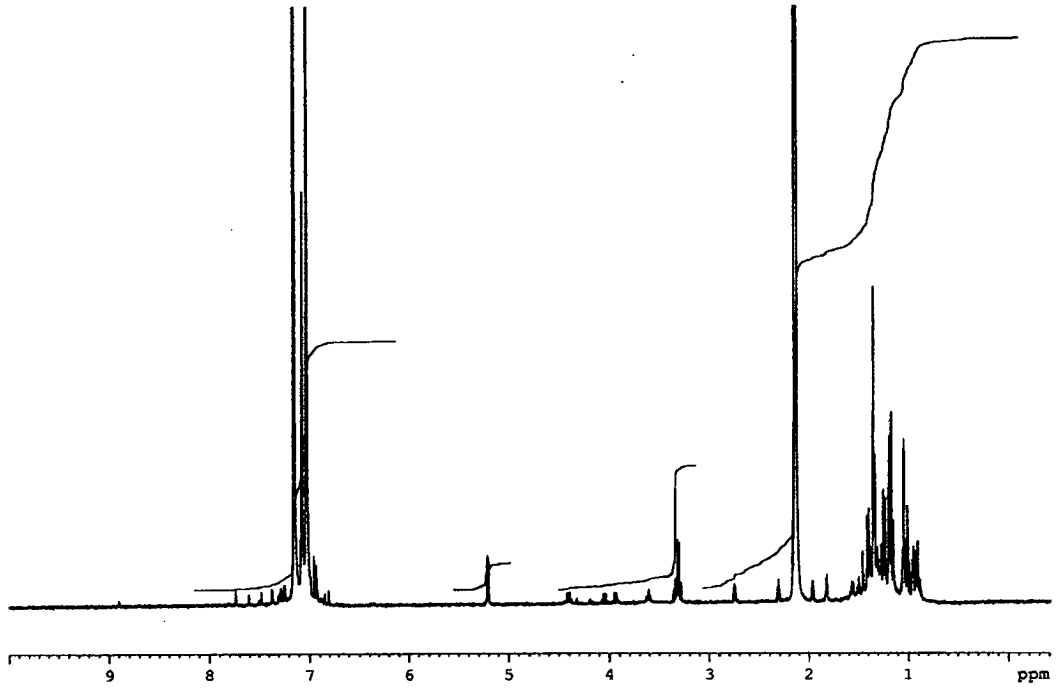

Figure 4.9 ^{1}H NMR spectrum in toluene-d_8 of 33.

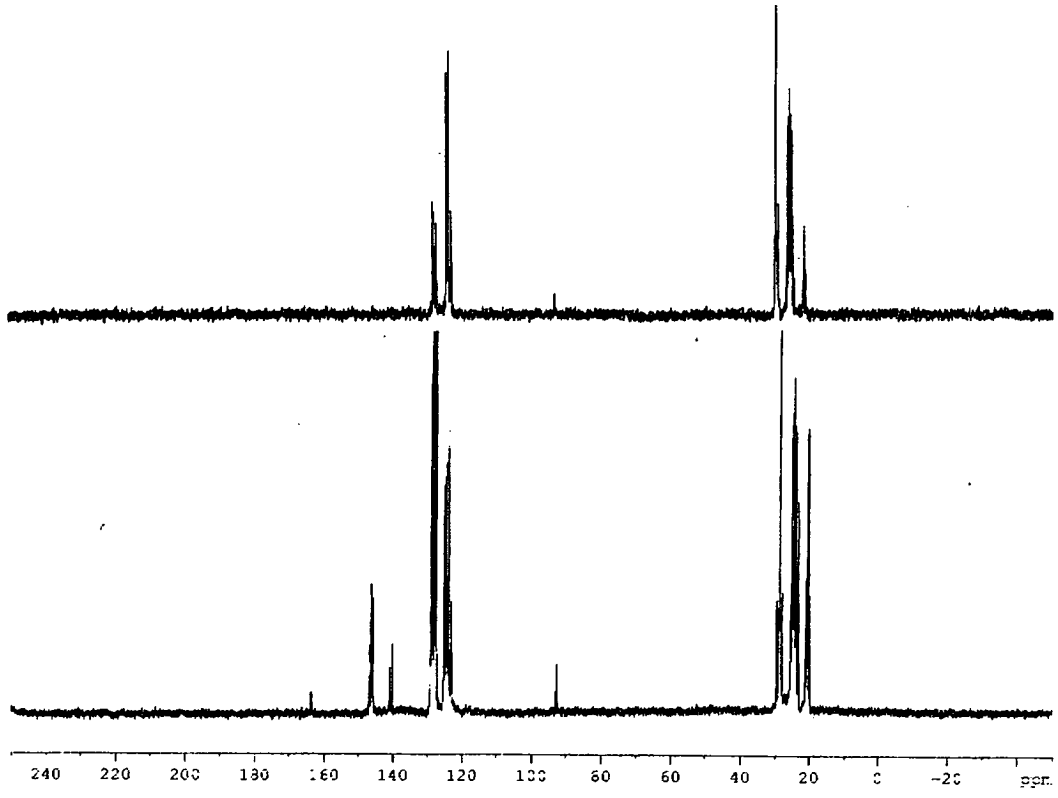

Figure 4.10 ^{13}C NMR spectrum in toluene-d_8 of 33.

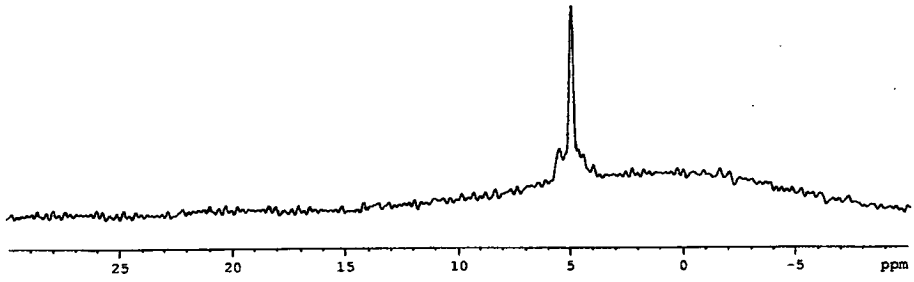

Figure 4.11 ^{11}B NMR spectrum in toluene-d_8 of 33.

4.2.2 Reactivity of [HC(MeCNAr')$_2$BCl$_2$] with MeLi

The alkylation of **33** with an equimolar amount of MeLi in ether at –78 °C, resulted in the formation of [HC(MeCNAr')$_2$B(Cl)Me] (**34**) as an orange oil (Figure 4.12). NMR spectra supported a monomeric structure with methylation of the boron atom. The ^1H NMR spectrum of **34** places the multiplet downfield peaks for the aromatic hydrogen atoms at δ 7.16, whilst the γ–C*H* singlet is shifted to δ 5.37. The isopropyl hydrogen atoms are placed in the region of δ 3.18, 1.27 and 1.17, whilst the singlet methyl hydrogen atoms are placed at δ 1.73 (Figure 4.13). In addition, the ^1H NMR spectrum shows an upfield peak of δ 0.13 which can be assigned to the boron-methyl group. The ^{13}C NMR spectrum places the downfield aromatic carbon atoms between δ 161.31 and 93.47, whilst the upfield methyl carbon atoms are found between δ 28.33 and 20.67 (Figure 4.14). The methylation of the boron atom is also confirmed by a signal at δ 0.94; there is no evidence of a methyl migration or nucleophilic attack of the α–carbon of the ring expected at δ 55.0, as reported for the fluoro analogue.[25] The ^{11}B NMR spectrum of **34** is also consistent with a characteristic tetrahedral boron centre, where a broad peak is placed at δ 21.47 (Figure 4.15).

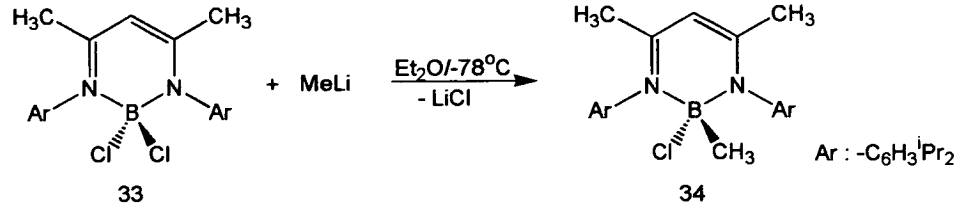

33 34

Figure 4.12 Reactivity of 33 with MeLi.

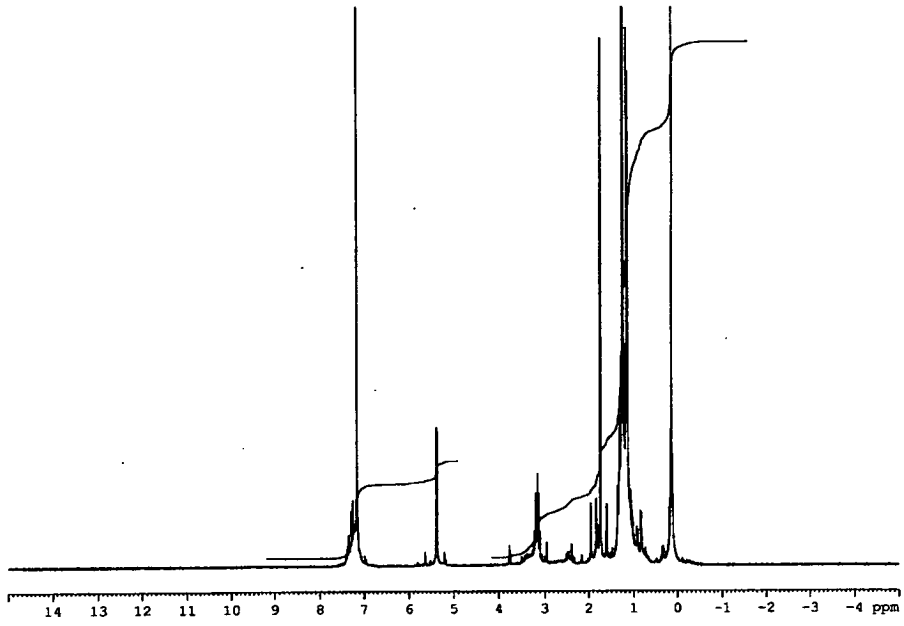

Figure 4.13 ^{1}H NMR spectrum in toluene-d_8 of 34.

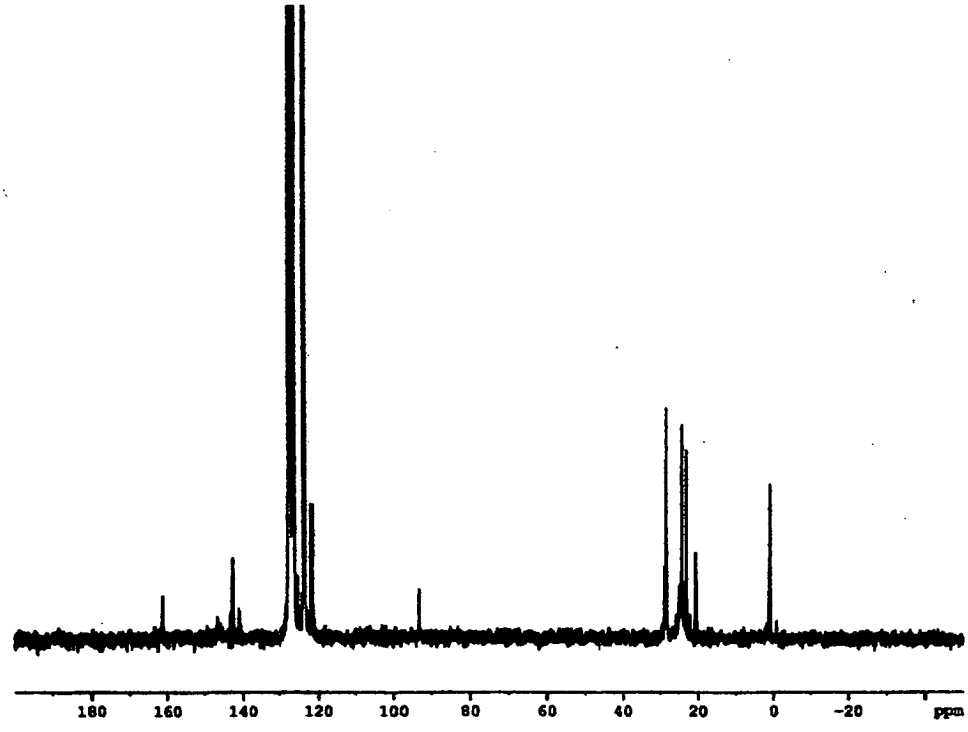

Figure 4.14 ^{13}C NMR spectrum in toluene-d_8 of 34.

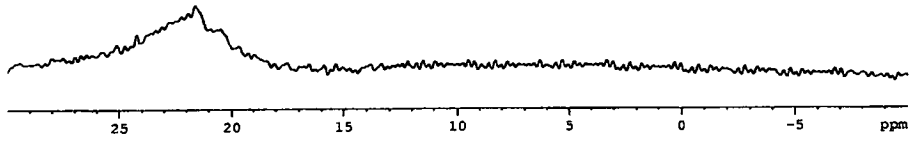

Figure 4.15 ^{11}B NMR spectrum in toluene-d_8 of 34.

Further alkylation of **34** with an equimolar amount of MeLi in toluene at –78 °C was carried out, and the reaction stopped after leaving overnight. The suspension was filtered, and the toluene solution concentrated and stored at –20 °C for two days to provide orange crystals of a radical species $[HC(MeCNAr')_2BCl]^{\bullet}$ **(35)** (Figure 4.16). The reaction between **33** and two equimolar amounts of MeLi at –78 °C gave the same radical. No meaningful NMR data could be obtained for this compound due the paramagnetic nature. The X-ray crystal structure (Figure 4.17) reveals a trigonal planar boron atom centre, where the boron and chlorine atoms are essentially coplanar with the diketiminate moiety (generating approximately C_{2v} molecular symmetry). The angles around the boron atom totalled 360°, whilst the bond angle N-B-N [120.89(14)°] is larger than the corresponding angle in trigonal planar boron structures reported by Smith *et al.*[25] of 118.5(4)° for [{η^2-$(Me)_2C(Ntolyl)CH=C(Ntolyl)Me$}BMe] (**I**) and 116.9(2)° for [{η^2-$CH_2=C(Ntolyl)CH=C(Ntolyl)Me$}$BCH_2SiMe_3$] (**II**), respectively. In addition, the B-N bond lengths [1.422(2) and 1.420(2) Å] are slightly shorter than **I** [1.431(6) and 1.425(6) Å] and **II** [1.438(3) and 1.445(3) Å], respectively. The chlorine to the boron bond length is 1.7763(19) Å. The β-diketiminate N-C and C-C ring distances, have average values of 1.413 and 1.392 Å, respectively, and the distances indicate the delocalization of π–electrons. Selected bond lengths and angles are shown in Table 4.1.

It can be suggested that the activated β-diketiminate ligand offers protection to the boron atom, and presumably since Me in **34** is more sterically demanding than Cl on the boron atom, the ejection of Me is favourable over a nucleophilic attack. Moreover, the ejection of one Cl in **33** has also been achieved by treatment with two equivalent amounts of MeLi (Figure 4.16).

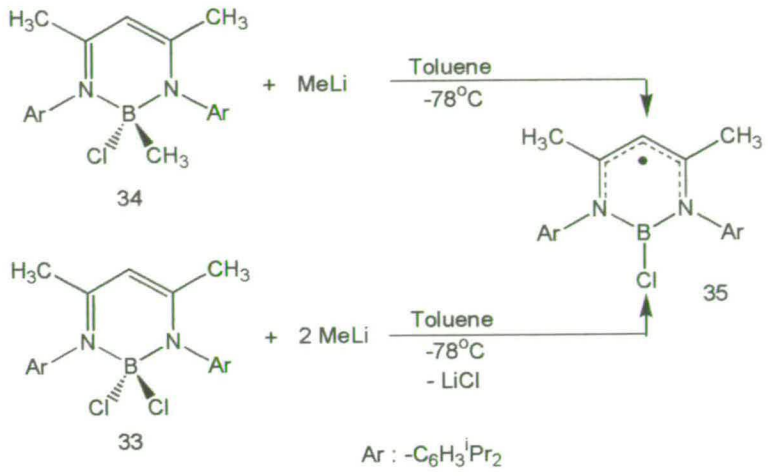

Figure 4.16 Methyl alkylation of β-diketiminate boron complexes.

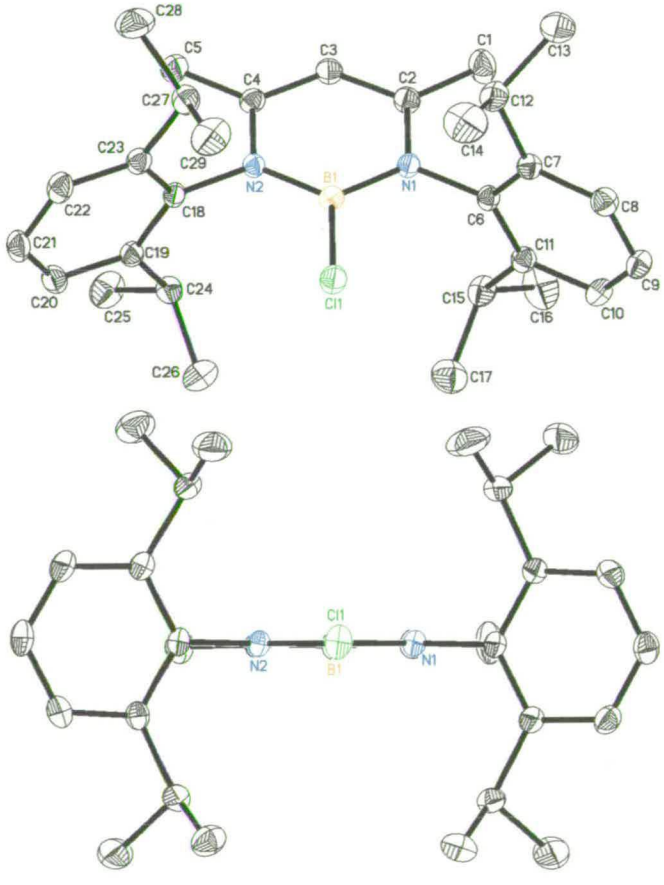

Figure 4.17 Crystallographic structure of 35 with different orientations. Displacement ellipsoids are shown at the 50% probability level. Hydrogen atoms have been omitted for clarity.

Table 4.1 Selected bond distances (Å), angles and torsion (°) for 35.

C(1)-C(2)	1.416(2)	C(2)-C(3)	1.393(2)	C(2)-N(1)	1.412(2)
C(3)-C(4)	1.391(2)	C(4)-N(2)	1.413(2)	C(4)-C(5)	1.431(2)
C(6)-C(11)	1.393(2)	C(6)-C(7)	1.404(2)	C(6)-N(1)	1.4496(18)
C(18)-C(19)	1.400(2)	C(18)-C(23)	1.404(2)	C(18)-N(2)	1.4446(18)
B(1)-N(2)	1.420(2)	B(1)-N(1)	1.422(2)	B(1)-Cl(1)	1.7763(19)
C(3)-C(2)-N(1)		117.83(13)	N(1)-C(2)-C(1)		120.07(14)
C(3)-C(4)-N(2)		117.27(13)	N(2)-C(4)-C(5)		120.32(13)
C(11)-C(6)-N(1)		119.18(13)	C(7)-C(6)-N(1)		119.19(13)
C(19)-C(18)-N(2)		119.14(13)	C(23)-C(18)-N(2)		118.90(13)
N(2)-B(1)-N(1)		120.89(14)	N(2)-B(1)-Cl(1)		119.72(12)
N(1)-B(1)-Cl(1)		119.39(12)	C(2)-N(1)-B(1)		119.20(12)
C(2)-N(1)-C(6)		118.43(12)	B(1)-N(1)-C(6)		122.35(13)
C(4)-N(2)-B(1)		119.79(12)	C(4)-N(2)-C(18)		117.06(12)
B(1)-N(2)-C(18)		123.15(13)	C(4)-C(3)-C(2)		125.01(14)
C(1)-C(2)-N(1)-B(1)		179.23(16)	C(3)-C(2)-N(1)-B(1)		-0.5(2)
Cl(1)-B(1)-N(1)-C(2)		-179.77(12)	N(2)-B(1)-N(1)-C(2)		-0.3(2)
Cl(1)-B(1)-N(1)-C(6)		2.0(2)	N(2)-B(1)-N(1)-C(6)		-178.56(13)
C(5)-C(4)-N(2)-B(1)		179.05(14)	C(3)-C(4)-N(2)-B(1)		-0.6(2)
Cl(1)-B(1)-N(2)-C(4)		-179.66(11)	N(1)-B(1)-N(2)-C(4)		0.9(2)
Cl(1)-B(1)-N(2)-C(18)		0.7(2)	N(1)-B(1)-N(2)-C(18)		-178.71(13)

The redox characteristics of **35** have been studied by cyclic voltammentry in $TBABF_4$/DCM(DMF) *vs.* ferrocene/ferrocenium. The cyclic voltammogram in DCM shows a reversible behaviour for the compound studied, where one-electron reduction wave at −1.21 V corresponds with the formation of the anion $[HC(MeCNAr')_2BCl]^-$ (Figure 4.18). There is no evidence, however, of oxidation of the **35**, which suggests that a high oxidation potential is needed to reach the unfavourable cation $[HC(MeCNAr')_2BCl]^+$. This is a surprising observation since $[HC(MeCNAr')_2BCl]^+$ is a 6π-aromatic system which may be considered to be a benzene-borazine hybrid. This therefore provides the first evidence for a boron(I) compound of the type $[HC(MeCNAr')_2B]$ since the aluminium and gallium analogues were reported.[22,23] In DMF however, the reduction is irreversible and an oxidation process is evident at +0.70 V (Figure 4.19) and is attributed to the electroactivity of the dimethylformamide, according to Figure 4.20.

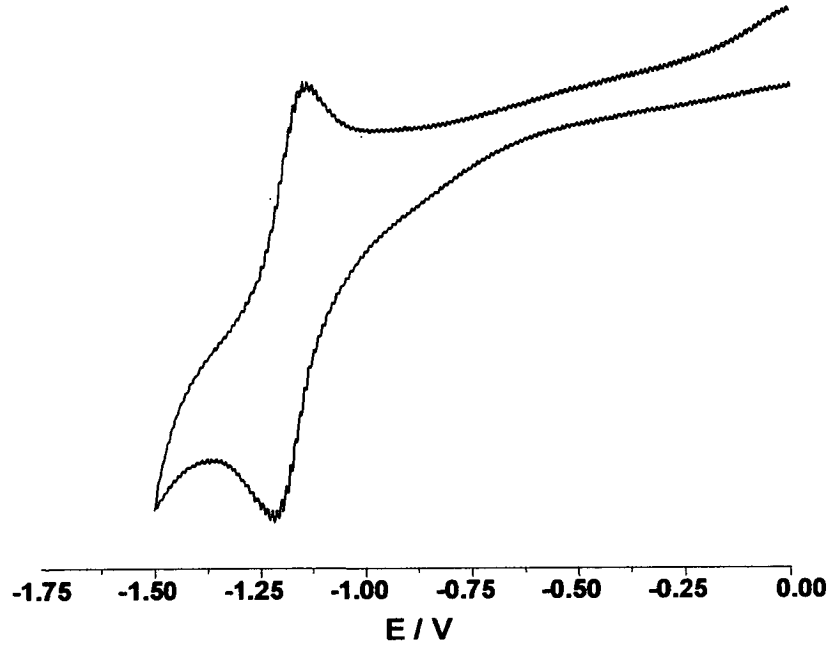

Figure 4.18 Reversible reduction cyclic voltammogram of 35 in DCM.

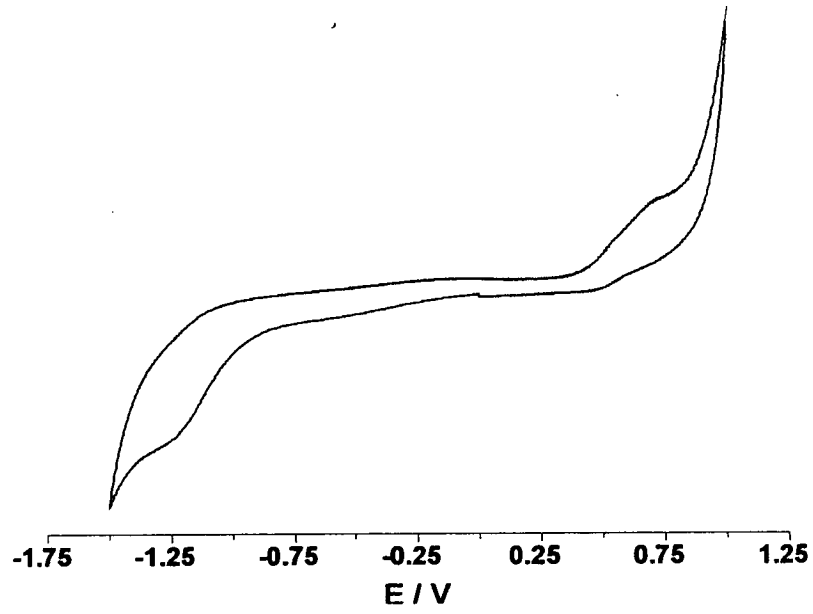

Figure 4.19 Redox cyclic voltammogram of 35 in DMF.

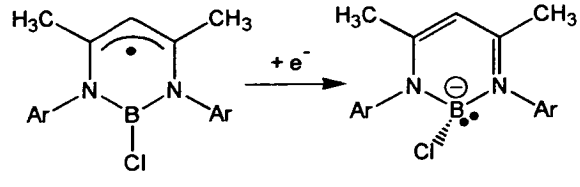

Figure 4.20 Possible reaction of 35 to produce the borane carbene analogue.

The EPR spectrum for **35** in toluene at room temperature suggests a hyperconjugative interaction of the boron-chloride with the π–systems of the β–diketiminate unit. The anisotropy of the *g*-factor is not strongly developed, which would be expected for a predominantly organic radical.[27] The EPR spectrum provides a *g*-value of 2.013 with a peak width of 16.2 G (Figure 4.21). A simulated EPR for **35** was satisfactorily obtained, revealing the coupling to both the methyne hydrogen on C3 [A_H= 32.99 G; ΔH_{pp}: 8G] and the boron isotopes [$A_{B(11)}$= 78.60 G; $A_{B(10)}$= 46.00 G], but no coupling to nitrogen was detected.

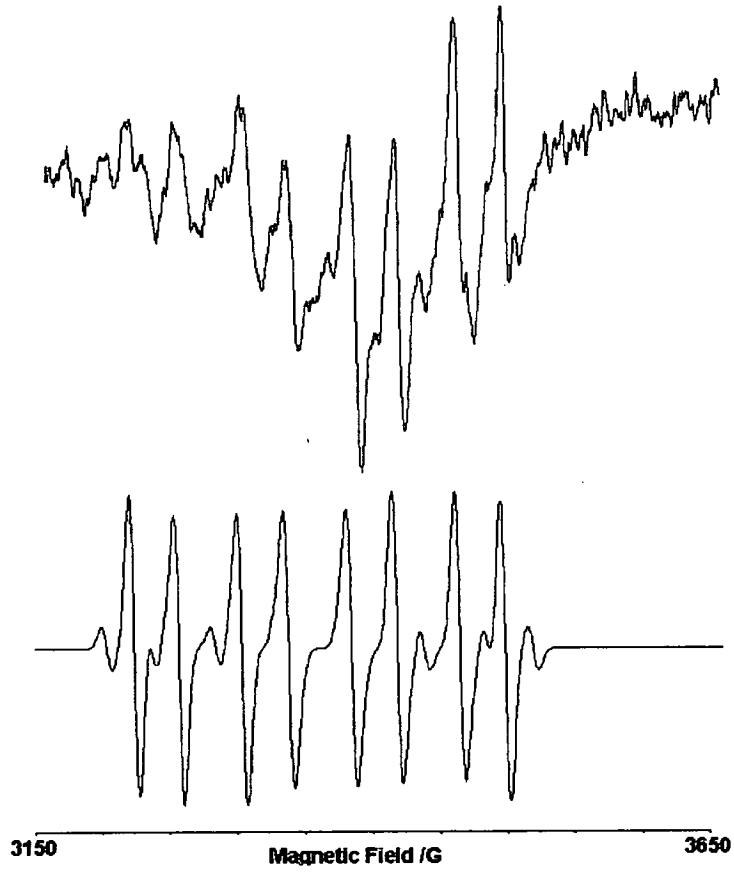

Figure 4.21 (Top) Experimetal EPR spectrum of 35. (Bottom) Computer simulation.

Further insight into the bonding in **35** is provided by the orbital energies and the spin density surface, which were obtained by DFT calculations using a C_{2v} symmetry. The SOMO of the radical **35** complex is mainly constructed from antibonding $2p_z$ orbitals of the C2, C4, N1 and N2, with smaller contributions from the nitrogen p_z orbitals (Figure 4.22). The result is inconsistent with the composition of this SOMO as shown by the EPR spectrum of **35**, which indicates that the unpaired electron density is located on boron and C3. HOMO-1 and HOMO-2 which are π-bonding, indicate that in the presence of bulky diisopropylphenyl rings the odd electron should be equally delocalized on both phenyl groups. The orbital most strongly associated with the B-N bonding is the HOMO-5 (which is π-bonding with respect to B-N and C2-C3-C4 and antibonding with respect to N-C), whilst there are no orbital contributions from the aromatic diisopropylphenyl groups. The HOMO-3 level, however, shows B-N σ-bonding amongst other σ-antibonding components, but there is a high π-bonding orbital contribution from the bulky diisopropylphenyl groups (which is π-bonding with respect to C23-C18-C19 and antibonding with respect to C22-C21-C20). In addition, a similar π-bonding orbital contribution from the phenyl rings is appreciated in HOMO-4, but less π B-N bonding contribution is observed (which is π-bonding with respect to B-N and C2-C3-C4 and antibonding with respect to N-C). The LUMO is associated with B and C3 $2p$ orbitals with smaller contributions of N and C p_z orbitals. The five doubly MOs (HOMO-1, HOMO-2, HOMO-3, HOMO-4 and HOMO-5) are all close in energy, whereas the SOMO and LUMO are considerably higher. The small SOMO-LUMO energy separation of 271.79 kJ/mol indicates a closed shell with high reactivity, where transposition of these two orbitals are possible.

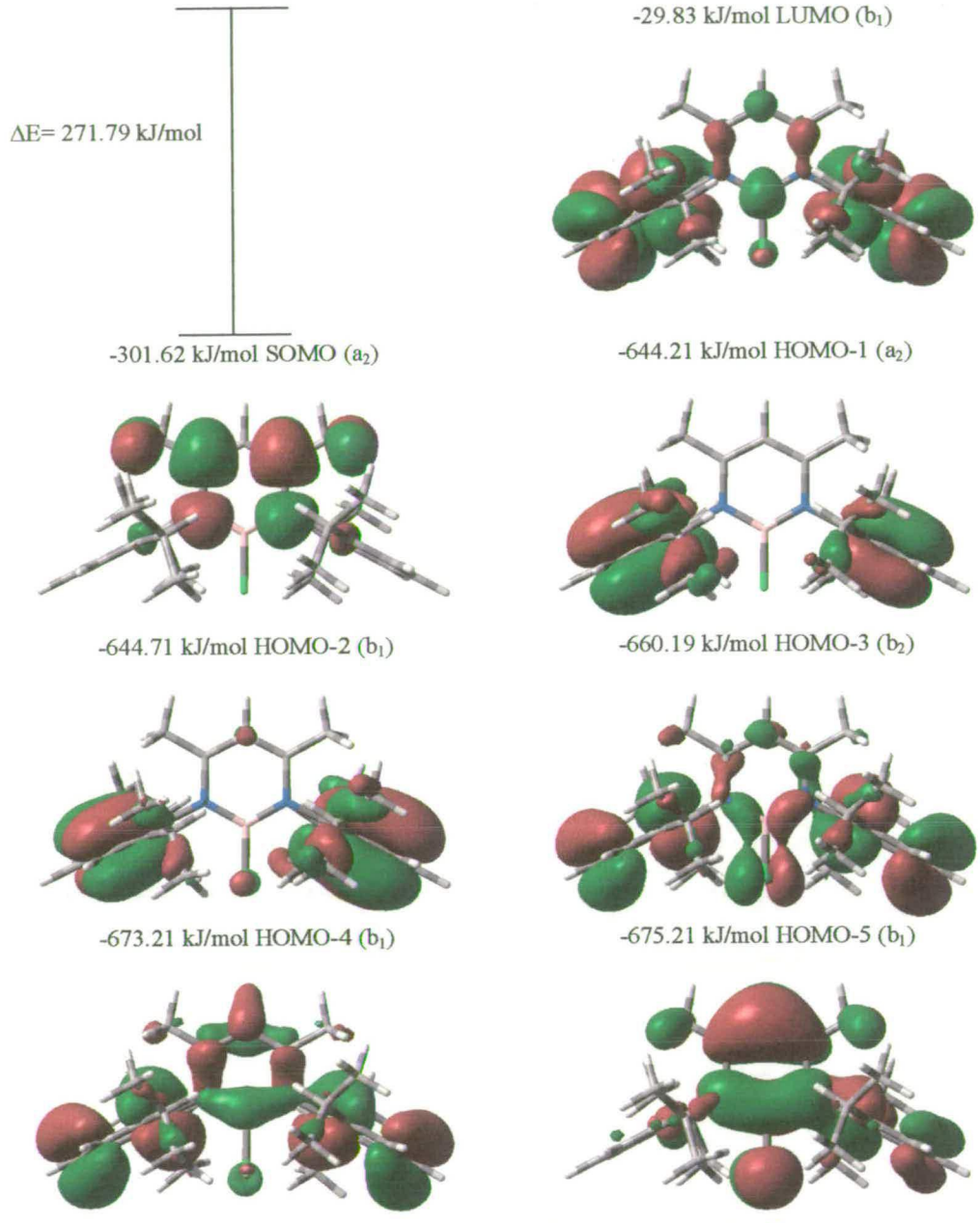

Figure 4.22 DFT calculated molecular orbitals for 35.

The spin density provided the shading for the isodensity surface, where the dark areas indicate positive (excess α) spin density and the light areas negative (excess β) spin density. DFT spin density study for **35** shows a positive concentration around the two backbone carbons (C2 and C4), and away from the central carbon (C3), according to Figure 4.23.

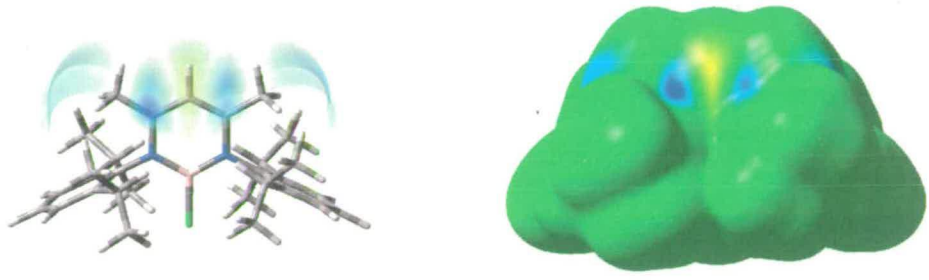

Figure 4.23 DFT calculated spin density for 35.

Table 4.2 Selected DFT spin densities calculated for 35.

Atom	C2	C3	C4	N1	N2	B1
pα	+0.691453	-0.490144	+0.661541	+0.106113	+0.096380	-0.027126

4.2.3 Potassium Reduction of [HC(MeCNAr')$_2$BCl]$^{\bullet}$

A potassium mirror was prepared and treated with an equimolar solution of **35** in toluene at room temperature (Figure 4.24). The solution was filtered, and the solvent removed under *vacuum*. Extraction with pentane, concentration of the solution and storage at –20 °C overnight provided [{HC(MeCNAr')$_2$BOK}$_2$] (**36**) as orange crystals. Although the inert atmosphere conditions (dried solvent, nitrogen atmosphere and glove-box technique) were used, the potassium reduction did not produce the desired borene compound.

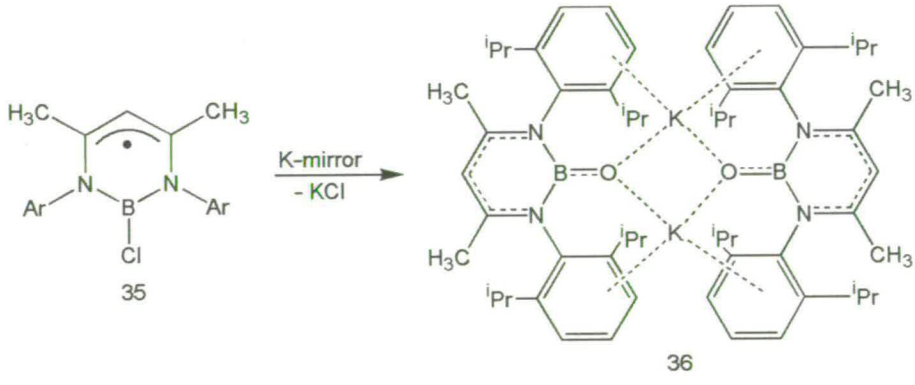

Figure 4.24 K-mirror reduction of 35.

The ^{1}H NMR spectrum for the compound **36** obtained, includes multiplet downfield peaks for the aromatic hydrogen atoms at δ 6.95, whilst the γ-C*H* singlet is shifted to δ 5.23 (Figure 4.25). The isopropyl hydrogen atoms are placed in the region of δ 3.23, 1.32 and 1.12, whilst the singlet methyl hydrogen atoms are located at δ 1.69. The ^{13}C NMR spectrum gives the downfield aromatic signals between δ 162.3 and 100.10, whilst the upfield resonances of methyl carbon atoms are found between δ 28.70 and 22.73 (Figure 4.26). The ^{11}B NMR spectrum of **36** shows two signals at δ 25.38 and 5.32 (Figure 4.27), where the upfield peak could have been produced by the incorporation of the boron atom in an aromatic ring system.[26]

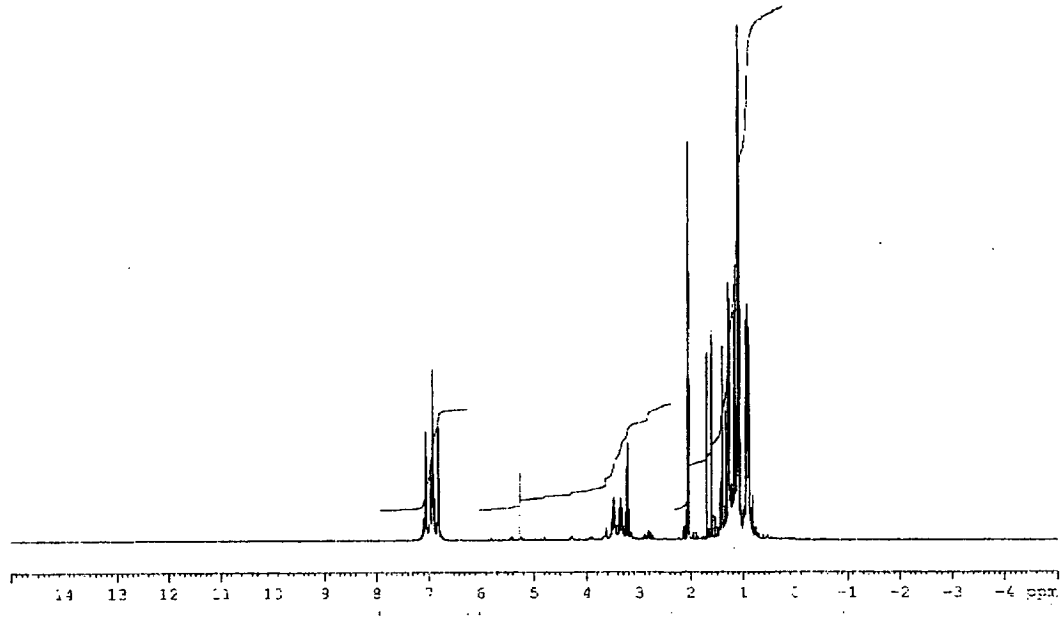

Figure 4.25 ^{1}H NMR spectrum in toluene-d_8 of 36.

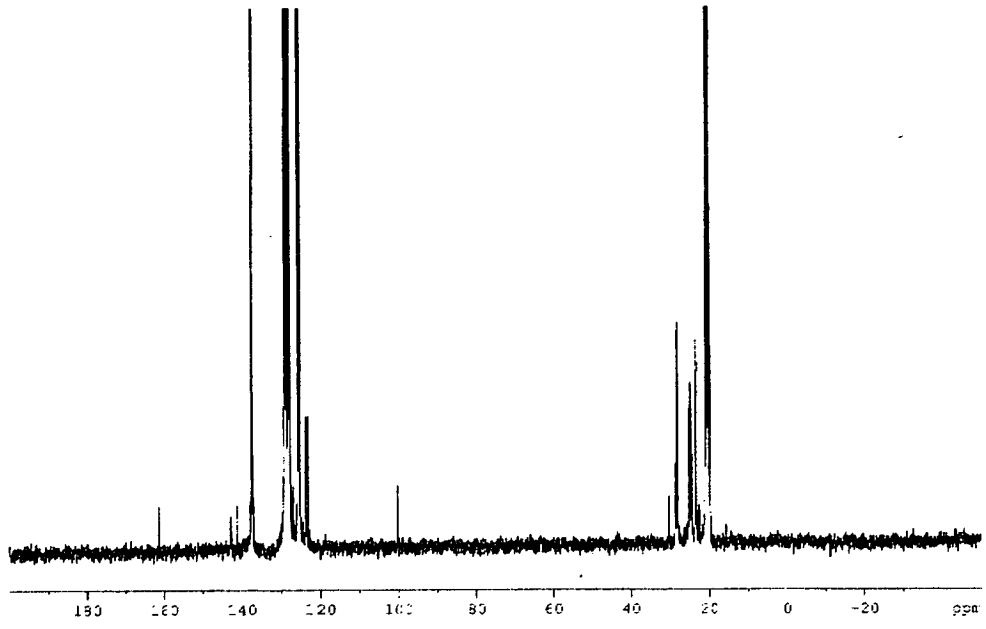

Figure 4.26 ^{13}C NMR spectrum in toluene-d_8 of 36.

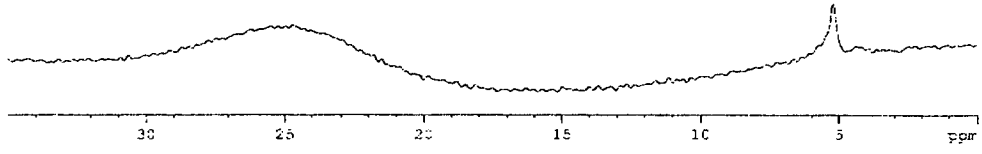

Figure 4.27 ^{11}B NMR spectrum in toluene-d_8 of 36.

The X-ray structure reveals a centrosymmetric dimer (Figure 4.28), where the trigonal planar boron atom centres are also coplanar with the β-diketiminate moieties. There is a centre of symmetry in the middle of the K_2O_2 core. The B-N bond lengths are 1.481(3) and 1.469(3)Å (longer than for the radical species), whilst the oxygen B-O bond lengths are 1.303(3) Å. The angles around each boron atom totalled 360°. There is significant electron π-delocalization in the ligand where the C-N and C-C distances in the ring have average values of 1.400 and 1.385 Å. The bond angle of N-B-N [113.1 (2) Å] is smaller than that of the corresponding radical **35**, whilst the bond angle is relatively wider than in the structures reported by Smith *et al.*[25] (**I** and **II**). In addition, the K-O distances are 2.5315(18) and 2.56261(19) Å, and

the η^6-interactions from the aromatic phenyl rings (the centre of ring) to K atom are 2.997 and 3.042 Å. Selected bond lengths and angles are shown in Table 4.3.

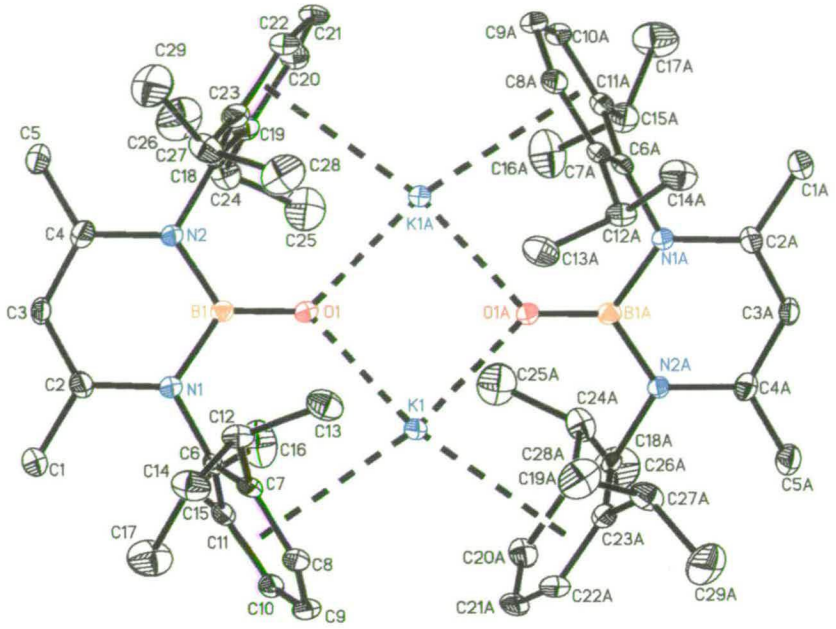

Figure 4.28 Crystallographic structure of 36. Displacement ellipsoids are shown at the 50% probability level. Hydrogen atoms have been omitted for clarity.

Table 4.3 Selected bond distances (Å), angles and torsion (°) for 36. Symmetry transformations used to generate equivalent atoms: $^{\#1}$ -x+1,y,-z+3/2.

K(1)-O(1)$^{\#1}$	2.5615(18)	K(1)-O(1)	2.5626(19)	K(1)-C(7)	3.211(2)
K(1)-C(18)$^{\#1}$	3.212(2)	K(1)-C(6)	3.220(2)	K(1)-C(19)$^{\#1}$	3.245(3)
K(1)-C(23)$^{\#1}$	3.303(3)	K(1)-C(8)	3.304(3)	K(1)-C(20)$^{\#1}$	3.315(3)
K(1)-C(11)	3.353(3)	K(1)-C(22)$^{\#1}$	3.371(3)	K(1)-C(21)$^{\#1}$	3.377(3)
O(1)-B(1)	1.303(3)	O(1)-K(1)$^{\#1}$	2.5615(18)	N(1)-C(2)	1.402(3)
N(1)-C(6)	1.429(3)	N(1)-B(1)	1.481(3)	N(2)-C(4)	1.399(3)
N(2)-C(18)	1.432(3)	N(2)-B(1)	1.469(3)	C(18)-K(1)$^{\#1}$	3.212(2)
C(19)-K(1)$^{\#1}$	3.245(3)	C(20)-K(1)$^{\#1}$	3.315(3)	C(21)-K(1)$^{\#1}$	3.377(3)
C(22)-K(1)$^{\#1}$	3.371(3)	C(23)-K(1)$^{\#1}$	3.303(3)		
O(1)$^{\#1}$-K(1)-O(1)		84.91(6)	B(1)-O(1)-K(1)$^{\#1}$		132.63(17)
B(1)-O(1)-K(1)		131.94(17)	K(1)$^{\#1}$-O(1)-K(1)		95.09(6)
C(2)-N(1)-B(1)		122.1(2)	C(6)-N(1)-B(1)		117.94(19)
C(4)-N(2)-B(1)		124.3(2)	C(18)-N(2)-B(1)		116.72(19)
O(1)-B(1)-N(2)		124.0(2)	O(1)-B(1)-N(1)		123.0(2)
N(2)-B(1)-N(1)		113.1(2)	O(1)$^{\#1}$-K(1)-O(1)-B(1)		173.2(2)
O(1)$^{\#1}$-K(1)-O(1)-K(1)$^{\#1}$		-0.52(9)	C(4)-N(2)-B(1)-O(1)		177.3(2)
C(4)-N(2)-B(1)-N(1)		-3.5(3)	C(18)-N(2)-B(1)-N(1)		178.8(2)
C(2)-N(1)-B(1)-O(1)		179.6(2)	C(6)-N(1)-B(1)-O(1)		0.9(4)
C(2)-N(1)-B(1)-N(2)		0.4(3)	C(6)-N(1)-B(1)-N(2)		-178.3(2)
B(1)-N(1)-C(2)-C(3)		2.9(4)	B(1)-N(1)-C(2)-C(1)		-174.6(2)
B(1)-N(2)-C(4)-C(3)		3.1(4)	B(1)-N(2)-C(4)-C(5)		-178.9(3)
B(1)-N(1)-C(6)-C(7)		76.0(3)	B(1)-N(1)-C(6)-C(11)		-100.4(3)

The redox properties of **36** were studied in $TBAPF_6$/DCM by differential pulse, and cyclic voltammetry (Figures 4.29 and 4.30). The differential pulse voltammogram at 289 K exhibits two single electron reduction waves at –0.870 and –1.670 V, and are attributed to the formation of radical anion and dianion. The reduction –1.670 V results in an unstable product and disappeared after a few cycles. The cyclic voltammogram of **36** at different temperatures (243 and 289 K) exhibits an irreversible reduction at –1.16 V.

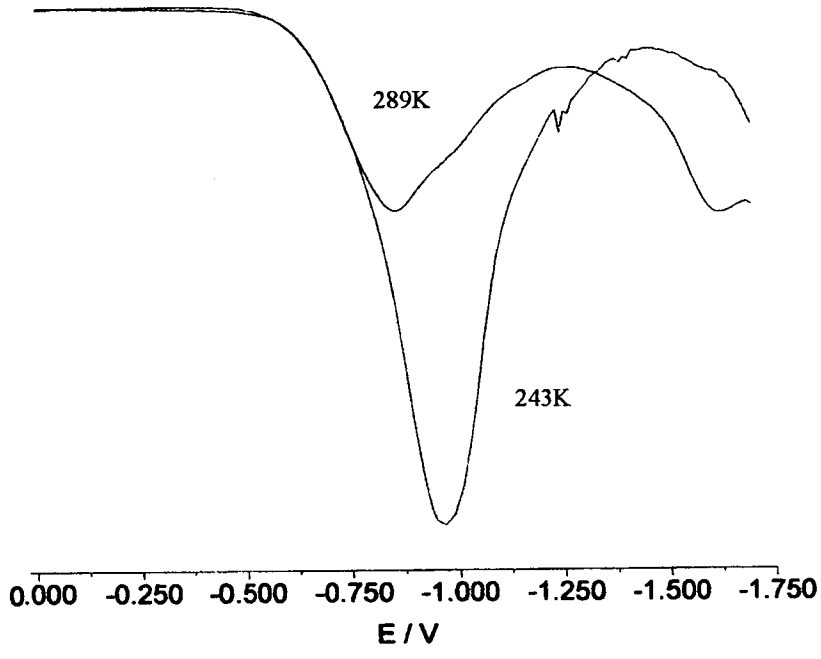

Figure 4.29 Differential pulse of voltammograms for reduction of 36.

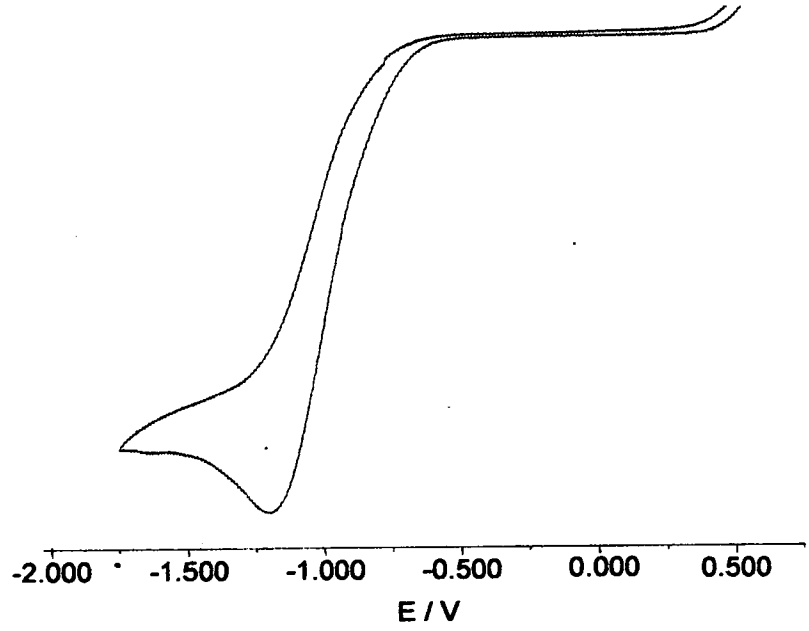

Figure 4.30 Cyclic voltammogram of 36.

4.2.4 Reactivity of Lithium β-Diketiminate with Me_2BBr

Treatment of **32** with an equimolar amount of Me_2BBr (**20**) in toluene at –78 °C was carried out. After standing at room temperature the solution was filtered off, concentrated, and stored at –20 °C to provide yellow co-crystals of [HC(MeCNAr')$_2$BO] (**37**) and [Li(BMe$_4$)] (**38**), according to Figure 4.31. NMR spectra of the mixed product show both methyl groups bonded to the boron atom centres, nevertheless diffraction of the crystals gave structures of **37** and **38** complexes. Perhaps the product [HC(MeCNAr')$_2$BMe$_2$] was obtained and it reacted further by means of the H_2O molecule thus providing the unexpected crystallised products. In addition, decomposition of **20** may include reaction with Li present to give MeLi, while **38** can be obtained by a further reaction between MeLi and **20**.

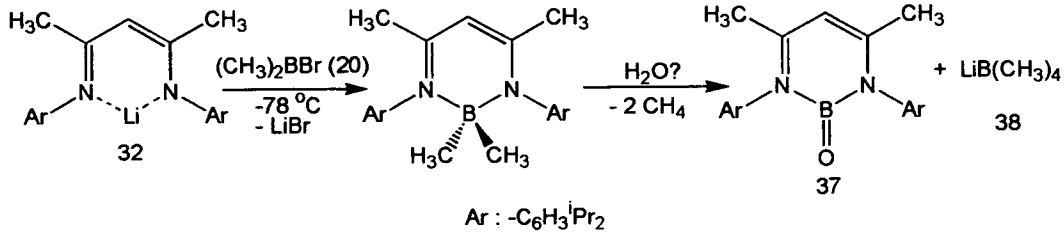

Figure 4.31 Reactivity of 32 with 20.

The ^{1}H NMR spectrum of the mixture products **37** and **38** gives downfield multiplet peaks for the aromatic hydrogen atoms at δ 7.15, whilst the γ-C*H* singlet is shifted to δ 5.05 (Figure 4.32). The isopropyl hydrogen atoms are located in the region of δ 3.32, 1.39 and 1.18, whilst the singlet resonance of the methyl hydrogen atoms is placed at δ 2.14. The presence of methyl atoms bonded to boron is confirmed by a singlet for the hydrogen atoms at δ 0.32. The ^{13}C NMR spectrum gives the downfield aromatic atom signals between δ 163.28 and 93.02, whilst the upfield methyl carbon atoms are found between δ 28.31 and 20.64 (Figure 4.33). The B-CH_3 group is confirmed by an upfield peak at δ 0.92. The ^{11}B NMR spectrum, however, gives two peaks at δ 31.0 and –1.92, which are consistent with tetrahedral boron centres (**38**). In addition, a third signal at δ 16.90 in the ^{11}B NMR spectrum supports a three co-ordinate boron centre (**37**).

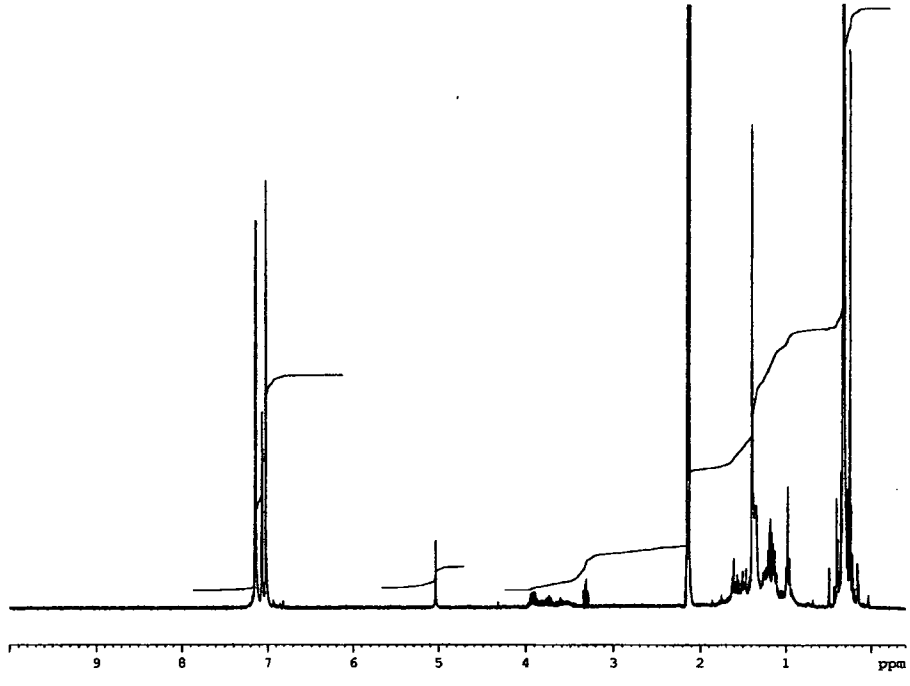

Figure 4.32 ^{1}H NMR spectrum in toluene-d_8 of 37 and 38.

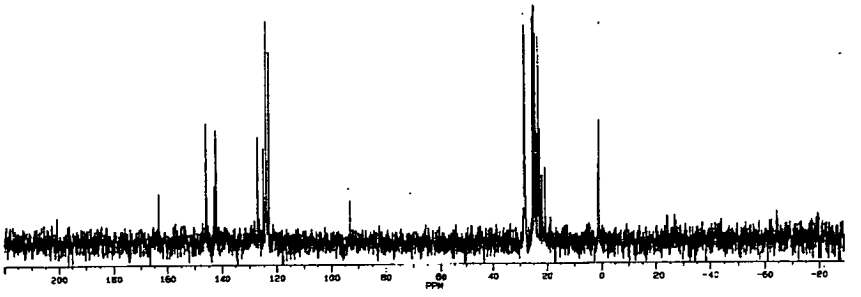

Figure 4.33 ^{13}C NMR spectrum in toluene-d_8 of 37 and 38.

The X-ray structure reveals the co-crystallisation of **37** and **38** (Figure 4.34). The boron and oxygen atoms are essentially coplanar with the β-diketiminate moiety, the angles around the boron atom totalling 360°. The B-N bond lengths are 1.488(3) Å, which is longer than bond lengths previously obtained for the trigonal planar structures **35** and **36**. The B-O bond length is 1.2721(4) Å, which is shorter than the 1.303(3) Å for **36**. The bond lengths of N-C and C-C in the ring [1.347 and 1.373(4) Å] show a significant electron π-delocalization in the ligand, and those bond distances are also shorter than corresponding bonds in **35** and **36** respectively. The structure **38** presents a tetrahedral boron atom centre with slightly longer B-C bond lengths [1.655(5) Å] than the same structure reported by Brown *et al.*[29a] [1.635 (5) Å]. Hydrogen bonds [Li···(H-C)] are observed in **38** with contacts [range 1.745(12) to 2.268(5) Å] slightly shorter than those reported by Peterson *et al.*[29b] for the same structure [range 2.204(15) to 2.274(25) Å]. Selected bond lengths and angles are shown in Table 4.4.

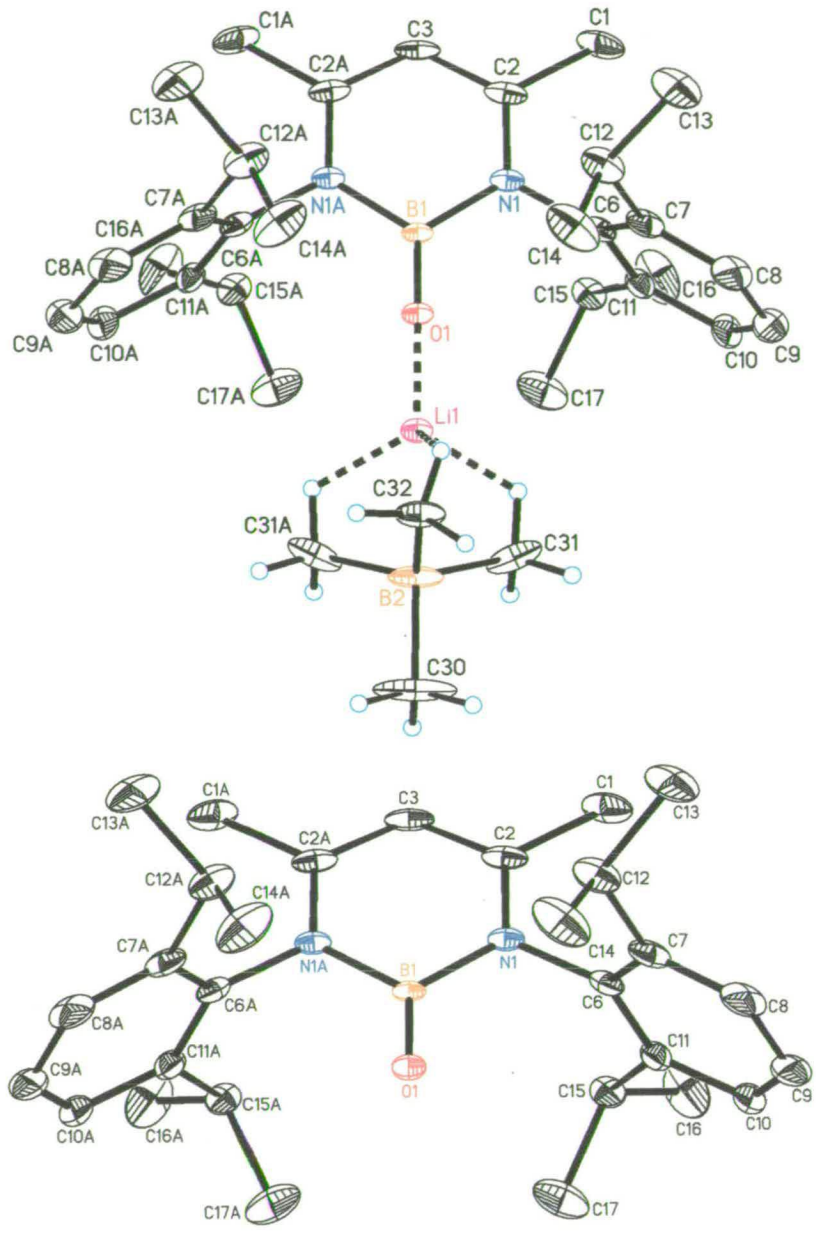

Figure 4.34 Crystallographic structure of 37 and 38. Displacement ellipsoids are shown at the 50% probability level. Hydrogen atoms have been omitted for clarity.

Table 4.4 Selected bond distances (Å), angles and torsion (°) for 37 and 38. Symmetry transformations used to generate equivalent atoms: #1 x,-y+1/2,z

C(1)-C(2)	1.489(5)	C(2)-N(1)	1.347(3)	C(2)-C(3)	1.373(4)
C(3)-C(2)#1	1.373(4)	C(6)-C(11)	1.393(4)	C(6)-C(7)	1.399(4)
C(6)-N(1)	1.449(4)	C(30)-B(2)	1.643(7)	C(31)-B(2)	1.655(5)
C(31)-Li(1)	2.268(7)	C(32)-B(2)	1.662(7)	C(32)-Li(1)	2.256(7)
N(1)-B(1)	1.488(3)	B(1)-O(1)	1.272(4)	B(1)-N(1)#1	1.488(3)
B(2)-C(31)#1	1.655(5)	B(2)-Li(1)	2.127(8)	O(1)-Li(1)	1.716(7)

Li(1)-C(31)$^{\#1}$	2.268(7)		
N(1)-C(2)-C(3)	119.1(3)	N(1)-C(2)-C(1)	119.7(4)
C(3)-C(2)-C(1)	121.2(3)	C(2)-C(3)-C(2)$^{\#1}$	123.3(3)
C(11)-C(6)-N(1)	119.4(3)	C(7)-C(6)-N(1)	119.1(3)
B(2)-C(31)-Li(1)	63.4(2)	B(2)-C(32)-Li(1)	63.7(3)
C(2)-N(1)-C(6)	120.4(2)	C(2)-N(1)-B(1)	123.7(3)
C(6)-N(1)-B(1)	115.8(2)	O(1)-B(1)-N(1)$^{\#1}$	124.51(14)
O(1)-B(1)-N(1)	124.51(14)	N(1)$^{\#1}$-B(1)-N(1)	111.0(3)
C(30)-B(2)-C(31)	107.5(3)	C(30)-B(2)-C(31)$^{\#1}$	107.5(3)
C(31)-B(2)-C(31)$^{\#1}$	111.5(4)	C(30)-B(2)-C(32)	108.2(4)
C(31)-B(2)-C(32)	111.0(3)	C(31)$^{\#1}$-B(2)-C(32)	111.0(3)
C(30)-B(2)-Li(1)	180.0(4)	C(31)-B(2)-Li(1)	72.5(2)
C(31)$^{\#1}$-B(2)-Li(1)	72.5(2)	C(32)-B(2)-Li(1)	71.9(3)
B(1)-O(1)-Li(1)	170.5(4)	O(1)-Li(1)-B(2)	177.5(5)
O(1)-Li(1)-C(32)	138.0(4)	B(2)-Li(1)-C(32)	44.5(2)
O(1)-Li(1)-C(31)	134.6(2)	B(2)-Li(1)-C(31)	44.09(18)
C(32)-Li(1)-C(31)	74.4(2)	O(1)-Li(1)-C(31)$^{\#1}$	134.6(2)
B(2)-Li(1)-C(31)$^{\#1}$	44.09(18)	C(32)-Li(1)-C(31)$^{\#1}$	74.4(2)
C(31)-Li(1)-C(31)$^{\#1}$	74.2(4)	C(3)-C(2)-N(1)-B(1)	-1.1(4)
C(1)-C(2)-N(1)-B(1)	177.1(3)	C(11)-C(6)-N(1)-B(1)	92.8(3)
C(7)-C(6)-N(1)-B(1)	-85.0(3)	C(2)-N(1)-B(1)-O(1)	-178.8(3)
C(6)-N(1)-B(1)-O(1)	2.5(5)	C(2)-N(1)-B(1)-N(1)$^{\#1}$	1.7(4)
C(6)-N(1)-B(1)-N(1)$^{\#1}$	-177.03(18)	N(1)$^{\#1}$-B(1)-O(1)-Li(1)	89.7(3)
N(1)-B(1)-O(1)-Li(1)	-89.7(3)	B(1)-O(1)-Li(1)-B(2)	0.00(6)

Further insight into the bonding of **37** is provided by the calculation of the orbital energies (Figure 4.35) using DFT and a C_{2v} symmetry. The HOMO of the **37** is mainly constructed from the lone pair from the oxygen atom, with a small contribution from the σ-antibonding interaction from the ring. The HOMO-1 represents a large π-contribution from the B-O bonding and antibonding with respect to B-N. The HOMO-2, HOMO-3 and HOMO-4 show a large π-bonding contribution from the bulky diisopropylphenyl rings, but no contribution from the NCCCNB ring is observed in HOMO-2 and HOMO-3. The LUMO of **37** is mainly constructed from $2p_z$ orbitals of the C2, C4, N1 and N2, but with little contribution from the nitrogen p_z orbitals. The five occupied MOs (HOMO, HOMO-1, HOMO-2, HOMO-3 and HOMO-4) are also close in energy, whilst the small energy gap between HOMO-LUMO (302.46 kJ/mol) indicates a closed shell with high reactivity.

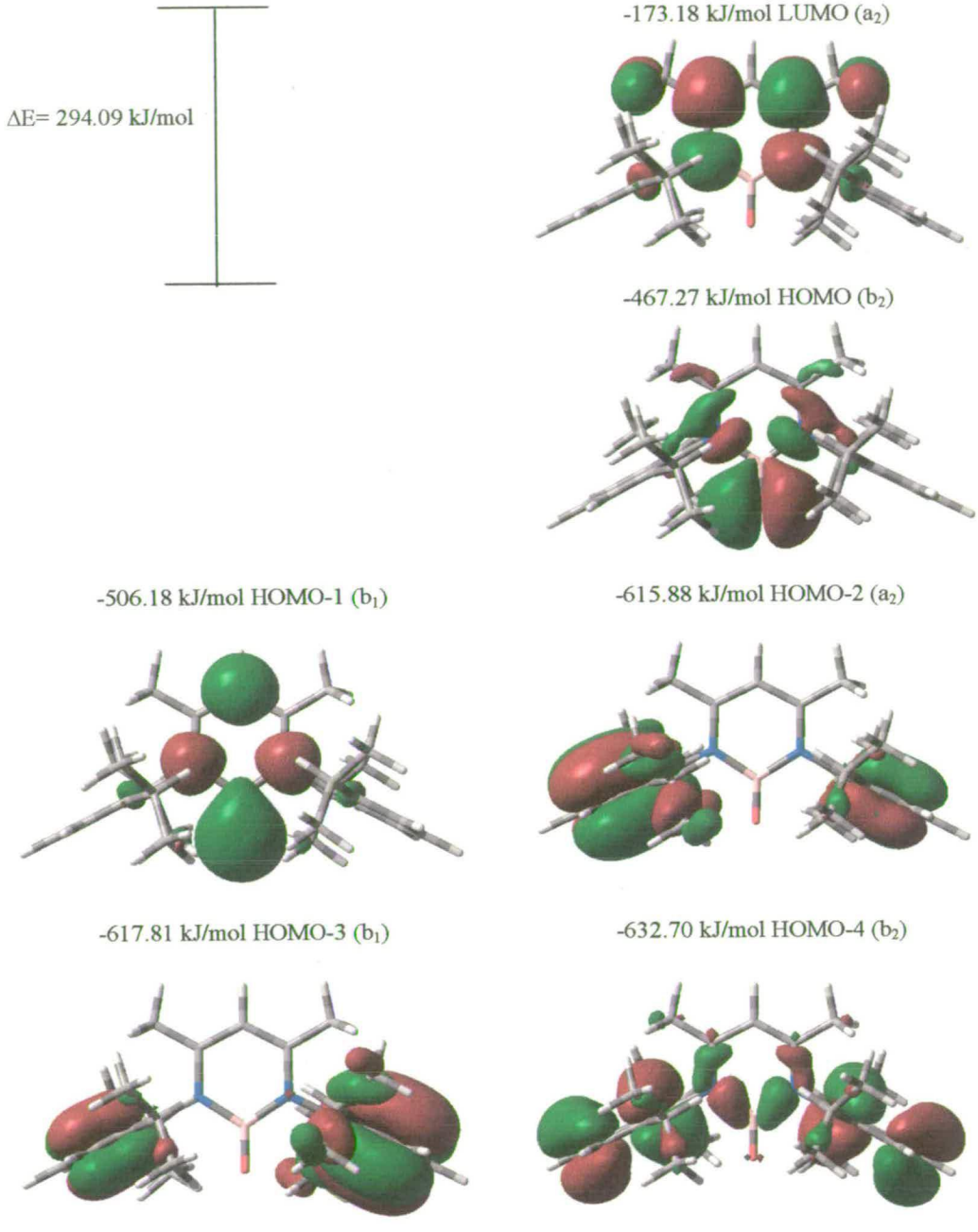

Figure 4.35 DFT calculated molecular orbitals for 37.

4.3 Conclusions

It is apparent that the steric properties of the aryl substituents play a key role in determining the structure, as well as the magnetic and spectral characteristics of the interesting boron compounds. Organolithium reagents need close interaction with a metal in order to produce alkylation (Figure 4.36), and due to the presence of bulky R groups such as 2,6-diisopropylphenyl, the possibility of interactions between boron and MeLi (for example) are low. Methyl substitution of the first chloride in $[CH(MeCNAr')_2BCl_2]$ (**33**) occurs, but the hindrance to substitution of the second chloride atom complex in $[HC(MeCNAr')_2B(Me)Cl]$ (**34**) makes such a process unfavourable. Moreover, chlorine atom ejection is also induced by MeLi treatment of **33** (2:1 molar ratio) to give $[CH(MeCNAr')_2BCl]^{\bullet}$ (**35**). The apparent ejection of chlorine or the methyl radical, induced by MeLi treatment of **33** (2:1 molar ratio) or **34** (1:1 molar ratio) are an unprecedented process and difficult to explain.

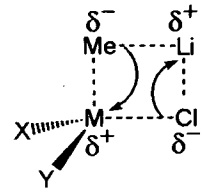

Figure 4.36 Trans-metallation requirement.

DFT orbital calculations have shown the high reactivity of the boron complexes obtained, where small energy gaps of SOMO-LUMO or HOMO-LUMO are present. The high π-bonding orbital contribution from the bulky 2,6-diisopropylphenyl groups can be deduced from all the calculations made, where the chelating β-diketiminate ligands present a high charge delocalization around the system thus stabilizing a particular metal (Figure 4.37). It has been proved that a simple modification of β-diketiminate ligands at a position away from the immediate site of co-ordination results in dramatic changes to the geometry around the metal atom.[21-23] Quantum calculations for **35** give a SOMO disagrees with the experimental EPR spectrum, which is more consistent with the occupation of the calculated LUMO by the unpaired electron. The small energy gap between SOMO

and LUMO indicates, however, that the two MOs are close in energy. The similar energy of the SOMO and LUMO and their high reactivity induce a nucleophilic character of the boron complex, and this effect is verified by the one-electron reduction wave obtained (CV experiment) producing the anion $[HC(MeCNAr')_2BCl]^-$. In addition, the spin density DFT study gave information about the concentration of electrons over C2 and C4, which support the hypothesis that a single electron is delocalized over the organic ligand.

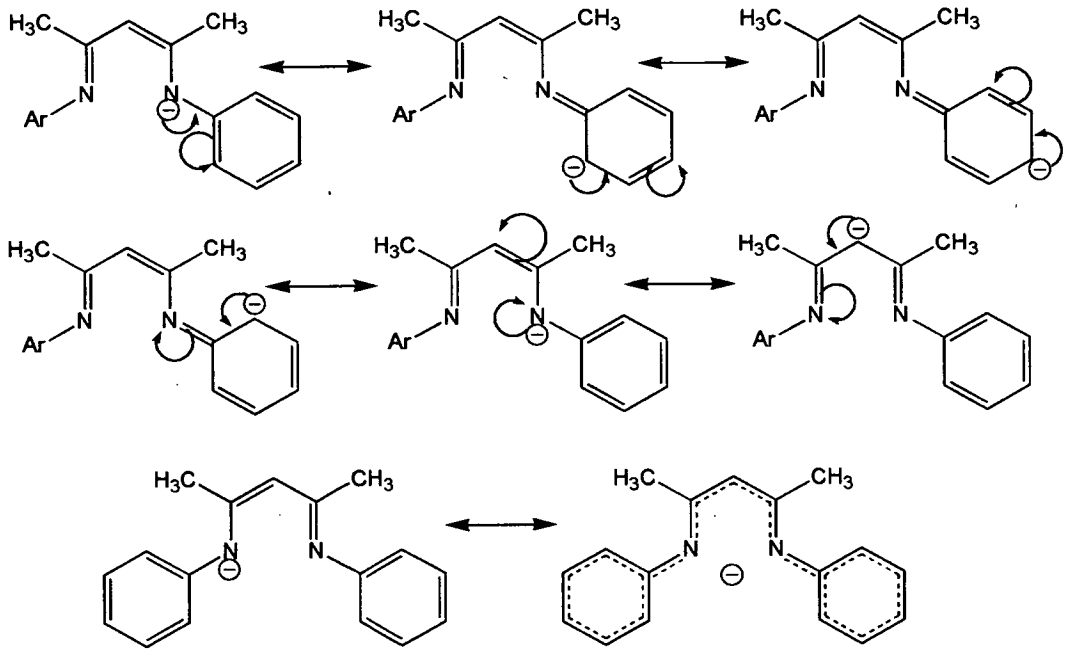

Figure 4.37 Delocalization of charge around the β-diketiminate.

Structural analysis could provide further explanation of the overprotected boron atom centre, due to the presence of a bulky group on the nitrogen atoms (2,6-diisopropylphenyl). Using the molecular modelling program MOPAC,[28] it is possible to compare the structure of **33** with similar reported $[HC(MeCNAr)_2BF_2]$ (Ar= *p*-tolyl),[25] and find a reasonable solution to the radical formation. Basically, the utilization of the *p*-tolyl group on the nitrogen atoms (Figure 4.38) has the advantage of inducing a more open structure producing a first alkylation with an organolithium reagent. A second alkylation may occur in the same way, because the ligand itself

has the ability to become twisted and there is a high probability of nucleophilic attack on the Cα.

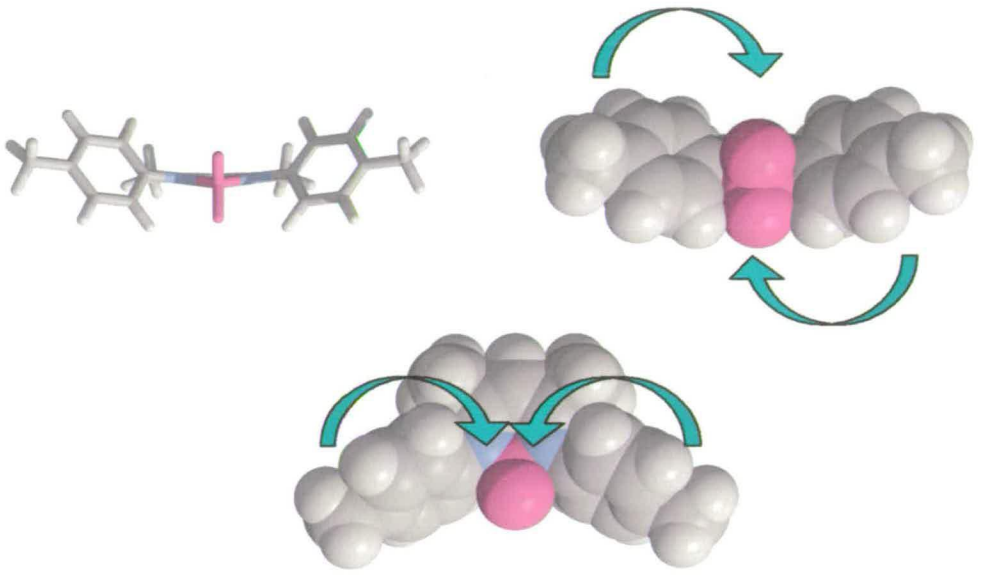

Figure 4.38 Possibility of alkylation on the structure reported for $[HC(MeCNAr)_2BF_2]$; (Ar=.*p*-tolyl).[25] The green arrow represents possible attacks of MeLi.

The simulation of **33** shows a distorted six membered ring, where the arrangement for alkylation is not very favourable (Figure 4.39). The addition of a second chlorine atom and rehybridisation of the boron to sp^3 results in considerable distortion of the molecule. The bulky groups protect the boron atom, so there may be a first alkylation, but the second is less likely, because once the first chloride is removed the bulky groups twist and protect the boron atom from further attack (Figure 4.40).

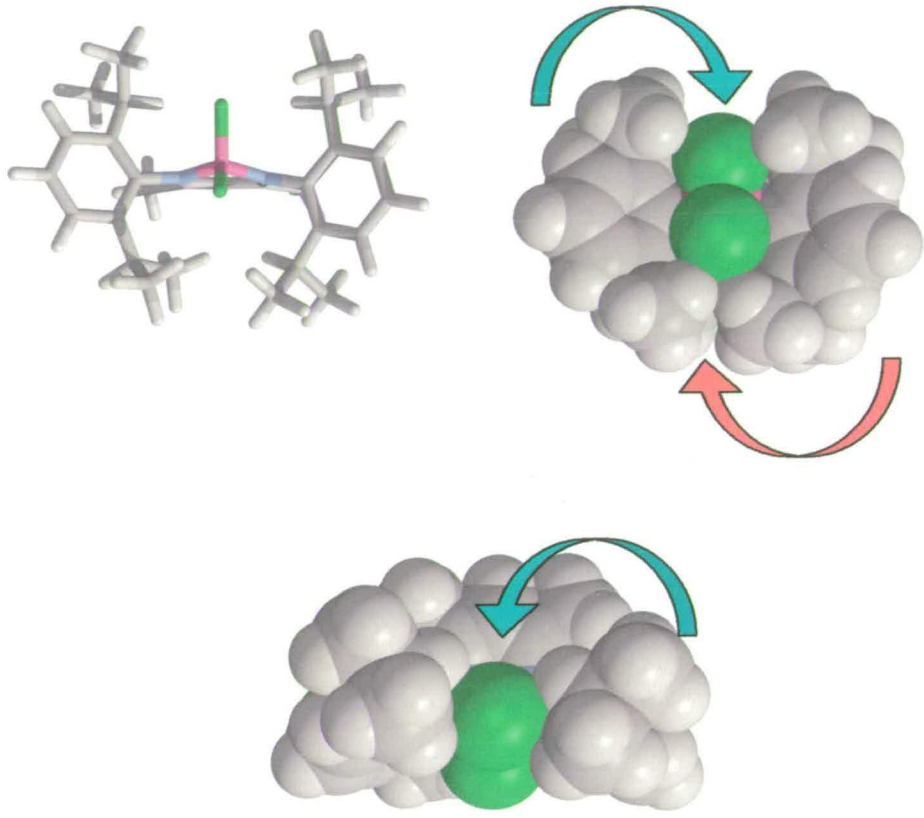

Figure 4.39 Alkylation on the modelled structure for 33. The green arrow represents possible attack routes of MeLi, whilst the red arrow represents a difficult attack to remove one chloride atom.

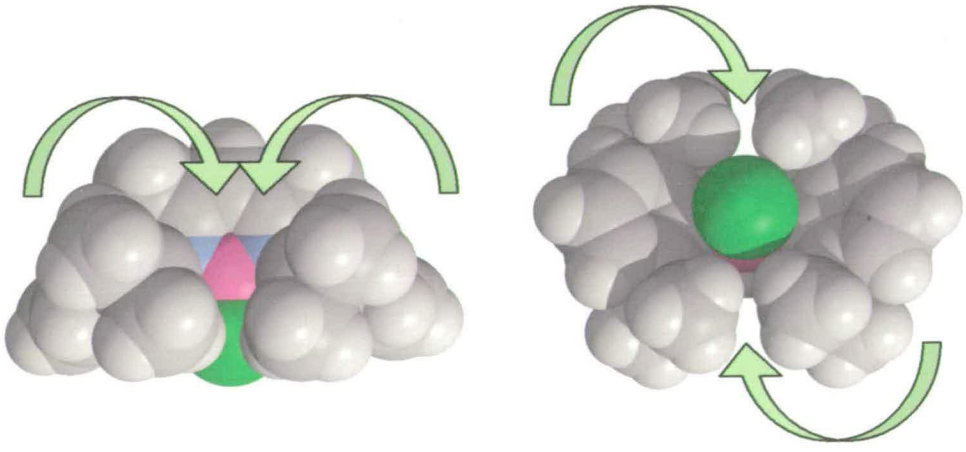

Figure 4.40 Alkylation of 35. The yellow arrows represent possible attack of MeLi.

The reduction of **35** by using a K-mirror was used in order to remove the remaining chlorine, with the aim of forming the borene compound. However, due to the presence of water during the reaction, an oxygen containing dimer complex is isolated. The reactivity of the lithium β–diketiminate with Me_2BBr (**20**) provided an alternative route to the borene compound, but instead a monomeric boron oxide complex is obtained, again due to the presence of traces of water.

4.4 Experimental

4.4.1 General Procedures

All manipulations were carried out under a nitrogen atmosphere using standard Schlenk and cannula techniques or in a conventional nitrogen-filled glove-box (Saffron Scientific), fitted with oxygen and water scavenging columns. Solvents were refluxed over an appropriate drying agent, and distilled and degassed prior to use. Solvents and reagents where commercially available were bought from Aldrich, Acros or Fischer, with exception of NMR solvents which were purchased from Goss Scientific. Diethyl ether, toluene, hexane, benzene and THF were all distilled from Na/benzophenone under a nitrogen atmosphere. NMR solvents were degassed using three freeze-pump-thaw cycles and stored over 4 Å molecular sieves.

4.4.2 Instrumentation

Elemental analyses were performed by sealing aluminium capsules containing approximately 1 mg of compound under nitrogen in the glove box, and performed using a Perkin-Elmer 2400 CHN Analyser. The NMR spectra were recorded on Bruker AC 250 MHz and Varian Gemini 200MHz spectrometers. Infrared spectra were obtained using a Perkin-Elmer 1600 Paragon Series FT-IR spectrometer as potassium bromide discs or as liquid thin films. Electron impact (EI) mass spectra were obtained either on a Finnigan MAT 4600 quadrupole spectrometer or on a Kratos MS50TC spectrometer. Fast atom bombardment (FAB) mass spectra were obtained on a MS50TC spectrometer. ^{1}H and ^{13}C NMR spectra were referenced to TMS and ^{11}B NMR spectra were referenced to $BF_3(Et_2O)$.

4.4.3 Synthesis

[Ar'N=C(CH$_3$)C(H)=C(CH$_3$)N(H)Ar']; (Ar': 2,6-diisopropylphenyl) (31)

To a solution of 2,4-pentadione (9.96 cm^3, 97.00 mmol) in ethanol (400 cm^3) and 2,6-diisopropylaniline (37 cm^3, 195.00 mmol) was added concentrated hydrochloride acid (8.17 cm^3, 96 mmol). After the mixture was stirred for three days under reflux (100 °C), ethanol was removed under *vacuum*. The brown residue was treated with dichloromethane (two portions of 250 cm^3) and water was added (200 cm^3). The organic phase was treated with an excess of Na_2CO_3, and the deep orange solution was filtered and dried over sodium sulphate (anhydrous). The solution was filtered again and the solvent removed under *vacuum* to obtain a red–orange oil. The red-orange oil was treated with hot methanol (200 cm^3), and the solution was filtered and stored at -5 °C for one day. The white solid obtained was filtered and dried overnight in *vacuum* at 70 °C (145.30 mmol, 81.0% yield).

^{1}H NMR ($C_2D_2Cl_4$/ppm): δ 12.01 (s, 1H, N*H*), δ 7.18 (m, 6H, -C_6H_3^{i}Pr), δ 5.40 (s, 1H, γ-C*H*), δ 3.47 [sept, 4H, C*H*(CH$_3$)$_2$], 1.96 [s, 6H, C(C*H*$_3$)], δ 1.29 [d, 12H, CH(C*H*$_3$)$_2$], δ1.20 [d, 12H, CH(C*H*$_3$)$_2$]. ^{13}C NMR ($C_2D_2Cl_4$/ppm): δ 164.0 (*p*-*C*), δ 150.6 [*C*(CH$_3$)], δ 141.5 [*o*-*C*(Dipp)], δ 123.3 [*m*-C(Dipp)], δ 93.0 (γ-*C*), δ 28.4 [*C*H(CH$_3$)$_2$], δ 24.8 [CH(*C*H$_3$)$_2$], δ 24.1 [C(*C*H$_3$)], δ 23.4 (*C*H$_2$). Elemental analysis for $C_{29}H_{42}N_2$: Expected: C, 83.20; H, 10.11; N, 6.69. Found: C, 83.01; H, 9.97; N, 6.60.

[HC(MeCNAr')$_2$Li] (32) and [HC(MeCNAr')$_2$BCl$_2$]; · (Ar'= 2,6-diisopropylphenyl) (33)

To a solution of Ar'N=C(CH$_3$)C(H)=C(CH$_3$)NHAr' (**A**) (2.51 g, 6 mmol) in diethyl ether (20 cm^3) was added ^{n}BuLi (2.4 cm^3, 2.5 M in hexanes, 6.0 mmol) at –78 °C. The mixture was allowed to warm to room temperature and stirred for 1 hour. The solvent and volatile components were removed under *vacuum* and the resulting solid of [HC(MeCNAr')$_2$Li] dissolved in toluene (20 cm^3). At –78 °C, BCl_3 in hexane (6.0 cm^3, 1.0 M, 6.0 mmol) was added to this solution and the mixture was

allowed to stir overnight. The resultant orange solution was filtered and LiCl removed to provide the final product **33** (3.12 mmol, 52% yield).

^{1}H NMR (toluene-d$_8$/ppm): δ 7.15 (m, 6H, -C$_6H_3$^{i}Pr), 5.18 (s, 1H, C*H*), 3.32 [sept, 4H, C*H*(CH$_3$)$_2$], 2.14 [s, 6H, C(C*H*$_3$)], 1.35 [d, 12H, CH(C*H*$_3$)$_2$], 1.17 [d, 12H, CH(C*H*$_3$)$_2$]. ^{13}C NMR (toluene-d$_8$/ppm): δ 161.0 (*p-C*), 141.91 [*C*(CH$_3$)], 140.70 [*o-C*(Dipp)], 126.30 [*p*-C(Dipp)], 123.30 [m-*C* (Dipp)], 94.70 (γ-*C*), 28.52 [*C*H(CH$_3$)$_2$], 24.60 [CH(*C*H$_3$)$_2$], 22.90 [C(*C*H$_3$)], 20.01 [CH(*C*H$_3$)$_2$]. ^{11}B NMR (toluene-d$_8$/ppm): δ 4.90. Satisfactory elemental analysis (CHN) and mass spectra could not be obtained due the reactivity of the sample.

[HC(MeCNAr')$_2$B(Me)Cl]; (Ar'= 2,6-diisopropylphenyl) (34)

A stirred solution of [HC(MeCNAr')$_2$BCl$_2$] (2.50g, 5.0 mmol) in 20 cm^3 of toluene was treated with MeLi in diethyl ether (3.6 cm^3, 1.4 M, 50 mmol) at –78 °C. The reaction mixture was warmed to room temperature and allowed to stir for 24 hours. The solvent and volatile components were removed under *vacuum* and the product extracted from LiCl in toluene (20 cm^3). The orange oil could not be crystallised (4.80 mmol, 96% yield).

^{1}H NMR (toluene-d$_8$/ppm): δ 7.16 (m, 6H, -C$_6H_3$^{i}Pr$_2$), 5.37 (s, 1H, C*H*), 3.18 [sept, 4H, C*H*(CH$_3$)$_2$], 1.73 [s, 6H, C(C*H*$_3$)], 1.27 [d, 12H, CH(C*H*$_3$)$_3$], 1.17 [d, 12H, CH(C*H*$_3$)$_2$], 0.13 (s, 3H, BC*H*$_3$). ^{13}C NMR (toluene-d$_8$/ppm): δ 161.31 (*p*-C), 142.68 [*C*(CH$_3$)], 141.04 [*o-C*(Dipp)], 125.20 [*p*-C(Dipp)], 123.09 [m-*C* (Dipp)], 93.47 (γ-C), 28.33 [*C*H(CH$_3$)$_2$], 24.19 [CH(*C*H$_3$)$_2$], 23.05 [C(*C*H$_3$)], 20.67 [CH(*C*H$_3$)$_2$], 0.94 (B*C*H$_3$). ^{11}B NMR (toluene-d$_8$/ppm): δ 21.47.

[HC(MeCNAr')$_2$BCl]$^•$; (Ar'= 2,6-diisopropylphenyl) (35)

a) From [HC(MeCNAr')$_2$B(Me)Cl]. The orange oil [HC(MeCNAr')$_2$B(Me)Cl] was redissolved in toluene (20 cm^3) and treated with MeLi (3.60 cm^3, 1.4 M, 5.0 mmol) at –78 °C. The reaction mixture was warmed to room temperature and allowed to stir overnight, The orange/red suspension was

filtered, concentrated (10 cm^3) and stored at –20 °C for 2 days to give orange crystals of $[HC(MeCNAr')_2BCl]^•$ complex (2.85 mmol, 57% yield).

b) From $[HC(MeCNAr')_2BCl_2]$. A stirred solution of $[HC(MeCNAr')_2BCl_2]$ (2.50 g, 5.0 mmol) in 20 cm^3 of toluene was treated with MeLi (7.20 cm^3, 1.4 M, 10.0 mmol) at –78 °C. The reaction mixture was warmed to room temperature and allowed to stir for 24 hours. The orange/red solution was filtered (LiCl removed), concentrated (10 cm^3) and stored for 2 days to give the final compound.

EIMS(*m/z*): 463; 447 (M-Me). UV-visible λ_{max}: 391.80 and 570.11 nm. CV: a reversible reduction at –1.21 V and a poorly defined oxidation at 1.69 V. Elemental analysis for $C_{29}H_{41}N_2BCl$: Found: C,75.06; H, 8.92; N, 6.04. Found: C, 74.60; H, 8.74; N, 5.93.

EPR. A orange solution of $[HC(MeCNAr')_2BCl]^•$ (0.080 g, 0.170 mmol) in toluene (25 cm^3) was transferred to a flat quartz cell for EPR analysis in the glove box and the EPR recorded at room temperature. The EPR analysis parameters were CF 3450, Gain $4x10^4$, Mod 4 Gpp, SW 200, Phase 180°, Power 100 mW, Freq 9.71 GHz. g = 2.013, peak width = 16.2 G. After simulation using WinEPR: g=2.015, $A_{B(11)}$=78.60 G, $A_{B(10)}$=46.00, A_H=32.99, Lorenzian line width 8 G

All potentials were recorded against the appropriate Pt reference electrode. The counter electrode was a similar Pt wire. To enable comparison between the solvent systems the ferrocene/ferrocinium redox couple was used as internal standard. The supporting electrolyte used was tetrabutylammonium tetrafluoroborate. Electrolyte concentrations of 0.1 M were used throughout. All solutions were degassed with nitrogen for five minutes and kept under a nitrogen atmosphere throughout the experiment. In DCM solvent a reversible reduction at –1.21 V was observed, whilst no oxidation was detected. In DMF solvent a irreversible reduction at –1.21 V and a irreversible oxidation at +0.70 V were observed.

Empirical formula	$C_{29}H_{41}BN_2Cl$	β/ °	104.074(5)
Formula weight	463.90	γ/ °	90
Crystal system	Monoclinic	Volume/ $Å^3$	2713.9(17)
Space group	$P2_1/n$	Z	4
a/ Å	12.587(5)	Z'	1
b/ Å	16.336(5)	Density calc./ Mgm^{-3}	1.135
c/ Å	13.607(5)	μ (Mo-K)/ mm^{-1}	0.160
α/ °	90		

Data were collected on a Bruker SMART APEX diffractometer[30] equipped with an Oxford Cryosystems low-temperature device at 150 K and using an orange block oil-coated crystal[31] with dimensions of 0.50x0.26x0.26 mm^3. The initial unit cell was indexed using a least-squares analysis of a random set of reflections collected from three series of 0.3° wide ω-scans, 10 s per frame, and 25 frames per series that were well distributed in reciprocal space. Data frames were collected [Mo Kα = 0.71073 Å] with 0.3° wide ω-scans, 10 s per frame and 600 frames per series. Three complete series were collected at varying ϕ angles (ϕ=0, 90, 180°). The crystal to detector distance was 6.0 cm, this providing a set of $3.96 \leq 2\theta \leq 57.96$. A total of 17080 reflections were collected and integrated using SAINT,[32] while absorption correction was applied using SADABS[33] with 6602 unique [R(int)=0.0202]. System symmetry, systematic absences and intensity statistics indicated the unique monoclinic space group $P2_1/n$. The structure was determined by direct methods with the location of nearly all non-hydrogen atoms using the program SHELXS[34] and refined by full-matrix least-squares on F^2 using SHELXL.[35] All non-hydrogen atoms were refined anisotropically, while hydrogen atoms were placed in calculated positions, constrained to ride on their carbon atoms with group U_{iso} values assigned ($U_{iso}(H) = 1.20U_{iso}$). The final structure was refined to convergence [$\Delta/\sigma \leq 0.001$] with R(F) = 0.0533 (for 6602 data with $F>4\sigma F$), GOF = 1.046 and *w*R2 = 0.1628 (all data). [$R1 = \Sigma|F_O - F_C|/ \Sigma |F_O|$, $wR2 = \{[\Sigma w(F_O^2 - F_C^2)^2]/ \Sigma wF_O^4\}^{0.5}$, $w = 1/[\sigma^2(F_O^2) + (xP)^2 + yP]$, $P = (F_O^2+2F_C^2/3)$]. The largest difference between peak and hole in the final difference map, 0.449 and –0.338 $eÅ^{-3}$.

Molecular Orbital Calculations for $[HC(MeCNAr')_2BCl]^•$

Ab initio calculations were performed with Gaussian 98[36] package at the density functional (DFT) level of theory, and by using the atomic co-ordinates from crystal structure data for the the $[HC(MeCNAr')_2BCl]^•$ complex. The DFT calculation employed of Becke gradient-corrected three-parameter hybrid exchange[37] combined with the gradient-corrected correlation functional of Lee *et al.*,[38] which

included both local and non-local terms B3LYP functional. The calculations were performed using the standard molecular split-valence 6-31G** basis set.[39]

[{HC(MeCNAr')$_2$BOK}$_2$]; (Ar'= 2,6-diisopropylphenyl) (36)

In a Schlenk flask a mirror of potassium metal (0.036 g, 1.08 mmol) was prepared. A solution of [HC(MeCNAr')$_2$BCl]$^\bullet$ (0.50 g, 1.08 mmol) in fresh toluene (20 cm^3) was added dropwise and stirred for 2 days at room temperature. The red solution was filtered and the solvent removed in *vacuum*. The product was extracted with n-pentane (20 cm^3), filtered and concentrated (10 cm^3) and stored at –20 °C to produce orange crystals suitable for X-rays.

^{1}H NMR (toluene-d$_8$/ppm): δ 6.95 (m, 12H, -C$_6$*H*$_3$^{i}Pr$_2$), 5.23 (s, 2H, C*H*), 3.23 [sept, 8H, C*H*(CH$_3$)$_2$], 1.69 [s, 12H, C(C*H*$_3$)], 1.32 [d, 24H, CH(C*H*$_3$)$_3$], 1.12 [d, 12H, CH(C*H*$_3$)$_2$]. ^{13}C NMR (toluene-d$_8$/ppm): δ 162.3 (*p*-C), 142.6 [*C*(CH$_3$)], 141.3 [*o*-*C*(Dipp)], 124.9 [*p*-C(Dipp)], 123.30 [m-*C*(Dipp)], 100.1 (γ-C), 28.70 [*C*H(CH$_3$)$_2$], 25.12 [CH(*C*H$_3$)$_2$], 23.83 [C(*C*H$_3$)], 22.73 [CH(*C*H$_3$)$_2$]. IR (KBr): 1550.5 cm^{-1} ν_a(B-O), 1442.4 cm^{-1} ν_s(B-O) and 1287.7 cm^{-1} ν_s(B-O). FABMS(*m/z*): 966 (M$^+$); 926 (M$^+$-K). UV-visible λ_{max}: 576.56 nm.

All potentials were recorded against the appropriate Pt reference electrode. The counter electrode was a similar Pt wire. To enable comparison between the solvent systems the ferrocene/ferrocinium redox couple was used as internal standard. The supporting electrolyte used was TBABF$_4$. Electrolyte concentrations of 0.1 M were used throughout. All solution were degassed with nitrogen for five minutes and kept under a nitrogen atmosphere throughout the experiment. In DCM the differential pulse for the π-dimer presents two reductions at –0.870 and –1.670 V. CV at different temperatures (289 and 243 K) show a irreversible reduction potential at –1.16 V.

Empirical formula	$C_{58}H_{82}B_2K_2N_4O_2$	β/°	111.249(5)
Formula weight	967.10	γ/°	90
Crystal system	Monoclinic	Volume/ Å^3	6658(3)
Space group	C 2/c	Z	4
a/ Å	20.931(5)	Z'	0.5
b/ Å	14.127(5)	Density calc./ Mgm^{-3}	0.965

c/ Å	24.160(5)	μ (Mo-K)/ mm^{-1}	0.179
α/ °	90		

Data were collected on a Bruker SMART APEX diffractometer[30] equipped with an Oxford Cryosystems low-temperature device at 150 K and using an orange block oil-coated crystal[31] with dimensions of 0.27x0.14x0.14 mm^3. The initial unit cell was indexed using a least-squares analysis of a random set of reflections collected from three series of 0.3° wide ω-scans, 10 s per frame, and 25 frames per series that were well distributed in reciprocal space. Data frames were collected [Mo Kα = 0.71073 Å] with 0.3° wide ω-scans, 20 s per frame and 600 frames per series. Four complete series were collected at varying ϕ angles (ϕ=0, 90, 120, 180°). The crystal to detector distance was 6.0 cm, this providing a set of $3.96 \leq 2\theta \leq 57.96$. A total of 20434 reflections were collected and integrated using SAINT,[32] while absorption correction was applied using SADABS[33] with 8748 unique [R(int)=0.0502]. System symmetry, systematic absences and intensity statistics indicated the unique monoclinic space group C 2/c. The structure was determined by direct methods with the location of nearly all non-hydrogen atoms using the program SHELXS[34] and refined by full-matrix least-squares on F^2 using SHELXL.[35] All non-hydrogen atoms were refined anisotropically, while hydrogen atoms were placed in calculated positions, constrained to ride on their carbon atoms with group U_{iso} values assigned ($U_{iso}(H)= 1.20U_{iso}$). The final structure was refined to convergence [$\Delta/\sigma \leq 0.001$] with R(F) = 0.0761 (for 8748 data with $F>4\sigma F$), GOF = 1.057 and *w*R2 = 0.1791 (all data). [$R1 = \Sigma|F_O - F_C|/ \Sigma |F_O|$, $wR2 = \{[\Sigma w(F_O^2 - F_C^2)^2]/ \Sigma wF_O^4\}^{0.5}$, $w = 1/[\sigma^2(F_O^2) + (xP)^2 + yP]$, $P = (F_O^2+2F_C^2/3)$]. The largest difference between peak and hole in the final difference map, 0.445 and –0.328 $eÅ^{-3}$.

[HC(MeCNAr')$_2$BO]; (Ar'= 2,6-diisopropylphenyl) (37) and [Li(BMe$_4$)] (38)

A stirred solution of [HC(MeCNAr')$_2$BCl$_2$] (2.50g, 5.0 mmol) in 20 cm^3 of toluene was treated with MeLi in diethyl ether (3.6 cm^3, 1.4 M, 50 mmol) at –78 °C. The reaction mixture was warmed to room temperature and allowed to stir for 24 hours. The solvent and volatile components were removed under *vacuum* and the product extracted from LiCl in toluene (20 cm^3). To a solution of

Ar'N=C(CH_3)C(H)=C(CH_3)NHAr' (2.5 g, 6.0 mmol) in toluene (20 cm^3) was added dropwise ^{n}BuLi in hexanes (2.4 cm^3, 2.5 M, 6.0 mmol) at –78 °C. The reaction mixture was allowed to warm to room temperature and stirred for 1 hour. The reaction mixture was treated with Me_2BBr (0.72 g, 6.0 mmol) in diethyl ether (10 mL) by adding dropwise within 10 minutes and the mixture allowed to warm to room temperature and stirred for 1 day. The orange solution was filtered, concentrated (10 cm^3) and stored at –20 °C for 2 days to give yellow co-crystals of **37** and **38**.

^{1}H NMR (toluene-d_8/ppm): δ 7.15 (m, 6H, -$C_6H_3{}^i Pr_2$), 5.05 (s, 1H, C*H*), 3.32 [sept, 4H, C*H*(CH_3)$_2$], 2.14 [s, 6H, C(C*H*$_3$)], 1.39 [d, 12H, CH(C*H*$_3$)$_3$], 1.18 [d, 12H, CH(C*H*$_3$)$_2$], 0.32 [s, 12H, B(C*H*$_3$)$_4$]. ^{13}C NMR (toluene-d_8/ppm): 163.28 (*p*-C), 145.94 [*C*(CH_3)], 142.34 [*o*-*C*(Dipp)], 126.30 [*p*-C(Dipp)], 122.90 [m-*C*(Dipp)], 93.02 (γ-C), 28.31 [*C*H(CH_3)$_2$], 24.67 [CH(*C*H$_3$)$_2$], 23.11 [C(*C*H$_3$)], 20.64 [CH(*C*H$_3$)$_2$], 0.92 (B*C*H$_3$). ^{11}B NMR (toluene-d_8/ppm): δ 31.0 (broad, *B*-CH_3), -1.92 (s, *B*-N), -16.90 (s, H_3C-*B*-CH_3).

Empirical formula	$C_{33}H_{53}B_2LiN_2O$	β/ °	115.423(12)
Formula weight	522.33	γ/ °	90
Crystal system	Monoclinic	Volume/ Å^3	1714.4(3)
Space group	$P2_1/m$	Z	2
a/ Å	9.4655(10)	Z'	0.5
b/ Å	19.0630(12)	Density calc./ Mgm^{-3}	1.012
c/ Å	10.5200(11)	μ (Mo-K)/ mm^{-1}	0.058
α/ °	90		

Data were collected on a Bruker SMART APEX diffractometer[30] equipped with an Oxford Cryosystems low-temperature device at 150 K and using an orange block oil-coated crystal[31] with dimensions of 0.27x0.15x0.15 mm^3. The initial unit cell was indexed using a least-squares analysis of a random set of reflections collected from three series of 0.3° wide ω-scans, 10 s per frame, and 25 frames per series that were well distributed in reciprocal space. Data frames were collected [Mo Kα = 0.71073 Å] with 0.3° wide ω-scans, 20 s per frame and 600 frames per series. Four complete series were collected at varying ϕ angles (ϕ=0, 90, 120, 180°). The crystal to detector distance was 6.0 cm, this providing a set of $3.58 \leq 2\theta \leq 57.76$. A total of 3481 reflections were collected and integrated using SAINT,[32] while absorption correction was applied using SADABS[33] with 3481 unique

[R(int)=0.0270]. System symmetry, systematic absences and intensity statistics indicated the unique monoclinic space group $P2_1/m$. The structure was determined by direct methods with the location of nearly all non-hydrogen atoms using the program SHELXS[34] and refined by full-matrix least-squares on F^2 using SHELXL.[35] All non-hydrogen atoms were refined anisotropically, while hydrogen atoms were placed in calculated positions, constrained to ride on their carbon atoms with group U_{iso} values assigned ($U_{iso}(H) = 1.20U_{iso}$). The final structure was refined to convergence [$\Delta/\sigma \leq 0.001$] with R(F) = 0.0945 (for 3481 data with $F>4\sigma F$), GOF = 1.087 and *w*R2 = 0.2263 (all data). [$R1 = \Sigma|F_O - F_C|/ \Sigma |F_O|$, $wR2 = \{[\Sigma w(F_O^2 - F_C^2)^2]/ \Sigma wF_O^4\}^{0.5}$, $w = 1/[\sigma^2(F_O^2) + (xP)^2 + yP]$, $P = (F_O^2+2F_C^2/3)$]. The largest difference between peak and hole in the final difference map, 0.215 and –0.184 eÅ^{-3}

Molecular Orbital Calculations for [HC(MeCNAr')$_2$BO]

Ab initio calculations were performed with Gaussian 98[36] package at the density functional (DFT) level of theory, and by using the atomic co-ordinates from crystal structure data for the [HC(MeCNAr')$_2$BO] complex. The DFT calculation employed Becke gradient-corrected three-parameter hybrid exchange[37] combined with the gradient-corrected correlation functional of Lee *et al.*,[38] which included both local and non-local terms B3LYP functional. The calculations were performed using the standard molecular split-valence 6-31G** basis set.[39]

4.5 References

1 J. P. Fackler Jr., *Prog. Inorg. Chem.*, **1966**, *7*, 361.

2 G. W. Everett Jr., *J. Am. Chem. Soc.*, **1963**, *37*, 2117.

3 P. A. White, J. Calabrese and K. H. Theopold, *Organometallics*, **1996**, *15*, 5473; Y. Liang, G. P. A. Yap, A. L. Rheingold and K. H. Theopold, *Organometallics*, **1996**, *15*, 5284; K. H. Theopold, *Eur. J. Inorg. Chem.*, **1998**, *1*, 15.

4 K. Ziegler, F. Krupp and K. Zosel, *Angew. Chem.*, **1955**, *67*, 425.

5 G. Schiebe, *Chem. Ber.*, **1923**, *56*, 137.

6 W. R. Brasen, H. E. Holmquist and R. E. Benson, *J. Am. Chem. Soc.*, **1961**, *83*, 3125.

7 L. C. Dolman, *Tetrahedron Lett.*, **1966**, *4*, 459.

8 P. H. M. Budzelaar, A. B. Van Ort and A. G. Orpen, *Eur. J. Inorg. Chem.*, **1998**, 1485; M. Stender, R. J. Wright, E. E. Barret, J. Prust, M. M. Olmstead, H. W. Roesky and P. P. Power, *J. Chem. Soc., Dalton Trans.*, **2001**, 3465.

9 P. B. Hitchcock, M. F. Lappert, D. S. Liu and R. Sablong, *Chem. Commun.*, **2002**, 1920.

10 M. F. Lappert and D. S. Liu, *J. Organomet. Chem.*, **1995**, *500*, 203.

11 C. F. Caro, P. B. Hitchcock and M. F. Lappert, *Chem. Commun.*, **1999**, 1433.

12 P. J. Bailey, C. M. E. Dick, S. Fabre and S. Parsons, *J. Chem. Soc., Dalton Trans.*, **2000**, 1655; P. J. Bailey, R. Coxall, C. M. E. Dick, S. Fabre and S. Parsons, *Organometallics*, **2001**, *20*, 798.

13 R. Eberhardt, M. Allmendinger, G. A. Luinstra and B. Drieger, *Organometallics*, **2003**, *22*, 211.

14 L. Bourget-Merle, M. F. Lappert and J. R. Severn, *Chem. Rev.*, **2002**, *102*, 3031.

15 P. L. Holland and W. B. Tolman, *J. Am. Chem. Soc.*, **1999**, *121*, 7270; P. L. Holland and W. B. Tolman, *J. Am. Chem. Soc.*, **2000**, *122*, 6331.

16 P. L. Holland, T. R. Cundari, L. L. A. Perez, N. A. Eckert and R. J. Lachicotte, *J. Am. Chem. Soc.*, **2002**, *124*, 14416; J. M. Smith, R. J. Lachicotte and P. L. Holland, *Chem. Commun.*, **2001**, 1542.

17 J. A. Jegier and W. L. Gladfelter, *Coord. Chem. Rev.*, **2000**, *631*, 206.

18 G. G. Hlatky, H. W. Turner and R. R. Eckman, *J. Am. Chem. Soc.*, **1989**, *111*, 2728; L. Ji, X. Yang, C. L. Stern and T. Marks, *Organometallics*, **1997**, *16*, 842.

19 M. P. Coles and R. F. Jordan, *J. Am. Chem. Soc.*, **1997**, *119*, 82125.

20 B. Qian, D. L. Ward and M. R. Smith III, *Organometallics*, **1998**, *17*, 3070.

21 N. Kuhn, J. Fahl, S. Fuchs and M. Steimann, *Z. Anorg. Allg. Chem.*, **1999**, *625*, 2108.

22 C. Cui, H. W. Roesky, H. G. Schmidt, M. Noltemeyer, H. Hao and F. Cimpesu, *Angew. Chem. Int. Ed. Engl.*, **2000**, *39*, 4274; N. J. Hardman, C. Cui, H. W. Roesky, W. Fink and P. P. Power, *Angew. Chem., Int. Ed. Engl.*, **2001**, *40*, 2172; M. Stender, B. Eichler, N. J.

Hardman, P. P. Power, J. Prust, M. Noltemeyer and H. W. Roesky, *Inorg. Chem.*, **2001**, *40*, 2794.

[23] P. B. Hitchcock, M. F. Lappert and M. Layh, *J. Chem. Soc., Dalton Trans.*, **2001**, 2409; W. Uhl, W. Hiller, M. Layh and W. Schwartz, *Angew. Chem., Int. Ed. Engl.*, **1992**, *31*, 1364; G. Linti, G. *J. Organomet. Chem.*, **1996**, *520*, 107; D. Loos, E. Baum, A. Ecker, H. Schöckel and A. J. Downs, *Angew. Chem., Int. Ed. Engl.*, **1997**, *36*, 860; A. Haaland, K. G. Martinsen, H. V. Volden and D. Loos, *Acta Chem. Scand.*, **1994**, *48*, 172.

[24] A. Sundermann, M. Reiher and W. W. Schoeller, *Eur. J. Inorg. Chem.*, **1998**, 305.

[25] B. Qian, S. W. Baek and M. R. Smith III, *Polyhedron*, **1999**, *18*, 2405.

[26] L. Weber, M. Schniede and P. Lönnecke, *J. Chem. Soc., Dalton. Trans.*, **2001**, 3459; L. Weber, E. Dobbert, H. Stammler, B. Newmann, R. Boese and D. Bläser, *Eur. J. Inorg. Chem.*, **1999**, 491.

[27] W. J. Kaim, *J. Am. Chem. Soc.*, **1984**, *106*, 1712.

[28] CambridgeSoft Corporation, *MOPAC*. Version 3.5.1. USA, **1995**.

[29] K. C. Williams and T. L. Brown, *J. Am. Chem. Soc.*, **1966**, *88*, 4134; W. Rhine, G. Stucky and S. W. Peterson, *J. Am. Chem. Soc.*, **1975**, *97*, 6401.

[30] Bruker. *SMART*. Bruker-AXS, Madison, Wisconsin, USA, **2001**.

[31] D. Stalke and T. Kottke, *J. Appl. Crystallogr.*, **1993**, 26, 615.

[32] Bruker. *SAINT*. Bruker-AXS, Madison, Wisconsin, USA, **2002**.

[33] G. M. Sheldrick, *SADABS*. Version 2.06. University of Gottingen, Germany, **2001**.

[34] G. M. Sheldrick, *SHELXS97*. University of Gottingen, Germany, **1997**.

[35] G. M. Sheldrick, *SHELXL97*. University of Gottingen, Germany, **1997**.

[36] Gaussian 98, Revision A.11. M. J. Frisch, G. W. Trucks, H. B. Schlegel, G. E. Scuseria, M. A. Robb, J. R. Cheeseman, V. G. Zakrzewski, J. A. Montgomery, R. E. Stratmann, J. C. Burant, S. Dapprich, J. M. Millam, A. D. Daniels, K. N. Kudin, M. C. Strain, O. Farkas, J. Tomasi, V. Barone, M. Cossi, R. Cammi, B. Mennucci, C. Pomelli, C. Adamo, C. Cliord, J. Ochterski, G. A. Petersson, P. Y. Ayala, Q. Cui, K. Morokuma, D. K. Malick, A. D. Rabuck, K. Raghavachari, J. B. Foresman, J. Cioslowski, J. V. Ortiz, B. B. Stefanov, G. Liu, A. Liashenko, P. Piskorz, I. Komaromi, R. Gomperts, R. L. Martin, D. J. Fox, T. Keith, M. A. Al-Laham, C. Y. Peng, A. Nanayakkara, C. Gonzalez, M. Challacombe, P. M. W. Gill, B. F. G. Johnson, W. Chen, M. W. Wong, J. L. Andres, M. Head-Gordon, E. S. Replogle and J. A. Pople, Gaussian Inc., Pittsburgh PA, **2001**.

[37] A. D. Becke, *J. Chem. Phys.*, **1993**, *98*, 5648.

[38] C. Lee, W. Yang R. G. Parr, *Phys. Rev. B.*, **1988**, *37*, 785.

[39] P. C. Haran and J. A. Pople, *Theor. Chim. Acta*, **1973**, *28*, 213.

Chapter 5:

6-Aminofulvene-2-Aldimine Magnesium Complexes

5.1 Introduction

5.1.1 Background

The present investigation involves attempts to explore the chemistry of *N,N'*-diaryl-6-aminofulvene-2-aldimines with Grignard reagents, in order to synthesise zwitterionic magnesium complexes (Figure 5.1). The negative charge should be stabilized at the five-membered-ring, so that there is a positive charge at the magnesium atom. The use of bulky groups at the nitrogen atoms should protect the metal and also prevent the complexes from dimerization. Finally, alkene polymerisation will be tested and the catalytic activity of the zwitterionic magnesium complex determined.

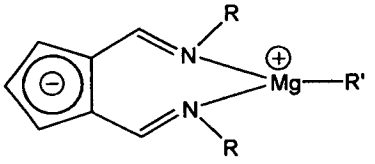

R : C_6H_5; C_6H_{11}; Aromatic group
R': Me or CH_2Ph

Figure 5.1 Possible zwitterionic magnesium complex to be synthesised.

Hafner *et al.*[1] have demonstrated that the reaction between dimethylformamide and dimethyl sulfate can produce a good yield of the *N,N'*-dimethylformamide-dimethylsulfate, according to the reaction illustrated in Figure 5.2. Further reaction of *N,N'*-dimethylformamide-dimethylsulfate with an equivalent amount of sodium cyclopentadienyl can provide the 6-dimethylaminofulvene (Figure 5.3).[2]

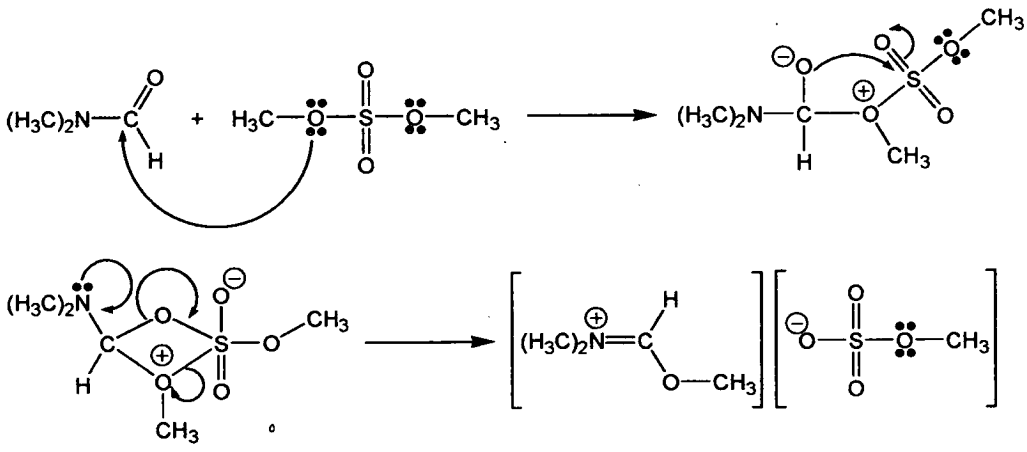

Figure 5.2 Synthesis of *N,N'*-dimethylformamide-dimethylsulfate.

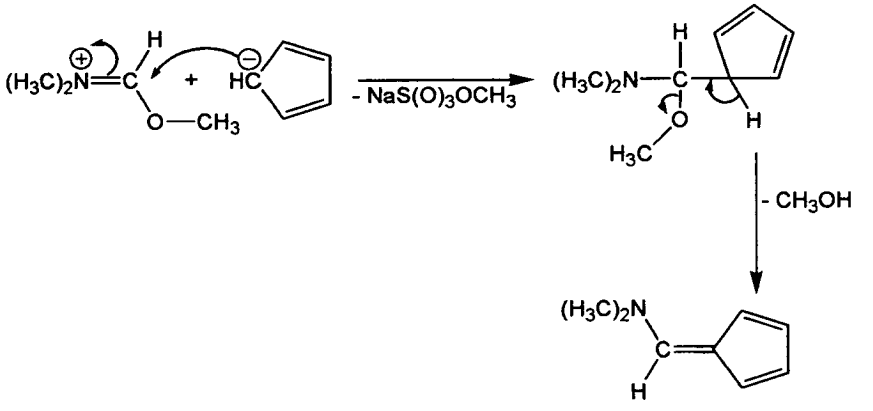

Figure 5.3 Synthesis of 6-dimethylaminofulvene.

Electrophilic substitutions of the 6-dimethylaminofulvenes are also possible when the product from oxalyl chloride and dimethylformamide is used to provide the 6-dimethylaminofulvene-2-*N,N'*-dimethylaldimmonium chloride (**A**), according to Figure 5.4. The reaction of **A** with two equivalent amounts of ammonia, or any primary aliphatic or aromatic amine, however, can produce the final *N,N'*-diaryl-6-aminofulvene-2-aldimine, [R_2AFA(H)], according to the reaction in Figure 5.5.[2] Intramolecular hydrogen bonds and proton transfer along hydrogen bonds have been considered to produce extra stability of the [R_2AFA(H)] ligands.[2-4] Regarding the hydrogen bonds, a vast number of theoretical and experimental studies have been undertaken,[3] and five tautomers have been proposed.[2,4] Moreover, if the two donor nitrogen atoms have the same affinity for the proton, a single potential energy well can be observed where the proton is centred between the nitrogen atoms [N···H···N].

A double potential energy well results, however, when the hydrogen atom jumps between both nitrogen atoms [N-H···N ⇌ N···H-N].[2] The obtained 6-aminofulvene derivatives have high resonance energy, due to the cyclopentadienyl unit, where the two contributing forms are of equal or nearly equal energy.[2]

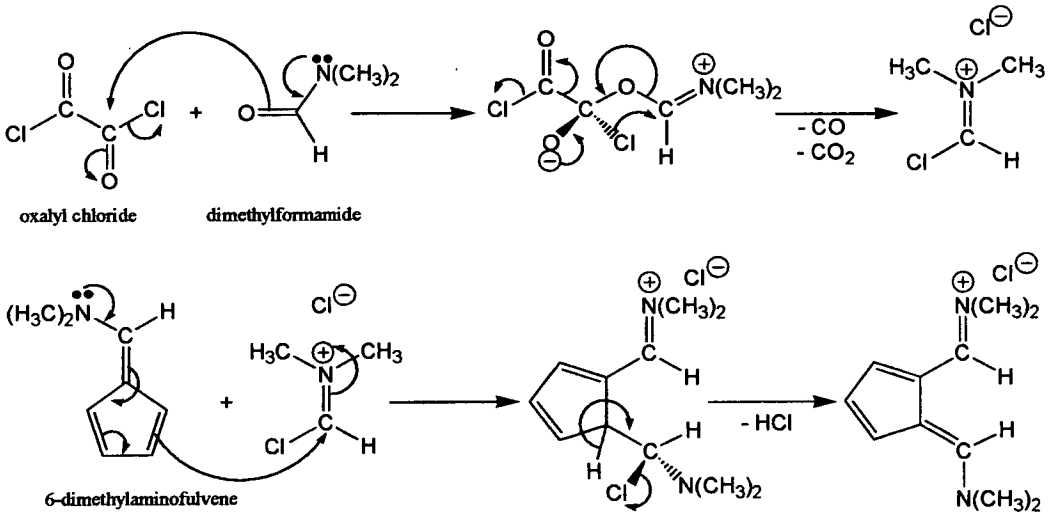

Figure 5.4 Synthesis of 6-dimethylaminofulvene-2-*N,N'*-dimethylaldimmonium chloride.

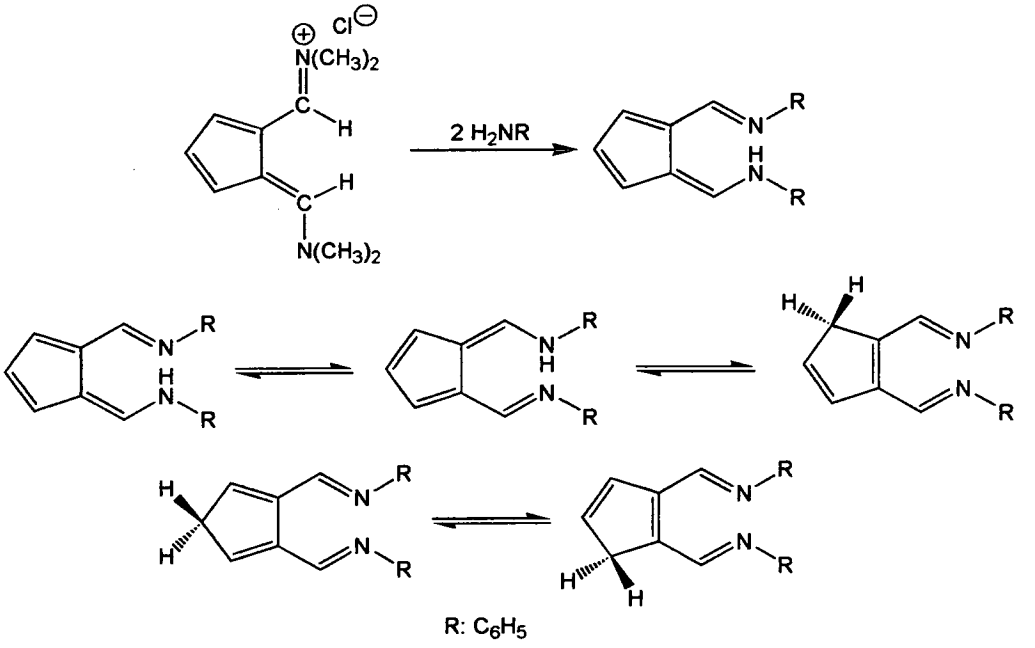

Figure 5.5 Synthesis of *N,N'*-diaryl-6-aminofulvene-2-aldimine and the hydrogen atom migration suggesting five possible tautomers.

In compounds such as the 1-amino-7-imino-1,3,5-cycloheptatrienes,[5] β-diketiminate ligands,[6] and the 6-aminopentafulvene-2-aldimine, the N-H···N moiety provides the structural environment for either facile tautomers or perhaps a symmetrical hydrogen bond, where the structures have been postulated to exhibit nonclassical aromaticity in the sense of cyclic delocalized π-electron systems (with ten or six π-electrons), according to Figure 5.6. The strong N-H···N hydrogen bond of the *N,N'*-diaryl-6-aminofulvene-2-aldimines and the 1-amino-7-imino-1,3,5-cycloheptatrienes can be compared to the 1,8-bis(dimethylamino)naphthalenes, which are a class of compounds known as Proton-Sponges.[7] The donor nitrogen atoms are forced into proximity, where the hydrogen atom can 'jump' between both nitrogen atoms. In addition to the hydrogen bonds, the aromaticity provides extra stabilization of a favourable planar symmetric structure.[8] Synthesis of 1,2-disubstituted cyclopentadienyl diimine ligands and the zirconium complexes have been reported,[9,10] whilst the synthesis of main group metal complexes has begun to be explored in order to test the complexes as alkene polymerisation catalysts (Figure 5.7).[11,12]

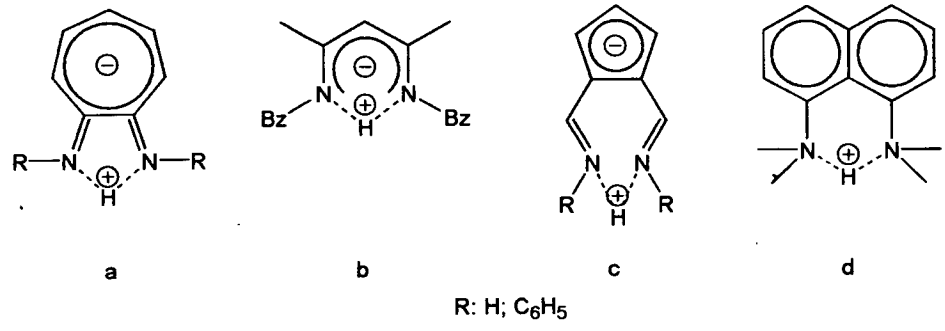

Figure 5.6 Proton-Sponge ligands: a) 1-amino-7-imino-1,3,5-cycloheptatrienes ligand; b) β-diketiminate ligand; c) *N,N'*-diaryl-6-aminofulvene-2-aldimine; d) Protonated 1,8-bis(dimethylamino)naphthalene.

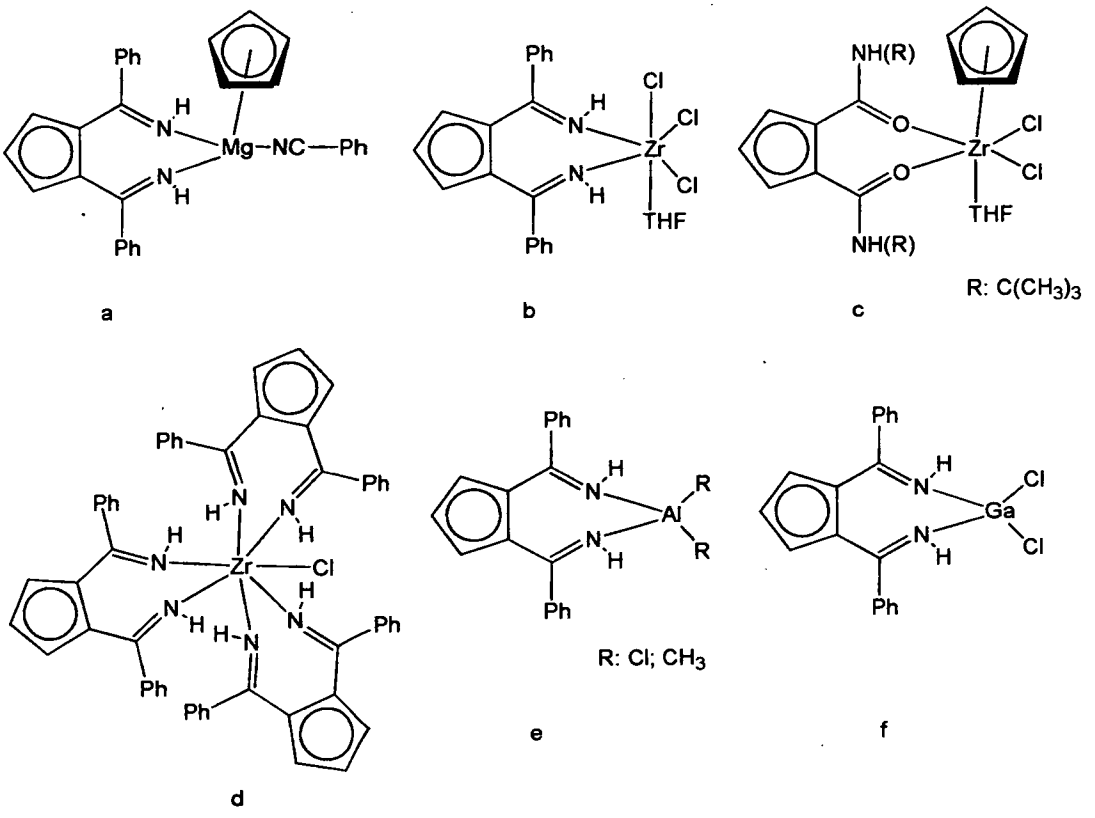

Figure 5.7 Transition and main group metal complexes of 1,2-disubstituted cyclopentadienyl diimines reported to date: a) (C_5H_3-1,2-(C(Ph)NH)$_2$])CpMg(NCPh);[9] b) (C_5H_3-1,2-(C(Ph)NH)$_2$)-$ZrCl_3$(THF);[9] c) [C_5H_3-1,2-(CONHCMe$_3$)$_2$]Cp$ZrCl_2$(THF);[10] d) (C_5H_3-1,2-(C(Ph)NH)$_2$)$_3$ZrCl;[9] e) [C_5H_3-1,2-(C(Ph)NH)$_2$]AlR_2;[11] f) [C_5H_3-1,2-(C(Ph)NH)$_2$]$GaCl_2$.[11]

5.2 Results

5.2.1 Reactivity of N-Chloromethylene-N-Methylmethan-ammonium Chloride

Treatment of 6-(dimethylamino)fulvene (**39**) with an equivalent amount of *N*-chloromethylene-*N*-methylmethanammonium chloride (**40**) in THF at −61 °C resulted in the formation of a yellow solid, 6-dimethylaminofulvene-2-*N,N'*-dimethylaldimmonium chloride, [{C_5H_3-$(HCNMe_2)_2$}Cl] (**41**). Crystals suitable for X-ray diffraction were obtained from a concentrated hexane/ether solution at room temperature to provide **41** as yellow crystals. NMR spectra were recorded and a high degree of π-resonance is assumed, where the positive charge could be delocalized over the aromatic system, according to Figure 5.8. The ^{1}H NMR spectrum for **41** places a downfield singlet peak at δ 9.76 for H1 and H7, whilst the aromatic Cp hydrogen atoms are located at δ 7.35 (H3/H5) and 6.78 (H4). The methyl hydrogen atom signals are placed at an upfield chemical shift of δ 3.83 and 3.42. The ^{13}C NMR spectrum shows the downfield aromatic carbon atoms at δ 160.60 and 119.32, for C2/C6 and C3/C5. In addition, the upfield signals for methyl carbon atoms are placed at δ 48.81 and 42.13, respectively.

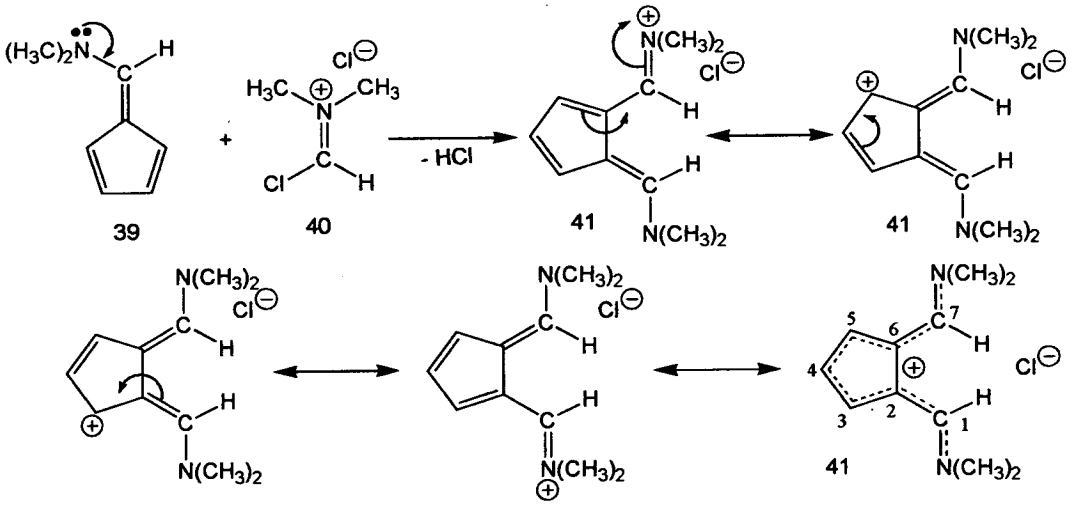

Figure 5.8 Synthesis of 41 and its π-resonance character.

The X-ray crystal structure of **41** displays C_{2v} symmetry, with all the main atoms lying within the same plane (Figure 5.9). The C-N distances are found at 1.337(4) and 1.310(4) Å, whilst the C-C distances range from 1.347(4) to 1.487(4) Å. The C-N and C-C bond lengths can be considered to be between those for single and double C-N and C-C bonds, whilst the coplanarity of the ligand shows a high degree of π-resonance delocalization effect. More information for selected bond lengths and angles are shown in Table 5.1.

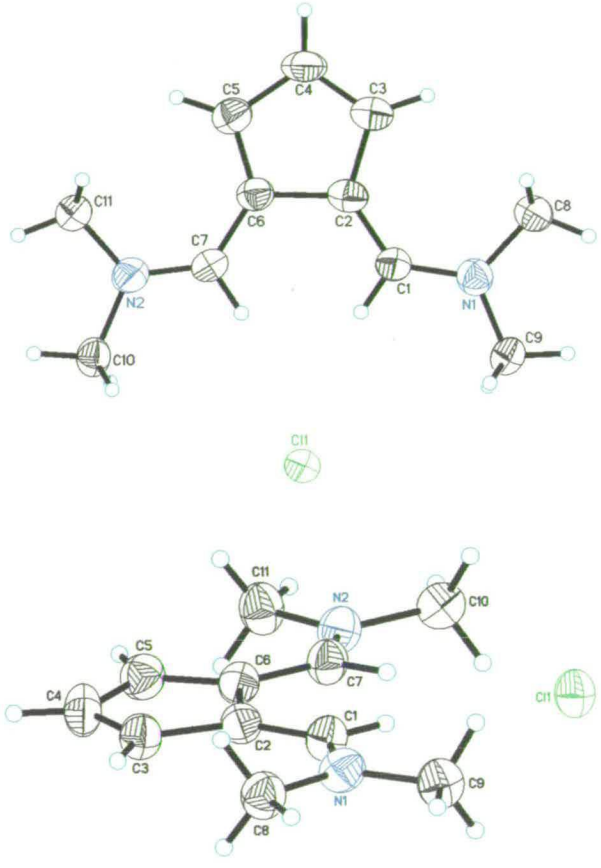

Figure 5.9 Crystallographic structure of 41 with different orientations. Displacement ellipsoids are shown at the 50% probability level.

Table 5.1 Selected bond distances (Å), angles and torsion (°) for 41.

N(1)-C(1)	1.337(4)	N(1)-C(8)	1.434(4)	N(1)-C(9)	1.438(4)
N(2)-C(7)	1.310(4)	N(2)-C(11)	1.402(4)	N(2)-C(10)	1.509(4)
C(1)-C(2)	1.368(4)	C(2)-C(3)	1.431(4)	C(2)-C(6)	1.487(4)
C(3)-C(4)	1.347(4)	C(4)-C(5)	1.426(4)	C(5)-C(6)	1.370(4)
C(6)-C(7)	1.403(4)				
C(1)-N(1)-C(8)		123.0(2)	C(1)-N(1)-C(9)		121.2(3)
C(8)-N(1)-C(9)		115.8(2)	C(7)-N(2)-C(11)		124.5(3)
C(7)-N(2)-C(10)		120.6(2)	C(11)-N(2)-C(10)		114.8(2)
N(1)-C(1)-C(2)		131.6(3)	C(1)-C(2)-C(3)		131.9(3)

C(5)-C(6)-C(7)	132.4(3)	C(7)-C(6)-C(2)		120.5(2)
N(2)-C(7)-C(6)	128.7(3)	C(8)-N(1)-C(1)-C(2)		-1.1(5)
C(9)-N(1)-C(1)-C(2)	177.6(3)	N(1)-C(1)-C(2)-C(3)		0.1(6)
N(1)-C(1)-C(2)-C(6)	177.4(3)	C(1)-C(2)-C(6)-C(7)		2.8(5)
C(11)-N(2)-C(7)-C(6)	1.4(5)	C(10)-N(2)-C(7)-C(6)		176.3(3)
C(5)-C(6)-C(7)-N(2)	-0.8(6)			
D-H...A	d(D-H)	d(H...A)	d(D...A)	<(DHA)
C(1)-H(1)...Cl(1)	0.95	2.76	3.690(3)	166.6
C(7)-H(7)...Cl(1)	0.95	2.76	3.691(3)	168.0

5.2.2 6-Aminofulvene-2-Aldimine Derivative Ligands

N,N'-disubstituted-6-aminofulvene-2-aldimine ligands [R_2AFA(H)] can be synthesised by refluxing an ethanolic solution of **41** with primary cycloalkyl or aromatic amines (R_2NH), according to Figure 5.10. The product can be extracted with hot hexane and purified with charcoal, whilst yellow or orange crystals suitable for X-ray diffraction were grown from concentrated hexane solution at room temperature.

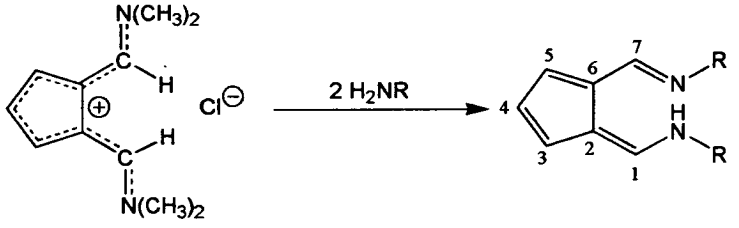

R: Cyclohexyl (42); Phenyl (43); 4-methylphenyl (44); 2,6-dimethylphenyl (45); 2,4,6-trimethylphenyl (46)

Figure 5.10 Synthesis of [R_2AFA(H)]: 42-46.

The synthesis and charactisation of five different 6-aminofulvene-2-aldimine derivatives (**42-46**) were carried out. NMR spectroscopy for all five ligands gave similar signals for the AFA base. The ^{1}H NMR spectra for the ligands show sharp downfield signals between δ 15.58 and 14.04 for the N-*H* atom. The sharp downfield peaks for N-*H* suggest high intramolecular hydrogen exchange with the other nitrogen atom (N-H···N), which is sterically favourable, according to Figure 5.11.

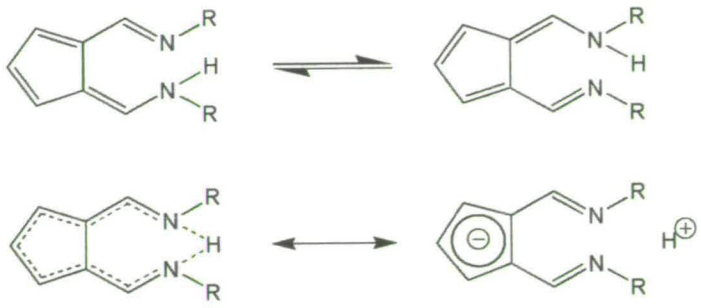

R: Cyclohexyl (42); Phenyl (43); 4-methylphenyl (44);
2,6-dimethylphenyl (45); 2,4,6-trimethylphenyl (46)

Figure 5.11 High intramolecular hydrogen exchange between nitrogen atoms for [R_2AFA(H)].

The X-ray crystal structures for the ligands (**42-46**) (Figure 5.12) reveal that the AFA bases are relatively planar, where the C-C and C-N bond lengths are situated between single and double bond distances [average distances of 1.453(5) and 1.293(5) Å, respectively]. The hydrogen bonds (N-H···N) are present for all the ligands synthesised, although for some ligands the hydrogen atoms bonded to the nitrogen atoms are located in disordered positions with occupancies of 0.5 over each nitrogen atom. These results confirm the sharp downfield peak for N-*H* in the ^{1}H NMR spectra obtained. More information for selected bond lengths and angles are shown in Tables 5.2-5.5.

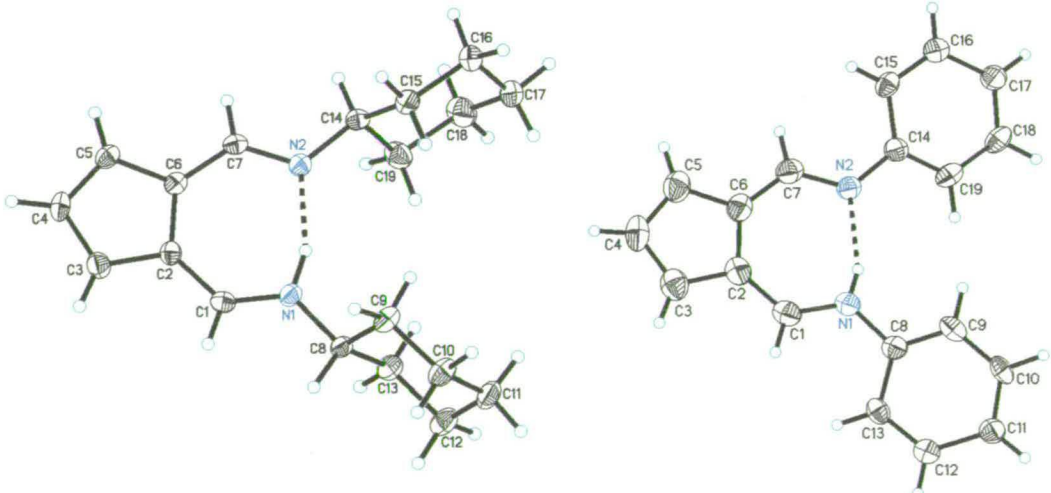

Figure 5.12 Crystallographic structure of: a) 42; b) 43.[2] Displacement ellipsoids are shown at the 50% probability level.

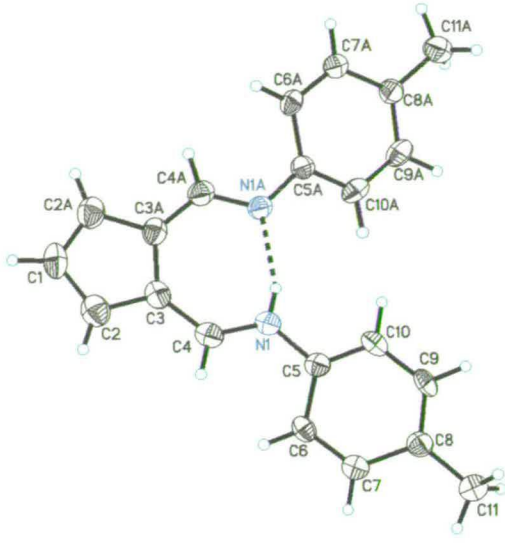

c

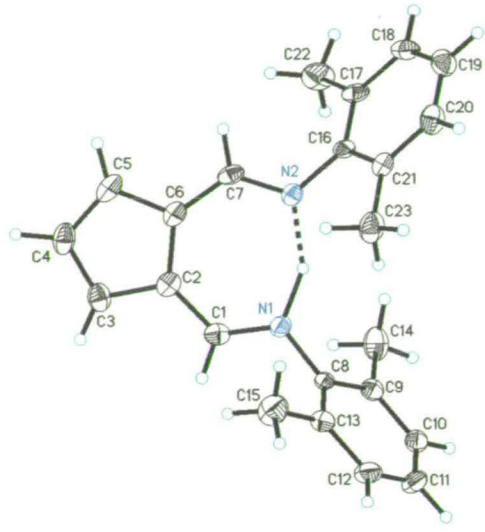

d

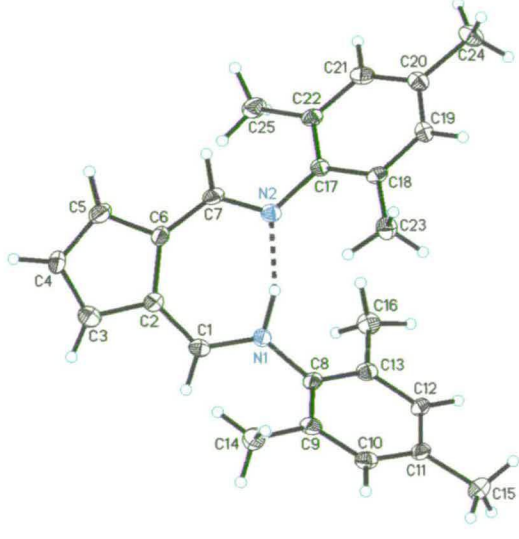

e

Figure 5.12 (Continued) Crystallographic structure of: c) 44; d) 45; e) 46. Displacement ellipsoids are shown at the 50% probability level.

Table 5.2 Selected bond distances (Å), angles and torsion (°) for 42.

N(1)-C(1)	1.303(2)	N(1)-C(8)	1.458(2)	N(2)-C(7)	1.291(2)
N(2)-C(14)	1.459(2)	C(1)-C(2)	1.403(2)	C(2)-C(3)	1.415(2)
C(2)-C(6)	1.450(2)	C(3)-C(4)	1.380(3)	C(4)-C(5)	1.401(3)
C(5)-C(6)	1.395(2)	C(6)-C(7)	1.427(2)	C(8)-C(13)	1.520(2)
C(8)-C(9)	1.526(3)	C(9)-C(10)	1.526(2)	C(10)-C(11)	1.518(3)
C(11)-C(12)	1.519(3)	C(12)-C(13)	1.530(3)	C(14)-C(19)	1.521(3)
C(14)-C(15)	1.522(3)	C(15)-C(16)	1.529(3)	C(16)-C(17)	1.518(3)
C(17)-C(18)	1.524(3)	C(18)-C(19)	1.525(3)		
C(1)-N(1)-C(8)		122.47(16)	C(7)-N(2)-C(14)		120.25(15)

N(1)-C(1)-C(2)	126.51(17)	C(1)-C(2)-C(3)		122.09(17)
C(5)-C(6)-C(7)	122.78(16)	C(5)-C(6)-C(2)		106.59(15)
N(2)-C(7)-C(6)	125.63(16)	C(8)-N(1)-C(1)-C(2)		175.12(17)
N(1)-C(1)-C(2)-C(3)	-178.02(18)	C(1)-C(2)-C(6)-C(7)		2.8(3)
C(14)-N(2)-C(7)-C(6)	-179.76(16)	C(5)-C(6)-C(7)-N(2)		175.68(17)
D-H...A	d(D-H)	d(H...A)	d(D...A)	<(DHA)
N(1)-H(1N)...N(2)	0.97(3)	1.78(3)	2.712(2)	160(2)

Table 5.3 Selected bond distances (Å), angles and torsion (°) for 44. Symmetry transformations used to generate equivalent atoms: $^{\#1}$ -x+3/2,-y+1/2,z.

N(1)-C(4)	1.308(4)	N(1)-C(5)	1.418(4)	C(1)-C(2)	1.387(4)
C(1)-C(2)$^{\#1}$	1.387(4)	C(2)-C(3)	1.412(4)	C(3)-C(4)	1.405(4)
C(3)-C(3)$^{\#1}$	1.452(6)	C(5)-C(10)	1.304(7)	C(5)-C(6)	1.432(6)
C(6)-C(7)	1.386(7)	C(7)-C(8)	1.471(6)	C(8)-C(9)	1.374(8)
C(8)-C(11)	1.508(4)	C(9)-C(10)	1.395(10)	C(6A)-C(7A)	1.382(7)
C(9A)-C(10A)	1.381(10)				
C(4)-N(1)-C(5)		123.3(3)	C(2)-C(1)-C(2)$^{\#1}$		107.7(4)
C(1)-C(2)-C(3)		110.0(3)	C(4)-C(3)-C(2)		122.7(3)
C(4)-C(3)-C(3)$^{\#1}$		131.04(17)	C(2)-C(3)-C(3)$^{\#1}$		106.18(19)
N(1)-C(4)-C(3)		126.3(3)	C(10)-C(5)-N(1)		118.0(4)
C(10)-C(5)-C(6)		122.1(4)	N(1)-C(5)-C(6)		119.5(3)
C(7)-C(6)-C(5)		116.4(5)	C(6)-C(7)-C(8)		122.8(5)
C(9)-C(8)-C(7)		113.4(4)	C(9)-C(8)-C(11)		125.4(4)
C(7)-C(8)-C(11)		120.6(3)	C(8)-C(9)-C(10)		123.7(6)
C(5)-C(10)-C(9)		120.6(6)	C(5)-N(1)-C(4)-C(3)		176.4(3)
C(2)-C(3)-C(4)-N(1)		-178.4(3)	C(3)$^{\#1}$-C(3)-C(4)-N(1)		-1.9(6)
D-H...A		d(D-H)	d(H...A)	d(D...A)	<(DHA)
N(1)-H(1N)...N(2)		0.97(3)	1.78(3)	2.712(2)	160(2)

Table 5.4 Selected bond distances (Å), angles and torsion (°) for 45.

C(1)-N(1)	1.306(5)	C(1)-C(2)	1.389(5)	C(2)-C(3)	1.418(5)
C(2)-C(6)	1.453(5)	C(3)-C(4)	1.364(6)	C(4)-C(5)	1.400(5)
C(5)-C(6)	1.401(5)	C(6)-C(7)	1.412(5)	C(7)-N(2)	1.293(5)
C(8)-C(9)	1.384(6)	C(8)-C(13)	1.407(5)	C(9)-C(10)	1.388(6)
C(9)-C(14)	1.502(6)	C(10)-C(11)	1.372(6)	C(11)-C(12)	1.368(6)
C(12)-C(13)	1.393(6)	C(13)-C(15)	1.491(6)	C(16)-C(17)	1.394(6)
C(16)-C(21)	1.396(5)	C(16)-N(2)	1.425(5)	C(17)-C(18)	1.393(6)
C(17)-C(22)	1.507(6)	C(18)-C(19)	1.371(7)	C(19)-C(20)	1.371(6)
C(20)-C(21)	1.383(5)	C(21)-C(23)	1.502(6)		
N(1)-C(1)-C(2)		128.3(4)	C(1)-C(2)-C(3)		122.9(4)
C(1)-C(2)-C(6)		131.0(4)	C(5)-C(6)-C(7)		122.9(4)
C(7)-C(6)-C(2)		130.5(4)	N(2)-C(7)-C(6)		125.7(4)
N(1)-C(1)-C(2)-C(3)		176.9(4)	C(1)-C(2)-C(6)-C(7)		-3.7(7)
C(5)-C(6)-C(7)-N(2)		-178.0(4)	C(2)-C(6)-C(7)-N(2)		-1.6(7)
D-H...A		d(D-H)	D(H...A)	d(D...A)	<(DHA)
N(1)-H(1N)...N(2)		0.97(3)	1.78(3)	2.712(2)	160(2)

Table 5.5 Selected bond distances (Å), angles and torsion (°) for 46.

N(1)-C(1)	1.327(4)	N(1)-C(8)	1.423(4)	N(2)-C(7)	1.287(4)
N(2)-C(17)	1.420(4)	C(1)-C(2)	1.400(4)	C(2)-C(3)	1.418(4)

C(2)-C(6)	1.451(4)	C(3)-C(4)	1.386(4)	C(4)-C(5)	1.403(4)
C(5)-C(6)	1.393(4)	C(6)-C(7)	1.428(4)	C(8)-C(9)	1.388(4)
C(8)-C(13)	1.402(4)	C(9)-C(10)	1.401(5)	C(9)-C(14)	1.511(4)
C(10)-C(11)	1.379(4)	C(11)-C(12)	1.383(4)	C(11)-C(15)	1.502(5)
C(12)-C(13)	1.395(4)	C(13)-C(16)	1.505(4)	C(17)-C(22)	1.406(4)
C(17)-C(18)	1.409(4)	C(18)-C(19)	1.382(4)	C(18)-C(23)	1.499(4)
C(19)-C(20)	1.386(4)	C(20)-C(21)	1.391(4)	C(20)-C(24)	1.499(4)
C(21)-C(22)	1.402(4)	C(22)-C(25)	1.503(5)		
C(1)-N(1)-C(8)		127.0(3)	C(7)-N(2)-C(17)		119.1(3)
N(1)-C(1)-C(2)		124.9(3)	C(1)-C(2)-C(3)		122.0(3)
C(5)-C(6)-C(7)		121.8(3)	C(7)-C(6)-C(2)		131.7(3)
N(1)-C(1)-C(2)-C(3)		-175.2(3)	C(8)-N(1)-C(1)-C(2)		164.6(3)
C(1)-C(2)-C(6)-C(7)		7.3(5)	C(17)-N(2)-C(7)-C(6)		176.7(3)
C(5)-C(6)-C(7)-N(2)		-177.9(3)	N(1)-C(1)-C(2)-C(6)		-3.3(5)
D-H...A		d(D-H)	d(H...A)	d(D...A)	<(DHA)
N(1)-H(1N)...N(2)		1.06(4)	1.68(4)	2.715(3)	162(3)

Although five ligands were prepared, only two of them showed reactivity with the Grignard reagent used. The synthesis of *N,N'*-diaryl-6-aminofulven-aldimine ligands involve very complicated steps; the reactions are light- and to some degree air-sensitive. The yield during the reaction can drop dramatically from 60% to 10% when the bulk of the substituent on the nitrogen atoms is changed. The ligands used are those for which the best yields were obtained.

Although reactions between [R_2AFA(H)] and equivalent amount of ^{n}BuLi were tested under different conditions in order to produce the complex [{R_2AFA}Li] no reactions occurred according to NMR spectroscopy. The use of an equimolar amount of MeLi, however, produces the expected removal proton and the lithiated complex, according to NMR spectroscopy.

5.2.3 Reactivity of Lithium N,N'-Diphenyl-6-Aminofulvene-2-Aldiminate with MeMgCl

Treatment of **43** in toluene with an equimolar amount of MeLi in toluene at – 78 °C was carried out, and the lithiated compound was further treated with an equimolar amount of MeMgCl. The suspension was filtered, the solvent concentrated and kept at – 20 °C to provide yellow crystals of the bischelate [(Ph_2AFA)$_2$Mg] (**47**) (Figure 5.13). Satisfactory NMR spectra were obtained, but the reactivity of the sample did not allow determination of mass spectra and elemental analysis. The ^{1}H NMR spectrum for **47** does not show the sharp downfield signal at δ 15.58 for the N-

H, whilst the singlet for H1/H7 is placed at δ 8.18 (Figure 5.14). In addition, the aromatic phenyl hydrogen resonances range from δ 7.33 to 7.12, but H3/H5 and H4 are found as a doublet at δ 6.96 and a triplet at δ 6.38, respectively. The ^{13}C NMR spectrum shows a downfield peak at δ 151.3 for the carbon atoms bonded to the nitrogen atoms (C1/C7), whilst C3/C5, C2/C6 and C4 are also placed at downfield chemical shifts of δ 134.0, 121.7 and 120.8, respectively (Figure 5.15). The aromatic phenyl carbon resonances, however, range between δ 144.8 and 119.0.

Two mechanisms have been suggested in order to interpret the result. Firstly, the monochelate of [(AFA)Mg(R)] reacts quickly with an unreacted ligand present to provide **47**. Secondly, the Schlenk equilibrium (Chapter 2) is possible, producing $MgCl_2$ which can react with two equivalents of [(AFA)Li] to provide the final product **47**, according to Figure 5.13.

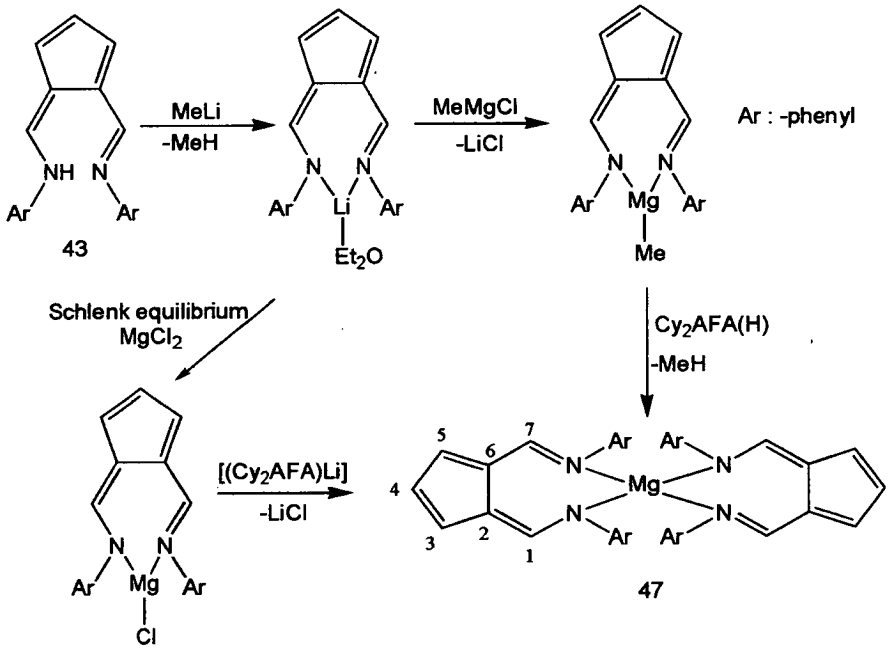

Figure 5.13 Reactivity of 43 with MeMgCl to produce 47.

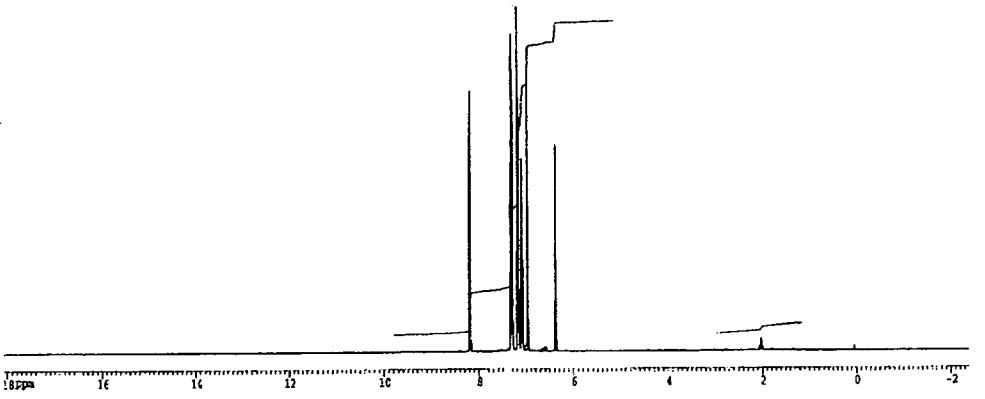

Figure 5.14 ^{1}H NMR spectrum in toluene-d_8 of 47.

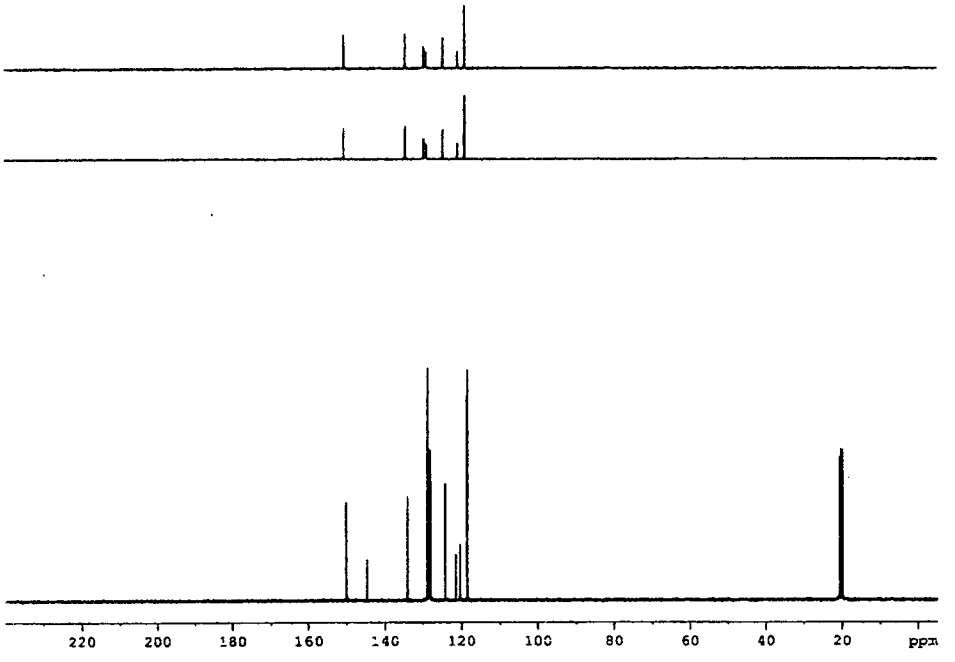

Figure 5.15 ^{13}C NMR spectrum in toluene-d_8 of 47.

The X-ray crystal structure of **47** (Figure 5.16) reveals a distorted tetrahedral magnesium atom centre, where the N-Mg-N angles range from 102.42(10) to 118.65(10)°. The two AFA ligands are almost orthogonal to one another, whilst the coplanarity of each ligand shows a high degree of π-resonance delocalization effect with N-C [range 1.302(3) to 1.309(3) Å] and C-C [range 1.380(3) to 1.458(4) Å] bond lengths. In addition to the planarity of each ligand, the magnesium atom is

located on average 0.15 Å out of plane. The Mg-N bond lengths [2.043(2), 2.044(2), 2.043(3) and 2.044(2) Å] in **47** are relatively shorter than the distances reported by Etkin *et al.*[9] [2.055(2) and 2.046(2) Å] for [{1,2-$C_5H_3(PhCNH)_2$}Mg(Cp)NCPh]. In addition, the Mg-N bond lengths in **47** are typical of σ-bonding interactions, and those distances are comparable to the bischelate magnesium complexes of [Mg{η^2-(^{i}Pr$_2$)ATI}$_2$] [(^{i}Pr$_2$)ATI = *N,N'*-diisopropylamino-troponiminate)[12a] (average distance of 2.048 Å)] and [{HC(C(Ph)=N(Bu^t)$_2$}$_2$Mg][13] (average value of 2.082 Å). Selected details of bond distances and angles are given in Table 5.6.

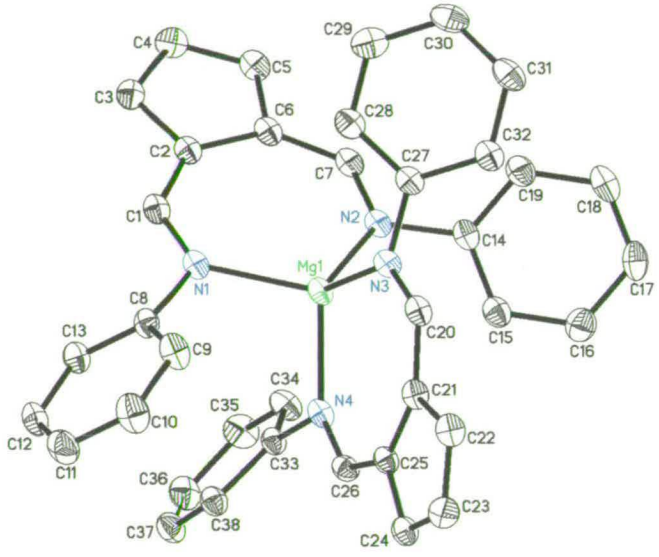

Figure 5.16 Crystallographic structure of 47. Displacement ellipsoids are shown at the 50% probability level.

Table 5.6 Selected bond distances (Å), angles and torsion (°) for 47.

C(1)-N(1)	1.309(3)	C(1)-C(2)	1.404(4)	C(2)-C(3)	1.414(4)
C(2)-C(6)	1.458(4)	C(3)-C(4)	1.390(4)	C(4)-C(5)	1.386(4)
C(5)-C(6)	1.408(4)	C(6)-C(7)	1.405(4)	C(7)-N(2)	1.302(3)
C(8)-N(1)	1.427(3)	C(14)-N(2)	1.431(3)	C(20)-N(3)	1.309(3)
C(20)-C(21)	1.400(4)	C(21)-C(22)	1.414(4)	C(21)-C(25)	1.450(4)
C(22)-C(23)	1.380(4)	C(23)-C(24)	1.390(4)	C(24)-C(25)	1.410(4)
C(25)-C(26)	1.412(4)	C(26)-N(4)	1.306(3)	C(27)-N(3)	1.430(3)
C(33)-N(4)	1.430(4)	N(1)-Mg(1)	2.043(2)	N(2)-Mg(1)	2.044(2)
N(3)-Mg(1)	2.043(3)	N(4)-Mg(1)	2.044(2)		
N(1)-Mg(1)-N(2)		107.60(10)	N(1)-Mg(1)-N(3)		118.65(10)
N(1)-Mg(1)-N(4)		102.70(10)	N(2)-Mg(1)-N(4)		118.57(10)
N(3)-Mg(1)-N(2)		102.42(10)	N(3)-Mg(1)-N(4)		107.74(10)
N(1)-C(1)-C(2)		129.8(3)	C(1)-C(2)-C(3)		118.0(3)
C(7)-C(6)-C(5)		117.7(2)	N(2)-C(7)-C(6)		129.9(2)
N(3)-C(20)-C(21)		130.2(3)	C(20)-C(21)-C(22)		118.2(3)
C(24)-C(25)-C(26)		117.5(2)	N(4)-C(26)-C(25)		129.9(3)

C(1)-N(1)-C(8)	117.5(2)	C(1)-N(1)-Mg(1)	129.77(18)
C(7)-N(2)-Mg(1)	129.77(19)	C(7)-N(2)-C(14)	116.9(2)
C(20)-N(3)-Mg(1)	129.66(19)	C(26)-N(4)-Mg(1)	129.5(2)
C(20)-N(3)-C(27)	116.4(2)	C(26)-N(4)-C(33)	115.9(2)
C(2)-C(1)-N(1)-Mg(1)	-1.2(4)	C(6)-C(7)-N(2)-Mg(1)	-8.7(5)
C(21)-C(20)-N(3)-Mg(1)	-0.5(4)	C(25)-C(26)-N(4)-Mg(1)	-5.8(4)

5.2.4 Reactivity of N,N'-Dicyclohexyl-6-Aminofulvene-2-Aldimine with Me_2Mg

A solution of **42** in benzene was refluxed with an equimolar amount of Me_2Mg (**48**), according to Figure 5.17. The solvent was removed under *vacuum* to provide the bischelate [$(Cy_2AFA)_2Mg$] (**49**) as a yellow solid, whilst crystals suitable for X-ray analysis were grown from a concentrated toluene solution at –20 °C. Satisfactory NMR spectra were recorded, but the reactivity of the sample did not allow mass spectra and elemental analysis to be obtained. The ^1H NMR spectrum for the complex **49** does not show the sharp downfield signal at δ 14.04 for the N-*H*, whilst a singlet for H1/H7 is placed at δ 7.74 (Figure 5.18). The H3/H5 and H4 are found as a doublet at δ 7.57 and a triplet at δ 6.29, respectively. The *ipso*-hydrogen atoms are located as multiplet signals upfield of δ 3.52, whilst the cyclohexyl hydrogen resonances are located between δ 1.83 and 0.21. The ^{13}C NMR spectrum shows a downfield peak at δ 158.2 for the carbon atoms bonded to the nitrogen atoms (C1/C7), whilst C3/C5, C2/C6 and C4 are also placed at downfield chemical shifts of δ 136.7, 118.8 and 116.3, respectively (Figure 5.19). The *ipso*-carbon atoms are assigned at δ 58.7, however, whilst the remaining cyclohexyl carbon resonances range between δ 31.8 to 26.6, respectively.

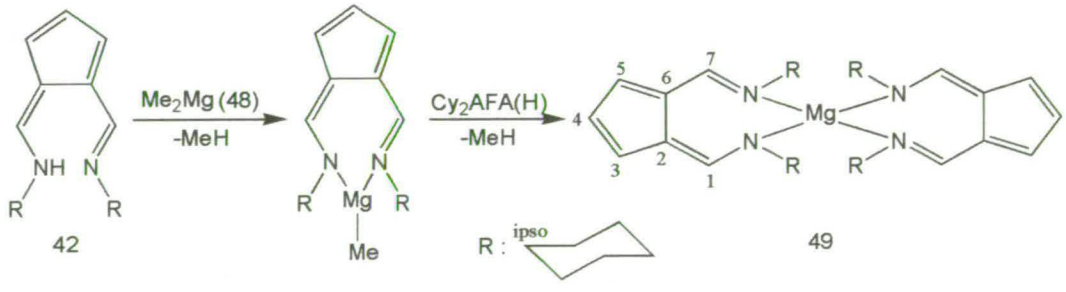

Figure 5.17 Reactivity of 42 with 48 to produce 49.

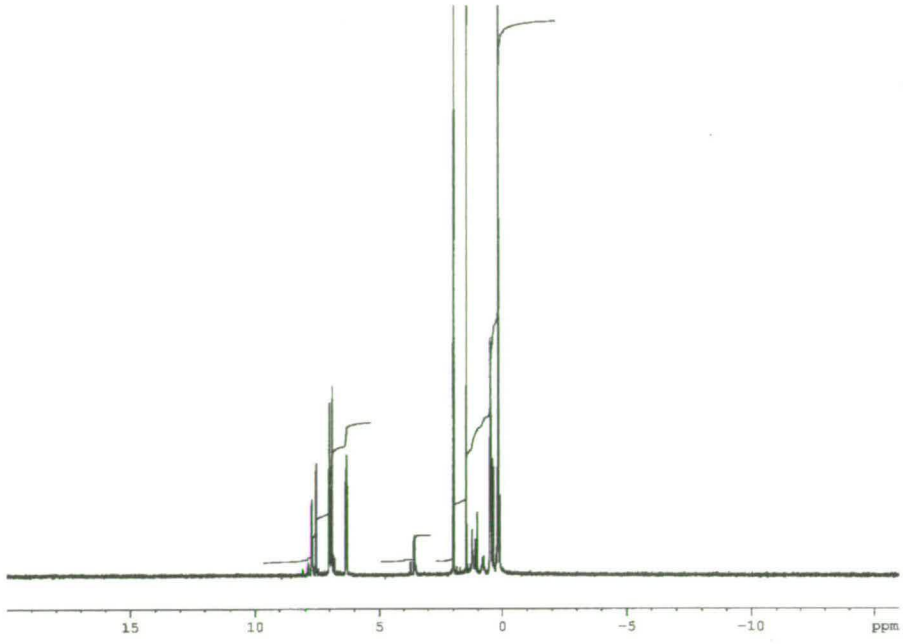

Figure 5.18 ^{1}H NMR spectrum in toluene-d_8 of 51.

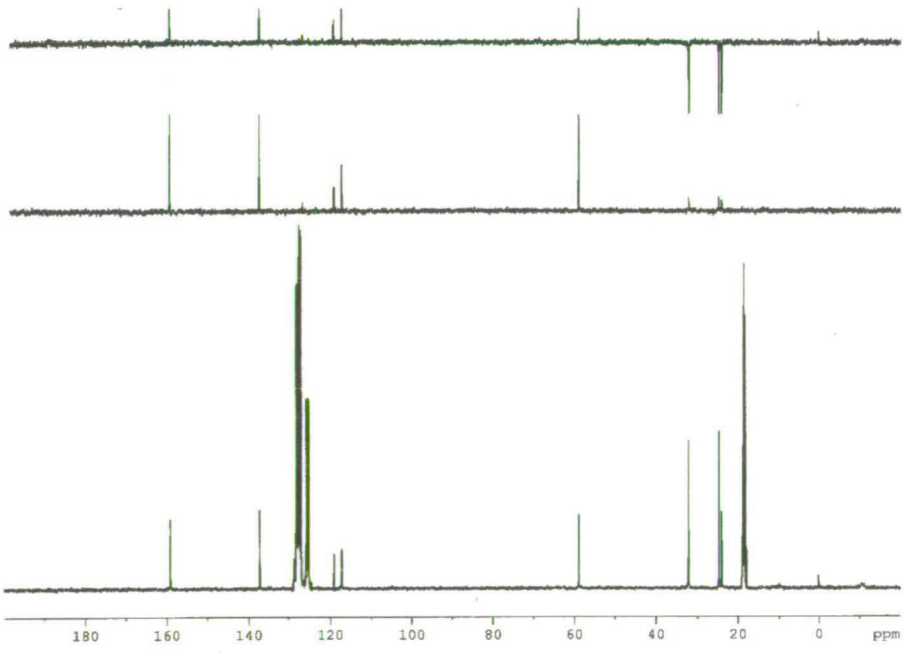

Figure 5.19 ^{13}C NMR spectrum in toluene-d_8 of 51.

X-ray crystallography of **49** was conducted revealing a structure containing a distorted tetrahedral magnesium centre with similar geometrical parameters to **47**. The N-Mg-N angles range from 102.42(10) to 118.65(10)°. The planarity of each

ligand shows that there is a degree of π-delocalization, but the large size of Mg cannot fit between the two N-atoms which means that Mg atom sits out of the plane at average distance of 0.16 Å. The two ligands are found almost orthogonal to one another, where the N-C bond lengths range from 1.302(3) to 1.309(3) Å and C-C bond lengths range from 1.380(3) to 1.458(4) Å. In addition, the Mg-N bond lengths [2.043(2), 2.044(2), 2.043(3) and 2.044(2) Å] are equal to those distances in **47**, and obviously shorter than the distances reported by Etkin *et al.*[9] [2.055(2) and 2.046(2) Å] for [{C_5H_3-1,2-(PhCNH)$_2$}Mg(Cp)NCPh]. Similar distances are comparable with those of the bischelate magnesium complex of [Mg{η^2-(^{i}Pr$_2$)ATI]$_2$] [(^{i}Pr$_2$)ATI = *N,N'*-diisopropylamino-troponiminate)][12a] (average distance of 2.048 Å). Selected bond lengths and angles are given in Table 5.7.

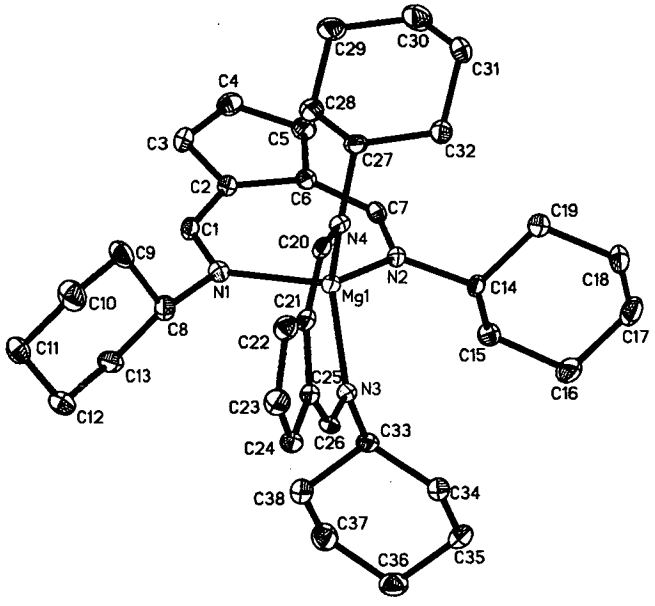

Figure 5.20 Crystallographic structure of 49. Displacement ellipsoids are shown at the 50% probability level.

Table 5.7 Selected bond distances (Å), angles and torsion (°) for 49.

C(1)-N(1)	1.309(3)	C(1)-C(2)	1.404(4)	C(2)-C(3)	1.414(4)
C(2)-C(6)	1.458(4)	C(3)-C(4)	1.390(4)	C(4)-C(5)	1.386(4)
C(5)-C(6)	1.408(4)	C(6)-C(7)	1.405(4)	C(7)-N(2)	1.302(3)
C(8)-N(1)	1.427(3)	C(14)-N(2)	1.431(3)	C(20)-N(3)	1.309(3)
C(20)-C(21)	1.400(4)	C(21)-C(22)	1.414(4)	C(21)-C(25)	1.450(4)
C(22)-C(23)	1.380(4)	C(23)-C(24)	1.390(4)	C(24)-C(25)	1.410(4)
C(25)-C(26)	1.412(4)	C(26)-N(4)	1.306(3)	C(27)-N(3)	1.430(3)
C(33)-N(4)	1.430(4)	N(1)-Mg(1)	2.043(2)	N(2)-Mg(1)	2.044(2)
N(3)-Mg(1)	2.043(3)	N(4)-Mg(1)	2.044(2)		

N(1)-Mg(1)-N(2)	107.60(10)	N(1)-Mg(1)-N(3)	118.65(10)
N(1)-Mg(1)-N(4)	102.70(10)	N(2)-Mg(1)-N(4)	118.57(10)
N(3)-Mg(1)-N(2)	102.42(10)	N(3)-Mg(1)-N(4)	107.74(10)
N(1)-C(1)-C(2)	129.8(3)	C(1)-C(2)-C(3)	118.0(3)
C(7)-C(6)-C(5)	117.7(2)	N(2)-C(7)-C(6)	129.9(2)
N(3)-C(20)-C(21)	130.2(3)	C(20)-C(21)-C(22)	118.2(3)
C(24)-C(25)-C(26)	117.5(2)	N(4)-C(26)-C(25)	129.9(3)
C(1)-N(1)-C(8)	117.5(2)	C(1)-N(1)-Mg(1)	129.77(18)
C(7)-N(2)-Mg(1)	129.77(19)	C(7)-N(2)-C(14)	116.9(2)
C(20)-N(3)-Mg(1)	129.66(19)	C(26)-N(4)-Mg(1)	129.5(2)
C(20)-N(3)-C(27)	116.4(2)	C(26)-N(4)-C(33)	115.9(2)
C(2)-C(1)-N(1)-Mg(1)	-1.2(4)	C(6)-C(7)-N(2)-Mg(1)	-8.7(5)
C(21)-C(20)-N(3)-Mg(1)	-0.5(4)	C(25)-C(26)-N(4)-Mg(1)	-5.8(4)

5.2.5 Reactivity of Lithium N,N'-Dicyclohexyl-6-Aminofulvene-2-Aldiminate with MeMgCl in Et_2O

A solution of **42** in diethyl ether was treated with an equimolar amount of MeLi at –78 °C and the lithiated compound was further treated with an equimolar amount of MeMgCl (Figure 5.21). The suspension was filtered, and the solvent and volatile components removed under *vacuum* to provide a yellow solid of [(Cy_2AFA)Mg(Cl)Et_2O] (**50**). Crystals suitable for X-ray analysis were grown from a toluene solution at –20 °C. Satisfactory NMR spectra were recorded, but the reactivity of the sample did not allow mass spectra and elemental analysis to be obtained. The characteristic resonance of a methyl group bonded to the magnesium atom was not observed, whilst signals of Et_2O solvated were detected by NMR spectra. The X-ray crystallographic structure, however, revealed a simple dissociation of the Grignard reagent by the Schlenk equilibrium had occurred, and the formation of a three-coordinate magnesium complex was obtained as shown in Figure 5.21.

The ^{1}H NMR spectrum of **50** shows a singlet for H1/H7 at δ 7.71 (Figure 5.22). The H3/H5 and H4 resonances are found as a doublet at δ 7.19 and a triplet at δ 6.89, respectively. The resonances of the *ipso*-hydrogen atoms is shifted upfield to δ 2.87, whilst the cyclohexyl hydrogen resonances are located between δ 2.23 and 1.18. An upfield quartet signal is observed at δ 3.45 which, after the integration, is equivalent to four hydrogen atoms, whilst six hydrogen resonances are also located between δ 2.23 and 1.18, indicating the presence of Et_2O solvate. The ^{13}C NMR spectrum shows a downfield peak at δ 154.8 for the carbon atoms bonded to the

nitrogen atoms (C1/C7), whilst C3/C5, C2/C6 and C4 are placed downfield at chemical shifts of δ 138.0, 121.1 and 118.5, respectively (Figure 5.23). The ^{13}C NMR spectrum gives two sets of signals at δ 48.10 and 19.2, which are assigned to the Et_2O solvated. Finally, the *ipso*-carbon atoms are assigned at δ 63.8, whilst the remaining cyclohexyl carbon resonances range between δ 35.49 and 25.44, respectively.

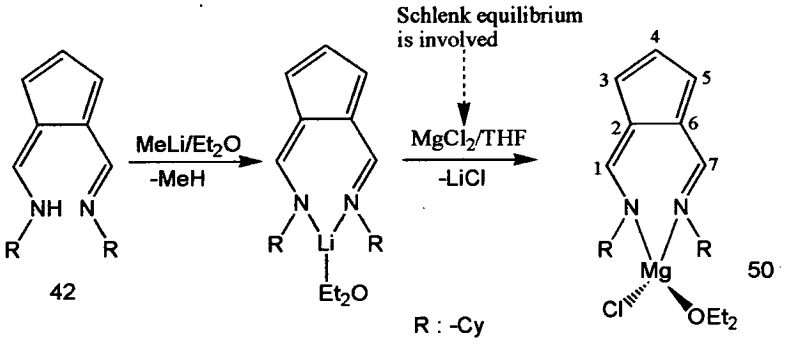

Figure 5.21 Reactivity of [{Cy_2AFA}Li] with MeMgCl to produce 50. The Schlenk equilibrium is involved.

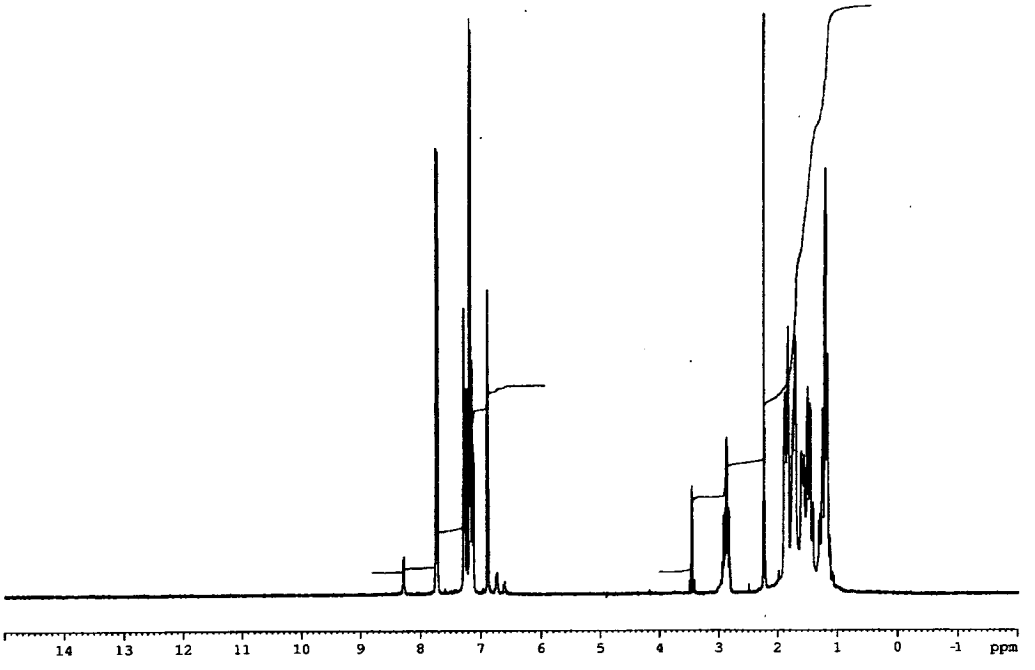

Figure 5.22 ^1H NMR spectrum in benzene-d_6 of 50.

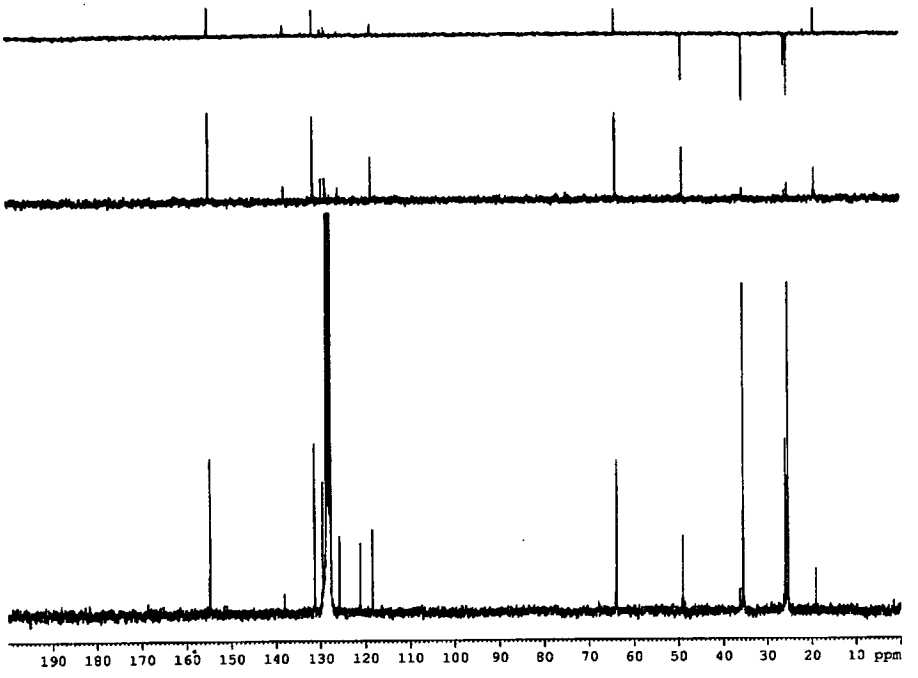

Figure 5.23 ^{13}C NMR spectrum in benzene-d_6 of 50.

The X-ray crystal structure of **50** shows the geometry of the magnesium atom to be approximately tetrahedral, where the two nitrogen atoms from the Cy_2AFA ligand are chelating the Mg atom, whilst the third and fourth co-ordination sites are occupied by a terminal chloride ligand and one Et_2O molecule (Figure 5.24). Within the Cy_2AFA ligand, the cylopentadienyl ring and the CN moieties are essentially planar, whilst the magnesium atom is situated 0.16 Å out of this plane. The L-Mg-L angles range from 102.06(9) to 117.23(8)° revealing the effect of the steric bulk of the co-ordinated ether and the cyclohexyl groups to prevent the co-ordination of an additional ligand. The cyclohexyl groups on the nitrogen atoms are orientated such that the planes are approximately orthogonal to that of the cyclopentadienyl ring in the ligand. The C-N [1.293(3) and 1.297(3) Å, respectively] and C-C [range 1.381(4) to 1.449(4) Å] bond lengths are found between those for single and double C-N and C-C bonds, and the distances are related to previous structures (Figure 5.9, 5.12, 5.16 and 5.20). The Mg-N bond lengths [2.080(2) and 2.087(2) Å] are typical of σ-bonding, but they are slightly larger than those seen in **47**, **49** and the distances reported by Etkin *et al.*[9] [2.055(2) and 2.046(2) Å] for [{C_5H_3-1,2-$(PhCNH)_2$}Mg(Cp)NCPh]. The Mg-O distance is 2.058(2) Å, whilst the Mg-Cl

distance of 2.3252(12) Å agrees well with other reported distances.[14] Selected bond lengths and angles are given in Table 5.8.

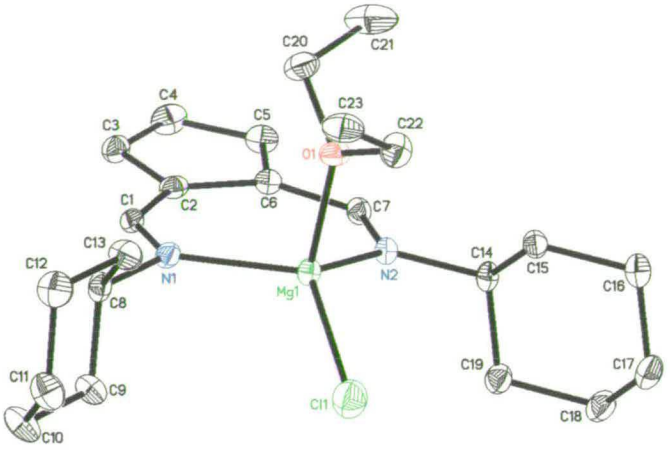

Figure 5.24 Crystallographic structure of 50. Displacement ellipsoids are shown at the 50% probability level.

Table 5.8 Selected bond distances (Å), angles and torsion (°) for 50.

C(1)-N(1)	1.293(3)	C(1)-C(2)	1.409(4)	C(2)-C(3)	1.410(4)
C(2)-C(6)	1.449(4)	C(3)-C(4)	1.381(4)	C(4)-C(5)	1.389(4)
C(5)-C(6)	1.406(4)	C(6)-C(7)	1.415(4)	C(7)-N(2)	1.297(3)
C(8)-N(1)	1.472(3)	C(8)-C(9)	1.516(4)	C(8)-C(13)	1.523(4)
C(9)-C(10)	1.522(4)	C(10)-C(11)	1.513(4)	C(11)-C(12)	1.506(5)
C(12)-C(13)	1.524(4)	C(14)-N(2)	1.476(3)	C(14)-C(15)	1.522(4)
C(14)-C(19)	1.525(4)	C(15)-C(16)	1.518(4)	C(16)-C(17)	1.511(4)
C(17)-C(18)	1.522(4)	C(18)-C(19)	1.520(4)	C(20)-O(1)	1.443(3)
C(20)-C(21)	1.487(5)	C(22)-O(1)	1.443(3)	C(22)-C(23)	1.501(4)
N(1)-Mg(1)	2.087(2)	N(2)-Mg(1)	2.080(2)	Mg(1)-Cl(1)	2.3252(12)
O(1)-Mg(1)	2.058(2)				
N(1)-C(1)-C(2)		131.4(2)	C(1)-C(2)-C(3)		118.5(2)
C(5)-C(6)-C(7)		117.3(2)	C(7)-C(6)-C(2)		135.9(2)
N(2)-C(7)-C(6)		131.0(2)	O(1)-C(20)-C(21)		113.4(3)
O(1)-C(22)-C(23)		112.8(2)	C(1)-N(1)-C(8)		115.1(2)
C(1)-N(1)-Mg(1)		128.51(18)	C(7)-N(2)-C(14)		114.7(2)
C(7)-N(2)-Mg(1)		128.18(17)	C(20)-O(1)-C(22)		115.1(2)
C(20)-O(1)-Mg(1)		121.93(17)	C(22)-O(1)-Mg(1)		122.54(17)
O(1)-Mg(1)-N(2)		102.06(9)	O(1)-Mg(1)-N(1)		100.70(9)
N(2)-Mg(1)-N(1)		106.94(9)	O(1)-Mg(1)-Cl(1)		111.32(7)
N(2)-Mg(1)-Cl(1)		116.43(7)	N(1)-Mg(1)-Cl(1)		117.23(8)
C(2)-C(1)-N(1)-Mg(1)		2.9(4)	C(6)-C(7)-N(2)-Mg(1)		-9.8(4)

5.2.6 Reactivity of N,N'-dicyclohexyl-6-aminofulvene-2-aldimine with MeMgBr in Toluene

A solution of **42** in toluene was refluxed with an equimolar amount of MeMgBr, and the solvent and volatiles were removed under *vacuum* to provide a yellow solid identified as [{(Cy_2AFA)MgBr}$_2$] (**51**) (Figure 5.25). Yellow crystals were obtained from a concentrated solution of **51** in toluene at –5 °C. Satisfactory NMR spectra were obtained, but the reactivity of the sample did not allow determination of mass spectra and elemental analysis. The ^{1}H NMR spectrum of **51** is significantly more complex than that for **50** indicating the presence of two Cy_2AFA ligands in different environments. Two singlets for H1/H7 are placed at δ 7.34 and 7.32. The resonances of H3/H5 are found as two doublets at δ 6.86 and 6.71, whilst two triplets are located at δ 6.74 and 6.40, which are assigned to H4. The *ipso*-hydrogen atoms are shifted upfield to δ 1.85, whilst the remaining cyclohexyl hydrogen resonances could be located between δ 1.70 and 0.70. The ^{13}C NMR spectrum shows a downfield peak at δ 157.20 for the carbon atoms bonded to the nitrogen atoms (C1/C7), whilst C3/C5, C2/C6 and C4 are also placed at downfield chemical shifts of δ 133.9, 124.2 and 121.0, respectively. Finally, the *ipso*-carbon atoms are assigned to δ 66.7, whilst the remaining cyclohexyl carbon resonances range between δ 38.1 and 28.1, respectively.

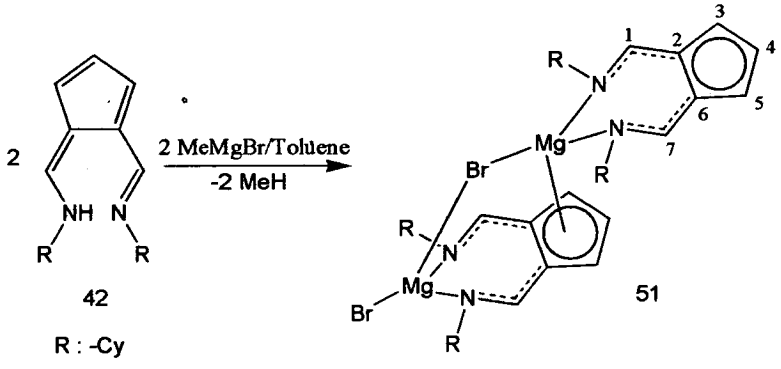

Figure 5.25 Reactivity of 42 with MeMgBr to produce 51.

The X-ray crystal structure of **51** reveals an asymmetric dimeric structure (Figure 5.26) in which one of the Cy_2AFA ligands is found in essentially the same environment as that in **50**, chelating one Mg ion through its two nitrogen donors. The

co-ordination sphere of this magnesium centre is completed by the symmetrical η^5-coordination of the cyclopentadienyl ring of a second Cy_2AFA ligand and a bromide ligand which bridges the two Mg centres in the molecule. The nitrogen atoms of this second ligand are also co-ordinated to Mg(1) whose fourth co-ordination site is occupied by a terminal bromide ligand. The symmetrical co-ordination of the C_5 ring to Mg(2) [Mg-C bond lengths range from 2.526(3) to 2.570(3) Å] and the C-C bond lengths supports an aromatic rather than a fulvene picture of the electronic structure, and thus the location of the negative charge within the C_5 ring being consistent with a cyclopentadienyldiimine description of the ligand rather than an amidofulvenealdimine (Figure 5.27).

Magnesium cyclopentadienyl complexes are relatively common, but the structure most closely related to **51** is that reported by Etkin *et al.*[9] of [{C_5H_3-1,2-$(PhCNH)_2$}Mg(Cp)NCPh], which was obtained from the reaction of magnesocene with benzonitrile. The structure [{C_5H_3-1,2-$(PhCNH)_2$}Mg(Cp)NCPh], provides an uncoordinated C_5 ring of the AFA ligand, whilst the magnesium atom co-ordination is completed by η^5-Cp and benzonitrile ligands, however, **51** is the first example of a complex in which the co-ordination of this part of the AFA ligand has been observed.

The N-Mg-N bite angles are 105.12(10) and 106.26(10)°, and the C-N bond lengths [range 1.280(3) to 1.297(3) Å] indicate that the C-N bonds are probably double bonds. In addition, the C-C bond lengths [range 1.385(4) to 1.463(4) Å] in the η^5-cyclopentadienyl ring show this to be aromatic thus indicating the location of a negative charge in this part of the ligand (Figure 5.27), and these distances are related to previous structures (Figure 5.9, 5.12, 5.16, 5.20, and 5.24). The Mg(1)-Br(2) distance is normal, being 2.4177(12) Å, whilst Mg(1)-[μ-Br(1)] is longer, 2.5710(13) Å. The Mg-(η^5-Cp) bond lengths [range 2.526(3) to 2.570(3) Å] are relatively longer than the similar interaction of 2.440 Å for [C_5H_3-1,2-$(C(Ph)NH)_2$)CpMg(NCPh)],[9] whilst Mg(2)-[μ-Br(1)] is 2.5912(12) Å. The planarity of the ligands show that there is a degree of π-delocalization, whilst the cyclohexanyl groups on the nitrogen atoms are orientated such that the planes are approximately orthogonal to that of the cyclopentadienyl ring in the ligand. The Mg(1)-N bond lengths [2.061(2) and 2.066(3) Å] are longer than the Mg(2)-N bond lengths [2.035(3) and 2.038(2) Å], and both of them are typical of σ-bonding. The Mg-N

distances, however, are shorter than in previous structures (Figures 5.9, 5.12, 5.16, 5.20 and 5.24) and also shorter than those found in the β-diketiminate system of $[HC(RCNAr')_2Mg(CH_3)THF]$ (Ar'=2,6-diisopropylphenyl; R=Me) [2.063(3) and 2.083(3) Å].[12b] Selected bond lengths and angles are given in Table 5.9.

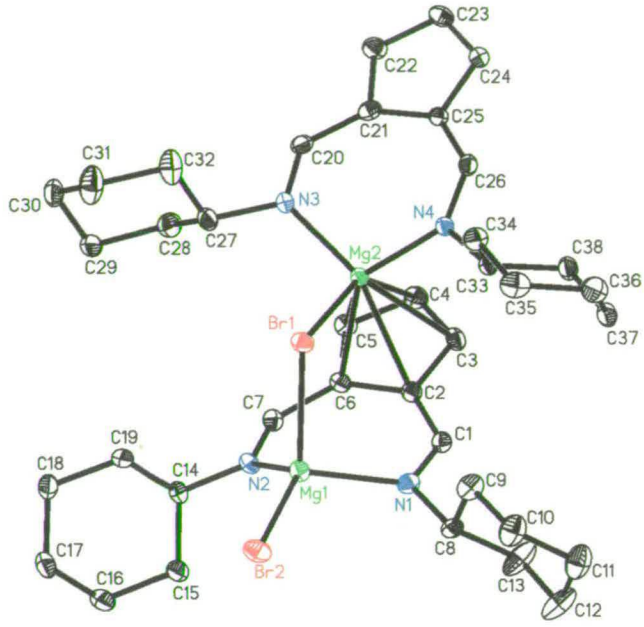

Figure 5.26 Crystallographic structure of 51. Displacement ellipsoids are shown at the 50% probability level.

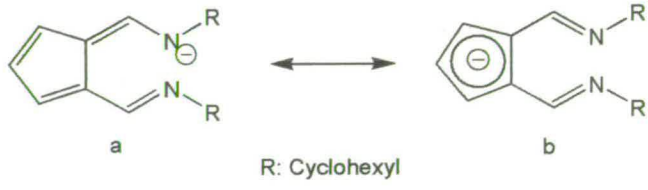

Figure 5.27 Resonance structures of R_2AFA: a).amidofulvenealdimine, b) cyclopentadienyldiimine.

Table 5.9 Selected bond distances (Å), angles and torsion (°) for 51. Symmetry transformations used to generate equivalent atoms: [#1] x,-y+1/2,z-1/2.

Br(1)-Mg(1)	2.5710(13)	Br(1)-Mg(2)	2.5912(12)	Br(2)-Mg(1)	2.4177(12)
Mg(1)-N(2)	2.061(2)	Mg(1)-N(1)	2.066(3)	N(1)-C(1)	1.280(3)
N(1)-C(8)	1.491(3)	N(2)-C(7)	1.282(3)	N(2)-C(14)	1.475(3)
C(1)-C(2)	1.439(4)	C(2)-C(3)	1.413(4)	C(2)-C(6)	1.451(4)
C(2)-Mg(2)	2.553(3)	C(3)-C(4)	1.393(4)	C(3)-Mg(2)	2.570(3)
C(4)-C(5)	1.398(4)	C(4)-Mg(2)	2.548(3)	C(5)-C(6)	1.410(4)
C(5)-Mg(2)	2.542(3)	C(6)-C(7)	1.442(4)	C(6)-Mg(2)	2.526(3)

Mg(2)-N(3)	2.035(3)	Mg(2)-N(4)	2.038(2)	N(3)-C(20)	1.296(4)
N(3)-C(27)	1.491(4)	N(4)-C(26)	1.297(3)	N(4)-C(33)	1.478(3)
C(20)-C(21)	1.412(4)	C(21)-C(22)	1.404(4)	C(21)-C(25)	1.463(4)
C(22)-C(23)	1.386(4)	C(23)-C(24)	1.385(4)	C(24)-C(25)	1.402(4)
C(25)-C(26)	1.413(4)	C(27)-C(28)	1.518(4)	C(27)-C(32)	1.521(5)
C(28)-C(29)	1.529(4)	C(29)-C(30)	1.505(5)	C(30)-C(31)	1.516(5)
C(31)-C(32)	1.531(4)	C(33)-C(34)	1.526(4)	C(33)-C(38)	1.531(4)
C(34)-C(35)	1.531(4)	C(35)-C(36)	1.524(5)	C(36)-C(37)	1.516(5)
C(37)-C(38)	1.521(4)				

Mg(1)-Br(1)-Mg(2)	104.50(4)	N(2)-Mg(1)-N(1)	105.12(10)
N(2)-Mg(1)-Br(2)	121.02(8)	N(1)-Mg(1)-Br(2)	113.40(8)
N(2)-Mg(1)-Br(1)	101.05(8)	N(1)-Mg(1)-Br(1)	98.82(8)
Br(2)-Mg(1)-Br(1)	114.50(4)	C(1)-N(1)-C(8)	118.3(2)
C(1)-N(1)-Mg(1)	122.0(2)	C(7)-N(2)-C(14)	115.2(2)
C(7)-N(2)-Mg(1)	119.53(19)	N(1)-C(1)-C(2)	128.2(3)
C(3)-C(2)-C(1)	119.8(3)	C(1)-C(2)-C(6)	134.1(3)
C(5)-C(6)-C(7)	118.2(3)	C(7)-C(6)-C(2)	134.8(3)
N(2)-C(7)-C(6)	130.1(3)	N(3)-Mg(2)-N(4)	106.26(10)
N(3)-Mg(2)-Br(1)	103.51(8)	N(4)-Mg(2)-Br(1)	102.24(7)
C(20)-N(3)-C(27)	116.8(2)	C(20)-N(3)-Mg(2)	122.4(2)
C(26)-N(4)-C(33)	118.1(2)	C(26)-N(4)-Mg(2)	124.28(19)
N(3)-C(20)-C(21)	129.7(3)	C(22)-C(21)-C(20)	118.9(3)
C(20)-C(21)-C(25)	134.1(3)	C(24)-C(25)-C(26)	119.3(3)
C(26)-C(25)-C(21)	134.9(3)	N(4)-C(26)-C(25)	130.4(3)
Mg(2)-Br(1)-Mg(1)-Br(2)	176.10(4)	Mg(1)-N(1)-C(1)-C(2)	-13.8(4)
Mg(1)-N(2)-C(7)-C(6)	13.4(4)	Mg(2)-N(3)-C(20)-C(21)	-21.4(4)
Mg(2)-N(4)-C(26)-C(25)	7.6(4)	Mg(2)-N(3)-C(27)-C(28)	-109.0(3)

D-H...A	d(D-H)	d(H...A)	D(D...A)	<(DHA)
C(7)-H(7)...Br(1)$^{\#1}$	0.95	2.84	3.686(3)	149.4

5.2.7 Reactivity of Lithium N,N'-Dicyclohexyl-6-Aminofulvene-2-Aldiminate with MeMgCl in Toluene

A solution of [{Cy_2AFA}Li] was produced by reacting equivalent amounts of **42** in toluene and MeLi at –78 °C. The solution was then treated with an equivalent amount of MeMgCl at room temperature, and the reaction mixture was stirred overnight. The suspension was filtered, the solution concentrated and stored at –5 °C to provide yellow crystals of complex [(Cy_2AFA)Mg(Me)THF] (**52**) (Figure 5.28). Satisfactory NMR spectra were recorded, but the reactivity of the sample did not allow determination of mass spectra and elemental analysis. The ^{1}H NMR spectrum of **52** contains an upfield signal at δ – 0.98 for the Mg bound methyl ligand. Other characteristic signals are an upfield quintet at δ 1.91 for the *ipso*-hydrogen atoms, whilst the remaining cyclohexyl hydrogen resonances could be located between δ 1.80 and 1.00. Moreover, a downfield singlet for H1/H7 is placed at δ 7.89, whilst

H3/H5 and H4 are found as a doublet at δ 6.66 and a triplet at δ 6.45, respectively. Finally, two upfield multiplet signals at δ 3.18 and 0.93 indicate the presence THF solvate. The ^{13}C NMR spectrum, however, shows a downfield peak at δ 162.8 for the carbon atoms bonded to the nitrogen atoms (C1/C7), whilst C3/C5, C2/C6 and C4 are also placed at downfield chemical shifts of δ 133.0, 115.9 and 113.8, respectively. Two sets of signals at δ 67.2 and 24.9 are assigned to the THF solvated, whilst the methyl carbon from the Mg-CH_3 is placed upfield at δ -10.6. Finally, the *ipso*-carbon resonances are assigned at δ 69.1, whilst the remaining cyclohexyl carbon resonances range between δ 33.1 and 23.9, respectively.

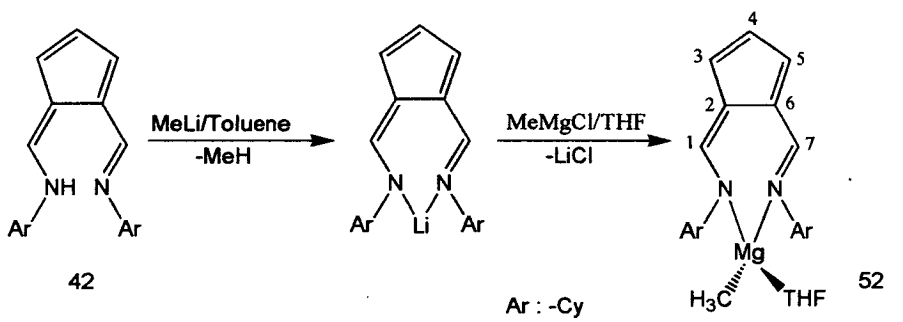

Figure 5.28 Reactivity of 42 with MeMgCl to produce 52.

The X-ray crystal structure of **52** reveals the co-ordination geometry of the magnesium atom to be approximately tetrahedral, where two nitrogen atoms from the Cy_2AFA ligand are chelating the magnesium atom, whilst the other sites are occupied by a terminal methyl carbon and one THF molecule (Figure 5.29). The Mg-C distance of 2.116(2) Å compares with values of 2.107(6) and 2.189(4) Å for the β-diketiminate complexes $[HC(RCNAr')_2Mg(CH_3)THF]$ (Ar'=2,6-diisopropylphenyl; R=^{t}Bu)[12b] The L-Mg-L angles range from 99.77(6) to 122.38(8)° revealing the effect of the steric bulk of the co-ordinated THF and the cyclohexyl groups to prevent the co-ordination of an additional ligand. The cyclohexyls group on the nitrogen atoms are orientated such that the planes are approximately orthogonal to that of the cyclopentadienyl ring in the ligand. The C-N [1.292(2) and 1.294(2) Å] and C-C bond lengths [range 1.378(3) to 1.447(3) Å] lie in between those for single and double C-N and C-C bonds, indicating that the co-ordinating ligand acts as a cyclopentadienyldiimine rather than an amidofulvenealdimine (Figure 5.27). The

cyclopentadienyl and imine portions of the Cy_2AFA ligand are coplanar but the magnesium centre is located 0.17 Å out of this plane. The Mg-N bond lengths [2.0821(16) and 2.0882(16) Å] are typical of σ-bonding, and the distances are longer than those found in the β-diketiminate system $[HC(RCNAr')_2Mg(CH_3)THF]$[12b] [2.063(3) and 2.083(3) Å]. The Mg-O distance is 2.0526(15) Å which is shorter than the value of 2.058(2) Å found in **50**. The THF molecule is disordered having two conformations with occupancies of 50% each [C2A-C3A, 50%; C2B-C3B, 50%]. Only the C2A-C3A conformation is shown in the structure plotted. Selected bond lengths and angles are given in Table 5.10.

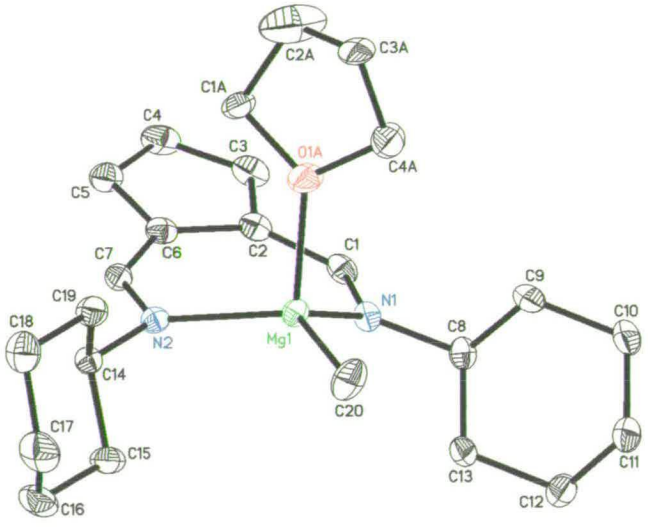

Figure 5.29 Crystallographic structure of 52. Displacement ellipsoids are shown at the 50% probability level.

Table 5.10 Selected bond distances (Å), angles and torsion (°) for 52.

Mg(1)-O(1)	2.0526(15)	Mg(1)-N(2)	2.0821(16)	Mg(1)-N(1)	2.0882(16)
Mg(1)-C(20)	2.116(2)	N(1)-C(1)	1.294(2)	N(1)-C(8)	1.478(2)
N(2)-C(7)	1.292(2)	N(2)-C(14)	1.479(2)	C(1)-C(2)	1.422(3)
C(2)-C(3)	1.412(3)	C(2)-C(6)	1.447(3)	C(3)-C(4)	1.378(3)
C(4)-C(5)	1.389(3)	C(5)-C(6)	1.411(3)	C(6)-C(7)	1.424(3)
C(8)-C(13)	1.520(3)				
O(1)-Mg(1)-N(2)		99.77(6)	O(1)-Mg(1)-N(1)		99.83(7)
N(2)-Mg(1)-N(1)		103.96(6)	O(1)-Mg(1)-C(20)		105.56(8)
N(2)-Mg(1)-C(20)		122.38(8)	N(1)-Mg(1)-C(20)		120.90(8)
C(1)-N(1)-C(8)		115.63(15)	C(1)-N(1)-Mg(1)		122.84(13)
C(7)-N(2)-C(14)		115.28(15)	C(7)-N(2)-Mg(1)		124.94(13)
N(1)-C(1)-C(2)		130.85(17)	C(3)-C(2)-C(1)		118.60(17)
C(5)-C(6)-C(7)		118.68(17)	N(2)-C(7)-C(6)		129.89(17)
C(4)-O(1)-Mg(1)		121.38(17)	C(1)-O(1)-Mg(1)		129.04(18)
Mg(1)-N(1)-C(1)-C(2)		-18.8(3)	Mg(1)-N(2)-C(7)-C(6)		13.2(2)

5.2.8 Removal of Co-ordinated THF from [(Cy$_2$AFA)Mg(CH$_3$)THF] (52)

The main objective for this part of the study has been the formation of three-co-ordinate methyl complexes for ethene polymerisation activity. The obtained complex **52** was heated at 135 °C under *vacuum* to produce a yellow oil of [(Cy$_2$AFA)Mg(CH$_3$)] (**53**) (Figure 5.29). Unfortunately, attempted crystallisation of the three co-ordinate magnesium methyl complex was unsuccessful. According to the NMR spectra there is no sign of the THF solvate, and it is not possible to say whether the structure is a three-coordinate monomeric structure or a methyl bridged dimer. However, this needs to be related to a discussion of the zwitterionic nature of the complex and the expectation of the positive charge on the magnesium would disfavour a dimeric structure.

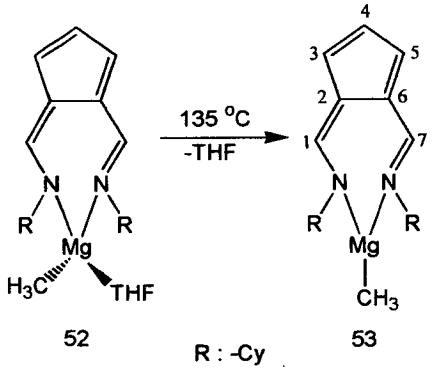

Figure 5.29 Synthesis of the three-coordinate methyl complex of 53.

The ^{1}H NMR spectrum for **53** gives a downfield singlet for H1/H7 at δ 8.33, whilst H3/H5 and H4 are found as a doublet at δ 6.88 and a triplet at δ 6.47, respectively (Figure 5.30). The *ipso*-hydrogen atoms are tentatively assigned to a resonance δ 3.06, however, the remaining cyclohexyl hydrogen resonances are located between δ 2.01 and 0.79. The methyl hydrogen atoms for the Mg-C*H*$_3$ signal give a shift to δ -0.54, which is downfield from δ -0.98 for the THF solvate complex. The ^{13}C NMR spectrum shows downfield peaks at δ 164.2 which could be assigned to C1/C7, while C3/C5, C2/C6 and C4 are also placed at downfield chemical shifts of δ 137.4, 117.8 and 115.9, respectively (Figure 5.31). The spectrum gives three sets

of signals at δ 63.1, 26.2 and 25.8 which could be assigned to *ipso*-hydrogen resonances in the cyclohexyl groups. The THF carbon resonances could not be found in the ^{13}C NMR spectrum, however, these could be confused with the peak at δ 63.1. Nevertheless the DEPT-135 shows a positive signal (δ 63.1) consistent with a CH group instead of a negative peak expected for a CH_2 from the THF solvate.

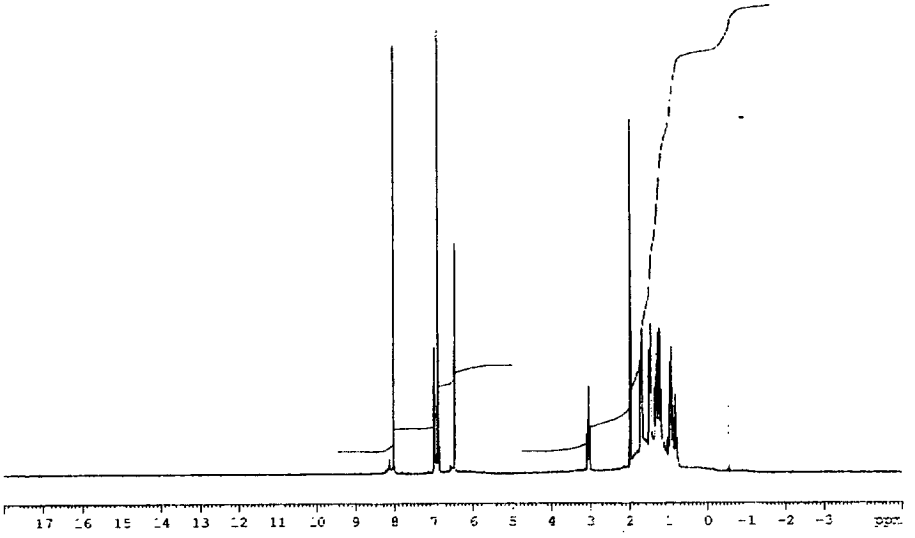

Figure 5.30 ^{1}H NMR spectrum in benzene-d_6 of 53.

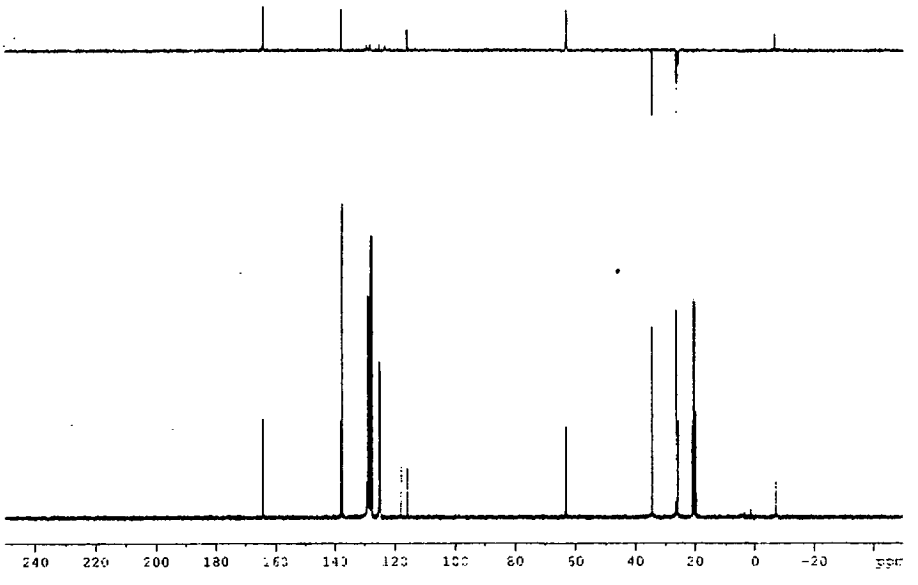

Figure 5.31 ^{13}C NMR spectrum in benzene-d_6 of 53.

Ab initio calculations (HF/6-31G**) show the favourable planar C_{2v} symmetric structure for **53**, where the N_2C_2Cp fragment is expected to be fully conjugated (Figure 5.32). Inspection of the space filling model reveals that the magnesium centre is not encapsulated in such a way that an alkene molecule will be able to approach significantly near to the magnesium centre to be able to react. In addition, MOs for **53** show that the HOMO is essentially π-bonding and centred on the cyclopentadienyl group (which is π-bonding with respect to C1-C2-C6-C7 and antibonding with respect to C3-C4-C5) with a smaller contribution from the nitrogen p_z orbitals (Figure 5.33). Moreover, a similar π-bonding orbital contribution from the cyclopentadienyl groups is found in HOMO-1 (which is π-bonding with respect to C1-C2-C3 and antibonding with respect to C4-C5-C6), whilst a smaller contribution of the nitrogen p_z orbitals is also observed. The HOMO-2 level had a Mg-CH_3 σ-antibonding contribution, and a smaller σ-antibonding contribution with respect to Mg-N. The HOMO-3 represents the highest π-bonding contribution centred on the cyclopentadienyl group (which is π-bonding with respect to C2-C3-C4-C5-C6), whilst π-bonding contribution could also be associated with the N-C bonds (which are π-bonding with respect to N1-C1 and N2-C7, but antibonding with respect to C1-C2 and C7-C6). Furthermore, the HOMO-4 level represents the π-bonding contribution for the AFA base (which is π-bonding with respect to N1-C1-C2-C3, but π-antibonding to the π-bonding C5-C6-C7-N2, respectively). There are σ-antibonding orbital contributions from the cyclohexyl groups for the HOMO-3 and HOMO-4, but no contribution from these group is observed for the other MOs levels. Finally, the LUMO level is largely π-antibonding on the cyclopentadienyl group. π-Bonding, however, could be shown for C1-C2, but antibonding for the C6-C7 and nitrogen atom contributions are observed.

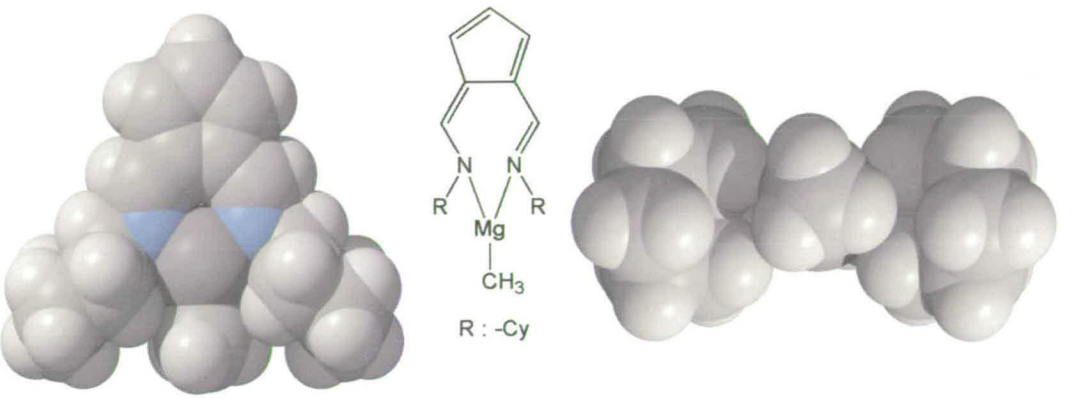

Figure 5.32 Spacefilling modelled structure of 53 at HF/6-31G level.**

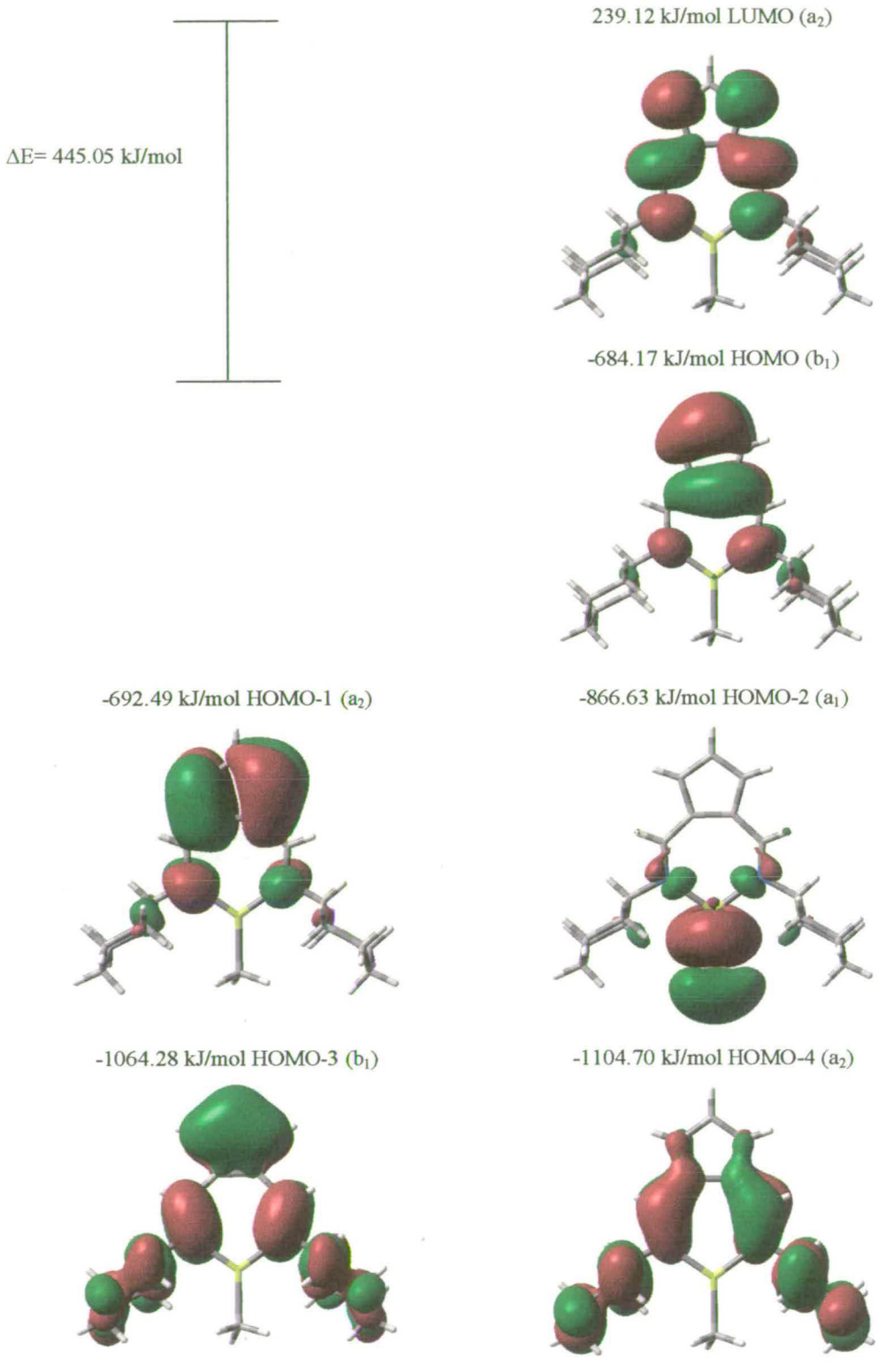

Figure 5.33 Molecular orbitals study for 53 at HF/6-31G.**

5.2.9 Ethene Polymerisation Testing of [(Cy_2AFA)Mg(CH_3)] Complex

Ethylene polymerisation of **53** like zwitterionic magnesium complexes without pre-activation by using MAO or $B(C_6F_5)_3$ were done in order to test the potential catalytic activity (Figure 5.34). Although the experimental conditions (temperature and pressure) were changed, no polymerisation activity was detected for the complex. NMR spectra were recorded for each reaction, but $-(CH_2)_n-$ was not detected.

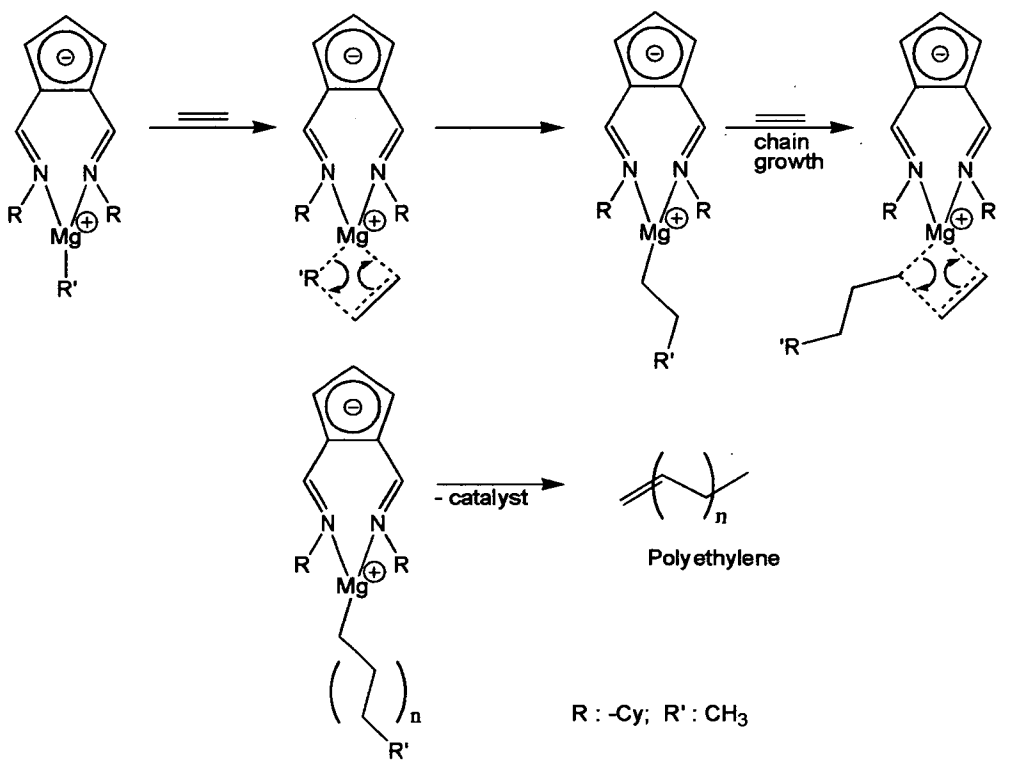

Figure 5.34 Anticipated mechanism of alkene polymerisation by 53.

5.3 Conclusions

The synthesis of $[C_5H_3\text{-}1,2\text{-}\{HC(NCH_3)_2\}_2Cl]$ (**41**), represents the starting point for the preparation of 6-aminofulvene-2-aldimine ligands, where the X-ray analysis reveals a planar structure with C_{2v} symmetry. In addition, a high π-resonance character with delocalisation of the charge toward the cyclopentadienyl ring could be deduced from the structure (Figure 5.35). Further reactivity with any primary aliphatic or aromatic amine, produces the 6-aminofulvene-2-aldimine $[R_2AFA(H)]$ system. The unusual strength of the intramolecular hydrogen bond is due to a maximum resonance to stabilize the possible charges on the ligand, where two resonances could be suggested (Figure 5.35). Lithiation of $[R_2AFA(H)]$ by using an equivalent amount of ^{n}BuLi did not provide reactivity under any condition, but the reaction with MeLi provides the appropriated removal of the N-*H* proton, according to the ^{1}H NMR spectrum (but no crystals suitable for X-ray analysis could not be obtained for the lithiated species).

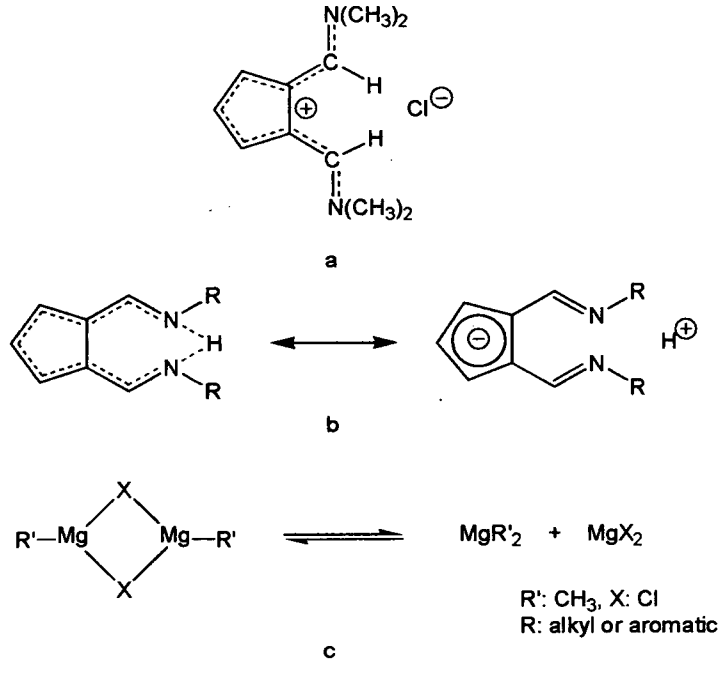

Figure 5.35 a) Internal charge resonance effect of 41; b) Resonance hybrids suggested for 42-46; c) Schlenk equilibrium for dissociation of the Grignard reagent.

Reaction between 6-aminofulvene-2-aldimine ligands (pure ligand or lithiated ligand) and Grignard reagents can give bischelate magnesium complexes, where the nitrogen atoms co-ordinate in a κ2 mode to the magnesium atom. All the complexes are obtained when non-coodinating solvents (benzene or toluene) are used, where the Schlenk equilibrium involving the magnesium reagents is also present, and it may explain the products obtained (Figure 5.35). However, reflux of a solution of the ligand with MeMgBr in a non-coordinating solvent provides the first example of a complex in which co-ordination of the cyclopentadienyl (η^5-Cp) portion of the ligand has been observed. The localization of negative charge on the Cp ring results in complexes of zwitterionic character in which a positive charge resides on the magnesium. The Schlenk equilibrium effect is also involved and this results in a reaction effectively of $MgCl_2$ to provide complexes [LMg(Cl)S] (S: Et_2O or THF). The complex [(Cy_2AFA)Mg(CH_3)THF] (**52**) could be treated under *vacuum* to remove the THF co-ordinated to the magnesium centre, where NMR spectra provide information about a three-coordinate magnesium sphere of **52**. Molecular models of the three-coordinate complex **53** shows that Mg is coplanar with the ligand. Molecular orbital analysis showed the hyper-conjugation of a zwitterionic magnesium complex, in which a localization of charge on the Cp ring provides electrophilic character at the magnesium atom.

The potential ethene polymerisation by [(Cy_2AFA)Mg(CH_3)] (**53**) has been explored, where the space filling model for the magnesium complex reveals the possible approach to produce activity, but no polymer was detected by using conventional techniques of analysis. Finally, although the experiment was unsuccessful, the research on zwitterionic magnesium complexes still needs to be done by using new amine ligands; perhaps changing for bigger groups at the nitrogen atoms may produce extra-stability of the metal sphere in order to produce catalytic activity.

5.4 Experimental

5.4.1 General Procedures

All manipulations were carried out under a nitrogen atmosphere using standard Schlenk and cannula techniques or in a conventional nitrogen-filled glove-box (Saffron Scientific), fitted with oxygen and water scavenging columns. Solvents were refluxed over an appropriate drying agent, and distilled and degassed prior to use. Solvents and reagents where commercially available were bought from Aldrich, Acros or Fischer, with exception of NMR solvents which were purchased from Goss Scientific. Diethyl ether, toluene, hexane, benzene and THF were all distilled from Na/benzophenone under a nitrogen atmosphere. NMR solvents were degassed using three freeze-pump-thaw cycles and stored over 4 Å molecular sieves.

5.4.2 Instrumentation

Elemental analyses were performed by sealing aluminium capsules containing approximately 1 mg of compound under nitrogen in the glove box, and performed using a Perkin-Elmer 2400 CHN Analyser. The NMR spectra were recorded on Brucker AC 250 MHz and Varian Gemini 200MHz spectrometers. Infrared spectra were obtained using a Perkin-Elmer 1600 Paragon Series FT-IR spectrometer as potassium bromide discs or as liquid thin films. Electron impact (EI) mass spectra were obtained either on a Finnigan MAT 4600 quadrupole spectrometer or on a Kratos MS50TC spectrometer. Fast atom bombardment (FAB) mass spectra were obtained on a MS50TC spectrometer. ^{1}H and ^{13}C NMR spectra were referenced to TMS.

5.4.3 Synthesis

$[C_5H_4=C(H)NMe_2]$ (39)

Dimethyl sulfate (400 cm^3, 200 mmol) was dropped into dimethylformamide (31.2 cm^3, 200 mmol) during 30 mins at 50-60 °C, under a nitrogen atmosphere. After the addition was completed, the mixture was heated for 2 h at 70-80 °C. Finally, a colourless oil of dimethylformamide-dimethylsulfate was obtained with a 97% yield.

N,N-dimethylformamide-dimethylsulfate (99.85 g, 200 mmol) was slowly added to a solution of sodium cyclopentadienyl (100 cm^3, 2.0 M in THF, 200 mmol) at –10 °C, under a nitrogen atmosphere. During the addition, the temperature was kept below –5 °C. After the addition was completed, the mixture was stirred at 20 °C for 2 h. The solution was filtered from the precipitate, which was washed with THF (two portions of 200 cm^3 each). Solvent and volatile components were removed under *vacuum* to obtain a black product. The final product was extracted using hot petroleum ether 60-80 °C (two portions of 100 cm^3 each), treated with activated charcoal, concentrated and cooled at 5 °C to yield **39**, 64% (15.51 g).

^{1}H NMR ($CDCl_3$/ppm): δ 7.15 (s, 1H, H2), 6.62 (m, 1H, H7, J= 8.4 Hz), 6.56 (m, 1H, H6, J=10.1 Hz), 6.44 (m, 1H, H5, J=8.6 Hz), 6.35 (m, 1H, H4, J=8.4 Hz), 3.29 (s, 6H, CH_3). ^{13}C NMR ($CDCl_3$, d): δ 148.70 (*C*2), 125.30 (*C*6), 124.50 (*C*5), 119.62 (*C*4), 116.92 (*C*3), 114.00 (*C*7), 30.41 (CH_3). EIMS (*m/z*): 122 (M^+), 107 (M^+-CH_3). Analysis elemental for $C_8H_{11}N$: Expected: C, 79.27; H, 9.17; N, 11.56. Found: C, 78.98; H, 9.10; N, 11.46.

$[\{H(Cl)CNMe_2\}Cl]$ (40)

A solution of oxalyl chloride (4.4 cm^3, 50 mmol) in THF (20 cm^3), at room temperature, under nitrogen atmosphere, was added slowly to a solution of DMF (3.7 cm^3, 50 mmol) in THF (20 cm^3) at 0 °C. After addition, the suspension was stirred for 3 h. A white suspension was obtained with a 98% yield.

[{C_5H_3-(HCNMe$_2$)$_2$}Cl] (41)

A solution of *N*-chloromethylene-*N*-methylmethanammoium chloride (6.50 g, 50 mmol) in THF (50 cm^3) was carefully added to a solution of 6-(dimethylamino)fulvene (6.06 g, 50 mmol) in THF (50 cm^3) at –61 °C. After 1 h, the reaction was warmed to room temperature and stirried for 2 h. Solvent and volatiles were removed under *vacuum*. The final product was washed with hexane/ether (100 cm^3, 50:50) to give yellow flecks of product (8.69 g, 98% yield).

^{1}H NMR ($CDCl_3$/ppm): δ 9.76 (s, 2H, C*H*N), 7.35 (d, 2H, Cp), 6.78 (t, 1H, Cp), 3.83 (s, 6H, CH_3), 3.42 (s, 6H, CH_3). ^{13}C NMR ($CDCl_3$/ppm): δ 160.60 (*C*2), 130.30 (*C*6), 125.81 (*C*5), 119.32 (*C*3), 48.81 (*C*H$_3$), 42.13 (*C*H$_3$).

Empirical formula	$C_{11}H_{17}N_2Cl$	β/ °	90
Formula weight	212.72	γ/ °	90
Crystal system	Tetragonal	Volume/ Å^3	8853(2)
Space group	I 4$_1$/a	Z	16
a/ Å	25.207(2)	Z'	1
b/ Å	25.207(2)	Density calc./ Mgm^{-3}	0.638
c/ Å	13.933(3)	μ (Mo-K)/ mm^{-1}	0.154
α/ °	90		

Data were collected on a Bruker SMART APEX diffractometer[15] equipped with an Oxford Cryosystems low-temperature device at 150 K and using a yellow needle oil-coated crystal[16] of dimension 0.20x0.05x0.05 mm^3. The initial unit cell was indexed using a least-squares analysis of a random set of reflections collected from three series of 0.3° wide ω-scans, 10 s per frame, and 25 frames per series that were well distributed in reciprocal space. Data frames were collected [Mo Kα = 0.71073 Å] with 0.3° wide ω-scans, 10 s per frame and 600 frames per series. Three complete series were collected at varying ϕ angles (ϕ=0, 90, 180°). The crystal to detector distance was 6.0 cm, this providing a set of $3.34 \leq 2\theta \leq 57.38$. A total of 30226 reflections were collected and integrated using SAINT,[17] while absorption correction was applied using SADABS[18] with 5356 unique [R(int)=0.1352]. System symmetry, systematic absences and intensity statistics indicated the unique tetragonal space group I 4$_1$/a. The structure was determined by direct methods with the location of nearly all non-hydrogen atoms using the program SHELXS[19] and refined by full-

matrix least-squares on F^2 using SHELXL.[20] All non-hydrogen atoms were refined anisotropically, while hydrogen atoms were placed in calculated positions, constrained to ride on their carbon atoms with group U_{iso} values assigned ($U_{iso}(H)$= $1.20U_{iso}$). The final structure was refined to convergence [$\Delta/\sigma \leq 0.001$] with R(F) = 0.0790 (for 5356 data with F>4σF), GOF = 0.980 and *w*R2 = 0.2210 (all data). [$R1 = \Sigma|F_O - F_C|/ \Sigma |F_O|$, $wR2 = \{[\Sigma w(F_O^2 - F_C^2)^2]/ \Sigma wF_O^4\}^{0.5}$, $w = 1/[\sigma^2(F_O^2) + (xP)^2 + yP]$, $P = (F_O^2+2F_C^2/3)$]. The largest difference between peak and hole in the final difference map, 0.276 and –0.308 eÅ^{-3}.

[Cy$_2$AFA(H)] (42)

A solution of 6-dimethylaminofulvene-2-*N,N*-dimethylaldimmonium chloride (8.00 g, 45.12 mmol) in absolute ethanol (250 cm^3) was refluxed with cyclohexylamine (10.3 cm^3, 90.24 mmol) for 4 h. The solvent and volatile components were removed under *vacuum*, and the product extracted with hot hexane (300 cm^3). The brown solution was treated with activated charcoal and filtered to produce yellow needles as the final product (10.30 g, 80.21% yield).

^{1}H NMR ($CDCl_3$/ppm): δ 14.04 (br, 1H, N*H*), 7.94 (s, 2H, H1/H7), 6.81 (d, 2H, H3/H5), 6.34 (t, 1H, H4), 3.25 (p, 2H, ipso-Cy), 1.20-2.01 (m, 20H, Cy). ^{13}C NMR ($CDCl_3$/ppm): δ 154.78 (C1/C7), 129.86 (C3/C5), 120.08 (C2/C6), 117.65 (C4), 64.19 (ipso-Cy), 35.39 (*o*-C), 26.00 (*p*-C), 25.49 (*m*-C). FABMS (*m/z*): 284 (M^+), 201 (M^+-C_6H_{11}). Analysis elemental for $C_{19}H_{28}N_2$: Expected: C, 80.21; H, 9.94; N, 9.85. Found: C, 80.00; H, 9.86; N, 9.80.

Empirical formula	$C_{19}H_{28}N_2$	β/ °	116.596(5)
Formula weight	284.43	γ/ °	90
Crystal system	Monoclinic	Volume/ Å^3	1955.6(6)
Space group	P 2_1/n	Z	4
a/ Å	15.635(3)	Z'	1
b/ Å	8.1020(15)	Density calc./ Mgm^{-3}	1.0.966
c/ Å	17.264(3)	μ (Mo-K)/ mm^{-1}	0.056
α/ °	90		

Data were collected on a Bruker SMART APEX diffractometer[15] equipped with an Oxford Cryosystems low-temperature device at 150 K and using an yellow

needle oil-coated crystal[16] of dimension 0.18x0.07x0.05 mm^3. The initial unit cell was indexed using a least-squares analysis of a random set of reflections collected from three series of 0.3° wide ω-scans, 10 s per frame, and 25 frames per series that were well distributed in reciprocal space. Data frames were collected [Mo Kα = 0.71073 Å] with 0.3° wide ω-scans, 10 s per frame and 600 frames per series. Three complete series were collected at varying ϕ angles (ϕ=0, 90, 180°). The crystal to detector distance was 6.0 cm, this providing a set of $2.92 \leq 2\theta \leq 52.86$. A total of 9709 reflections were collected and integrated using SAINT,[17] while absorption correction was applied using SADABS[18] with 3760 unique [R(int)=0.0248]. System symmetry, systematic absences and intensity statistics indicated the unique monoclinic space group $P2_1/n$. The structure was determined by direct methods with the location of nearly all non-hydrogen atoms using the program SHELXS[19] and refined by full-matrix least-squares on F^2 using SHELXL.[20] All non-hydrogen atoms were refined anisotropically, while hydrogen atoms were placed in calculated positions, constrained to ride on their carbon atoms with group U_{iso} values assigned ($U_{iso}(H) = 1.20U_{iso}$). The final structure was refined to convergence [$\Delta/\sigma \leq 0.001$] with R(F) = 0.0596 (for 3760 data with F>4σF), GOF = 1.122 and *w*R2 = 0.1346 (all data). [$R1 = \Sigma|F_O - F_C| / \Sigma |F_O|$, $wR2 = \{[\Sigma w(F_O^2 - F_C^2)^2] / \Sigma wF_O^4\}^{0.5}$, $w = 1/[\sigma^2(F_O^2) + (xP)^2 + yP]$, $P = (F_O^2 + 2F_C^2/3)$]. The largest difference between peak and hole in the final difference map, 0.306 and –0.198 $eÅ^{-3}$.

[Ph_2AFA(H)] (43)

A solution of 6-dimethylaminofulvene-2-*N,N*-dimethylaldimmonium chloride (8.00 g, 45.12 mmol) in absolute ethanol (250 cm^3) was refluxed with an excess of aniline (12.33 cm^3, 135.36 mmol) overnight. The solvent and volatile components were removed under *vacuum*, and the product extracted with hot hexane (300 cm^3). The red/brown solution was treated with activated charcoal and filtered to produce yellow needles as the final product (7.74 g, 63.0% yield).

^{1}H NMR ($CDCl_3$/ppm): δ 15.58 (br, 1H, N*H*), 8.25 (s, 2H, H1/H7), 7.38 (t, 4H, C_6H_5), 7.23 (d, 4H, C_6H_5), 7.18 (t, 2H, C_6H_5), 7.04 (d, 2H, H3/H5), 6.44 (t, 1H,

H4). ^{13}C NMR ($CDCl_3$/ppm): δ 150.63 (CN, C1/C7), 145.25 (*C*, Ar), 134.68 (C3/C5), 129.56 (*m*-C, Ar), 124.84 (*p*-C, Ar), 122.08 (C2/C6), 120.96 (C4), 119.12 (*o*-C, Ar). EIMS (*m/z*): 273 (M^+). Analysis elemental for $C_{19}H_{16}N_2$: Expected: C, 83.78; H, 5.73; N, 10.29. Found: C, 82.25; H, 5.87; N, 10.20.

[(4-methyl)Ph$_2$AFA(H)] (44)

A solution of 6-dimethylaminofulvene-2-*N,N*-dimethylaldimmonium chloride (5.30 g, 25.00 mmol) in absolute ethanol (100 cm^3) was refluxed with an excess of *p*-toluidine (8.04 cm^3, 75.00 mmol) overnight. The solvent and volatile components were removed under *vacuum*, and the product extracted with hot hexane (200 cm^3). The orange/red solution was treated with activated charcoal and filtered to produce orange needles as the final product (0.75 g, 10.00% yield).

^1H NMR ($CDCl_3$/ppm): δ 14.94 (br, 1H, N*H*), 8.28 (s, 2H, H6/H7), 7.30 (d, 4H, *m*-C), 7.22 (d, 4H, *o*-C), 7.05 (d, 2H, H3/H5), 6.46 (t, 1H, H4), 2.16 (s, 6H, CH_3). ^{13}C NMR ($CDCl_3$/ppm): δ 150.58 (CN), 145.19 (*C*, ipso-Ar), 134.50 (C3/C5), 129.30 (*m*-C), 121.87 (C3), 121.03 (C5), 119.00 (*o*-C), 20.02 (CH_3). FABMS (*m/z*): 300 (M^+), 285 (M^+-CH_3). Analysis elemental for $C_{21}H_{20}N_2$: Expected: C, 83.95; H, 6.72; N, 9.33. Found: C, 83.89; H, 6.70; N, 9.25.

Empirical formula	$C_{10.50}H_{10}N$	β/ °	90
Formula weight	150.19	γ/ °	90
Crystal system	Orthorhombic	Volume/ Å^3	1647.1(17)
Space group	P ccn	Z	8
a/ Å	5.286(5)	Z'	0.5
b/ Å	14.808(5)	Density calc./ Mgm^{-3}	1.211
c/ Å	21.042(5)	μ (Mo-K)/ mm^{-1}	0.071
α/ °	90		

Data were collected on a Bruker SMART APEX diffractometer[15] equipped with an Oxford Cryosystems low-temperature device at 150 K and using an orange needle oil-coated crystal[16] of dimension 0.18x0.07x0.06 mm^3. The initial unit cell was indexed using a least-squares analysis of a random set of reflections collected from three series of 0.3° wide ω-scans, 10 s per frame, and 25 frames per series that were well distributed in reciprocal space. Data frames were collected [Mo Kα =

0.71073 Å] with 0.3° wide ω-scans, 10 s per frame and 600 frames per series. Three complete series were collected at varying ϕ angles (ϕ=0, 90, 180°). The crystal to detector distance was 6.0 cm, this providing a set of $3.88 \leq 2\theta \leq 52.84$. A total of 11930 reflections were collected and integrated using SAINT,[17] while absorption correction was applied using SADABS[18] with 1700 unique [R(int)=0.0809]. System symmetry, systematic absences and intensity statistics indicated the unique orthorhombic space group Pccn. The structure was determined by direct methods with the location of nearly all non-hydrogen atoms using the program SHELXS[19] and refined by full-matrix least-squares on F^2 using SHELXL.[20] All non-hydrogen atoms were refined anisotropically, while hydrogen atoms were placed in calculated positions, constrained to ride on their carbon atoms with group U_{iso} values assigned ($U_{iso}(H) = 1.20U_{iso}$). The final structure was refined to convergence [$\Delta/\sigma \leq 0.001$] with R(F) = 0.0991 (for 1700 data with F>4σF), GOF = 1.291 and *w*R2 = 0.1603 (all data). [$R1 = \Sigma|F_o - F_c| / \Sigma |F_o|$, $wR2 = \{[\Sigma w(F_o^2 - F_c^2)^2] / \Sigma wF_o^4\}^{0.5}$, $w = 1/[\sigma^2(F_o^2) + (xP)^2 + yP]$, $P = (F_o^2 + 2F_c^2/3)$]. The largest difference between peak and hole in the final difference map, 0.185 and –0.151 eÅ^{-3}.

[(2,6-dimethyl)Ph$_2$AFA(H)] (45)

A solution of 6-dimethylaminofulvene-2-*N*,*N*-dimethylaldimmonium chloride (5.30 g, 25.00 mmol) in absolute ethanol (100 cm^3) was refluxed with an excess of 2,6-dimethylaniline (9.24 cm^3, 75.00 mmol) for four days. The solvent and volatile components were removed under *vacuum*, and the product extracted with hot hexane (200 cm^3). The brown solution was treated with activated charcoal and filtered to produce orange needles as the final product (0.84 g, 10.23% yield).

^{1}H NMR ($CDCl_3$/ppm): δ 14.89 (br, 1H, N*H*), 7.45 (d, 2H, H6/H7), 7.01 (d, 2H, H3/H5), 6.87 (s, 6H, Ar), 6.66 (t, 1H, H4), 2.03 (s, 12H, C*H*$_3$). ^{13}C NMR ($CDCl_3$/ppm): δ 156.63 (CN), 144.91 (*C*, ipso-Ar), 134.82 (C3/C5), 131.11 (*o*-C), 128.83 (*m*-C), 125.40 (*p*-C), 122.12 (C1/C2), 120.43 (C4), 18.74 (*C*H$_3$). FABMS (*m/z*): 328 (M$^+$). Analysis elemental for $C_{23}H_{24}N_2$: Expected: C, 84.11; H, 7.37; N, 8.53. Found: C, 83.78; H, 7.27; N, 8.475.

Empirical formula	$C_{23}H_{24}N_8$	β/ °	91.733(3)
Formula weight	328.44	γ/ °	90
Crystal system	Monoclinic	Volume/ $Å^3$	1909(2)
Space group	P $2_1/c$	Z	4
a/ Å	23.176(3)	Z'	4
b/ Å	20.402(3)	Density calc./ Mgm^{-3}	0.638
c/ Å	16.159(2)	μ (Mo-K)/ mm^{-1}	1.143
α/ °	90		

Data were collected on a Bruker SMART APEX diffractometer[15] equipped with an Oxford Cryosystems low-temperature device at 150 K and using an yellow needle oil-coated crystal[16] of dimension 0.22x0.08x0.06 mm^3. The initial unit cell was indexed using a least-squares analysis of a random set of reflections collected from three series of 0.3° wide ω-scans, 10 s per frame, and 25 frames per series that were well distributed in reciprocal space. Data frames were collected [Mo Kα = 0.71073 Å] with 0.3° wide ω-scans, 10 s per frame and 600 frames per series. Three complete series were collected at varying ϕ angles (ϕ=0, 90, 180°). The crystal to detector distance was 6.0 cm, this providing a set of $3.88 \leq 2\theta \leq 52.84$. A total of 15672 reflections were collected and integrated using SAINT,[17] while absorption correction was applied using SADABS[18] with 15672 unique [R(int)=0.1291]. System symmetry, systematic absences and intensity statistics indicated the unique monoclinic space group P $2_1/c$. The structure was determined by direct methods with the location of nearly all non-hydrogen atoms using the program SHELXS[19] and refined by full-matrix least-squares on F^2 using SHELXL.[20] All non-hydrogen atoms were refined anisotropically, while hydrogen atoms were placed in calculated positions, constrained to ride on their carbon atoms with group U_{iso} values assigned ($U_{iso}(H) = 1.20U_{iso}$). The final structure was refined to convergence [$\Delta/\sigma \leq 0.001$] with R(F) = 0.1192 (for 1700 data with $F>4\sigma F$), GOF = 1.188 and *w*R2 = 0.1915 (all data). [$R1 = \Sigma|F_o - F_c|/ \Sigma |F_o|$, $wR2 = \{[\Sigma w(F_o^2 - F_c^2)^2]/ \Sigma wF_o^4\}^{0.5}$, $w = 1/[\sigma^2(F_o^2) + (xP)^2 + yP]$, $P = (F_o^2+2F_c^2/3)$]. The largest difference between peak and hole in the final difference map, 0.337 and –0.235 $eÅ^{-3}$.

[(2,4,6-trimethyl)Ph_2AFA(H)] (46)

A solution of 6-dimethylaminofulvene-2-*N,N*-dimethylaldimmonium chloride (9.24 g, 43.42 mmol) in absolute ethanol (150 cm^3) was refluxed with an excess of 2,4,6-trimethylaniline (18.29 cm^3, 130.26 mmol) for four days. The solvent and volatile components were removed under *vacuum*, and the product extracted with hot hexane (200 cm^3). The brown solution was treated with activated charcoal and filtered to produce orange needles as the final product (10.22 g, 66.0% yield).

^{1}H NMR ($CDCl_3$/ppm): δ 14.96 (br, 1H, N*H*), 7.81 (s, 2H, H6/H7), 6.91 (d, 2H, H4), 6.74 (s, 4H, Ar), 2.18 (s, 6H, *p*-CH_3), 2.08 (s, 12H, CH_3). ^{13}C NMR ($CDCl_3$/ppm): δ 156.81 (CN), 141.68 (*C*, ipso-Ar), 134.65 (*o*-C), 132.71 (C3), 130.73 (*p*-C), 129.91 (*m*-C), 120.85 (C1/C2), 119.14 (C4), 20.65 (*p*-CH_3), 18.44 (*o*-CH_3). EIMS (*m/z*): 357 (M^+), 238 (M^+-C_9H_{11}). Analysis elemental for $C_{25}H_{28}N_2$: Expected: C, 84.21; H, 7.93; N, 7.86. Found: C, 84.19; H, 7.88; N, 7.66.

Empirical formula	$C_{25}H_{28}N_2$	β/ °	90
Formula weight	356.49	γ/ °	90
Crystal system	Orthorhombic	Volume/ $Å^3$	1973.4(16)
Space group	P $ca2_1$	Z	4
a/ Å	14.257(7)	Z'	1
b/ Å	8.792(4)	Density calc./ Mgm^{-3}	1.200
c/ Å	15.743(7)	μ (Mo-K)/ mm^{-1}	0.070
α/ °	90		

Data were collected on a Bruker SMART APEX diffractometer[15] equipped with an Oxford Cryosystems low-temperature device at 150 K and using an orange needle oil-coated crystal[16] of dimension 0.21x0.09x0.06 mm^3. The initial unit cell was indexed using a least-squares analysis of a random set of reflections collected from three series of 0.3° wide ω-scans, 10 s per frame, and 25 frames per series that were well distributed in reciprocal space. Data frames were collected [Mo Kα = 0.71073 Å] with 0.3° wide ω-scans, 10 s per frame and 600 frames per series. Three complete series were collected at varying ϕ angles (ϕ=0, 90, 180°). The crystal to detector distance was 6.0 cm, this providing a set of $3.88 \leq 2\theta \leq 52.84$. A total of 18273 reflections were collected and integrated using SAINT,[17] while absorption correction was applied using SADABS[18] with 4736 unique [R(int)=0.0772]. System

symmetry, systematic absences and intensity statistics indicated the unique orthorhombic space group P $ca2_1$. The structure was determined by direct methods with the location of nearly all non-hydrogen atoms using the program SHELXS[19] and refined by full-matrix least-squares on F^2 using SHELXL.[20] All non-hydrogen atoms were refined anisotropically, while hydrogen atoms were placed in calculated positions, constrained to ride on their carbon atoms with group U_{iso} values assigned ($U_{iso}(H) = 1.20U_{iso}$). The final structure was refined to convergence [$\Delta/\sigma \leq 0.001$] with R(F) = 0.0723 (for 4736 data with F>4σF), GOF = 1.048 and *w*R2 = 0.1345 (all data). [$R1 = \Sigma|F_O - F_C|/ \Sigma |F_O|$, $wR2 = \{[\Sigma w(F_O^2 - F_C^2)^2]/ \Sigma wF_O^4\}^{0.5}$, $w = 1/[\sigma^2(F_O^2) + (xP)^2 + yP]$, $P = (F_O^2+2F_C^2/3)$]. The largest difference between peak and hole in the final difference map, 0.273 and –0.212 eÅ^{-3}.

[(Ph$_2$AFA)$_2$Mg] (47)

A solution of *N,N'*-diphenyl-6-aminofulvene-2-aldimine [Ph$_2$AFA(H)] (0.235 g, 0.863 mmol) in toluene (7 cm^3) at –78 °C was treated with MeLi in diethyl ether (0.54 cm^3, 1.6 M, 0.863 mmol). The reaction mixture was left to warm to room temperature and allowed to stir over night. At room temperature, MeMgCl in THF (0.30 cm^3, 3.0 M, 0.863 mmol) was added to the lithiated ligand solution and the mixture was allowed to stir for three days. The resultant orange solution was filtered and LiCl removed to provide the final product (0.1941 mmol, 45% yield).

^{1}H NMR (toluene-d$_8$/ppm): δ 8.18 (s, 2H, H1/H7), 7.33 (t, 4H, C$_6H_5$), 7.18 (d, 4H, C$_6H_5$), 7.12 (t, 2H, C$_6H_5$), 6.96 (d, 2H, H3/H5), 6.38 (t, 1H, H4). ^{13}C NMR (toluene-d$_8$/ppm): δ 151.30 (CN), 144.8 (*C*, ipso-Ar), 134.01 (C4), 127.07 (*m*-C), 123.25 (*p*-C), 121.72 (C3), 120.82 (C5), 119.03 (*o*-C).

Empirical formula	$C_{38}H_{30}N_4Mg$	β/ °	89.881(4)
Formula weight	566.97	γ/ °	87.266(4)
Crystal system	Triclinic	Volume/ Å^3	2943.5(11)
Space group	P-1	Z	4
a/ Å	10.133(2)	Z'	2
b/ Å	15.302(3)	Density calc./ Mgm^{-3}	1.279
c/ Å	19.005(4)	μ (Mo-K)/ mm^{-1}	0.095
α/ °	89.926(4)		

Data were collected on a Bruker SMART APEX diffractometer[15] equipped with an Oxford Cryosystems low-temperature device at 150 K and using an yellow rod oil-coated crystal[16] of dimension 0.27x0.14x0.12 mm^3. The initial unit cell was indexed using a least-squares analysis of a random set of reflections collected from three series of 0.3° wide ω-scans, 10 s per frame, and 25 frames per series that were well distributed in reciprocal space. Data frames were collected [Mo Kα = 0.71073 Å] with 0.3° wide ω-scans, 20 s per frame and 600 frames per series. Four complete series were collected at varying ϕ angles (ϕ=0, 90, 120, 180°). The crystal to detector distance was 6.0 cm, this providing a set of $3.96 \leq 2\theta \leq 57.96$. A total of 19361 reflections were collected and integrated using SAINT,[17] while absorption correction was applied using SADABS[18] with 13270 unique [R(int)=0.0502]. System symmetry, systematic absences and intensity statistics indicated the unique triclinic space group Pī. The structure was determined by direct methods with the location of nearly all non-hydrogen atoms using the program SHELXS[19] and refined by full-matrix least-squares on F^2 using SHELXL.[20] All non-hydrogen atoms were refined anisotropically, while hydrogen atoms were placed in calculated positions, constrained to ride on their carbon atoms with group U_{iso} values assigned ($U_{iso}(H)= 1.20U_{iso}$). The final structure was refined to convergence [$\Delta/\sigma \leq 0.001$] with R(F) = 0.0752 (for 13270 data with F>4σF), GOF = 1.017 and *w*R2 = 0.1853 (all data). [$R1 = \Sigma|F_o - F_c|/ \Sigma |F_o|$, $wR2 = \{[\Sigma w(F_o^2 - F_c^2)^2]/ \Sigma wF_o^4\}^{0.5}$, $w = 1/[\sigma^2(F_o^2) + (xP)^2 + yP]$, $P = (F_o^2+2F_c^2/3)$]. The largest difference between peak and hole in the final difference map, 0.564 and –0.686 $eÅ^{-3}$.

[Me_2Mg] (48)

A stirred solution of MeMgCl (50.60 cm3, 3.0 M, 151 mmoles) in THF was added to a 500 cm^3 Schlenk flask and diluted with THF (100 cm^3). To this solution MeLi (95 cm^3, 1.6 M, 152 mmoles) in Et_2O was added with stirring at room temperature. The reaction mixture was stirred over night, after time all the solvent was removed in *vacuum*. Dried Et_2O was added (250 cm3) and the solution stirred for 30 mins before filtered to remove LiCl. The solvent was then removed under

vacuum, and then dried at 120 °C for 2 hours to give a fine white powder in 99.0% yield.

^{1}H NMR (THF-d_8/ppm): δ -1.82 (s, Mg-CH_3). Analysis elemental for C_2H_6Mg: Expected: C, 44.18; H, 11.12. Found: C, 42.05; H, 8.30.

[(Cy$_2$AFA)$_2$Mg] (49)

A stirred solution of *N,N'*-dicyclohexyl-6-aminofulvene-2-aldimine [Cy$_2$AFA(H)] (0.510 g, 1.790 mmol) in benzene (15 cm^3) was refluxed with Me_2Mg in THF (0.90 cm^3, 2.0 M, 1.790 mmol) for 30 min and then stirred at room temperature over night. The solvent and volatiles were removed under *vacuum* and the resulting solid dissolved in toluene (10 cm^3). Storage of at –5 °C over night gave yellow crystals as the product (0.555 mmol, 62.0% yield).

^{1}H NMR (toluene-d_8/ppm): δ 7.74 (s, 4H, H1/H7), 7.57 (d, 4H, H3/H5), 6.29 (t, 2H, H4), 3.52 (m, 4H, ipso-Cy), 1.83-0.21 (m, 40H, H4). ^{13}C NMR (toluene-d_8/ppm): δ 158.2 (C1/C7), 136.7 (C3/C5), 118.83 (C2/C6), 116.3 (C4), 58.7 (ipso-Cy-CH), 31.8 (o-Cy-CH_2), 24.20 (p-Cy-CH_2), 23.63 (m-Cy-CH_2).

Empirical formula	$C_{45}H_{62}N_4Mg$	β/ °	98.351(3)
Formula weight	683.30	γ/ °	98.351(3)
Crystal system	Triclinic	Volume/ Å^3	1964.7(5)
Space group	P-1	Z	2
a/ Å	9.2767(15)	Z'	1
b/ Å	11.1419(17)	Density calc./ Mgm^{-3}	1.155
c/ Å	19.352(3)	μ (Mo-K)/ mm^{-1}	0.081
α/ °	93.843(4)		

Data were collected on a Bruker SMART APEX diffractometer[15] equipped with an Oxford Cryosystems low-temperature device at 150 K and using an yellow rod oil-coated crystal[16] of dimension 0.25x0.12x0.11 mm^3. The initial unit cell was indexed using a least-squares analysis of a random set of reflections collected from three series of 0.3° wide ω-scans, 10 s per frame, and 25 frames per series that were well distributed in reciprocal space. Data frames were collected [Mo Kα = 0.71073 Å] with 0.3° wide ω-scans, 20 s per frame and 600 frames per series. Four complete series were collected at varying ϕ angles (ϕ=0, 90, 120, 180°). The crystal to detector

distance was 6.0 cm, this providing a set of $3.96 \leq 2\theta \leq 57.96$. A total of 6727 reflections were collected and integrated using SAINT,[17] while absorption correction was applied using SADABS[18] with 6381 unique [R(int)=0.0107]. System symmetry, systematic absences and intensity statistics indicated the unique triclinic space group P$\bar{1}$. The structure was determined by direct methods with the location of nearly all non-hydrogen atoms using the program SHELXS[19] and refined by full-matrix least-squares on F^2 using SHELXL.[20] All non-hydrogen atoms were refined anisotropically, while hydrogen atoms were placed in calculated positions, constrained to ride on their carbon atoms with group U_{iso} values assigned ($U_{iso}(H)= 1.20U_{iso}$). The final structure was refined to convergence [$\Delta/\sigma \leq 0.001$] with R(F) = 0.0574 (for 6381 data with $F>4\sigma F$), GOF = 1.002 and *w*R2 = 0.1380 (all data). [$R1 = \Sigma|F_O - F_C|/ \Sigma |F_O|$, $wR2 = \{[\Sigma w(F_O^2 - F_C^2)^2]/ \Sigma wF_O^4\}^{0.5}$, $w = 1/[\sigma^2(F_O^2) + (xP)^2 + yP]$, $P = (F_O^2+2F_C^2/3)$]. The largest difference between peak and hole in the final difference map, 0.535 and –0.315 eÅ^{-3}.

[(Cy$_2$AFA)Mg(Cl)Et$_2$O] (50)

A stirred solution of *N,N'*-dicyclohexyl-6-aminofulvene-2-aldimine [Cy$_2$AFA(H)] (0.507 g, 1.779 mmol) in diethyl ether (15 cm^3) at –78 °C was treated with MeLi in diethyl ether (1.30 cm^3, 1.6 M, 1.779 mmol), allowed to warm to room temperature and the left to stir over night. The lithiated ligand was treated with a solution of MeMgCl (0.59 cm^3, 3.0 M, 1.779 mmol) in THF and the resulting solution was stirred over night. The orange solution was filtered (LiCl removed), while the solvent and volatile components were removed under *vacuum* and the resulting solid dissolved in toluene (10 cm^3). Storage of at –5 °C over night gave yellow crystals as the product (0.98 mmol, 55.1% yield).

^{1}H NMR (benzene-d$_6$/ppm): δ 7.71 (s, 4H, H1/H7), 7.19 (d, 4H, H3/H5), 6.89 (t, 2H, H4), 3.45 (q, 4H, Et$_2$O), 2.87 (m, 4H, ipso-Cy), 2.23-1.18 (m, 26H, Cy, Et$_2$O); ^{13}C NMR (benzene-d$_6$/ppm): δ 154.80 (C1/C7), 138.04 (C3/C5), 121.19 (C2/C6), 118.50 (C4), 63.81 (ipso-Cy-CH), 48.1 (Et$_2$O, CH$_2$), 35.49 (o-Cy-CH$_2$), 26.05 (p-Cy-CH$_2$), 25.44 (m-Cy-CH$_2$). 19.22 (Et$_2$O, CH$_3$).

Empirical formula	$C_{23}H_{37}N_2MgOCl$	β/ °	83.713(2)
Formula weight	417.31	γ/ °	70.746(2)
Crystal system	Triclinic	Volume/ Å^3	1165.6(3)
Space group	P-1	Z	2
a/ Å	8.0275(10)	Z'	1
b/ Å	11.2403(16)	Density calc./ Mgm^{-3}	1.189
c/ Å	14.3153(17)	μ (Mo-K)/ mm^{-1}	0.206
α/ °	72.937(3)		

Data were collected on a Bruker SMART APEX diffractometer[15] equipped with an Oxford Cryosystems low-temperature device at 150 K and using an yellow rod oil-coated crystal[16] of dimension 0.27x0.12x0.10 mm^3. The initial unit cell was indexed using a least-squares analysis of a random set of reflections collected from three series of 0.3° wide ω-scans, 10 s per frame, and 25 frames per series that were well distributed in reciprocal space. Data frames were collected [Mo Kα = 0.71073 Å] with 0.3° wide ω-scans, 20 s per frame and 600 frames per series. Four complete series were collected at varying ϕ angles (ϕ=0, 90, 120, 180°). The crystal to detector distance was 6.0 cm, this providing a set of $3.96 \leq 2\theta \leq 57.96$. A total of 14117 reflections were collected and integrated using SAINT,[17] while absorption correction was applied using SADABS[18] with 5590 unique [R(int)=0.0453]. System symmetry, systematic absences and intensity statistics indicated the unique triclinic space group P$\bar{1}$. The structure was determined by direct methods with the location of nearly all non-hydrogen atoms using the program SHELXS[19] and refined by full-matrix least-squares on F^2 using SHELXL.[20] All non-hydrogen atoms were refined anisotropically, while hydrogen atoms were placed in calculated positions, constrained to ride on their carbon atoms with group U_{iso} values assigned ($U_{iso}(H)= 1.20U_{iso}$). The final structure was refined to convergence [$\Delta/\sigma \leq 0.001$] with R(F) = 0.00677 (for 5590 data with F>4σF), GOF = 1.041 and *w*R2 = 0.1715 (all data). [$R1 = \Sigma|F_O - F_C|/ \Sigma |F_O|$, $wR2 = \{[\Sigma w(F_O^2 - F_C^2)^2]/ \Sigma wF_O^4\}^{0.5}$, $w = 1/[\sigma^2(F_O^2) + (xP)^2 + yP]$, $P = (F_O^2+2F_C^2/3)$]. The largest difference between peak and hole in the final difference map, 0.441 and –0.771 eÅ^{-3}.

[{(Cy_2AFA)MgBr}$_2$] (51)

A stirred solution of *N,N'*-dicyclohexyl-6-aminofulvene-2-aldimine (Cy_2AFAH) (0.400 g, 1.400 mmol) in benzene (15 cm^3), under a nitrogen atmosphere, was refluxed with MeMgBr in diethyl ether (0.47 cm^3, 3.0 M, 1.400 mmol) for 30 min and then allowed to stir at room temperature for three days. The solvent and volatile components were removed under *vacuum* and the resulting solid dissolved in toluene (10 cm^3). Storage of at –5 °C over night gave yellow crystals as the final product (0.434 mmol, 62.0% yield).

^{1}H NMR (toluene-d_8/ppm): δ 7.34 (s, 2H, H1/H7), 7.32 (s, 2H, H1/H7), 6.86 (d, 2H, H3/H5), 6.74 (t, 1H, H4), 6.71 (d, 2H, H3/H5), 6.40 (t, 1H, H4), 1.85 (q, 2H, ipso-Cy), 1.70-0.70 (m, 20H, Cy). ^{13}C NMR (toluene-d_8/ppm): δ 157.2 (C1/C7), 133.9 (C3/C5), 124.2 (C2/C6), 121.0 (C4), 66.7 (ipso-Cy-CH), 38.1 (o-Cy-CH_2), 28.7 (p-Cy-CH_2), 28.10 (m-Cy-CH_2).

Empirical formula	$C_{38}H_{54}N_4MgBr_2$	β/ °	100.925(5)
Formula weight	778.29	γ/ °	90
Crystal system	Monoclinic	Volume/ Å^3	3748(2)
Space group	$P2_1/c$	Z	4
A/ Å	11.354(5)	Z'	1
B/ Å	26.306(5)	Density calc./ Mgm^{-3}	1.374
C/ Å	12.779(5)	μ (Mo-K)/ mm^{-1}	2.229
α/ °	90		

Data were collected on a Bruker SMART APEX diffractometer[15] equipped with an Oxford Cryosystems low-temperature device at 150 K and using a yellow block oil-coated crystal[16] of dimension 0.30x0.25x0.10 mm^3. The initial unit cell was indexed using a least-squares analysis of a random set of reflections collected from three series of 0.3° wide ω-scans, 10 s per frame, and 25 frames per series that were well distributed in reciprocal space. Data frames were collected [Mo Kα = 0.71073 Å] with 0.3° wide ω-scans, 20 s per frame and 600 frames per series. Four complete series were collected at varying ϕ angles (ϕ=0, 90, 120, 180°). The crystal to detector distance was 6.0 cm, this providing a set of $3.10 \leq 2\theta \leq 58.06$. A total of 33990 reflections were collected and integrated using SAINT,[17] while absorption correction was applied using SADABS[18] with 10006 unique [R(int)=0.0604].

System symmetry, systematic absences and intensity statistics indicated the unique monoclinic space group P $2_1/c$. The structure was determined by direct methods with the location of nearly all non-hydrogen atoms using the program SHELXS[19] and refined by full-matrix least-squares on F^2 using SHELXL.[20] All non-hydrogen atoms were refined anisotropically, while hydrogen atoms were placed in calculated positions, constrained to ride on their carbon atoms with group U_{iso} values assigned ($U_{iso}(H)= 1.20U_{iso}$). The final structure was refined to convergence [$\Delta/\sigma \leq 0.001$] with R(F) = 0.0491 (for 33990 data with F>4σF), GOF = 1.024 and *w*R2 = 0.1009 (all data). [$R1 = \Sigma|F_o - F_c|/ \Sigma |F_o|$, $wR2 = \{[\Sigma w(F_o^2 - F_c^2)^2]/ \Sigma wF_o^4\}^{0.5}$, $w = 1/[\sigma^2(F_o^2) + (xP)^2 + yP]$, $P = (F_o^2+2F_c^2/3)$]. The largest difference between peak and hole in the final difference map, 0.674 and –0.490 eÅ^{-3}.

[(Cy$_2$AFA)Mg(Me)THF] (52)

A stirred solution of *N,N'*-dicyclohexyl-6-aminofulvene-2-aldimine (Cy_2AFAH) (0.238 g, 0.835 mmol) in toluene (5 cm^3), under a nitrogen atmosphere, was added dropwise to a solution of MeLi (0.52 cm^3, 1.6 M, 0.835 mmol) in diethyl ether at –78 °C. The reaction mixture was allowed to warm to room temperature and stirred for 20 min. After 20 min the lithiated ligand was treated with a solution of MeMgCl (0.30 cm^3, 3.0 M, 0.835 mmol) in THF and the resulting solution was stirred over night. The orange solution was filtered (LiCl removed) and stored at –5 °C for 2 days to give yellow crystals (0.55 mmol, 66% yield).

^{1}H NMR (toluene-d_8/ppm): δ 7.89 (s, 2H, H1/H7), 6.66 (d, 2H, H3/H5), 6.45 (t, 1H, H4), 3.18 (m, 4H, THF), 1.91 (p, 2H, ipso-Cy), 1.18-1.00 (m, 20H, Cy); 0.93 (m, 4H, THF). –0.98 (s, 3H, CH_3) ^{13}C NMR (toluene-d_8/ppm): δ 162.8 (C1/C7), 133.0 (C3/C5), 115.9 (C2/C6), 113.8 (C4), 69.1 (ipso-Cy-CH), 67.5 (THF, CH_2), 33.1 (o-Cy-CH_2), 24.9 (p-Cy-CH_2), 24.3 (m-Cy-CH_2), 23.9 (THF, CH_2), -10.6 (Mg*C*H3).

Empirical formula	$C_{24}H_{38}N_2OMg$	β/°	90
Formula weight	394.87	γ/°	90
Crystal system	Orthorhombic	Volume/ Å^3	4701.9(6)
Space group	Pbca	Z	8

A/ Å	11.3464(9)	Z'	1
B/ Å	15.2076(13)	Density calc./ Mgm^{-3}	1.116
C/ Å	27.249(2)	μ (Mo-K)/ mm^{-1}	0.091
α/ °	90		

Data were collected on a Bruker SMART APEX diffractometer[15] equipped with an Oxford Cryosystems low-temperature device at 150 K and using a yellow block oil-coated crystal[16] of dimension 0.38x0.25x0.24 mm^3. The initial unit cell was indexed using a least-squares analysis of a random set of reflections collected from three series of 0.3° wide ω-scans, 10 s per frame, and 25 frames per series that were well distributed in reciprocal space. Data frames were collected [Mo Kα = 0.71073 Å] with 0.3° wide ω-scans, 20 s per frame and 600 frames per series. Four complete series were collected at varying ϕ angles (ϕ=0, 90, 120, 180°). The crystal to detector distance was 6.0 cm, this providing a set of $3.02 \leq 2\theta \leq 58.12$. A total of 28371 reflections were collected and integrated using SAINT,[17] while absorption correction was applied using SADABS[18] with 5846 unique [R(int)=0.0490]. System symmetry, systematic absences and intensity statistics indicated the unique orthorhombic space group P bca. The structure was determined by direct methods with the location of nearly all non-hydrogen atoms using the program SHELXS[19] and refined by full-matrix least-squares on F^2 using SHELXL.[20] All non-hydrogen atoms were refined anisotropically, while hydrogen atoms were placed in calculated positions, constrained to ride on their carbon atoms with group U_{iso} values assigned ($U_{iso}(H)= 1.20U_{iso}$). The final structure was refined to convergence [$\Delta/\sigma \leq 0.001$] with R(F) = 0.0652 (for 5846 data with F>4σF), GOF = 1.078 and *w*R2 = 0.1469 (all data). [$R1 = \Sigma|F_o - F_c|/ \Sigma |F_o|$, $wR2 = \{[\Sigma w(F_o^2 - F_c^2)^2]/ \Sigma wF_o^4\}^{0.5}$, $w = 1/[\sigma^2(F_o^2) + (xP)^2 + yP]$, $P = (F_o^2+2F_c^2/3)$]. The largest difference between peak and hole in the final difference map, 0.540 and –0.373 $eÅ^{-3}$.

[(Cy$_2$AFA)Mg(Me)] (53)

Yellow crystals of [(Cy$_2$AFA)Mg(Me)THF] (0.200 g 0.506 mmol) were heated to 135 °C under dynamic *vacuum* (10^{-2} torr) for 2 h to give [(Cy$_2$AFA)Mg(Me)] as a yellow oil (0.153 g, 0.474 mmol, 93.7% yield).

^{1}H NMR (toluene-d_8/ppm): δ 8.33 (s, 2H, H1/H7), 6.88 (d, 2H, H3/H5), 6.47 (t, 1H, H4), 3.06 (p, 2H, ipso-Cy), 2.01-0.79 (m, 20H, Cy), –0.54 (s, 3H, CH_3). ^{13}C NMR (toluene-d_8/ppm): δ 164.2 (C1/C7), 137.4 (C3/C5), 117.8 (C2/C6), 115.9 (C4), 63.1 (ipso-Cy-*C*H), 26.2 (o-Cy-*C*H_2), 25.8 (p-Cy-*C*H_2), 25.2 (m-Cy-*C*H_2), -10.6 (Mg*C*H_3).

Modelling Structure for [(Cy$_2$AFA)Mg(CH$_3$)]

Ab initio calculations were obtained from the Gaussian 98[21] package at 6-31G** basis set, and by using the atomic co-ordinates from crystal structure data for the AFA base.

Ethene Polymerisation Testing of [(Cy$_2$AFA)Mg(CH$_3$)]

Polymerisation reactions were performed in a 30 cm^3 Büchi miniclave equipped with a magnetic stir bar and a stainless steel pressure head fitted with inlet and outlet needle valves, a check valve for safety, and a pressure gauge (Figure 5.39). In a glovebox, the miniclave was charged with [(Cy$_2$AFA)Mg(CH$_3$)] complex (0.200 g, 0.620 mmol) and dry toluene (20 cm^3) and sealed. The minicalve was removed from the glovebox and attached to a stainless steel double manifold (*vacuum*/ethylene) line. The nitrogen atmosphere was removed under *vacuum*, and the solution was saturated with ethylene and thermally equilibrated at 55 °C for 10 min, followed by an immediate increase of the ethylene pressure to 7 bar. After 2 h, polymerisation was stopped by cooling and venting the reaction vessel, followed by quenching of the reaction with methanol. No polymers were detected by NMR spectroscopy.

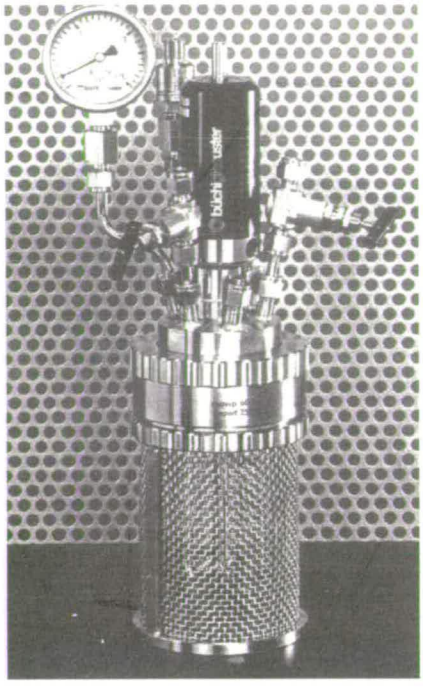

Figure 5.36 Schematic diagram of the Büchi miniclave used.

5.5 References

1 a) K. Hafner, K. H. Vöpel, G. Ploss and C. König, *Org. Syn.*, **1967**, *47*, 52; b) K. Hafner, K. H. Vöpel, G. Ploss and C. König, *Justus Liebigs Ann. Chem.*, **1963**, *661*, 52; c) K. Hafner and K. H. Vöpel, *Angew. Chem.*, **1959**, *71*, 672.

2 U. Müller-Westerhoff, *J. Am. Chem. Soc.*, **1970**, *92:6*, 4849.

3 J. Emley, *Chem. Rev.*, **1980**, *9*, 1.

4 S. P. Brown, M. Pérez-Torrealba, D. Sanz, R. M. Claramount and L. Emsley, *Chem. Commun.*, **2002**, 1852.

5 W. R. Brasen, H. E. Holmquist and R. E. Benson, *J. Amer. Chem. Soc.*, **1961**, *83*, 3125.

6 a) L. C. Dorman, *Tetrahedron Lett.*, **1966**, 459; b) E. Daltrozzo and K. Feldmann, *Tetrahedron Lett.*, **1968**, 4983.

7 a) R. W. Alder, *Chem. Rev.*, **1989**, *89*, 1215; b) H. A. Staab and T. Saupe, *Angew. Chem. Int. Ed. Engl.*, **1988**, *27*, 865.

8 L. McCoy, *J. Am. Chem. Soc.*, **1967**, *89*, 1673.

9 E. Etkin, C. M. Ong and D. W. Stephan, *Organometallics*, **1998**, *17*, 3656.

10 K. Klaβ, L. Duda, L. Kleigrewe, G. Erker, R. Fröhlich and E. Wegelius, *Eur. J. Inorg. Chem.*, **1999**, 11.

11 C. M. Ong and D. W. Stephan, *Inorg. Chem.*, **1999**, *38*, 5189.

12 a) P. J. Bailey, C. M. E. Dick, S. Fabre and S. Parsons, *J. Chem. Soc., Dalton Trans.*, **2000**, 1655; b) P. J. Bailey, R. Coxall, C. M. E. Dick, S. Fabre and S. Parsons, *Organometallics*, **2001**, *20*, 798; c) P. J. Bailey, S. Liddle, C. Morrison and S. Parsons, *Angew. Chem. Int. Ed. Engl.*, **2001**, *40*, 4463.

13 C. F. Caro, P. B. Hitcock and M. F. Lappert, *Chem. Commun.*, **1999**, 1433.

14 S. Halut-Desportes and C. Bois, *Acta Crystallogr. Sect. B.*, **1979**, *35*, 2205.

15 Bruker. *SMART*. Bruker-AXS, Madison, Wisconsin, USA, **2001**.

16 D. Stalke and T. Kottke, *J. Appl. Crystallogr.*, **1993**, 26, 615.

17 Bruker. *SAINT*. Bruker-AXS, Madison, Wisconsin, USA, **2002**.

18 G. M. Sheldrick, *SADABS*. Version 2.06. University of Gottingen, Germany, **2001**.

19 G. M. Sheldrick, *SHELXS97*. University of Gottingen, Germany, **1997**.

20 G. M. Sheldrick, *SHELXL97*. University of Gottingen, Germany, **1997**.

21 Gaussian 98, Revision A.11. M. J. Frisch, G. W. Trucks, H. B. Schlegel, G. E. Scuseria, M. A. Robb, J. R. Cheeseman, V. G. Zakrzewski, J. A. Montgomery, R. E. Stratmann, J. C. Burant, S. Dapprich, J. M. Millam, A. D. Daniels, K. N. Kudin, M. C. Strain, O. Farkas, J. Tomasi, V. Barone, M. Cossi, R. Cammi, B. Mennucci, C. Pomelli, C. Adamo, C. Cliord, J. Ochterski, G. A. Petersson, P. Y. Ayala, Q. Cui, K. Morokuma, D. K. Malick, A. D. Rabuck, K. Raghavachari, J. B. Foresman, J. Cioslowski, J. V. Ortiz, B. B. Stefanov, G. Liu, A. Liashenko, P. Piskorz, I. Komaromi, R. Gomperts, R. L. Martin, D. J. Fox, T. Keith, M. A.

Al-Laham, C. Y. Peng, A. Nanayakkara, C. Gonzalez, M. Challacombe, P. M. W. Gill, B. F. G. Johnson, W. Chen, M. W. Wong, J. L. Andres, M. Head-Gordon, E. S. Replogle and J. A. Pople, Gaussian Inc., Pittsburgh PA, **2001**.

Chapter 6:

Experimental Charge Density Analysis of Magnesium bis[hydrotris(pyrazolyl)borate]. Chloroform Solvate

6.1 Introduction

6.1.1 Background

In this work the technique of high-resolution X-ray diffraction has been used to determine the electron density in the complex of $[Mg\{(pz)_3BH\}_2]$, and hence experimentally to investigate the structure and the nature of the Mg-N and B-N bonding beyond the level attainable in a regular crystal structure determination.

After extensive development of experimental and calculational methods and concepts, experimental charge densities from X-ray diffraction measurements are now being more widely applied to chemical and physical problems. Examples are the calculations of Coulombic contributions to molecular interactions, the study of bonding-induced charges in transition-metal ligands, the establishment of the electronic ground state of transition-metal complexes, and the calibration of theoretical calculations.[1] Further experimental advances may be expected from the availability of the new synchrotron sources, which allow the use of smaller crystals, harder radiation, and shorter data collection times. The possibility of measuring the charge density in a crystal from its X-ray diffraction pattern was envisioned many years ago when Debye and Scherrer discussed the possibility that the halos on a powder photograph were images of the electron orbits around the atoms.[2] It took more theoretical developments, in particular the application of the theory of Fourier transforms, to establish the basic relationships between elastic X-ray scattering and the electron density distribution.[1,2] Even then the correspondence of experimental errors in the measurements, and the success of the spherical atom description of the density, raised doubts about the feasibility of such studies.[3] As a result, electron density studies in the 1960s and early 1970s were directed toward establishing the feasibility of the method and its limitations, given the sources and equipment available at that time.[1] More recently the emphasis has shifted to applications to chemical and physical problems, including comparison with theoretical results, calculation of intermolecular interactions, and determination of the ground state in metal co-ordination complexes.[1-3]

The most commonly used methods of electron density analysis are the calculation of electron density maps and the least-squares fitting of parametrized analytical functions to the experimental structures factors.[1-3] The electron density maps are obtained by usual Fourier inversion of the structure factors and require knowledge of the phase of the observed structure factors.[2] In X-ray scattering experiments on crystals, which are the most common sort, the diffraction pattern is determined by the repeating unit cell, characteristic of the crystal, and by the particular crystallographic plane (Miller indices) from which the scattering occurs. Thus for crystals one defines a structure factor $F(hkl)$ which is expressed as the Equation 1:

$$F(hkl) = \Sigma f_j e^{(2\pi h.r_j)} \qquad \text{Equation 1}$$

f: atomic scattering factor of the j^{th} atom in the unit cell

r_j : is its position within the Born-Oppenheimer approximation.

h :components vector of h/a, k/b and l/c, where a, b and c denote the dimensions of the unit cell.

The charge distribution at a point $\boldsymbol{r}$ within a unit cell, is expressed as the following Equation 2:[1,4,5]

$$\rho(r) = V^{-1}\sum_h\sum_k\sum_l F(hkl)\, e^{(-2\pi h.r_j)} \qquad \text{Equation 2}$$

V: volume of the unit cell

Parameter indeterminacies are especially severe for noncentrosymmetric structures for which the least square solution can lead to a physically meaningless result.[6] Haouzi *et al.*[6] have discussed that certain parameters or combinations of parameters are insensitive to the change in the structure factor amplitudes but are markedly affected by the phases. As a consequence, their estimates become indeterminate; typical parameters of this nature are odd-order multipoles being invariant under crystal-class symmetry.[6] In such a situation, application of chemical

and/or non-crystallographic symmetry constraints is essential to retrieve a physically meaningful static density. For centrosymmetric crystals the spherical atom treatment is quite adequate; such crystals are therefore inherently more suitable for the density analysis. Nevertheless, successful studies on acentric crystals have been reported; an example of such is the a study of tetraphenylporhyrin iron(II) structure factors.[7] Since the total electron density is dominated by the core electrons and only very slightly affected by chemical bonding, difference densities are employed to illustrate bonding effects. The most widely used function is the "atom deformation density" or "standard deformation density" which is simply the difference between the total density and the density corresponding to superimposed spherical atoms (Equation 3), where R_i is the nuclear position of atom i.[1,8]

$$\Delta\rho(r) = \rho_{total}(r) - \sum_{\substack{all \\ atoms}} \rho(r - R_i) \qquad \text{Equation 3}$$

The density obtained experimentally is the total density averaged over the vibrational modes of the crystal. In order to apply the Equation 3, the atomic densities subtracted must be thermally averaged, or the thermal motion must be deconvoluted from the total density.[9] In the former case the thermally averaged deformation density [$\Delta\rho(r)$] is obtained. Either procedure requires a model for the thermal motion in the crystal, which is often based on the atomic thermal parameters from the X-ray experiment. In the case of a molecule the second term in Equation 3 is referred to as the pro-molecule density; it is the density prior to bond formation between the atoms.[9] Such deformation densities can be excellent demonstrations of accumulation of density in the bond and lone-pair regions of a molecule. The Figure 6.1 shows density in the bonds and the lone-pair regions near the oxygen atoms of the molecule of oxalic acid.[10] But for elements with more than half-filled valence shells, bond peaks in the standard deformation density tend to be lower than expected or may even be absent.[9,11] The effect has been very elegantly demonstrated in a study on a molecule that contains C-N, C-O, N-N, and O-O bonds. Because of this, the standard deformation density has been criticised by theoreticians,[12] and alternative definitions of the deformation density have been proposed in which either oriented atoms or hybridized atoms are subtracted, as was in fact done in much earlier work

on the F_2 molecule by Bader *et al.*[13] While the alternative definitions are helpful, in particular in illustrating the bonding density, the spherically averaged atomic density is the only reference state that is unambiguously defined and does not depend on assumptions regarding orientation and hybridisation of the atoms.[13] An extension of the idea of subtraction of a prepared entity is to subtract a chemical fragment, or ligand, from a molecular density. This was done in 1976 by Rees[14] for $Cr(CO)_6$, for which subtraction of a theoretical density of the carbon monoxide molecule clearly showed the decrease in σ- and increase in π-density in the ligand due to the bonding, in accordance with the σ-donation, π-back-donation concept of Chatt *et al.*[15]

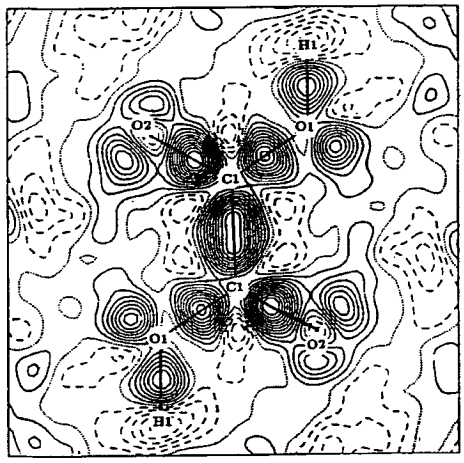

Figure 6.1 Standard model deformation density in the plane of the oxalic acid molecule at 15 K. Contour at 0.05 e Å^{-3}, zero dotted lines; negative contour dashed.

To obtain more quantitative information on the charge distribution than is possible from electron density maps, the refinement of charge density parameters such as valence shell population, a valence shell "shape" parameter, and populations of atomic dipole, quadrupole, and higher functions has been developed.[16,17] They are usually refined together with the conventional structural parameters which include atomic positional and temperature parameters. The most widely applied charge density model of this kind consists of an expansion of atom-centred spherical harmonic functions y_{lmp}. The radial dependence or "shape" of the valence shell density in this "multipole model" is allowed to vary by the adjustment of a parameter κ, which scales the radial coordinate r,[17] where p is plus or minus for $m \geq 1$, P_v is the valence shell population which multiplies the spherical valence density $\rho(r)$, and the

radial function R can have either a Slater type or a Hartree-Fock radial dependence (Equation 4).

$$\rho(r) = \rho_c(r) + P_v \kappa^3 \rho_{valence}(\kappa r) + \sum_{l=0}^{l_{max}} \kappa'^3 R_l(\kappa' r) \sum_{m=0}^{l} P_{lmp} y_{lmp}(\vartheta, \varphi) \qquad \text{Equation 4}$$

When this expression is truncated after the second term a simple spherical atom model is obtained, which allows the determination of the net charge and the change in the radial dependence of the valence shell that must accompany any deviation from electron neutrality of an atom, because of the change in electron-electron repulsion. This "kappa refinement" model[18] is quite successful in giving net atomic charges of atoms, which can be used in molecular force field calculations, or in the calculation of molecular dipole moments for molecules in crystals. The continuous electron density in the crystal is then modelled as a sum of atom centred charge distributions, according to the Equation 5.

$$\rho(r) = \sum_j \rho_j(r_j) \qquad \text{Equation 5}$$

6.1.2 Atoms in Molecules

In the topological theory of Bader "Atoms in Molecule" (AIM)[19-22] the chemical bonds and molecular reactivity is interpreted in terms of the total molecular electronic density, $\rho(r)$, and its corresponding Laplacian, $\nabla^2\rho(r)$. The values of $\rho(r)$ and $\nabla^2\rho(r)$ at the bond critical point (bcp) allow the characterisation of the chemical bonds of the atoms in the molecules (see for example, Figure 6.2). Any bonded pair of atoms has a bond path, which is a line of the highest electron density linking them. According to the AIM theory, $\nabla^2\rho(r)$ provides information concerning electronic charge. $\nabla^2\rho(r) > 0$ implies locally depleted charge while, on the contrary, $\nabla^2\rho(r) < 0$ signifies locally concentrated charge.[20-22] Thus, classical covalent bonds or shared interactions have values at the bcp of $\nabla^2\rho_{bcp} < 0$ and ρ_{bcp} large, while classical ionic bonds (closed-shell interactions) have $\nabla^2\rho_{bcp} > 0$ and ρ_{bcp} low. Intermediate bonds are associated with $\nabla^2\rho_{bcp} > 0$ and ρ_{bcp} medium or large, i.e.; values between shared

and closed-shell. On the other hand, Cremer and Kraka[23] have shown that for covalent and intermediate bonds the energy density H_{bcp} has negative values. Another parameter used to describe a bond is the ellipticity (ε) that shows if the electronic charge is preferentially accumulated in a given direction between two bonded atoms. The ellipticities at the BCPs are also defined in terms of the ratio of the curvature of the $\rho(r)$ in directions normal to the bond, and represent the deviations of the bonding density from cylindrical symmetry. Sigma bonds have $\varepsilon = 0$, while π bonds, in general, have $\varepsilon > 0$. Beside the BCP there is another type of critical point (cp) called the ring CP, which is present in ring structures such as benzene, thiophene, etc. It has been proposed[24] that there is a correlation between the interaction energies of some compounds and either $\rho(r)$ or $\nabla^2\rho(r)$ at the ring CP.

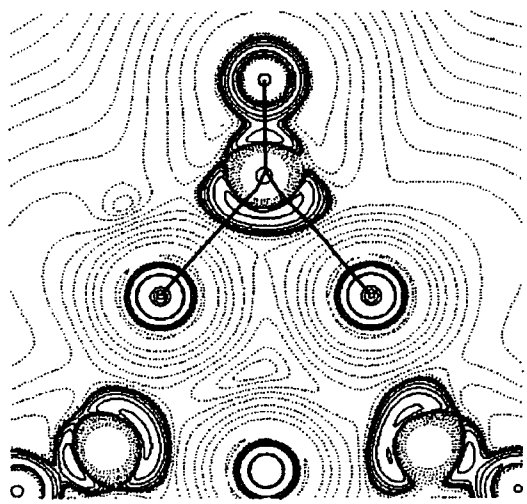

Figure 6.2 Laplacian distribution and bond paths for a bridging carbonyl in $Co_4(CO)_8(\mu_2\text{-}CO)_3PPh_3$.[25]

6.2 Results

6.2.1 Reactivity of Potassium Hydrotris(1-pyrazoly)borate with MeMgCl

The potassium hydrotris(1-pyrazolyl)borate, $[K\{(pz)_3BH\}]$ (**54**), (Figure 6.3) was prepared satisfactorily by reacting potassium borohydride with pyrazole.[26] Treatment of **54** with an equimolar amount of MeMgCl in THF at room temperature was carried out. After subsequent removal of the solvent in *vacuum* and extraction from diethyl ether gave **55** as white powder. Colourless crystals for X-ray analysis were grown from a concentrated chloroform solution of **55** at room temperature. The NMR spectra show only one type of pyrazole group at room temperature. The ^1H NMR spectrum shows the three pyrazole hydrogen atoms as doublets for H5 and H3 at δ 7.65 and 7.30, with a triplet for H4 at δ 6.15 in a 1:1:1 ratio, respectively. The ^{13}C NMR spectrum gives the three pyrazole carbon resonances at δ 140.31, 135.96 and 104.09 for C3, C5 and C4, respectively.

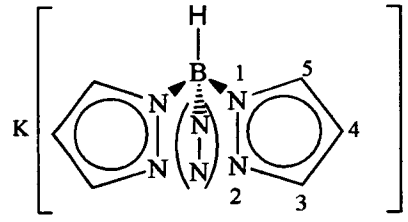

-(N-N)- is the third, hidden, pyrazolyl group

Figure 6.3 Labelling reference for 54.

The X-ray crystal structure (Figure 6.4) reveals a bischelate magnesium complex, with an octahedral geometry around the magnesium atom centre for the $[Mg\{(pz)_3BH\}_2].2[CHCl_3]$ (**55**). The crystal structure is located in the cubic Pa3 space group, making it a good candidate for electron density measurements. The $[HB(pz)_3]^-$ ligands are co-ordinating in a $\kappa 3$ fashion, in which the complex has the local geometry of C_3 and sits along the unit cell diagonal. The chloroform co-molecules are also found on the three-fold axis. The Mg-N bond distances of 2.1772(4) Å in the chelate ligands are typical σ-bonding distances. The co-ordinative

effect on the octahedral magnesium atom could be also explained by a simple dissociation of the alkyl magnesium compound by a Schlenk equilibrium. Selected bond length and angles are shown in Table 6.1.

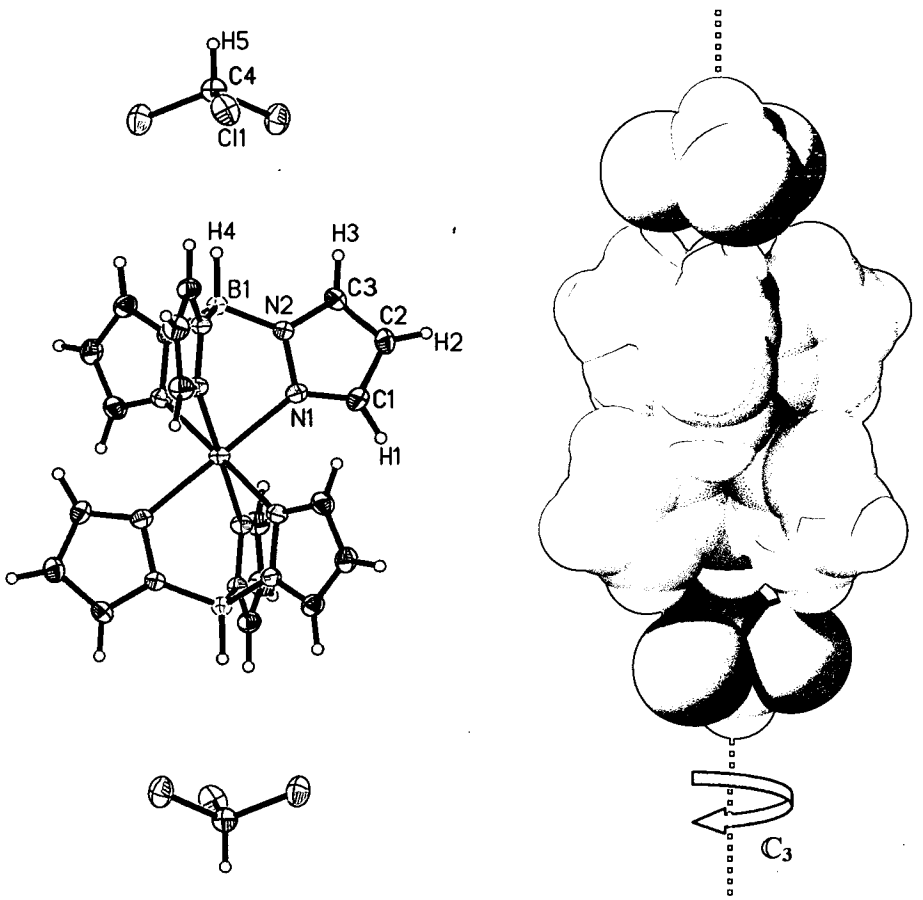

Figure 6.4 Crystallographic structure of 55; a) Displacement ellipsoids are shown at the 50 % probability level; b) Spacefilling structure showing a three-fold rotation axis (C_3).

Table 5.1 Selected bond distances (Å) and angles (°) for 55. Symmetry transformations used to generate equivalent atoms: #1 –z,-x,-y; #2 y,z,x; #3 –y,-z,-x; #4 z,x,y; #5 –x,-y,-z.

Mg(1)-N(1)	2.1772(4)	Mg(1)-N(1)$^{\#1}$	2.1772(4)	Mg(1)-N(1)$^{\#2}$	2.1772(4)
Mg(1)-N(1)$^{\#3}$	2.1772(4)	Mg(1)-N(1)$^{\#4}$	2.1772(4)	Mg(1)-N(1)$^{\#5}$	2.1772(4)
B(1)-N(2)	1.5439(4)	B(1)-N(2)$^{\#2}$	1.5439(4)	B(1)-N(2)$^{\#4}$	1.5439(4)
N(1)-C(1)	1.3361(5)	N(1)-N(2)	1.3588(5)	N(2)-C(3)	1.3461(5)
C(1)-C(2)	1.4044(5)	C(2)-C(3)	1.3888(5)	Cl(1)-C(4)	1.7617(9)
N(1)$^{\#1}$-Mg(1)-N(1)		94.89(4)	N(1)$^{\#1}$-Mg(1)-N(1)$^{\#3}$		85.11(4)
N(1)$^{\#2}$-Mg(1)-N(1)$^{\#3}$		180.00(5)	N(1)-Mg(1)-N(1)$^{\#5}$		180.00(5)
N(1)$^{\#4}$-Mg(1)-N(1)$^{\#5}$		94.89(4)	N(2)$^{\#2}$-B(1)-N(2)		108.74(10)
C(1)-N(1)-N(2)		105.83(10)	C(1)-N(1)-Mg(1)		135.96(9)
N(2)-N(1)-Mg(1)		118.10(8)	C(3)-N(2)-N(1)		110.11(11)
C(3)-N(2)-B(1)		129.26(13)	N(1)-N(2)-B(1)		120.61(12)
N(1)-C(1)-C(2)		110.89(12)	C(3)-C(2)-C(1)		104.71(12)

N(2)-C(3)-C(2)	108.46(12)	Cl(1)$^{\#2}$-C(4)-Cl(1)	110.70(7)

6.2.2 Residual Density

The residual density can be used as a tool in structure analysis; its result is a measure for the shortcomings of the least-squares minimisation, and the functions which constitute the least-square model for the scattering density. Observation of the residual map of **55** (Figure 6.5) shows an excellent and coherent relationship between the observed and calculated scattering densities after completion of the multipole refinement. The range of residual density values over the whole asymmetric unit is –0.211 and 0.210 e.Å^{-3}.

Figure 6.5 Residual map for 55 in the Mg-pyrazolyl-B plane. Contours at 0.1 eÅ^{-3} intervals, first contours at 0.05 eÅ^{-3}.

6.2.3 Deformation Density

Deformation densities of **55** routinely show both bonding and non-bonded (lone-pair) regions of charge density in a pictorial manner. The deformation density in the plane of one aromatic heterocycle and including the Mg and B atoms is shown in Figure 6.6. Considering firstly the ring portion of the structure, one sees well structured deformation peaks in the bonds. The C-H bonds show the redistribution of

density from behind the H atoms into the bonds while the C-C and C-N bond peaks lie slightly outside the direct vector. If one considers the C and N atoms to be sp^2 hybridised, the ideal bonds angles would be 120°. This is not possible in a 5-membered ring and therefore a degree of strain is to be expected. This is mirrored in the positions of the bonding peaks being outside the ring as found in porphyrin compounds.[27]

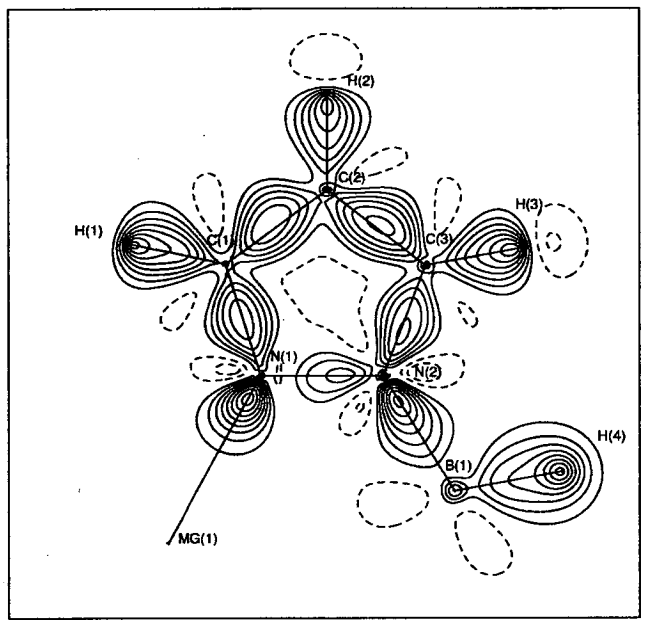

Figure 6.6 Experimental static deformation map for 55 in the Mg-pyrazolyl-B plane. Contours at 0.1 eÅ^{-3} intervals, positive contours solid.

The character of the H atom in the B-H bond is very different from that of the three C-H bonds. The hydrogen atom on boron atom, H(4), actually gains electrons compared to its free atom state, and it is reflected in the diffuseness of its deformation density. Of major interest in this study is the nature of the Mg-N bonding modes. Since both N(1) and N(2) are chemically equivalent from the point of view of the ring, they have the same capacity for bonding. Indeed both show similar peaks in the deformation map pointing charge directly at Mg and B, respectively. There is a difference in diffuseness of the peaks however. N(1) has a contracted peak, reminiscent of a possible lone-pair, while the N(2) peak stretches further toward B, indicating more of sharing of electrons. Since this deformation peak originates at N(2) it has the character of a dative bond from N(2) to B(1). On

the other hand, N(1) looks more to present an electron density close to its nucleus but pointing to the magnesium atom. The N(1)-N(2) bonding deformation is slight, and less than would be expected. This is a common occurrence in the deformation maps (see Section 6.1.1).

6.2.4 Topology of the Total Electron Density

Another important function of the electron density is the Laplacian $[\nabla^2\rho(r_c)]$ of **55**, defined as the second derivative of its total density (Figure 6.7). A total topological analysis of **55** has been done, and several experimental CP properties were obtained, and they are listed in Table 6.2.

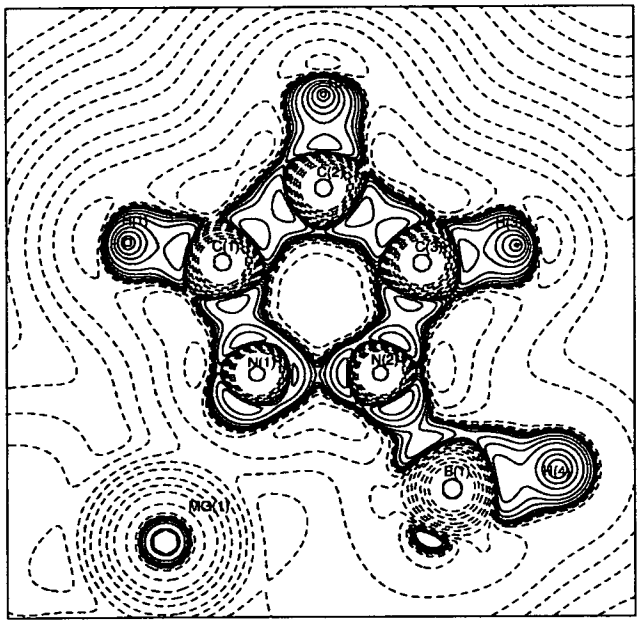

Figure 6.7 Experimental Laplacian map for 55 in the Mg-pyrazolyl-B plane. Contours at 0.1 eÅ^{-5} intervals, positive contours solid.

Table 6.2 Experimental determined CP properties for 55. R_{ij} is the length of bond path. d1 and d2 are the distances of bcp from atoms.

Bond	Length/Å	$\rho(r_c)$/eÅ^{-3}	$\nabla^2\rho(r_c)$/eÅ^{-5}	R_{ij}/Å	d1/Å	d2/Å	ε
Mg(1)-N(1)	2.1772(3)	0.24(1)	4.4(1)	2.1775	0.9292	1.2483	0.02
B(1)-N(2)	1.5439(4)	1.03(1)	7.9(1)	1.5443	0.4795	1.0648	0.08
N(1)-N(2)	1.3588(4)	2.37(2)	-3.5(1)	1.3588	0.6673	0.6915	0.07
N(1)-C(1)	1.3361(5)	2.36(2)	-25.2(1)	1.3361	0.7889	0.5472	0.19
N(2)-C(3)	1.3461(5)	2.26(2)	-22.4(1)	1.3463	0.7987	0.5475	0.21
C(1)-C(2)	1.4044(5)	2.05(2)	-18.3(1)	1.4065	0.7190	0.6875	0.21
C(2)-C(3)	1.3888(5)	2.13(2)	-19.1(1)	1.3896	0.6923	0.6974	0.26
C(4)-Cl(1)	1.7641(2)	1.28(1)	-2.6(1)	1.7642	0.8230	0.9411	0.04
C(1)-H(1)	1.0770(-)	1.87(4)	-19.4(1)	1.0773	0.7091	0.3682	0.11
C(2)-H(2)	1.0770(-)	1.77(4)	-17.9(1)	1.0771	0.6829	0.3942	0.08
C(3)-H(3)	1.0770(-)	1.83(3)	-19.5(1)	1.0771	0.6829	0.3942	0.11
B(1)-H(4)	1.2000(-)	1.16(1)	-10.1(1)	1.2000	0.5198	0.6801	0.00
C(4)-H(5)	1.0590(-)	1.98(3)	-24.9(1)	1.0500	0.7230	0.3270	0.00
Cl(1)···H(3)	3.0461(2)	0.02(1)	0.3(2)	3.0999	1.9655	1.1344	0.27
Cl(1)···H(4)	3.3000(2)	0.03(1)	0.3(1)	3.3052	1.9434	1.3618	0.14

According to the topological features obtained for the experimental charge density for **55**, the following points emerge. The averaged topological density, $\rho(r_c)$, over the two C-N CP is 2.31 eÅ^{-3}, and its value cannot be considered as clearly double or single bond, which suggest that both interactions support π-delocalization. The Laplacian map of **55** (Figure 6.7) in the ring section demonstrates clearly the concentration of its negative values in the interatomic region C-N (-23.8 eÅ^{-5}); this is due to the shared electrostatic attraction of electrons by both nucleus acting as a typical covalent bond. The ellipticity for the C-N BCP is shown to be 0.20, which is characteristic of a double bond. In addition, the CP properties of the C-C bond (average) present a relatively high density of 2.09 eÅ^{-3}, while the negative Laplacian [$\nabla^2\rho(r_c)$= -18.7 eÅ^{-5}] indicates a local concentration of charge in the C-C bonds and hence covalence where the potential energy dominates the local electronic energy. The charge delocalization, around the C-C bonds is supported by high ellipticities (0.24) in the BCP. The N-N bond from the 5-membered ring appears rather pinched here and has a low charge accumulation [$\nabla^2\rho(r_c)$= -3.5 eÅ^{-5}], although the density itself is reasonably high at 2.37 eÅ^{-3}, higher than for the C-N bonds (2.31 eÅ^{-3}). The ellipticity is not significantly different from zero (0.07), however, the N-N bond [1.3588(4) Å] may confirm a π contribution to the bond. As a complement, the Laplacian distribution around the central N(1) atom shows only one non-bonded valence shell charge concentration (VSCC).

Analysing the CP properties for Mg-N and B-N bonds, the densities at their critical points are very low (0.24 and 1.03 eÅ^{-3}, respectively), with positive values of $\nabla^2\rho(rc)$ (4.4 and 7.9 eÅ^{-5}, respectively). According to the Laplacian map a higher covalent character can be suggested for the B-N bond than for the Mg-N bond, unlike those for covalent bonds between first-row atoms. These features correspond to an absence of potential-energy lowering typical for covalent bonds, which results from the shared interaction of the electron with other close nucleus. The B-H bond shows a small value of $\rho(r_c)$ (1.16 eÅ^{-3}), and high concentration of charge according to $\nabla^2\rho(r_c)$ (-10.1 eÅ^{-5}).

The Cl-atoms of the chloroform solvent molecule point towards the boron-bound hydrogen atom, involving weak Cl···H hydrogen bonds [3.0461(2) and 3.3000(2) Å, respectively]. The B-H···Cl-C and C-H···Cl-C interactions can be appreciated by analysing the different bond paths observed in Figure 6.8. The corresponding CPs for B-H···Cl-C and C-H···Cl-C interactions have associated a low value of ρ and positive $\nabla^2\rho$ (averaged values of 0.02 e.Å^{-3} and 0.3 e.Å^{-5}, respectively), whilst the long R_{ij} value (> 2.2 Å) represent the weakest types of interactions,[28] and according to the AIM[20-22] suggests the presence of a closed-shell interaction consistent with a long hydrogen bond.

Finally, the relative experimental atomic charges on the Mg^{2+} have been integrated in the volume of the atomic basin by using the TOPXD[36] program, providing an electrophilic magnesium atom with charge of +1.4e.

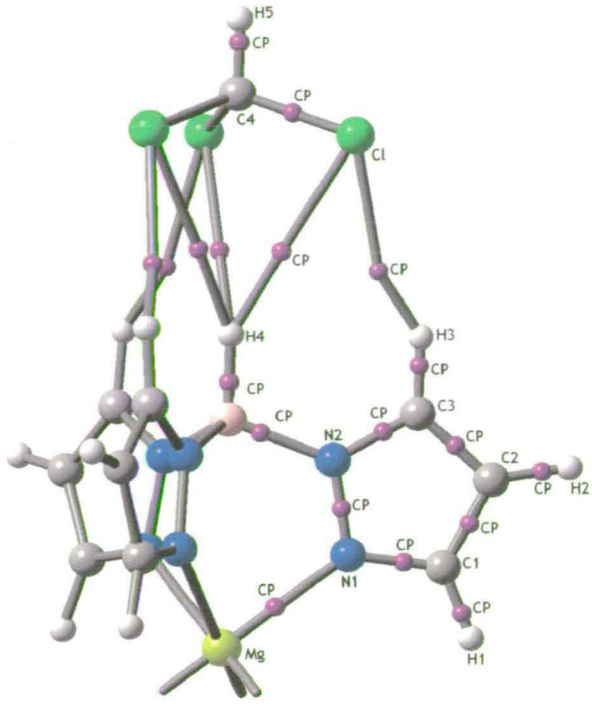

Figure 6.8 Interaction lines, lines along which charge is concentrated and on which critical points are situated. Positions of critical points are labelled CP for 55.

6.3 Conclusions

The structure and bonding of magnesium bis[hydrotris(pyrazolyl)borate] as its chloroform solvate has been investigated by high-resolution X-ray diffraction. The topological properties of $\rho(r)$ and $\nabla^2\rho(r)$ have been investigated, and deformation density maps produced. The charge on the formally Mg^{2+} ion obtained by integrating the electron density in the volume of the atomic basin is $+1.4e$, while the directional lone-pairs on the six ligating nitrogen atoms in the hydrotris(1-pyrazolyl)borate ligands have similar properties in the deformation density, being donation from nitrogen lone-pairs to B, however the Laplacian maps show this to have much more covalent character than the Mg-N bond. It is also possible that nitrogen atoms present a sharing electron character or a tight peak (lone pair), where electron charge transference is present. An equilibrium between two structures can be suggested, according to the Figure 6.9. The deformation density maps show a rather diffuse B-H bond, where the hydrogen atom is attracted toward the chloride atoms in the chloroform solvate, where weak types of Cl···H hydrogen bonding are appreciated. The topological analysis of the ligand charge density shows strain in the aromatic five-membered heterocycles since both the maxima in the deformation maps and the bond critical point positions from topological analysis sit outside of the interatomic vectors.

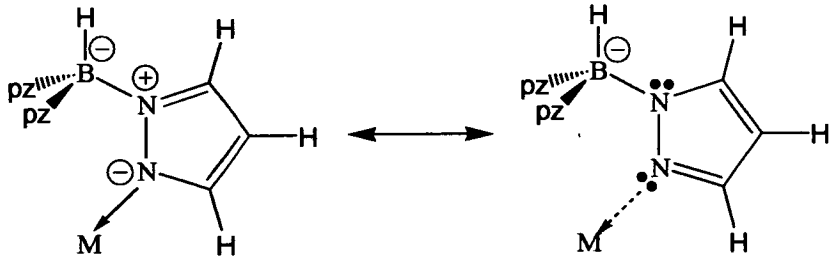

Figure 6.9 The two particular resonance forms for 55 show alternation within the π-system.

6.4 Experimental

6.4.1 General Procedures

All manipulations were carried out under a nitrogen atmosphere using standard Schlenk and cannula techniques or in a conventional nitrogen-filled glove-box (Saffron Scientific), fitted with oxygen and water scavenging columns. Solvents were refluxed over an appropriate drying agent, and distilled and degassed prior to use. Solvents and reagents where commercially available were bought from Aldrich, Acros or Fischer, with exception of NMR solvents which were purchased from Goss Scientific. Diethyl ether and THF were all distilled from Na/benzophenone under a nitrogen atmosphere. NMR solvents were degassed using three freeze-pump-thaw cycles and stored over 4 Å molecular sieves.

6.4.2 Instrumentation

The NMR spectra were recorded on Bruker AC 250 MHz and Varian Gemini 200MHz spectrometers. Infrared spectra were obtained using a Perkin-Elmer 1600 Paragon Series FT-IR spectrometer as potassium bromide discs or as liquid thin films. ^{1}H and ^{13}C NMR spectra were referenced to TMS.

6.4.3 Synthesis

$[Mg\{(pz)_3BH\}_2]$ (55)[29]

A solution of potassium hydrotris(1-pyrazolyl)borate (1.00 g, 5.36 mmol) in THF (10 cm^3) at room temperature was treated with MeMgCl in THF (1.80 cm^3, 5.36 mmol) and the mixture was allowed to stir overnight. Solvent and volatile components were removed under *vacuum,* and the product was extracted using diethyl ether (20 cm^3). The resultant solution was filtered through Celite 521 under nitrogen atmosphere and KCl removed to provide the final product (1.072 mmol,

40% yield). The crystallisation process of colourless crystals suitable for X-ray diffraction was carried out by slow evaporation of chloroform at room temperature.

IR: ν(BH): 2510 cm^{-1}; ^{1}H NMR ($CDCl_3$/ppm): δ 7.65 (s, 1H, H2), 7.30 (s, 1H, H3), 6.15 (s, 1H, H1). ^{13}C NMR ($CDCl_3$/ppm): δ 140.319 (*C*3), 135.96 (*C*1), 104.09 (*C*1). ^{11}B NMR ($CDCl_3$/ppm): δ -6.51.

Data Collection and Reduction

Data collection was performed on a Bruker SMART APEX CCD diffractometer[30] using graphite-monochromated Mo-Kα (λ= 0.71073Å) radiation with a nominal detector distance of 50 mm. Two separate crystals of differing sizes were used during the data collection, both being mounted under oil and cooled to 100 K using a liquid nitrogen cryostream. The large crystal (approximately 0.65 mm in all directions) was used to ensure adequate observed intensity at high angle. A scan through 180° in ω in 0.3° steps was performed with ϕ fixed at 0°, 120° and 240° and 2θ = 65°. Each 0.3° scan was exposed for 300 s. This data was integrated using SAINT[31] with a box size of 1.5° x 1.5° x 1.3°. The averaged profiles from the 9 regions of the detector were blended together.

The slightly smaller second crystal was used for low angle data collection. The same range was scanned, exposing for 30 s per 0.2° scan and with 2θ at +20° and –20°. The box size used in SAINT for integration of these exposures was 1.2° x 1.2° x 0.8°. The profiles for the nine detector regions were not blended for the low angle data.

The unit cell was refined using 6579 reflections in the range 4.91° ≤ 2θ ≤ 52.69° giving a value of a= 14.3698(2) Å. The two groups of data were separately run through SADABS[31] to correct for anisotropic diffraction effects such as variation in the volume irradiated due to centring errors, incident beam inhomogeneity, absorption and decay as well as a theta-dependent absorption correction, followed by merging these two sets in SORTAV[32] to give a single set of unique, commonly scaled reflection data.

Multipole Refinements

The crystal structure was solved and refined using the SHELXTL package[33] and provided the starting point for charge density refinement. Multipole refinements of a structured model against the experimental structure factors were performed using the XD package.[34] The topological properties of the charge density were calculated with the program TOPXD.[34] The static molecular charge density in this model is described as a sum of rigid pseudoatoms[35] at the nuclear positions (R_j).

$$\rho(r) = \sum_j \rho_j(r_j R_j)$$

Each pseudoatom density has the form

$$\rho_j(r_j) = P_c\rho_c(r_j) + P_v\kappa^3\rho_v(\kappa r_j) + \sum_{l=0}^{l_{max}}\sum_{m=-1}^{m=+1}\kappa'^3 P_{lm} R_l(\kappa' r_j) d_{lmp}(\theta_j,\phi_j)$$

where $r_j = r - R_j$. Thus each atom is described by a frozen core density of form ρ_c with a fixed population Pc, and spherical valence density ρ_υ, with the population P_υ varied in the least squares procedures to allow charge transfer between atoms and the κ' variable allowing for concentration or expansion of the charge cloud of the pseudoatom. Both and ρ_υ are derived from the Clementi-Roetti Hartree-Fock wavefunctions.[36] The final term in the expansion describes the deviation from sphericity of the valence density by a set of deformation functions taking the shape of density normalised spherical harmonics d_{lmp}. The radial term for these functions is a simple Slater-type function $Rl(r) = Nr^n\exp(-\kappa'\zeta r)$ with the expansion-contraction coefficient κ' again available to improve the radial dependence of the fit. The values chosen for n and ζ are based on orbital product arguments.[37]

An electroneutrality constraint was applied to refinements, and the formal charge for the magnesium complex and chloroform were kept neutral. The level of expansion was truncated at the octapole level (l_{max} = 3) for non hydrogen atoms, applying appropriate site-symmetry constraints.[38] The asphericity of hydrogen atoms was modelled by a single bond-directed dipole. The refinement of the radial functions corresponded to the NRMM method introduced by Abramov *et al.*[39] where

κ is freely refined while κ' is fixed at average values obtained by refinement against theoretical structure factors[40] for H, C and N; κ' was fixed at 1.0 for Mg and B.

In the absence of neutron diffraction data for precise determination of hydrogen atom structural parameters, the C-H bond lengths were renormalised to average values from neutron refinement.[41] No such values are available for B-H bonds and the few relevant entries in the Cambridge Database showed a wide variation, so a DFT B3LYP/6-31G** optimisation of the complex was undertaken, yielding a distance of 1.2000 Å which was used for renormalisation of the B-H bond length.

Treatment of the thermal motion was within the anisotropic harmonic approximation for non-hydrogen atoms, while hydrogen atoms were assigned an anisotropic harmonic temperature factor equal to 1.5 times the isotropic equivalent of the atom to which they were bonded.

The refinement converged smoothly with stable values for all parameters and no large least-squares correlation coefficients. A facility which provides a useful indicator of the reliability of the temperature factors and hence the static charge density model is Hirshfeld's rigid bond test.[42,43] For atoms of similar masses, and at least as heavy at carbon, it is assumed that there is an effectively vanishing component of the relative vibrational motion of a pair of bonded atoms in the bond direction. If $z^2_{A,B}$ denotes the mean square displacement amplitude of atom A in the direction of atom B, the difference of amplitudes of a bonded pair of atoms in the bond direction ($\Delta_{A,B} = z^2_{A,B} - z^2_{B,A}$) should tend to zero and certainly be less than 0.001Å^2. All bonded pairs of atoms satisfy this criterion.

Empirical formula	$C_{20}H_{22}N_{12}B_2Mg_{12}Cl_6$	N°. Reflections measured	116187
Crystal system	Cubic	Density calc./ Mgm^{-3}	1.135
Space group	Pa3	μ (Mo-K)/ mm^{-1}	0.160
a/ Å	14.3698(2)	N°. symmetry-independent reflections	4982
T/K	100(1)	Average multiplicity	23.3
Volume/ Å^3	2967.2(1)	Agreement factor R = $\Sigma \mid I-\bar{I} \mid / \Sigma I$	0.0276
Z	4	Refined on	F^2
Crystal 1/mm^3	0.18 x 0.12 x 0.10	R(F^2)	0.0347
Crystal 2/mm^3	0.18 x 0.12 x 0.10	$R\omega$ (F^2)	0.0360
Radiation (λ/Å)	Mo-Kα (0.71073)	S	1.7623
Scan type	ω	N_{data}/N_{params}	23/878
sin θ/λ_{max}/Å^{-1}	1.00	Weighting scheme, ω	$\omega=[\sigma^2(F^2)]^{-1}$

Optimisation of the B-H Bond Length for the [Mg{(pz)$_3$BH}$_2$]

Ab initio calculations were performed with Gaussian 98[44] package at the density functional (DFT) level of theory, and by using the atomic co-ordinates from crystal structure data for the [Mg{(pz)$_3$BH}$_2$] complex. The DFT calculation employed Becke gradient-corrected three-parameter hybrid exchange[45] combined with the gradient-corrected correlation functional of Lee *et al.*,[46] which included both local and non-local terms B3LYP functional. The calculations were performed using the standard molecular split-valence 6-31G** basis set.[47]

6.5 References

1 P. Coppens and T. S. Koritsanszky, *Chem. Rev.*, **2001**, *101*, 1583.

2 P. Debye and P. Scherrer, *Phys. Z.*, **1918**, *19*, 474.

3 L. Massa, M. Goldberg, C. Frishberg, R. F. Boehme and S. Laplaca, *J. Phys. Rev. Lett.*, **1985**, *55*, 622; M. P. C. M. Krijn, *J. Chem. Phys.*, **1988**, *89*, 4199.

4 M. P. C. M. Krijn, *J. Chem. Phys.*, **1988**, *89*, 4199.

5 E. D. Stevens, J. Rys and P. Coppens, *J. Am. Chem. Soc.*, **1978**, *100*, 2324.

6 M. A. Kampermann, R. J. Rubble and B. M. Craven, *Acta Crystallogr.*, **1994**, *B50*, 737; A. El Haouzi, N. K. Hansen, C. Le Hénaff and J. Prota, *Acta Crystallogr.*, **1996**, *A52*, 291; P. Coppens, *Acta Crystallogr.*, **1974**, *B30*, 255.

7 N. Li, P. Coppens and J. Landrum, *Inorg. Chem.*, **1988**, *27*, 482.

8 C. Gatti, R. Bianchi, R. Destro and F. Merati, *J. Mol. Struct. (Theochem.)*, **1992**, *255*, 409; C. Gatti, V. R. Saunders and C. Roetti, *J. Chem. Phys.*, **1994**, *101*, 10686; C. Gatti, B. Silvi and F. Colonna, *Chem. Phys. Lett.*, **1995**, *247*, 135.

9 P. Coppens, *Chem. Rev.* **2001**, *101*, 1583; V. G. Tsirelson and R. P. Ozerov, *Electron Density and Bonding in Crystals*, Institute of Physics, London (1996); P. Coppens, *X-ray Charge Densities and Chemical Bonding*, Oxford University Press, Oxford (1997).

10 D. Zobel, P. Luger, W. Dressig and T. Koritsanszky, *Acta Cryst.*, **1992**, *B48*, 837.

11 J. M. Savariault and M. Lehmann, *J. Am. Chem. Soc.*, **1980**, *102*, 1298.

12 K. Kunze and M. B. Hall, *J. Am. Chem. Soc.*, **1986**, *108*, 5122.

13 R. F. W. Bader, W. H. Henneker and P. E. Cade, *J. Chem. Phys.*, **1967**, *46*, 3341.

14 J. Rees, *J. Am. Chem. Soc.*, **1976**, *98*, 7918.

15 J. Chatt and L. Ducanson, *J. Am. Chem. Soc.*, **1953**, 2939.

16 R. F. Stewart, *Acta Crystallogr.*, **1976**, *A32*, 565.

17 N. K. Hansen and P. Coppens, *Acta Crystallogr.*, **1978**, *A34*, 909.

18 P. Coppens, T. N. Guru-Row, P. Leung, P. J. Becker, Y. W. Yang and E. D. Stevens, *Acta Crystallogr.*, **1979**, *A35*, 63.

19 R. F. W. Bader, *J. Phys. Chem.*, **1998**, *A102*, 7314.

20 R. F. W. Bader, *Atoms in Molecules: A Quantum Theory; Oxford University* Press: Oxford, UK. **1990**.

21 R. F. W. Bader, *Chem. Rev.*, **1991**, *91*, 893.

22 R. W. F. Bader and H. Essen, *J. Chem. Phys.*, **1984**, *80*, 1943.

23 D. Cremer and E. Kraka, *Angew. Chem. Int. Ed. Engl.*, **1984**, *109*, 5917; D. Cremer and E. Kraka, *Angew. Chem. Int. Ed. Engl.*, **1984**, *23*, 627.

24 D. Quiñonero, A. Frontera, P. Ballester, C. Garau, A. Costa and P. M. Deya, *Chem. Phys. Lett.*, **2001**, *339*, 369.

[25] J. Epstein and D. J. Swanton, *J. Chem. Phys.*, **1982**, *77*, 1048; Z. Su and P. Coppens, *J. Appl. Crystallogr.*, **1994**, *27*, 89.

[26] S. Trofimenko, *J. Am. Chem. Soc.*, **1966**, *88*, 1842; S. Trofimenko, *J. Am. Chem. Soc.*, **1967**, *89*, 3170.

[27] P. Coppens and L. Li, *J. Chem. Phys.*, **1984**, *81*, 1983-1993; K. Tanaka, E. Elkain, L. Liang, N. J. Zhu, P. Coppens and J. Landrum, *J. Chem. Phys.*, **1986**, *84*, 6969.

[28] U. Koach and P. L. A. Popelier, *J. Phys. Chem.*, **1995**, *99*, 9747; P. A. Popelier, *J. Phys. Chem. A.*, **1998**, *102*, 1873.

[29] S. Trofimenko, *Scorpionates – The Coordination Chemistry of Polypyrazolylborate Ligands*, Imperial College Press, London, (1999); S. Trofimenko, *Chem. Revs.*, **1993**, *93*, 943; N. Kitajima and W. B. Tolman, *Prog. Inorg. Chem.*, **1995**, *43*, 418; G. Parkin, *Adv. Inorg. Chem.*, **1995**, *42*, 291; S. Trofimenko, *Prog. Inorg. Chem.*, **1986**, *34*, 115.

[30] Bruker. *SMART*. Bruker-AXS, Madison, Wisconsin, USA, **2001**.

[31] *SAINT* and *SADABS*. Version 2.06. Data Collection and Processing Software for the SMART System. Siemens Analytical X-ray Instruments Inc., Madison, Wisconsin, USA, **2002**.

[32] R. H. Blessing, *Acta Crystallogr.*, **1997**, *A51*, 33.

[33] G. M. Sheldrick, *SHELXS97* and *SHELXS97*. University of Göttingen, Germany, **1997**.

[34] T. Koritsanszky, S. T. Howard, P. R. Mallinson, Z. Su, T. Richter and N. K. Hansen, *XD* – a computer program package for multipole refinement and analysis of charge densities from diffraction data, **1995**.

[35] R. F. Stewart, *Acta Crystallogr.*, **1976**, *A32*, 565.

[36] E. Clementi and C. Roetti, *Atomic Data and Nuclear Data Tables*, **1974**, *14*, 177.

[37] N. K. Hansen and P. Coppens, *Acta Crystallogr.*, **1978**, *A34*, 909.

[38] K. Kurki-Suonio, *Israel J. Chem.*, **1977**, *16*, 115.

[39] Y. A. Abramov, A. Volkov and P. Coppens, *Chem. Phys. Lett.*, **1999**, *81*, 311.

[40] A. Volkov, Y. A. Abramov and P. Coppens, *Acta Crystallogr.*, **2001**, *A57*, 272.

[41] F. H. Allen, O. Kenard, D. G. Watson, L. Brammer, A. G. Orpen and R. Taylor, *International Tables for Crystallography – Volume C*, Kluwer, **1992**.

[42] M. Harel and F. L. Hirshfeld, *Acta Crystallogr.*, **1975**, *B31*, 162.

[43] F. L. Hirshfeld, *Acta Crystallogr.*, **1976**, *A34*, 909.

[44] Gaussian 98, Revision A.11. M. J. Frisch, G. W. Trucks, H. B. Schlegel, G. E. Scuseria, M. A. Robb, J. R. Cheeseman, V. G. Zakrzewski, J. A. Montgomery, R. E. Stratmann, J. C. Burant, S. Dapprich, J. M. Millam, A. D. Daniels, K. N. Kudin, M. C. Strain, O. Farkas, J. Tomasi, V. Barone, M. Cossi, R. Cammi, B. Mennucci, C. Pomelli, C. Adamo, C. Cliord, J. Ochterski, G. A. Petersson, P. Y. Ayala, Q. Cui, K. Morokuma, D. K. Malick, A. D. Rabuck, K. Raghavachari, J. B. Foresman, J. Cioslowski, J. V. Ortiz, B. B. Stefanov, G. Liu, A. Liashenko, P. Piskorz, I. Komaromi, R. Gomperts, R. L. Martin, D. J. Fox, T. Keith, M. A. Al-Laham, C. Y. Peng, A. Nanayakkara, C. Gonzalez, M. Challacombe, P. M. W. Gill, B. F.

G. Johnson, W. Chen, M. W. Wong, J. L. Andres, M. Head-Gordon, E. S. Replogle and J. A. Pople, Gaussian Inc., Pittsburgh PA, **2001**.

[45] A. D. Becke, *J. Chem. Phys.*, **1993**, *98*, 5648.

[46] C. Lee, W. Yang and R. G. Parr, *Phys. Rev. B.*, **1988**, *37*, 785.

[47] H. P. Haran and J. A. Pople, *Theor. Chim. Acta*, **1973**, *28*, 213.